UNIVERSIDADE FEDERAL DE SÃO CARLOS
CENTRO DE CIÊNCIAS BIOLÓGICAS E DA SAÚDE
PROGRAMA DE PÓS-GRADUAÇÃO EM ECOLOGIA E RECURSOS NATURAIS

THAIS RABITO PANSANI

TRACEOLOGICAL STUDY OF GROUND SLOTH FOSSILS IN SANTA ELINA (MT): IMPLICATIONS ON PALEOECOLOGY AND HUMAN/MEGAFAUNA INTERACTION IN BRAZIL

ESTUDO TRACEOLÓGICO DE FÓSSEIS DE PREGUIÇAS TERRÍCOLAS EM SANTA ELINA (MT): IMPLICAÇÕES SOBRE PALEOECOLOGIA E INTERAÇÃO SER HUMANO/MEGAFAUNA NO BRASIL

SÃO CARLOS - SP
2023

THAIS RABITO PANSANI

ESTUDO TRACEOLÓGICO DE FÓSSEIS DE PREGUIÇAS TERRÍCOLAS EM SANTA ELINA (MT): IMPLICAÇÕES SOBRE PALEOECOLOGIA E INTERAÇÃO SER HUMANO/MEGAFAUNA NO BRASIL

Tese apresentada ao Programa de Pós-Graduação em Ecologia e Recursos Naturais, ao Centro de Ciências Biológicas e da Saúde da Universidade Federal de São Carlos, para obtenção do título de Doutora em Ciências, área de concentração em Ecologia e Recursos Naturais.

Orientadora: Dr. Mírian Liza Alves Forancelli Pacheco
Co-orientador: Dr. Mário André Trindade Dantas

São Carlos - SP

2023

UNIVERSIDADE FEDERAL DE SÃO CARLOS

Centro de Ciências Biológicas e da Saúde
Programa de Pós-Graduação em Ecologia e Recursos Naturais

Folha de Aprovação

Defesa de Tese de Doutorado da candidata Thais Rabito Pansani, realizada em 20/03/2023.

Comissão Julgadora:

Profa. Dra. Mírian Liza Alves Forancelli Pacheco (UFSCar)

Prof. Dr. Hermínio Ismael de Araújo Júnior (UERJ)

Profa. Dra. Taissa Rodrigues Marques da Silva (UFES)

Profa. Dra. Briana Pobiner (NMNH)

Profa. Dra. Alison Spence Brooks (GWU)

O Relatório de Defesa assinado pelos membros da Comissão Julgadora encontra-se arquivado junto ao Programa de Pós-Graduação em Ecologia e Recursos Naturais.

In dedication to Águeda Vilhena Vialou,
Mother of Santa Elina

ACKNOWLEDGEMENTS

AGRADECIMENTOS

ABSTRACT

The Santa Elina rock shelter, in Mato Grosso State, Central Brazil, stands out as a pivotal zooarchaeological site in the study of the prehistory of South America, especially on the debate on the peopling of the Americas. Its successive human occupations dating from the late Pleistocene to the early Holocene exhibit lithic industry, rock painting, an exceptional abundance of ground sloth bone remains and cultural ornaments from different periods. Although the material culture of Santa Elina has been extensively explored, its paleontological potential have remained poorly investigated. This thesis aimed to provide an in-depth investigation of several aspects of the giant ground sloth from Santa Elina, including updating its taxonomy, new paleoecological inferences, natural aspects of their dermal bones (osteoderms), and their association with prehistoric human occupation, evidenced by the modification and use of osteoderms as personal ornaments during the Last Glacial Maximum (LMG). For this purpose, several traditional and advanced techniques were applied to study the bones and teeth of the ground sloth from Santa Elina. Diverse techniques (Carbon and oxygen stable isotopes analysis, Radiocarbon dating, Stereomicroscopy, Scanning Electron Microscopy, Energy Dispersive Spectroscopy, Photoluminescence, and synchrotron-based Computerized Microtomography, X-Ray Fluorescence and X-Ray Diffraction) were applied to the study of 22 fossil samples. The first paper resulting from this thesis updates the taxonomic status of the mylodontid from Santa Elina, explores its isotopic paleoecology, and provides new radiocarbon dating from dental fragments from units II2 and III4. This study reveals the generalist diet of *Glossotherium phoenesis* with preference for C4 grasses and reinforces the stratigraphy of unit III4 to the LGM. The second paper explores the human modification of giant sloth bones in Santa Elina during the LGM. This paper provides solid evidence for human manufacturing and use-wear of these artifacts as personal objects during the Ice Age. Finally, the third paper presents preliminary results on paleobiological aspects of natural osteoderms of the mylodontid from Santa Elina. In sum, this thesis contributes to paleoecological and paleobiological aspects of the tropical giant sloth *G. phoenesis*, as well as to the Zooarchaeology and the Pleistocene occupation of the Americas. The core of this thesis reinforces the co-existence and interaction of prehistoric human populations with the Pleistocene megafauna during the LGM in Brazil, feeding the feverous discussion on the early human settlements in South America.

keywords: Xenarthra; Megafauna; South America; Peopling of Americas; Last Glacial Maximum

RESUMO

O abrigo rupestre de Santa Elina, no estado de Mato Grosso, Brasil Central, destaca-se como um sítio zooarqueológico fundamental no estudo da pré-história da América do Sul, especialmente no debate acerca do povoamento das Américas. As suas sucessivas ocupações humanas, datadas desde o Pleistoceno tardio até ao Holoceno inicial, exibem uma rica indústria lítica, pintura rupestre, uma abundância excepcional de restos ósseos de preguiça gigante, e ornamentos culturais de diferentes épocas. Embora a cultura material de Santa Elina tenha sido amplamente explorada, seu potencial fossilífero permaneceu pouco investigado. Esta tese teve como objetivo fornecer uma investigação profunda sobre diversos aspectos da preguiça gigante de Santa Elina, incluindo atualização da sua taxonomia, inferências paleoecológicas inéditas, aspectos naturais dos seus ossos dérmicos (osteodermos), e a sua associação com ocupações humanas pré-históricas, evidenciada pela modificação e utilização de osteodermos como adornos pessoais durante o Último Máximo Glacial (UMG). Para este fim, várias técnicas tradicionais e avançadas foram aplicadas no estudo de ossos e dentes da preguiça de Santa Elina. Diversas técnicas (análises de isótopos estáveis de carbono e oxigênio, datação por radiocarbono, microscopia e Microscopia Eletrônica de Varredura, Espectroscopia Dispersiva de Energia, Fotoluminescência, e Microtomografia Computadorizada, Fluorescência de Raios X, Difração de Raios X sob radiação síncrotron) foram aplicadas no estudo de 22 amostras fósseis. O primeiro artigo resultante desta tese atualiza o status taxonômico do milodontídeo de Santa Elina, explora a sua paleoecologia isotópica e apresenta novas datações por radiocarbono a partir de fragmentos dentários provenientes das unidades II2 e III4. Este estudo revela a dieta generalista de *Glossotherium phoenesis*, com preferência por gramíneas C4, e reforça a estratigrafia da unidade III4 para o UMG. O segundo artigo explora a modificação humana de ossos de preguiça gigante em Santa Elina durante o UMG. Esse artigo apresenta sólidas evidências referentes à produção humana e uso desses artefatos como adornos pessoais durante a "idade do gelo". Finalmente, o terceiro artigo apresenta resultados preliminares sobre a paleobiologia dos osteodermos naturais do milodontídeo de Santa Elina. Esta tese contribui com aspectos paleoecológicos e paleobiológicos da preguiça gigante tropical *G. phoenesis*, assim como com a zooarqueologia e a ocupação humana no Pleistoceno das Américas. O âmago desta tese reforça a coexistência e interação das populações humanas pré-históricas com a megafauna Pleistocênica durante o UMG no Brasil, alimentando a discussão fervorosa sobre os primeiros assentamentos humanos na América do Sul.

palavras-chave: Xenarthra; Megafauna; América do Sul; Povoamento das Américas; Último Máximo Glacial

LIST OF FIGURES

ABBREVIATIONS

BP: Before Present

BSM: Bone Surface Modifications

CNPEM: Centro Nacional de Pesquisa em Energia e Materiais

EDS: Energy Dispersive X-Ray Spectroscopy

ESRF: European Synchrotron Radiation Facility

K-Pg: Cretáceo–Paleógeno

kyr: Thousand years

LGM: Last Glacial Maximum

Ma: Million years

MAE: Museu de Arqueologia e Etnologia

MNHN: Muséum National d'Histoire Naturelle

PL: Photoluminescence

PPSM: Photochimie et Photophysique Supramoléculaires et Macromoléculaires

SEM: Scanning Electron Microscopy

μCT: Computerized Microtomography

USP: Universidade de São Paulo

UFCAT: Universidade Federal de Catalão

UFSCar: Universidade Federal de São Carlos

XRD: X-Ray Diffraction

XRF: X-Ray Fluorescence

SUMMARY

SUMÁRIO

1. CHAPTER 1: INTRODUCTION

1.1. Background: Pleistocene megafauna

The Pleistocene megafauna (large-sized mammals, > 45 kg by the classic definition of Martin, 1967) has experienced and survived climatic and ecological changes since the Pliocene, with oscillations of glacial and interglacial cycles with consequent changes in sea level, and expansion and retreat of savannas and forested landscapes across the globe (Lisiecki et al., 2007; Salzmann et al., 2011; Louys & Roberts, 2020), becoming extinct in the Pleistocene-Holocene transition (Barnosky et al., 2004). Its paleoecological and paleoenvironmental importance, as well as the causes and consequences of its extinction, are still debated (Barnosky et al., 2004). In this context, megafauna fossils are significant proxies for paleoecological and paleoenvironmental studies of the Quaternary. The South American megafauna was highly diverse, including autochthones species from the Notoungulata, Litopterna, Pilosa, Cingulata, and Rodentia orders, as well as allochthonous species from the Perissodactyla, Artiodactyla, Proboscidea, and Carnivora that entered the continent through the dispersal events during the Great American Biotic Interchange – GABI (Marshal, 1998; Pelegrin et al., 2018). South American megafauna dominated the most diverse niches, extending from the open Pampean plain grasslands (e.g., Prado et al., 2015) to the Amazon mosaic landscapes (e.g., Antoine et al., 2017; Asevedo et al., 2021) and intertropical regions (e.g., Dantas et al., 2013; 2017). This great diversity, however, experienced the most severe consequences of the Pleistocene-Holocene extinction, and South America stands out as the continent with the greatest loss of megafauna genera, but without well-established explanations yet (Barnosky et al., 2004).

A particularly important group of South American megamammals with great paleoecological importance are the extinct giant sloths (Xenarthra, Folivora) that emerged in the Oligocene in South America (Pujos et al., 2021), and diversified over thousands of years into several families (Megatheriidae, Megalonychidae, Nothrotheriidae, and Mylodontidae; Cartelle et al., 2009; McDonald et al., 2018; Cartelle et al., 2019), up to North America. Their species encompass great diversity, such as terrestrial representatives with Pan-American distribution (Cartelle & De Iullis, 1995), including aquatic behavior (De Los Arcos et al., 2017), presenting diverse diets and diverse sizes (Tejada, 2021; Dantas, 2022), and configuring as key species of their ecological environment (Dantas et al., 2017). The coexistence and ecological interaction of these animals with prehistoric human populations in the Americas are

still discussed (e.g., Redmond et al., 2012; Fariña et al., 2014; Bustos et al., 2018; Iriarte et al., 2022).

1.2. Background: Peopling of the Americas

Although it is an academic consensus that the Americas was the last continent to be inhabited, questions regarding its antiquity and possible routes remain open (Lesnek et al., 2018; Hoffecker et al., 2019). The most widely known hypothesis concerning the colonization of the Americas suggests that it occurred overland, shortly after the last peak of the Ice Age, through the ice-free corridor bridge that connects Asia (Siberia) and North America (Alaska), known as the Bering Strait (Martin, 1973). This hypothesis is mainly supported by genetic studies that reveal the Asian ancestry of current native Americans (Fagundes et al., 2008; O'Rourke & Raff, 2010). Martin (1973) suggested that the first populations that entered the continent by this route would have been those of the Clovis culture, ~13 kyr BP, associated with the *overkill* culture of the Pleistocene megafauna in the continent. However, the hypothesis of the Clovis culture as the first Americans is no longer valid, as recent discoveries and studies evidence an earlier colonization and possibly by other routes (Dillehay et al., 2008, 2015; Erlandson & Braje, 2011; Potter et al., 2018; Gruhn, 2020; Becerra-Valdivia & Highman, 2020). Hypothesis regarding the routes of this migration have also expanded, such as the model via the Pacific coast shorelines. In this model, the human arrival in the Americas would have happened before the deglaciation of the Laurentide and Cordillera glaciers (Fagundes et al., 2008; Clark et al., 2022).

Evidence for a more ancient settlement than previously accepted in the Americas has grown significantly in recent decades. Recent studies suggesting human presence on the continent around or even before the Last Glacial Maximum (LGM; ~26,000–19,000 kyr BP; Clark et al., 2009) have generated a fervent debate in academia. In this context, the following stand out: the Chiquihuite cave in Mexico, with lithic industry from strata dated to ~30 kyr BP (Ardelean et al., 2020); the White Sands National Park, in the USA, where human footprints in context with megafauna footprints are dated to ~23–21 kyr BP (Bennett et al., 2021); the archaeological site Arroyo del Vizcaíno, in Uruguay, with cut-marked giant sloth bones dated to ~30 kyr PB (Fariña et al., 2014); the archaeological site Vale da Pedra Furada, inserted in the Serra da Capivara complex, in northeast Brazil, with a rich lithic culture contextualized to at least ~24 kyr BP (Boëda et al., 2021); and the Santa Elina rock shelter, in Central

Brazil. Santa Elina displays clear spatial association of fossils of ground sloths with material in two Pleistocene layers, where the older (Unit III4) is dated to ~27–25 kyr BP (Vialou et al., 2005; 2017; 2019).

Rowe et al. (2022) suggest the human presence in North America dated to at least ~38–36 kyr BP, through primitive lithic industry and cut-marked fossils of mammoth found at the "Hartley mammoth" locality in New Mexico, USA. In this context, the authors suggest that the American continent was colonized by genetically diverse human lineages, and while the ancestors of current Native Americans may have introduced the elaborate stone tool technology that is most often found in sites in the American continent (generally ~16 kyr BP), representatives of older lineages (prior to the LGM) could have had simpler and more convenient technology for that time. An even older human occupation in North America is suggested by Holen et al., (2017). The authors argue that *Homo* species were in the continent during the Early Pleistocene (~130 kyr BP), through the investigation of broken bones of a mastodon found in association with artifacts in the Cerutti Mastodon site, in California, USA. This claim is rejected by some critics (e.g., Braje et al., 2017; Ferraro et al., 2018; Ferrell, 2019; Sutton et al., 2019), while also supported by other researches (e.g., Gruhn, 2018; Bordes et al., 2020).

Finally, studies of prehistoric human relationships with megafauna on the American continent, and the possible human role in the population decline and even extinction of these communities, foster a debate of great proportion, in which South America presents a prominent position. North America presents an extensive record of evidence for human exploitation of Pleistocene megamammals (e.g., Fisher, 1984; Shipman et al., 1984; Waters et al., 2011; 2015; Redmond et al., 2012; Bourgeon, 2021; Bourgeon & Burke, 2021; Haynes, 2022) compared to South America. However, this scenario is reshaping as recent studies feed this debate with evidence for the South American continent (e.g., Fariña et al., 2014; Vialou et al., 2017; Politis et al., 2019; Mothé et al., 2020; Domínguez-Rodrigo et al., 2021; Carlini et al., 2022). Meticulous studies about the traces of this interaction in Brazil, as in the case of the modified osteoderms from Santa Elina (Vialou et al, 2017), help elucidate questions within archaeology, paleoecology, and paleobiogeography, such as: 1) when did the first human occupations arrive in South America?; 2) did humans coexist and interact with the Pleistocene megafauna on this continent?; 3) what types of interactions were established (e. g. subsistence, hunting)?; 4) may these interactions have triggered

significant consequences for the megafauna extinction on this continent?; 5) how understanding these dynamics can contribute to current ecological investigations, particularly within "conservation paleobiology"?. Understanding the possible role of prehistoric human populations in the extinction of megafauna is fundamental to understanding recent extinctions and their possible consequences (Galetti et al., 2017), as well as the wide debate on the human role in the increasing defaunation during the Anthropocene (Zalasiewicz et al., 2011; Malhi et al., 2016). In this context, this thesis aimed to explore and complement these questions, synthesized in the study of paleoecological and zooarchaeological relationships of prehistoric humans with the Pleistocene megafauna in Brazil.

1.3. Santa Elina rock shelter

The state of Mato Grosso, located in Central Brazil, is a significant locality for zooarchaeological research in the country and on the continent (Vialou et al., 2017; Vialou et al., 2020), where the archaeological site of Santa Elina, in central South America (Figure 1a), stands out for the record of consecutive prehistoric human occupations since the Last Glacial Maximum (LGM) to the early Holocene. The Santa Elina rock shelter is in the present-day Serra das Araras region (Figure 1b) and is inserted between two dolomitic limestone walls (Figure 1c), one of them decorated with hundreds of paintings. The faunal and anthropomorphized sketches recorded in the rocky limestones of Santa Elina (Figure 1e-f), probably made with natural pigments, highlight the artistic manifestation of its prehistoric occupations. In the open shelter (figure 1d), excavated areas dated from the late Pleistocene to the early Holocene reveal traces of human activity (lithic industry, Figure 2), campfires, personal adornments, and worked vegetables, such as armbands and sandals (Vialou, 2005; Vialou & Vialou, 2019; 2020). The site was excavated and has been studied since the 1980s by Brazilian-French teams. The main contribution to the site has been made by the archaeologists Águeda Vilhena Vialou and Denis Vialou, associated to the MAE/USP in São Paulo and the MNHN in Paris.

The stratigraphy of Santa Elina is well established, with well-defined stratigraphic layers. The excavation area of the rock shelter is characterized by continuous sediments, whose only disturbances refer to localized impact areas due to rockfall in blocks 22-24/Z-B at the height of unit II1 (Vialou et al., 2017). The division of the archaeological layers of Santa Elina is divided into four main units, some with

subdivisions. Unit IV, the oldest, shows no trace of human or megafauna presence, and presents an OSL quartz dating of ~27.8 thousand years ago (Vialou et al., 2017). Unit I, the most recent, has continuous occupations from 1.6 to 6.8 kyr BP, and is predominantly powdery, thin, showing a high amount of worked rock and plant materials, ash, and coal deposits (Vialou, 2003; Vialou et al., 2017). All units show evidence of human occupation. Two units (II and III) show evidence of human activity (through the presence of material culture, i.e., lithic industry) in clear association with Pleistocene megafauna (through bone remains of an extinct giant sloth; Figure 1g). They are only subdivided due to evidence of illuviation process in units III3 and III4 (Vialou et al., 2017). Finally, unit II2 and unit III4 are the ones of interest in this thesis, characterized by their Pleistocene occupation and associated megafaunal remains (Figuti, 2005). Unit II2 is dated to approximately 13–15 thousand years ago; and unit III4 is dated to approximately 25–27 thousand years ago. Unit II is 2 meters deep and is characterized by four sub-layers of homogeneous, sandy sediments. A layer of limestone blocks with no presence of fire, fauna, or lithic material separates unit II from unit III. Unit III is 3 meters deep and is characterized by predominantly sandy sediments, rich in boulders (Vialou et al., 2017).

Santa Elina is one of the most thoroughly dated archaeological sites in the Americas, with approximately 50 published dates (Vialou, 2005; Vialou et al., 2017). Evidence of human presence in units II and III is characterized by the presence of lithic artifacts (e.g., flakes, platelets, cores, pebbles, fragments, and stone tools made from limestone, silex, and sandstone), in addition to the use of hematite pigments in rocks (painted blocks), and allochthonous material, such as quartz crystals (Figure 3). Evidence of Pleistocene megafauna in both units is characterized by bones and dental fragments, including thousands of osteoderms (i.e., dermal ossicles) of a giant sloth identified as *Glossotherium phoenesis* Cartelle, De Iuliis, Boscaini & Pujos, 2019 (Pansani et al., *submitted*). There are bonfire structures in unit II, and three osteoderms were found to be possibly modified into personal ornaments in unit III (Vialou, 2005; Vialou et al., 2017, Vialou & Vialou, 2019; Figure 1h). These ornaments, however, had not been thoroughly analyzed so far, but are key pieces for an understanding of the cultural manifestation of the prehistoric occupations of Santa Elina. Therefore, it was necessary to perform a deep investigation on these objects and search for strong evidence of their possibly anthropic nature, which was the main goal of this thesis.

The excavations carried out in Santa Elina (1984–2004) consisted of a precise archaeological plan where the meters were divided into horizontal/spatial squares: Z, A, B, C, and D (in X), 18–31 (in Y); and vertical: Z (depth), reaching up to nearly 400 cm deep (Figure 1d). The pieces have since been cataloged and deposited in the Santa Elina collection of the MAE/USP. All archaeological and paleontological data from units II and III, available in the Santa Elina inventories (1980–2004 excavations) were accessed and reviewed during the development of this work, along with the analysis and review of all osteoderms present in the collection (n=7,069). Thereby, statistical analyses developed in R Studio software reveal the clear spatial and temporal association of human and megafauna remains in two distinct periods during the late Pleistocene (Figure 3).

This thesis contributes to the zooarchaeological and paleontological aspects of the fossil remains in Santa Elina. Among thousands of osteoderms analyzed at the MAE/USP, it was possible to observe and document their natural morphological and taphonomic aspects, as well as to confirm that the three perforated and polished osteoderms are human-made, rare artifacts. The osteoderms of the giant sloth from Santa Elina were meticulously analyzed for the first time, using traditional and advanced methods such as stereomicroscopes and high-resolution microscopes (Leica, Nikon SMZ-25), Scanning Electron Microscopy (SEM, Zeiss Supra 55VP) Energy Dispersive X-Ray Spectroscopy (EDS), Photoluminescence Spectroscopy (PL), Computed Microtomography (μCT), X-Ray Fluorescence (XRF), and X-Ray Diffraction (XRD).

Additionally, two tooth fragments of *G. phoenesis*, from units II and III, were isotopically analyzed and dated (calibrated radiocarbon). The carbon (δ^{13}C) and oxygen (δ^{18}O) isotopic analyses, as well as the radiocarbon dating, were performed at the Center for Applied Isotope Studies at the University of Georgia, USA, revealing new paleoecological inferences for tropical mylodontids and corroborating the temporal context of the oldest human occupation in Santa Elina around the LGM.
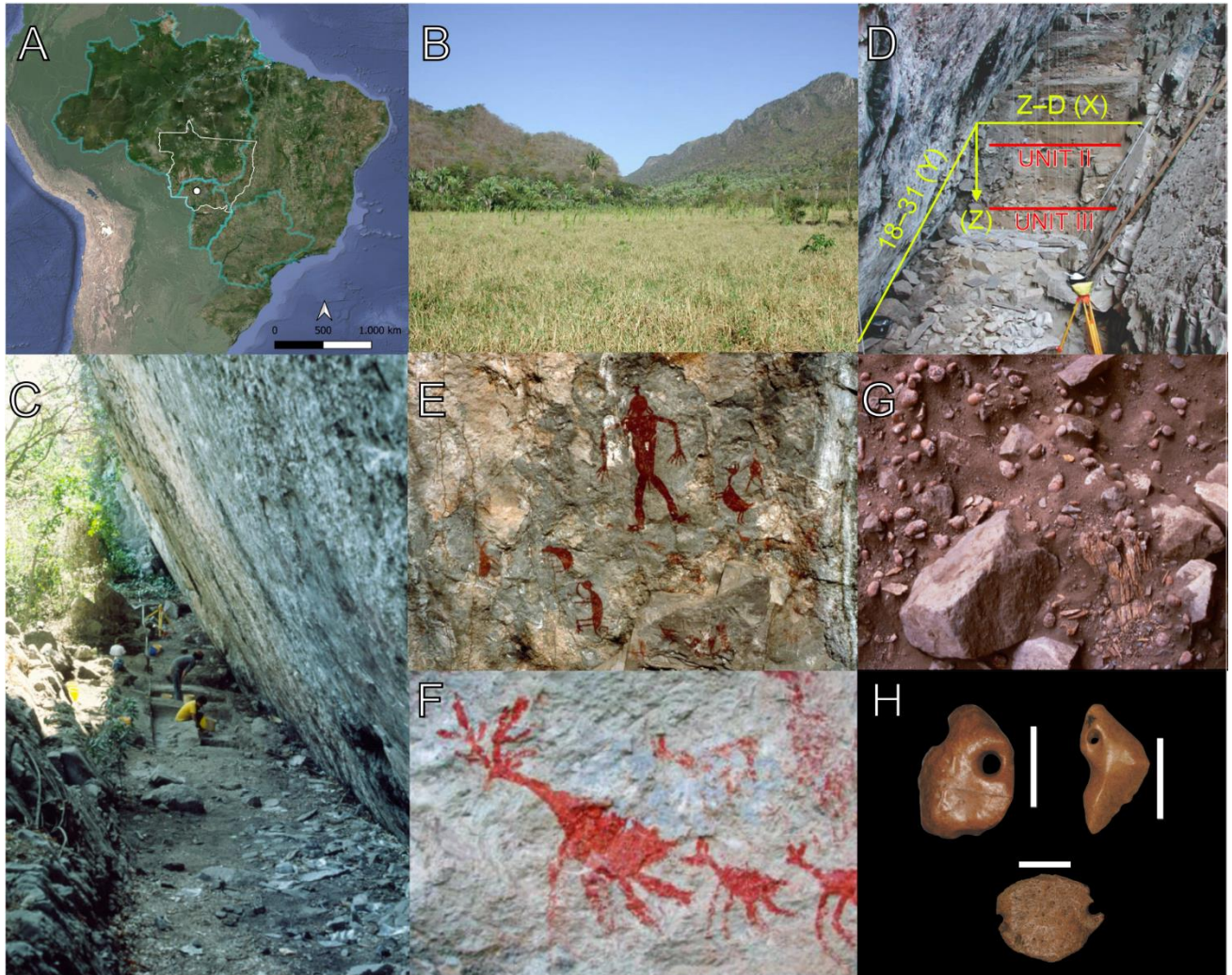
Figure 1. Santa Elina rock shelter. A) South America map, highlighting Brazil. Mato Grosso state, Central Brazil, is delimited in White. The Amazon (above) and Paraná-Paraguay (below) watersheds are delimited in blue. White dot indicate the geographical location of Santa Elina archaeological site, in Jangada municipality. B) Photograph of Serra das Araras region, where the rock shelter is located. C) Rock shelter, inserted between two limestone walls. D) Excavation area. Notice location of units II (II1b+II2) and III (III3+III4) delimited in red, and simplified excavation grid in yellow (X–Y squares and Z depth) in. E-F) Rock paintings on the shelter's walls. G) Ground sloth bone fragments and several osteoderms displayed in unit III4. IPhotos: Águeda V. Vialou. H) three perforated ground sloth osteoderms that suggest anthropic modification. Scale bars: 1 cm.

A

Unit II2	Limestone	Calcite	Hematite	Silex	Sandstone	Quartz
Stone tool*	68			3	1	5
Platelet	8		3	2		
Flake	143	8	1	16	4	8
Small Flake	52	24		2		1
Burnt flake	2					
Blade	1			1		
Block	9			3		
Coloured block	32		1			
Fragment	11	44		5	2	16
Pebble	1					2
Core	2			1	1	
Pigment			85			
Crystal						5
Grain			1			1

B

Unit III4	Limestone	Calcite	Hematite	Silex/Silica	Quartz	Iron?
Stone tool*	129	5	6	1	2	
Platelet	7	1		2	1	
Flake	105	1	1	3	5	
Small flake	21			1	5	
Blade					1	
Block	5					1
Coloured block	1					
Fragment	2		1		6	
Pebble	2					
Core	1					
Pigment			2			
Crystal					7	
Grain					1	

Figure 2. Lithic industry in Santa Elina. A) Unit II2. B) Unit III4. Details are available in the electronic supplementary material of the paper of chapter 3. After a rigorous review of the Santa Elina inventory, it is considered only undisputable data with all the following reliable information: object and raw material identification, and square and depth of origin. Total materials for Unit II2: 575. Total materials for Unit III4: 231. *Stone tool identification considers every retouched material. Notice the predominance of flakes (adding large and small), representing 33,91% for lithics of Unit II2 and 54,55% for lithics of Unit III4.
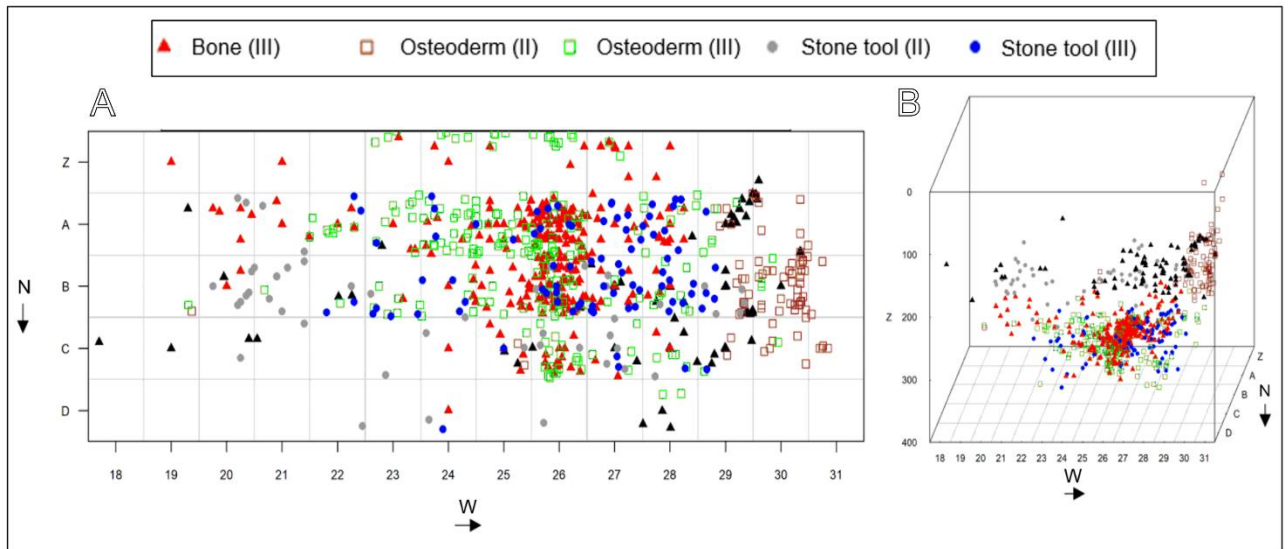
Figure 3. 2D e 3D association maps. Spatial distribution and association between lithic industry (stone tools), giant sloth bones, and osteoderms in Santa Elina. A) Spatial distribution is divided into the *x* and *y* meters, corresponding to archaeological squares. X axis represents North Direction, Y axis represents West Direction. B) Spatial distribution including the Z axis (depth).

1.4. Goals

This thesis aimed to:

      1) Investigate and test the hypothesis that the three perforated osteoderms from Unit III4 of Santa Elina are anthropically modified;

      2) Investigate if these osteoderms were modified in fresh of fossilized bones;

      3) Update the taxonomy of the mylodontid from Santa Elina, and investigate its paleoecological and paleoenvironmental aspects during the late Pleistocene;

1.5. Traceology and Paleometry

In order to achieve the goals described above, this thesis carried out taphonomic, traceological, and paleoecological analyses of bones and teeth of the giant sloth from Santa Elina. Traceology studies the physical and chemical traces in the context of material culture, such as in the investigation of residues or surface alterations of stone tools and ornaments (e.g., manufacturing marks and use-wear traces; Thomas et al., 2011; Marreiros et al., 2015; Stemp et al., 2015). Cultural objects may come from a variety of raw materials, such as animal bones and teeth, shells, minerals, and rocks (Klein, 2000; Gijn, 2006; d'Errico & Backwell, 2009; d'Errico & Stringer, 2011; Cuenca-Solana et al., 2013; Eren et al., 2014).

Traceological analyses can be made on a macro or microscopic scale. Besides anthropic action, other agents can cause marks, polishing, perforations, and breakages in rocks and other raw materials. Some examples commonly found in bone materials are natural erosion and polishing events made by wind and/or water; chemical dissolution by diagenetic processes; roots growing; excavation or laboratory handling; eco-interaction of bacteria, fungi, and insects; interaction of herbivores and carnivores, either by the trampling of large herbivores whose marks might mimic cut marks, bite marks of carnivores that resemble human percussive blows, or digestion of carnivores that might cause rounding and perforations (Behrensmeyer et al. , 1986; Olsen & Shipman, 1988; d'Errico & Villa, 1997; Andrews & Fernández-Jalvo, 2012; Fernández-Jalvo et al., 2014; Fernández-Jalvo & Andrews, 2016). Therefore, caution and rigor are needed during taphonomic and traceological investigartion, in order to avoid misassignments concerning prehistoric human behavior. In this context, there is

a recent demand for additional effective protocols and methods for identifying traces, especially BSMs of anthropogenic origin, beyond microscopy (e.g., Pante et al., 2017). Thus, techniques from paleo-archaeometry stand out as strong alternatives to address these issues.

Paleometry and Archaeometry are interdisciplinary fields that use analytical techniques from other sciences for the investigation of archaeological and paleontological materials (Gomes et al., 2019; Rousaki et al., 2018; Pronti et al., 2020). In Brazil, this field of research has only recently been explored and disseminated within biology, paleontology, geology, and astrobiology (e.g., Delgado et al., 2014; Callefo et al., 2019; Gomes et al., 2019; Prado et al., 2021).

The interdisciplinary field that uses these techniques focused on paleontology is called Paleometry (Gomes et al., 2019). Due to their often non-destructive nature, these techniques possess a high potential for the study of rare and valuable fossils, such as the Santa Elina bone ornaments. Among several rising interdisciplinary methodologies, advanced techniques coming from synchrotron light (radiation) laboratories have been widely used - and enhanced - in recent decades within paleontology and archaeology (Tafforeau et al., 2006; Bergmann et al., 2012; Bertrand et al., 2012; Gueriau et al., 2016; Osés et al., 2016).

Synchrotron light techniques generate high-resolution data due to the high energy and sensitivity of the light used in the laboratory (particles traveling near the speed of light; Gueriau et al., 2016). The contact between light and matter generates signals that are captured by the detectors, generating information about the structure and chemical composition of bio-geological samples (Gueriau et al., 2016; Callefo et al., 2019). The development of this thesis relied on the collaboration with several experts in diverse scientific areas within the natural sciences (e.g., biology, physics, chemistry, paleontology, archaeology), making it possible to investigate the paleontological materials of Santa Elina in an unprecedented way. The osteoderms of *G. phoenesis* from Santa Elina were analyzed under the following techniques and at the following institutions:

- Stereomicroscopes and Scanning Electron Microscope (SEM) (UFSCar, USP, and CNPEM, Brazil, and IPANEMA, France)

Stereomicroscope and scanning electron microscope (SEM) analysis are the most traditional in zooarchaeological studies. The SEM has an exceptional advantage

compared to conventional microscopes due to its property of capturing three-dimensional structures in high resolution and its wide range of depth and magnification of images (Shipman, 1981). Its classical use in the identification of fossil bone modifications stands out (Shipman, 1981; Olsen, 1988; Olsen & Shipman, 1988; Fernández-Jalvo & Monfort, 2008), being possible to distinguish typical marks of anthropic nature or natural processes following established protocols (Domínguez-Rodrigo et al., 2009; Fernández-Jalvo et al., 2014; Fernández-Jalvo & Andrews, 2016). In this context, the modified ornaments from Santa Elina were investigated under various magnifications using binocular microscopes (Leica microscope, Nikon SMZ25 Stereomicroscope with high-resolution zoom; covering scales from ~500 to 100 mm) and SEM (Zeiss and Hitachi TM3000; covering scales from ~200 to 10 μm). The investigation of several marks, under different magnifications, allowed accurate identification of the anthropic traces generated from the impact of lithic tools on the object (modified osteoderms) and their use-wear traces.

- XRF and XRD (PUMA beamline, SOLEIL, France)

The PUMA beamline of the SOLEIL synchrotron is equipped with 2D imaging instruments that provide chemical and structural contrast information regarding elemental and structural characterization of the samples studied (Gianoncelli et al., 2020). XRF spectroscopy analyses generate microscale data and allow the identification of chemical elements as well as the taphonomic history of the bones; while XRD analyses indicate their mineral characterization, diversity, and crystalline organization (Gueriau et al., 2020). Elemental identification is possible through element-specific chemical spectra generated from the emission and detection of specific X-rays (Abdollahi et al., 2020). Mineral identification, in turn, is possible through the identification of the crystalline organization that differentiates the minerals (e.g., apatite, fluorapatite, hydroxyapatite, calcite, etc.; Gueriau et al., 2020). XRF analyses of unmodified osteoderms generated data that allowed histological and diagenetic characterization of these bones in giant sloths. XRF and XRD analyses on the anthropically-modified bones generated data regarding their diagenetic history, crystallography, and new insights into the extremely polished and worn surface of the ornaments.

- μCT (PSICHÉ beamline, SOLEIL, and BM05, ESRF, France)

X-Ray phase-contrast computed microtomography (µCT) is an already popular technique within the natural sciences by enabling the internal investigation and three-dimensional reconstruction of a material in a non-destructive way. The µCT method using X-rays from the synchrotron light source has a higher sensitivity than traditional microtomography. Consequently, it generates data at the highest resolution, enabling fine-scale anatomical and histological investigation and the differentiation of tissues and organs (Tafforeau et al., 2006; Legland et al., 2022). X-Ray µCT uses multiple X-ray measurements at different angles to project images, which generate three-dimensional images of an entire specimen or parts at any desired angles or depths (Legland et al., 2022). The adornments and other fossil osteoderms from Santa Elina were investigated at beamlines in the SOLEIL and ESRF synchrotrons. The data generated enabled histological investigation of the natural osteoderms, in addition to 3D reconstruction in images and videos of the ornaments that enable the observation of the perforation holes and anthropic modifications present on the bone surface at high resolution, at different angles, and are easily accessible by anyone from any location.

- Photoluminescence Spectroscopy (IPANEMA, France)

Photoluminescence (PL) is a phenomenon whose spontaneous emission of luminescence is generated due to the stimulation of a material (electron, atom, crystal) excited by photons (Bertrand et al., 2017). Photoluminescence spectroscopy has been recently applied in the archaeological and artistic context due to its non-destructive characteristic, high sensitivity, and investigative potential regarding the composition of organic and inorganic materials (Thoury et. al., 2011; Gonzales et al., 2017; Hageraats et al., 2019). Recently, fluorescence using ultraviolet (UV) light has been explored to investigate structures not observable to the naked eye, primarily in vertebrates (Kaye et al., 2015). An advanced and innovative technique that has recently been improved is ultraviolet photoluminescence (UV/PL), in which excitation wavelengths from the deep ultraviolet to the visible range are utilized (Bertrand et al., 2017). In addition to enabling mapping large areas at high resolution, this technique promotes the visualization of reflected spectra by excitation and/or emission, which represent the chemical and/or structural contrast of heterogeneous samples (Echard et al., 2015; Bertrand et al., 2017). The histology of the osteoderms was analyzed by UV/PL spectroscopy at the IPANEMA laboratory in France, allowing observation and

differentiation of histological structures. The ornaments analyzed under this technique, as well as experimentally modified fossil bones, enabled an innovative discussion regarding the moment of modification of the ancient ornaments. The homogeneous contrast between bone, marks, and perforation, in comparison with the heterogeneous contrast of these structures in the perforated fossil osteoderms, provides evidence that the ornaments were modified before their fossilization (see discussion in the paper available in chapter 3).

1.6. General remarks

Anthropic marks (e.g., incision marks, scrapes, notches) were identified as resulting from interaction between lithic tools and the osteoderms, in addition to their polished, deformed, and worn characteristics resulting from intensive use and likely interaction of these objects with other materials (e.g., other ornaments, skin contact, string suspension, etc). Comparison with the other thousands of osteoderms from the site confirms that the three perforated osteoderms (SEI6059, SEI6368, and SEI6557) are the result of an anthropic modification. The evidence present in this thesis reinforces that they are rare and unique artifacts from the Last Glacial Maximum.

These main findings demonstrate that this thesis has fulfilled its main objective, which was to search for evidence, nonexistent until then, of the nature of these modified bones, and to investigate whether these modifications would have been made by human populations contemporaneously around the Last Glacial Maximum or by more recent populations in a period after the fossilization of osteoderms. It is expected that this contribution fosters the debate on human-megafauna interaction in South America and intensifies the contentious discussion on the peopling of the Americas.

Additionally, this thesis contributes to paleoecological and paleoenvironmental aspects of Santa Elina. Isotopic analyses of *G. phoenesis* highlight its generalist feeding behavior, corroborating the suggestion of an open environment (savanna with sparsely forested vegetation) for the Santa Elina region during the Pleistocene. Other contributions concern the use of analytical techniques such as synchrotron light sources and UV/PL in histological characterization, taphonomic investigation, and BSMs of prehistoric material. Experimental data regarding the difference between human modifications performed on fossil and fresh bones have also been generated. Scraping, polishing, and perforation of extant osteoderms of a giant armadillo

(*Priodontes maximus*) and fossil osteoderms of a giant sloth (*G. phoenesis* from Santa Elina) were compared (Figure 4). These data are still being processed in an additional manuscript under development.
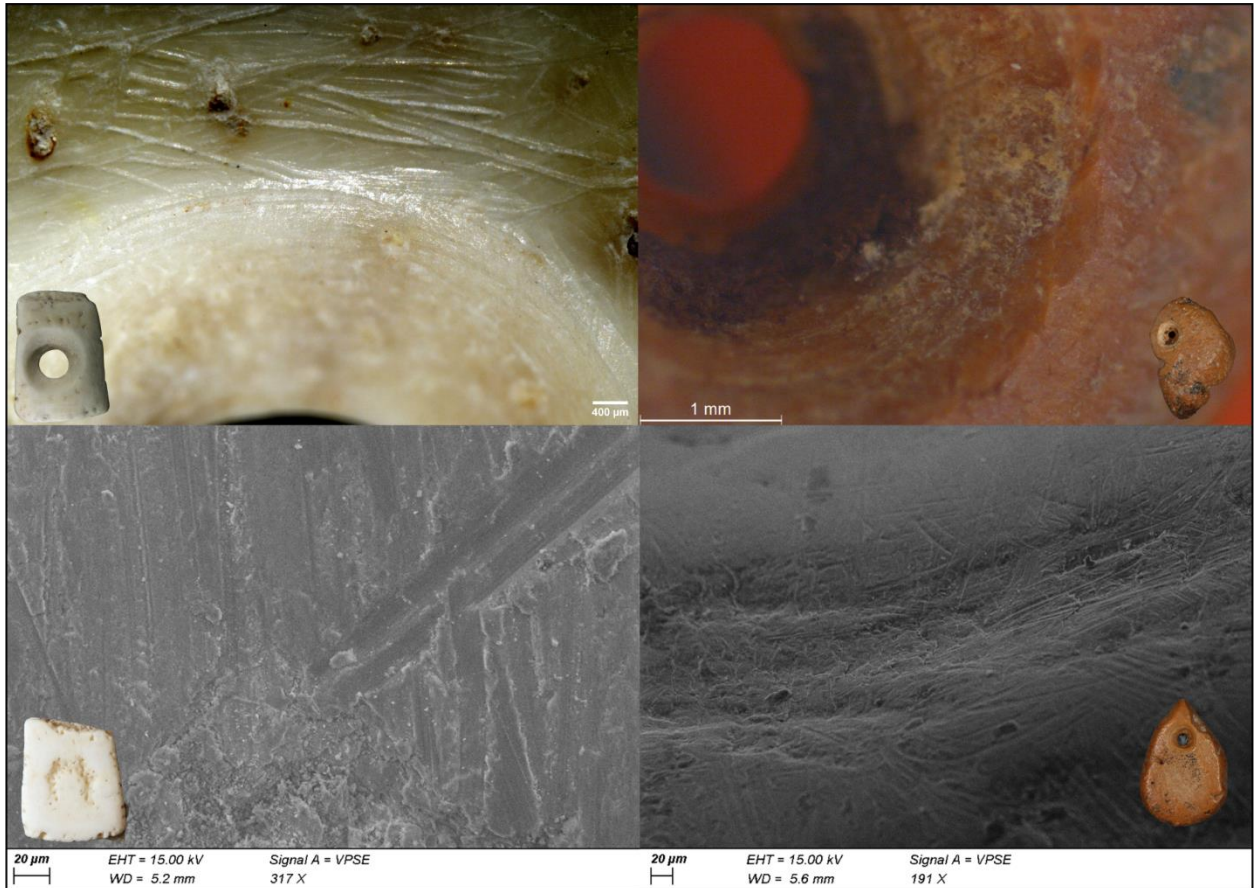
Figure 4. Experimental zooarchaeology. A-B) Perforated and polished osteoderms of extant armadillo (fresh bone). C-D) Perforated and polished osteoderms of giant ground sloth (fossil bone). Preliminary data regarding the investigation of the human-made traces made on fresh and fossil bones. Analyses under stereomicroscopy and SEM.

References

Andrews, P., Fernández-Jalvo, Y., 2012. How to approach perimortem injury and other modifications. Forensic Microscopy for Skeletal Tissues, 191–225.

Antoine, P.O., Salas-Gismondi, R., Pujos, F., Ganerød, M., Marivaux, L., 2017. Western Amazonia as a hotspot of mammalian biodiversity throughout the Cenozoic. Journal of Mammalian Evolution 24(1), 5–17.

Ardelean, C.F. et al., 2020. Evidence of human occupation in Mexico around the Last Glacial Maximum. Nature 584(7819), 87–92.

Asevedo, L., Pansani, T.R., Cordeiro, V.M., Silva-Caminha, S.A.F., Paixão, J.D.S., Cozzuol, M.A., Dantas, M.A.T., 2021. Diversity of Pleistocene megamammals from southern Amazon, Mato Grosso state, Brazil. Journal of South American Earth Sciences 112, 103552.

Barnosky, A.D., Koch, P.L., Feranec, R.S., Wing, S.L., Shabel, A.B., 2004. Assessing the Causes of Late Pleistocene Extinctions on the Continents. Science 306, 70–75.

Becerra-Valdivia, L., Higham, T., 2020. The timing and effect of the earliest human arrivals in North America. Nature 584(7819), 93–97.

Behrensmeyer, A.K., Gordon, K.D., Yanagi, G.T., 1986. Trampling as a cause of bone surface damage and pseudo-cutmarks. Nature 319(6056), 768–771.

Bennett, M.R. et al., 2021. Evidence of humans in North America during the last glacial maximum. Science 373(6562), 1528–1531.

Bergmann, U., Manning, P.L., Wogelius, R.A., 2012. Chemical mapping of paleontological and archeological artifacts with synchrotron X-rays. Annual Review of Analytical Chemistry 5, 361–389.

Bertrand, L., Robinet, L., Thoury, M., Janssens, K., Cohen, S.X., Schöder, S., 2012. Cultural heritage and archaeology materials studied by synchrotron spectroscopy and imaging. Applied Physics A 106(2), 377–396.

Bertrand, L., et al., 2017. Emerging approaches in synchrotron studies of materials from cultural and natural history collections. Analytical Chemistry for Cultural Heritage, 1–39.

Boëda, E. et al., 2021. 24.0 kyr cal BP stone artefact from Vale da Pedra Furada, Piauí, Brazil: Techno-functional analysis. PLoS ONE 16(3), e0247965.

Bordes, L., Hayes, E., Fullagar, R., Deméré, T., 2020. Raman and optical microscopy of bone micro-residues on cobbles from the Cerutti mastodon site. Journal of Archaeological Science: Reports 34, 102656.

Bourgeon, L., 2021. Revisiting the mammoth bone modifications from Bluefish Caves (YT, Canada). Journal of Archaeological Science: Reports 37, 102969.

Bourgeon, L., Burke, A., 2021. Horse exploitation by Beringian hunters during the Last Glacial Maximum. Quaternary Science Reviews 269, 107140.

Braje, T.J. et al., 2017. Were hominins in California~ 130,000 years ago?. PaleoAmerica 3(3), 200–202.

Bustos, D. et al., 2018. Footprints preserve terminal Pleistocene hunt? Human-sloth interactions in North America. Science Advances 4(4), eaar7621.

Callefo, F. et al., 2019. Evaluating biogenicity on the geological record with synchrotron-based techniques. Frontiers in Microbiology 10, 2358.

Carlini, A.A. et al., 2022. Damaged glyptodontid skulls from Late Pleistocene sites of northwestern Venezuela: evidence of hunting by humans?. Swiss Journal of Palaeontology 141, 11.

Cartelle, C., De Iuliis, G., 1995. *Eremotherium laurillardi*: the Panamerican late Pleistocene megatheriid sloth. Journal of Vertebrate Paleontology 15(4), 830–841.

Cartelle, C., 2005. A Preguiça-terrícola de Santa Elina. In: Vialou, A.V. Pré-história do Mato Grosso. EdUSP, São Paulo, 159–162.

Cartelle, C., De Iuliis, G., Ferreira, R.L., 2009. Systematic revision of tropical Brazilian scelidotheriine sloths (Xenarthra, Mylodontoidea). Journal of Vertebrate Paleontology 29(2), 555–566.

Cartelle, C., De Iuliis, G., Boscaini, A., Pujos, F., 2019. Anatomy, possible sexual dimorphism, and phylogenetic affinities of a new mylodontine sloth from the late Pleistocene of intertropical Brazil. Journal of Systematic Palaeontology 17(23), 1957–1988.

Clark, P. U. et al., 2009. The Last Glacial Maximum. Science 325, 710–714.

Clark, J. et al, 2022. The age of the opening of the Ice-Free Corridor and implications for the peopling of the Americas. Proceedings of the National Academy of Sciences 119(14), e2118558119.

Cuenca-Solana, D. et al., 2013. Shell technology, rock art, and the role of marine resources during the Upper Paleolithic. Current Anthropology 54(3), 370–380.

D'Errico, F., Villa, P., 1997. Holes and grooves: the contribution of microscopy and taphonomy to the problem of art origins. Journal of Human Evolution 33(1), 1–31.

D'Errico, F., Backwell, L., 2009. Assessing the function of early hominin bone tools. Journal of Archaeological Science 36(8), 1764–1773.

D'Errico, F., Stringer, C.B., 2011. Evolution, revolution or saltation scenario for the emergence of modern cultures?. Philosophical Transactions of the Royal Society B: Biological Sciences 366(1567), 1060–1069.

Dantas, M.A.T., Dutra, R.P., Cherkinsky, A., Fortier, D.C., Kamino, L.H.Y., Cozzuol, M. A., Ribeiro, A.S. Vieira, F.S., 2013. Paleoecology and radiocarbon dating of the Pleistocene megafauna of the Brazilian Intertropical Region. Quaternary Research 79(1), 61–65.

Dantas, M.A.T., et al., 2017. Isotopic paleoecology of the Pleistocene megamammals from the Brazilian Intertropical Region: Feeding ecology (δ^{13}C), niche breadth and overlap. Quaternary Science Reviews 170, 152–163.

Dantas, M.A.T., 2022. Estimating the body mass of the Late Pleistocene megafauna from the South America Intertropical Region and a new regression to estimate the body mass of extinct xenarthrans. Journal of South American Earth Sciences 119, 103900.

De Los Arcos, S., Partarrieu, D., Carrillo-Briceño, J., Amson, E., 2017. The Southernmost occurrence of the aquatic sloth *Thalassocnus* (Mammalia, Tardigrada) in two new Pliocene localities in Chile. Ameghiniana 54(4), 351–369.

Delgado, A.D.O., Buck, P.V., Osés, G.L., Ghilardi, R.P., Rangel, E.C., Pacheco, M.L.A.F., 2014. Paleometry: a brand new area in Brazilian science. Materials Research 17, 1434–1441.

Dillehay, T.D., Ramírez, C., Pino, M., Collins, M.B., Rossen, J., Pino-Navarro, J.D., 2008. Monte Verde: Seaweed, food, medicine, and the peopling of South America. Science 320, 784–786.

Dillehay, T.D. et al., 2015. New Archaeological Evidence for an Early Human Presence at Monte Verde, Chile. PLoS ONE 10(11), e0141923.

Domínguez-Rodrigo, M., De Juana, S., Galan, A.B., Rodríguez, M., 2009. A new protocol to differentiate trampling marks from butchery cut marks. Journal of Archaeological Science 36(12), 2643–2654.

Domínguez-Rodrigo, M., Baquedano, E., Varela, L., Tambusso, P.S., Melián, M.J., Fariña, R.A., 2021. Deep classification of cut-marks on bones from Arroyo del Vizcaíno (Uruguay). Proceedings of the Royal Society B 288(1954), 20210711.

Echard, J. P. et al., 2015. Synchrotron DUV luminescence micro-imaging to identify and map historical organic coatings on wood. Analyst 140(15), 5344–5353.

Eren, M.I., Roos, C.I., Story, B.A., von Cramon-Taubadel, N., Lycett, S.J., 2014. The role of raw material differences in stone tool shape variation: an experimental assessment. Journal of Archaeological Science, 49, 472–487.

Erlandson, J.M., Braje, T.J., 2011. From Asia to the Americas by boat? Paleogeography, paleoecology, and stemmed points of the northwest Pacific. Quaternary International 239(1-2), 28–37.

Fagundes, N.J. et al., 2008. Mitochondrial population genomics supports a single pre-Clovis origin with a coastal route for the peopling of the Americas. The American Journal of Human Genetics 82(3), 583–592.

Fariña, R.A., Tambusso, P.S., Varela, L., Czerwonogora, A., Di Giacomo, M., Musso, M., Bracco, R., Gascue, A., 2014. Arroyo del Vizcaíno, Uruguay: a fossil-rich 30-ka-old

16

megafaunal locality with cut-marked bones. Proceedings of the Royal Society B 281, 20132211.

Fernández-Jalvo, Y., Monfort, M.D.M., 2008. Experimental taphonomy in museums: Preparation protocols for skeletons and fossil vertebrates under the scanning electron microscopy. Geobios 41(1), 157–181.

Fernández-Jalvo, Y., Andrews, P., Sevilla, P., Requejo, V., 2014. Digestion versus abrasion features in rodent bones. Lethaia 47(3), 323–336.

Fernández-Jalvo, Y., Andrews, P., 2016. Atlas of taphonomic identifications: 1001+ images of fossil and recent mammal bone modification. Vertebrate Paleobiology and Paleoanthropology, Springer Science+Business Media Dordrecht.

Ferraro, J.V., Binetti, K.M., Wiest, L.A., Esker, D., Baker, L.E., Forman, S.L., 2018. Contesting early archaeology in California. Nature 554(7691), E1–E2.

Ferrell, P.M., 2019. The Cerutti Mastodon site reinterpreted with reference to freeway construction plans and methods. PaleoAmerica 5(1), 1–7.

Figuti, L., 2005. Considerações sobre a distribuição da megafauna em Santa Elina. In: Vialou, A.V. Pré-história do Mato Grosso. EdUSP, São Paulo, 163–66.

Fisher, D.C., 1984. Taphonomic analysis of late Pleistocene mastodon occurrences: evidence of butchery by North American Paleo-Indians. Paleobiology 10(3), 338–357.

Galetti, M. et al., 2017. Ecological and evolutionary legacy of megafauna extinctions. Biological Reviews 93, 845–862.

Gianoncelli, A. et al., 2020. Synchrotron μ-XRF imaging and μ-XANES of black-glazed wares at the PUMA beamline: Insights on technological markers for colonial productions. Microchemical Journal 154, 104629.

Gijn, A.L., 2006. Ornaments of jet, amber and bone. In: Louwe, K.L.P. & Jongste, P.F.B. Analecta Praehistorica Leidensia, Leiden: Faculty of Archaeology, Leiden University, 195–205.

Gomes, A.L., et al., 2019. Paleometry as a key tool to deal with paleobiological and astrobiological issues: some contributions and reflections on the Brazilian fossil record. International Journal of Astrobiology 18(6), 575–589.

Gonzalez, V., Gourier, D., Calligaro, T., Toussaint, K., Wallez, G., Menu, M., 2017. Revealing the origin and history of lead-white pigments by their photoluminescence properties. Analytical Chemistry,89(5), 2909–2918.

Gruhn, R., 2018. Observations concerning the Cerutti Mastodon site. PaleoAmerica 4(2), 101–102.

Gruhn, R., 2020. Evidence grows that peopling of the Americas began more than 20,000 years ago. Nature 584, 47–48.

Gueriau, P., Bernard, S., Bertrand, L., 2016. Advanced synchrotron characterization of paleontological specimens. Elements 12(1), 45–50.

Gueriau, P. et al., 2020. Visualizing mineralization processes and fossil anatomy using synchronous synchrotron X-ray fluorescence and X-ray diffraction mapping. Journal of the Royal Society Interface 17(169), 20200216.

Hageraats, S., Keune, K., Réfrégiers, M., van Loon, A., Berrie, B., Thoury, M., 2019. Synchrotron deep-UV photoluminescence imaging for the submicrometer analysis of chemically altered zinc white oil paints. Analytical Chemistry 91(23), 14887–14895.

Haynes, G., 2022. Sites in the Americas with Possible or Probable Evidence for the Butchering of Proboscideans. PaleoAmerica 8(3), 1–28.

Hoffecker, J.F. et al., 2019. Native American origins: An interdisciplinary critique of current models, in American Journal of Physical Anthropology 168, 105–105.

Holen, S.R. et al., 2017. A 130,000-year-old archaeological site in southern California, USA. Nature 544(7651), 479–483.

Kaye, T.G. et al., 2015. Laser-stimulated fluorescence in paleontology. PloS One 10(5), e0125923.

Klein, R.G., 2000. Archeology and the evolution of human behavior. Evolutionary Anthropology: Issues, News, and Reviews 9(1), 17–36.

Legland, D. et al., 2022. Synchrotron Based X-ray Microtomography Reveals Cellular Morphological Features of Developing Wheat Grain. Applied Sciences 12(7), 3454.

Lesnek, A.J., Briner, J.P., Lindqvist, C., Baichtal, J.F., Heaton, T.H., 2018. Deglaciation of the Pacific coastal corridor directly preceded the human colonization of the Americas. Science Advances 4(5), eaar5040.

Lisiecki, L.E., Raymo, M.E., 2007. Plio–Pleistocene climate evolution: trends and transitions in glacial cycle dynamics. Quaternary Science Reviews 26(1-2), 56–69.

Louys, J., Roberts, P., 2020. Environmental drivers of megafauna and hominin extinction in Southeast Asia. Nature 586(7829), 402–406.

Malhi, Y., Doughty, C.E., Galetti, M., Smith, F.A., Svenning, J., Terborgh, J.W., 2016. Megafauna and ecosystem function from the Pleistocene to the Anthropocene. Proceedings of the National Academy of Sciences 113(4), 838–846.

Marreiros, J., Mazzucco, N., Gibaja, J.F., Bicho, N., 2015. Macro and micro evidences from the past: the state of the art of archeological use-wear studies. Use-wear and Residue Analysis in Archaeology, 5–26.

Marshall, L.G., 1988. Land mammals and the great American interchange. American Scientist 76(4), 380–388.

Martin, P.S., 1967. Prehistoric overkill. In: Martin & Wright. Pleistocene extinctions: the search for a cause. New Haven, CT: Yale University Press, 75–120.

Martin, P.S., 1973. The discovery of America. Science 179, 969–974.

McDonald, H.G., 2018. An overview of the presence of osteoderms in sloths: implications for osteoderms as a plesiomorphic character of the Xenarthra. Journal of Mammalian Evolution 25(4), 485–493.

Mothé, D., Avilla, L.S., Araújo-Júnior, H.I., Rotti, A., Prous, A., Azevedo, S.A.K., 2020. An artifact embedded in an extinct proboscidean sheds new light on human-megafaunal interactions in the Quaternary of South America. Quaternary Science Reviews 229, 106125.

O'Rourke, D.H., Raff, J.A., 2010. The human genetic history of the Americas: the final frontier. Current Biology 20(4), R202–R207.

Olsen, S.L., 1988. The identification of stone and metal tool marks on bone artefacts. In: Oslen, S.L., Scanning electron microscopy in archaeology. British Archaeological Reports, International Series 452, BAR, Oxford, 337–360.

Olsen, S.L., Shipman, P., 1988. Surface modification on bone: trampling versus butchery. Journal of Archaeological Science 15(5), 535–553.

Osés, G.L. et al., 2016. Deciphering the preservation of fossil insects: a case study from the Crato Member, Early Cretaceous of Brazil. PeerJ 4, e2756.

Pante, M.C., Muttart, M.V., Keevil, T.L., Blumenschine, R.J., Njau, J.K., Merritt, S.R., 2017. A new high-resolution 3-D quantitative method for identifying bone surface modifications with implications for the Early Stone Age archaeological record. Journal of Human Evolution 102, 1–11.

Pelegrin, J.S., Gamboa, S., Menéndez, I., Fernández, M.H., 2018. El gran intercambio biótico Americano: una revisión paleoambiental de evidencias aportadas por mamíferos y aves neotropicales. Ecosistemas 27(1), 5–17.

Politis, G.G., Messineo, P.G., Stafford Jr, T.W., Lindsey, E.L., 2019. Campo Laborde: a Late Pleistocene giant ground sloth kill and butchering site in the Pampas. Science Advances 5(3), eaau4546.

Potter, B.A. et al., 2018. Current evidence allows multiple models for the peopling of the Americas. Science Advances 4(8), eaat5473.

Prado, G. et al., 2021. Synchrotron radiation in palaeontological investigations: Examples from Brazilian fossils and its potential to South American palaeontology. Journal of South American Earth Sciences 108, 102973.

Prado, J.L., Martinez-Maza, C., Alberdi, M.T., 2015. Megafauna extinction in South America: A new chronology for the Argentine Pampas. Palaeogeography, Palaeoclimatology, Palaeoecology 425, 41–49.

Prevosti, F.J., Vizcaíno, S.F., 2006. Paleoecology of the large carnivore guild from the late Pleistocene of Argentina. Acta Palaeontologica Polonica 51 (3), 407–422.

Pronti, L., Romani, M., Viviani, G., Stani, C., Gioia, P., Cestelli-Guidi, M., 2020 Advanced methods for the analysis of Roman wall paintings: Elemental and molecular detection by means of synchrotron FT-IR and SEM micro-imaging spectroscopy. Rendiconti Lincei. Scienze Fisiche e Naturali 31(2), 485–493.

Pujos, F. et al., 2021. The late Oligocene xenarthran fauna of Quebrada Fiera (Mendoza, Argentina) and its implications for sloth origins and the diversity of Palaeogene cingulates. Papers in Palaeontology 7(3), 1613–1656.

Redmond, B.G., McDonald, H.G., Greenfield, H.J., Burr, M.L., 2012. New evidence for Late Pleistocene human exploitation of Jefferson's Ground Sloth (*Megalonyx jeffersonii*) from northern Ohio, USA. World Archaeology 44(1), 75–101.

Rousaki, A., Moens, L., Vandenabeele, P., 2018. Archaeological investigations (archaeometry). Physical Sciences Reviews 3(9), 20170048.

Rowe, T.B. et al., 2022. Human Occupation of the North American Colorado Plateau~ 37,000 Years Ago. Frontiers in Ecology and Evolution, 534.

Salzmann, U. et al. 2011. Climate and environment of a Pliocene warm world. Palaeogeography, Palaeoclimatology, Palaeoecology 309(1-2), 1–8.

Shipman, P., 1981. Applications of scanning electron microscopy to taphonomic problems. Annals of the New York Academy of Sciences 376(1), 357–385.

Shipman, P., Fisher, D.C., Rose, J.J., 1984. Mastodon butchery: microscopic evidence of carcass processing and bone tool use. Paleobiology 10(3), 358–365.

Stemp, W.J., Watson, A.S., Evans, A.A., 2015. Surface analysis of stone and bone tools. Surface Topography: Metrology and Properties 4(1), 013001.

Sutton, M.Q., Parkinson, J., Rosen, M.D., 2019. Observations Regarding the Cerutti Mastodon. PaleoAmerica 5(1), 8–15.

Tafforeau, P., et al., 2006. Applications of X-ray synchrotron microtomography for non-destructive 3D studies of paleontological specimens. Applied Physics A 83(2), 195–202.

Tejada, J.V. et al., 2021. Isotope data from amino acids indicate Darwin's ground sloth was not an herbivore. Scientific Reports, 11:18944.

Thomas, T.R., Rosén, B.G., Zahouani, H., Blunt, L., El Mansori, M., 2011. Traceology, quantifying finishing machining and function: A tool and wear mark characterisation study. Wear 271(3-4), 553–558.

Thoury, M., Delaney, J.K., de la Rie, E.R., Palmer, M., Morales, K., Krueger, J., 2011. Near-infrared luminescence of cadmium pigments: in situ identification and mapping in paintings. Applied Spectroscopy 65(8),939–51.

Vialou, A.V., 2003. Santa Elina rockshelter, Brazil: evidence of the coexistence of man and *Glossotherium*. In: L. Miotti, M. Salemme, N. Flegenheimer (Ed.) Where the south winds blow: ancient evidence of Paleo South Americans: 21–28. College Station: Center for the Study of the First Americans, Texas A&M University.

Vialou, A.V., 2005. Pré-história do Mato Grosso. Vol. 1, Santa Elina. São Paulo: Editora da Universidade de São Paulo. 256 p. ISBN: 85-314-0861-x.

Vialou, D., Benabdelhadi, M., Feathers, J., Fontugne, M., Vialou, A.V., 2017. Peopling South America's centre: the late Pleistocene site of Santa Elina. Antiquity 91(358), 865–884.

Vialou, A.V., Vialou, D., 2019. Manifestações simbólicas em Santa Elina, Mato Grosso, Brasil: representações rupestres, objetos e adornos desde o Pleistoceno ao Holoceno recente. Boletim do Museu Paraense Emílio Goeldi. Ciências Humanas, Belém 14(2), 343–365.

Vialou, A.V., Vialou, D., dos Santos, M.V., 2020. Arqueologia: do passado ao presente, das paisagens ao território: Archaeology: from the past to the present, from landscape to territories. Revista Nordestina de História do Brasil 2(4), 143–174.

Waters, M.R. et al., 2011. The buttermilk creek complex and the origins of Clovis at the DebraL. Friedkin site, Texas. Science 331, 1599–1603.

Waters, M.R. et al., 2015. Late Pleistocene horse and camel hunting at the southern margin of the ice-free corridor: Reassessing the age of Wally's Beach, Canada. Proceedings of the National Academy of Sciences 112(14), 4263–4267.

Zalasiewicz, J., Williams, M., Haywood, A., Ellis, M., 2011. The Anthropocene: a new epoch of geological time?. Philosophical Transactions of the Royal Society A: Mathematical, Physical and Engineering Sciences 369(1938), 835-841.

2. CHAPTER 2: PAPER 1- PALEOECOLOGY
Manuscript submitted to *Journal of Quaternary Sciences*.

Radiocarbon dating and isotopic paleoecology of *Glossotherium phoenesis* from the Late Pleistocene of the Santa Elina rock shelter, Central Brazil

Thais Rabito Pansani[1,2,*], Mário André Trindade Dantas[3], Lidiane Asevedo[3,4], Alexander Cherkinsky[5], Denis Vialou[6], Águeda Vilhena Vialou[6,7], Mírian Liza Alves Forancelli Pacheco[1, 2]

Mylodontids from Santa Elina, Brazil

[1]*Programa de Pós-Graduação em Ecologia e Recursos Naturais, Universidade Federal de São Carlos, São Carlos, SP, 13565-905, Brazil*

[2]*Laboratório de Paleobiologia e Astrobiologia, Universidade Federal de São Carlos, Sorocaba, SP, 18052-780, Brazil*

[3]*Laboratório de Ecologia e Geociências, Instituto Multidisciplinar em Saúde, Universidade Federal da Bahia campus Anísio Teixeira, Vitória da Conquista, BA, 45029-094, Brazil*

[4]*Programa de Pós-Graduação em Ecologia e Conservação, Universidade Federal de Sergipe, São Cristóvão, SE, 49100-000, Brazil*

[5]*Center for Applied Isotope Studies, University of Georgia, Athens, GA, 30602, USA*

[6]*Muséum National d'Histoire Naturelle, Paris, 75005, France*

[7]*Universidade de São Paulo, São Paulo, SP, 05508-900, Brazil*

*Corresponding author: thais-pansani@hotmail.com, +5519982397758

Abstract: The Santa Elina rock shelter, in Central Brazil, stands out with human occupation layers, two in association with ground sloth fossil remains from the Late Pleistocene. Here, we explore the paleontological aspect of this site. We update the taxonomic assignment of the ground sloth found in the shelter to *Glossotherium phoenesis.* Radiocarbon dating performed on bioapatite ($^{14}C_{bioapatite}$) of two tooth specimens reveal ages of 12,690±40 cal a BP (unit II2) and 18,580±40 cal a BP (unit III4), which were converted to collagen using a novel approach and presented calibrated ages of 17,450–17,906 cal a BP ($^{14}C_{collagen}$ = 14,547±40) and 25,994–26,396 cal a BP ($^{14}C_{collagen}$ = 22,042±40). We reinforce the chronology of the oldest unit of Santa Elina with material culture in association with megafauna bones to around the Last Glacial Maximum (LGM). Carbon isotopic signatures suggest a mixed feeding diet for both specimens. The most recent ground sloth presents a higher isotopic value ($\delta^{13}C$ = –1.8 ‰) and narrower niche breadth (B_A = 0.50) than the oldest one ($\delta^{13}C$ = –3.3 ‰; B_A = 0.74). We interpret that *G. phoenesis* lived in an arboreal savanna habitat during the phases studied. Slightly different oxygen isotopic values ($\delta^{18}O$ = 26.2 ‰ and 27.9 ‰) might suggest a decrease in humidity over time. Our results provide insights into the paleoecology of the tropical Pleistocene *G. phoenesis* and to the paleoenvironmental setting of Santa Elina when occupied by early humans and megafauna during the Late Pleistocene.

keywords: Quaternary, South America, Stable Isotopes Analysis, Last Glacial Maximum

1. Introduction

Megamammal fossils are significant proxies for paleoecological and paleoenvironmental studies of Quaternary communities worldwide (*e.g.,* Kuitems et al., 2015; Tomassini et al., 2020; Ma et al., 2021; Dantas et al., 2022). Among them, the extinct ground sloths (Xenarthra, Folivora) stand out due to their abundant fossil record and significant paleoecological importance (McDonald & De Iuliis, 2008).

Giant ground sloths were a diverse group that emerged in the Late Oligocene-Early Miocene in South America (Boscaini et al., 2019; Pujos et al., 2021), reaching Central and North America during the Great American Biotic Interchange (i.e., GABI) intensified after the total establishment of the Isthmus of Panama in the Late Pliocene (Webb, 1976; Marshall, 1998; Woodburne, 2010; O'Dea et al., 2016). The group diversified over thousands of years into four families: Megatheriidae, Megalonychidae, Nothrotheriidae, and Mylodontidae (Cartelle et al. 2009; McDonald et al, 2018; Cartelle et al., 2019).

The ground sloths were adapted to different biomes over the Quaternary, with geographic distribution from tropical and subtropical forests to temperate and arid environments throughout the American continent (Ribeiro et al., 2012; McDonald, 2021). Their representatives include species with Pan-American distribution (Cartelle & De Iuliis, 1995), a wide range of body sizes (from tens of kg to almost two tons), and a variety of dietary and locomotory habits and social behaviors (Bargo et al., 2006; Bargo & Vizcaíno, 2008; McDonald & De Iuliis, 2008; Vízcaíno et al., 2008; Pujos et al., 2007, 2012; Amson et al., 2015; De Los Arcos et al., 2017; Tomassini et al., 2020).

The paleoecology of the South American ground sloths has been studied mainly through stable isotopes (MacFadden et al., 1994; Bocherens et al., 2017; Dantas et al., 2017; Oliveira et al., 2020; Asevedo et al., 2021), dental microwear (Oliveira et al., 2020), and ecomorphology analyses (Fariña & Vizcaíno, 2001; Bargo et al., 2006; Figueirido & Soibelzon, 2010; Prevosti & Martin, 2013; Dantas & Santos, 2022).

Giant ground sloths are generally described as herbivore animals (McDonald, 2005; Bocherens et al., 2017), although Fariña & Blanco (1996) challenged this view when proposed that *Megatherium* could have omnivorous habits. A recent study by Tejada et al. (2021) suggested an opportunistic omnivore behavior for the mylodontid *Mylodon darwinii* Owen, 1840 based on nitrogen isotopic analyses (δ^{15}N) from amino acids. However, high concentrations of δ^{15}N in tropical primates in Africa, for example, have been attributed to highly enriched-δ^{15}N plants they ate, being plant food their main protein source (e.g., Oezle et

al., 2011). The $\delta^{15}N$ levels in leaves from the upper crown are predicted to be higher than the lower crown (canopy stratification), as well as leaf age (Blumenthal et al., 2016). Thus, the consumption of distinct leaves might reflect distinct isotopic nitrogen values in herbivores' diets.

The Mylodontidae family was abundant and widely diverse in South America since the Late Oligocene (Shockey & Anaya, 2011), and the Pleistocene ground sloths have been considered a key species of Brazilian communities (Dantas et al., 2017). During the Late Pleistocene, the Mylodontinae subfamily was represented in South America by the species *M. darwinii*, *Glossotherium robustum* Owen 1842, and *Lestodon armatus* Gervais 1855 in temperate regions of Argentina, Uruguay, Bolivia, and southern Brazil (Bargo et al., 2006; Varela et al., 2021; Vargas-Peixoto et al., 2021), and *Glossotherium tropicorum* Hoffstetter 1952, *Glossotherium phoenesis* Cartelle, De Iuliis, Boscaini & Pujos 2019, *Glossotherium wegneri* Spillmann 1931, *Mylodonopsis ibseni* Cartelle 1991, and *Ocnotherium giganteum* Lund 1839 in tropical regions of Ecuador, Peru, and Brazil (De Iuliis et al., 2017; Barbosa et al., 2019; Cartelle et al., 2019, De Iuliis et al., 2020).

The genus *Glossotherium* is present in South America (Pampean region of Argentina) since the Pliocene, with irradiation of the species during the Pleistocene (Boscaini et al., 2022). The species assigned to *Glossotherium tarijensis* Ameghino 1902, from Bolivia, is under review and their validity has not been well-established yet (Boscaini et al., 2018; Cartelle et al., 2019).

Although the anatomy and systematics of South American Mylodontinae taxa have been widely explored (*e.g.,* Czerwonogora & Fariña, 2012; Haro et al., 2016; De Iuliis et al., 2017; Cartelle et al., 2019) there is little information concerning their paleoecological aspects. Regarding the paleoecology of *Glossotherium* species, a higher consumption of C_3 plants with digger behavior is suggested for *G. robustum* (Bargo et al., 2000; Czerwonogora & Fariña, 2012). The only available isotopic data for *Glossotherium* in South America until now is for an individual in Argentina (Czerwonogora et al., 2011; Bocherens et al., 2017).

The human exploitation of ground sloths in the Americas, especially in the Southern continent, is still an open and intriguing discussion (*e.g.,* Vialou et al., 2003; Redmond et al., 2012; Fariña et al., 2014; Bustos et al., 2018; Politis et al., 2019; Iriarte et al., 2022). The Santa Elina rock shelter, in Brazil, stands out in this debate due to their Pleistocene layers containing clear association of giant sloth bones with elements of material culture, including anthropogenic perforated osteoderms (Vialou et al., 2017), which suggests human-megafauna co-habitation and interaction there.

Whereas the archaeological context of Santa Elina has been well explored, the paleontological aspects of their ground sloth fossils remain poorly explored. Therefore, here we aim to provide new information concerning the taxonomic assignment, and chronological and paleoecological aspects of the mylodontid from the tropical region of Santa Elina, Central Brazil.

1.2. Geological setting

Santa Elina (Mato Grosso, Brazil; Figure 1) is an open rock shelter that documents evidence of successive human occupations from the Late Pleistocene (~27,000 years ago) to the Early Holocene (Vialou et al., 2017). The prehistoric settlements (3–4 m wide, 20 m long) are located at the base of a cliff between two dolomitic limestone walls, covered by ~1,000 paintings (Vialou, 2005; Vialou et al., 2017). Among more than 25,000 elements of material culture, the archaeofauna (including sub-recent species from Central Brazil and megafauna fossils) attests to one of the most complete (zoo)archaeological sequences of Brazilian prehistory (Figuti, 2005a; Pacheco, 2009). It highlights important aspects of the interaction between fauna and humans (*e.g.,* hunting, massive gathering, feeding patterns and stylistic uses of animal remains) over the past 25,000 years (Pacheco, 2009; Vialou & Vialou, 2019).

The 20-year period of excavations at Santa Elina (1984–2004) followed meticulous archaeological methods for the study of its stratigraphy and its archaeological and paleontological material (Vialou & Vialou, 1994; Vialou et al., 2017). The stratigraphy of Santa Elina is clearly layered and is divided into four main units (I–IV), which are categorized due to the nature of sediments (e.g., color, texture) and their archaeological and paleontological material (Benabdelhadi, 2005; Vialou et al., 2017). The most recent unit (I, superior), of Holocene age and composed of fine and powdery sediments, presents abundant organic material and high anthropic nature with unique remains in excellent preservation, such as stakes, charcoal, personal adornments, hematite and colorant fragments with abrasion facets, remains of fruits, hearth structures, and worked plants (*e.g.,* sandals, strings, braided fibers, body ornaments) (d'Errico & Dubreuil, 2005; D'Errico & Vialou, 2007; Vialou & Vialou, 2019). Unit IV, dated by OSL to ~27.8–2.7 ka, does not present paleontological remains or evidence of material culture (Vialou et al., 2017). More detailed information on the stratigraphy of the site can be found in previous works (*e.g.,* Vialou, 2003; Benabdelhadi, 2005; Vialou et al., 2017).

Two layers present evidence of material culture (lithic assemblage) and ground sloth fossils in spatial association (unit II1b–2 and unit III3–4), which are interesting to this study (Figure 2). One layer consisting of limestone blocks without fire structures, fauna, or lithic material separates units II (intermediate) and III (inferior). Material culture in both units is displayed by lithic assemblage, including stone tools (*e.g.,* retouched limestone flakes, siliceous microblade cores), painted blocks, pigments (*e.g.,* hematite), and exogenous minerals (*e.g.,* quartz crystals) (Vialou et al., 2017). In unit II (2 m deep), composed of sandy sedimentological layers (Benabdelhadi, 2005), there is evidence of hearth structures (Vialou et al., 2017). In unit III (3 m deep), composed of coarser sands and rubble, with a high frequency of blocks (Benabdelhadi, 2005), highlights three anthropically perforated giant sloth osteoderms likely used as personal ornaments (Vialou et al., 1995; Vialou et al., 2017).

The only megamammal fossil present in Santa Elina is the extinct ground sloth. Thousands of osteoderms (~7,000 pieces) were found on the site along with post-cranial bones and tooth fragments (Cartelle, 2005; Figuti, 2005b). Information on the recognition of one individual in two distinct layers, and the spatial distribution of their bones is available in book chapters (Cartelle, 2005; Figuti, 2005b). The identification of one individual in each of the two archaeological layers relies on analyses of the skeletal materials (Figuti, 2005b), the ontogenetic identification of a young and an older individual, and dating of the bones (Vialou et al., 2017). There is no detailed taphonomic study on the giant sloth bones of Santa Elina to date. Although the ground sloth bones present a poor state of preservation, a detailed investigation of their weathering stages is needed.

Previous identification of the mylodontid from Santa Elina assigned it to *Glossotherium* aff. *G. lettsomi* (Vialou et al., 1995; Cartelle, 2005). However, a recent study concerning the phylogenetic affinities of Pleistocene mylodontids of Brazil suggested a review of this assignment (Cartelle et al., 2019). This is reexamined in this study.

1.3. Isotopic Paleoecology ($\delta^{13}C$, $\delta^{18}O$)

Isotopic paleoecology is successfully applied to investigate the dietary behavior and ecological preferences (*e.g.,* habitat preferences, trophic level) of extinct Pleistocene megamammals and to reconstruct their past landscape and environmental conditions worldwide (Domingo et al., 2012a; Bocherens, 2015; Mendoza et al., 2018; Dantas et al., 2020; Pushkina et al., 2020). The use of stable isotopes in paleoecological analyses consists of measuring the isotopic composition (*e.g.,* carbon, oxygen, nitrogen, among others) present in

animal tissues extracted from collagen or hydroxyapatite of fossil teeth and bones (Ben-David & Flaherty 2012; Bocherens & Drucken, 2013). In this context, studies on tooth samples stand out as a more reliable paleodietary and paleoclimatic proxy due to their good preservation in the fossil record and lower diagenetic alteration than bone tissues (Koch, 2007; Clementz, 2012).

Stable isotopes of carbon (δ^{13}C) and oxygen (δ^{18}O) are commonly used for reconstructing megamammal paleoecology. Carbon isotopic data are related to the different photosynthetic cycles of plants (C$_3$/Calvin–Benson, C$_4$/Hatch–Slack, and CAM pathways). Each distinct pathway fractionates carbon differently, allowing the discrimination of the plant resources consumed by herbivores. C$_3$ plants, such as trees, shrubs, and closed canopy vegetation, present lower values (average of -27 ± 3 ‰) than C$_4$ plants (average of -13 ± 2 ‰), such as grasslands of more arid and warmer growing seasons (Koch et al., 1998; Collatz et al., 1998). CAM plants present intermediate values between C$_3$ and C$_4$ plants (MacFadden, 2005). This approach helps us infer the dietary behavior and food preferences of past herbivores, discerning browser (*i.e.,* woody plant consumers), grazer (*i.e.,* C$_4$ grass consumers), and mixed feeders (Cerling & Harris, 1999; Clementz, 2012; Bocherens & Drucker, 2013). Consequently, uncovering the resources available for consumption also allows paleoenvironmental inferences related to phytophysiognomies.

In turn, oxygen isotopic data reflect body water values, which are related to oxygen uptake during an organism's lifetime (Kohn, 1996; Sponheimer & Lee-Thorp, 1999). The δ^{18}O content is related to bioclimatic sources (*e.g.,* atmospheric O$_2$, amount of precipitation), ecological behavior (*e.g.,* obligate drinker or water uptake from leaf-feeding), physiological conditions (*e.g.,* inspiration, expiration), and biogeographical variables (*e.g.,* latitude, altitude, and distance from the coast) (Bryant & Froelich, 1995; Kohn et al., 1996; Sponheimer & Lee-Thorp, 1999; Domingo et al., 2012b; Bocherens & Drucken, 2013).

Stable oxygen isotope analysis can constitute alternative data to the palynology, phytoliths, speleothems, and other sources, and support paleoclimate investigation mainly through the reconstruction of the temperature and humidity of past environments (Luz & Kolodny, 1989; Bryant & Froelich, 1995). The isotopic approach can provide paleoecological reconstructions in a study area (e.g., DeSantis et al., 2019; Dantas et al., 2022) or a refined reconstitution when studying a larger dataset of samples in a broader geographical range (*e.g.,* Sánz-Pérez et al., 2022; Szabó et al., 2022).

2. Material and methods

2.2. Taxonomic identification

Because giant sloth bones are poorly preserved, the only reliable structure that we could (re)analyze was the partial right maxilla (stratigraphic location: unit III4, 25C, 307 cm), which is the same material analyzed by Vialou et al. (1995). The partial right maxilla was compared with the specialized literature (Cartelle, 1991; 1992; Pitana et al., 2013; De Iuliis et al., 2017; Cartelle et al., 2019; De Iuliis et al., 2020), and, therefore, we were able to update the species identification.

2.3. Isotopic paleoecology ($\delta^{13}C$, $\delta^{18}O$)

For isotopic paleoecology interpretation and radiocarbon dating, we selected two tooth fragments from stratigraphic unit II (square 25C, z = 200 cm) and stratigraphic unit III (square 27B, z = 327) of Santa Elina, Mato Grosso state, Brazil. The samples came from the Santa Elina collection stored at the Museu de Arqueologia e Etnologia of the Universidade de São Paulo (MAE/USP). Analyses on the dentine tissues were conducted at the Center for Applied Isotope Studies, University of Georgia, USA.

The bone was cleaned and washed, using an ultrasonic bath. After cleaning, the dried bone was gently crushed into small fragments and treated with diluted 1N acetic acid to remove surface-absorbed and secondary carbonates. Periodic evacuation ensured that evolved carbon dioxide was removed from the interior of the sample fragments and that fresh acid was allowed to reach even the interior micro-surfaces. The chemically-cleaned sample was then reacted under vacuum with 100% phosphoric acid to dissolve the bone mineral and release carbon dioxide from bioapatite.

The resulting carbon dioxide was cryogenically purified from the other reaction products and catalytically converted to graphite using the method of Vogel et al. (1984). Graphite $^{14}C/^{13}C$ ratios were measured using the CAIS 0.5 MeV accelerator mass spectrometer. The sample ratios were compared to the ratio measured from Oxalic Acid I (NBS SRM 4990). The sample $^{13}C/^{12}C$ ratios were measured separately using a stable isotope ratio mass spectrometer and expressed as $\delta^{13}C$ with respect to PDB, with an error of less than 0.1‰. All results are reported using delta notation, $\delta = [(R_{sample}/R_{standard} - 1)*1000]$ (Coplen, 1994). The reference for carbon isotope values (R = $^{13}C/^{12}C$) is V-PDB, and for oxygen isotope values (R = $^{18}O/^{16}O$) it is in V-SMOW (Coplen, 1995).

Interpretation of results was performed based on $\delta^{13}C$ standards defined for plants C_3 ($\delta^{13}C = -27\pm3$ ‰) and C_4 ($\delta^{13}C = -13\pm2$ ‰) (MacFadden, 2005 and references therein), and considering the body enrichment of +14 ‰, which is a value used largely in the literature (Cerling & Harris, 1999). We interpret that $\delta^{13}C$ values lower than −13 ‰ are characteristic of animals that feed on C_3 plants, while values of $\delta^{13}C$ higher than 1 ‰ are characteristic of a diet based on C_4 plants. Between these values, the diet consists of both types of plants.

The measurement of the proportion (f_1, f_2) of different plants in the animal's diet ($f_1 = C_3$ plants; $f_2 = C_4$ plants) was estimated through the isotope mixing model using carbon (1,2) isotopic data below (Phillips, 2012). The food resources are represented by the isotopic signature of the C_3 plants ($\delta^{13}C_1$) and C_4 plants ($\delta^{13}C_2$), and the carbon isotopic signatures found in the studied species = $\delta^{13}C_{mix}$.

$$\delta^{13}C_{mix} = \delta^{13}C_1 f_1 + \delta^{13}C_2 f_2 \ (1)$$
$$1 = f_1 + f_2 \ (2)$$

Additionally, the niche breadth (B) was calculated by Levins' (1968) measure (3), where p_i = proportion of resources consumed. These values were standardized (B_A) from 0 to 1, where N = total amount of resources (4).

$$B = 1/\sum p_i^2 \ (3)$$
$$B_A = B - 1\ /N - 1 \ (4)$$

Finally, considering the enrichments value of +14 ‰, and the expected $\delta^{13}C$ values in different habitats of South America (Domingo et al., 2012b), we could suggest the habitats in which this taxon lived during the Late Pleistocene tropical regions, such as the Brazilian Intertropical Region (BIR). Values between −22 ‰ to −16 ‰ represent closed-canopy forests; −16 ‰ to −11 ‰ represent low density forest; −11 ‰ to −8 ‰, arboreal savanna; −8 ‰ to −1 ‰, arboreal to open savanna; and, −1 ‰ to 5 ‰, open savanna.

2.4. Radiocarbon dating (^{14}C AMS)

For radiocarbon dating, the quoted uncalibrated dates are given in radiocarbon years before 1950 (years BP), using the ^{14}C half-life of 5,568 years. The error is quoted as one

standard deviation and reflects both statistical and experimental errors. The date has been corrected for isotope fractionation.

The reliability of the applied technique for the purification of hydroxyapatite was previously demonstrated, especially due to the demand for dating archaeological samples that present little or no collagen (Cherkinsky, 2009). However, radiocarbon dating in bioapatite promotes younger dates than those made in collagen (Zazzo & Saliège, 2011; Zazzo, 2014), thus, radiocarbon dating in bioapatite should be considered as minimum dates.

Because of the lack of collagen in fossils from tropical regions, as is the case for the giant sloth fossil bones from Santa Elina, we corrected the radiocarbon dating in bioapatite ($^{14}C_{bioapatite}$) to collagen ($^{14}C_{collagen}$) as proposed by Dantas & Cherkinsky (in press) using the following equation (5). This new regression presents a strong correlation ($R^2 = 0.98$), a lower percent predicted error (%PE = 0.01), and a standard error of the estimate (%SEE = 21.83), being a reliable tool to convert the bioapatite radiocarbon dating ($^{14}C_{bioapatite}$) to collagen ($^{14}C_{collagen}$) patterns, aiming the acquisition of more reliable dates.

$$\log_{10}{^{14}C_{collagen}} = 1.09*\log_{10}{^{14}C_{bioapatite}} - 0.31 \ (5)$$

The dates were calibrated into calendar ages before the present, using the same standard error found in the $^{14}C_{bioapatite}$, CALIB 8.1 program (Reimer et al., 2020), and SHCal20 curve (Hogg et al., 2020). The 2σ measured ages are reported in Table 2.

3. Results
3.1. Systematic Paleontology

Xenarthra Cope, 1889
Pilosa Flower, 1883
Folivora Delsuc et al., 2001
Mylodontidae Gill, 1872
Mylodontinae Gill, 1872

Glossotherium phoenesis Cartelle, De Iuliis, Boscaini & Pujos, 2019

Material. Partial right maxilla, with the first superior caniform, and a partial alveolus of the first molariform.

Comments. Among the Mylodontidae taxa of the Late Pleistocene of South America, only the genera *Ocnotherium*, *Lestodon*, *Mylodonopsis*, and *Glossotherium* present caniforms, and only *Ocnotherium* possessed two caniforms (Figure 3A-G).

To assign the material from Santa Elina, we measured the angle between the C1 and M1 to the medial part of the skull and the diastema between both teeth (Table 1; Figure 3). Based on these measurements, we exclude the possibility that this material could belong to *Ocnotherium* or *Lestodon*, as the angle was superior to 24º and the diastema superior to 40 mm (Table 1). The species belonging to the genus *Mylodonopsis* (*M. ibseni*) and *Glossotherium* (*G. phoenesis*, *G. tropicorum*, *G. wegneri*, and *G. robustum*) present similar values to the observed in the material from Santa Elina. However, the most similar measurements were found in the species *G. phoenesis* and *G. tropicorum*, as the angle was lower than 15º and the C1-M1 diastema was lower than 11 mm (Table 1; Figure 3).

To attribute to one of these species, we observed the morphology of the suture between the maxilla and the pre-maxilla. In *G. tropicorum* the suture is less angular than that observed in *G. phoenesis*, such that the partial maxilla found in Santa Elina/MT is more similar to the latter (Figure 3E).

3.2. Radiocarbon dating and Isotopic Paleoecology

The specimen from unit II (UGAMS 51687) presented a calibrated radiocarbon dating on bioapatite of 14,944–15,239 cal a BP ($^{14}C_{bioapatite}$ = 12,690±40; Table 2). This could be the minimum age for this unit. However, using the corrected radiocarbon dating for collagen (see Material and methods), a calibrated age of 17,450–17,906 cal a BP was found ($^{14}C_{collagen}$ = 14,547±40; Table 2). The specimen from unit III (UGAMS 51688) presented a minimum calibrated radiocarbon dating on bioapatite of 22,339–22,534 cal a BP ($^{14}C_{bioapatite}$ = 22,042±45; Table 2). However, with collagen correction, we observe an older calibrated radiocarbon dating of 25,994–26,395 cal a BP ($^{14}C_{collagen}$ = 22,042±45; Table 2).

The carbon isotopic signature (Table 2) shows that *G. phoenesis* from Santa Elina was a mixed feeder with a preference for C_4 plants living in arboreal savanna habitats (Figure 4) in both phases studied. The youngest individual (unit II2) had a generalist diet consisting of 79%

of C_4 plants and 21% of C_3 plants, and a niche breadth (B_A) of 0.50. Its $\delta^{18}O$ value is 27.9‰. The oldest individual (unit III4) also presents a generalist diet consisting of 69% of C_4 plants and 31% of C_3 plants.

Its $\delta^{18}O$ value is 26.2‰, lower than the one found in the ground sloth from unit II. The oldest ground sloth, from unit III4, present slightly higher consumption of C_3 plants than the one from unit II. It also reflects its broader niche breadth (B_A = 0.79), owing to a more balanced diet in C_3/C_4 resources than the ground sloth from unit II2.

4. Discussion

4.1. Isotopic Paleoecology

McDonald (2005) highlights the diversity of feeding habitats among the Xenarthra in the Late Pleistocene of North America. The *Glossotherium* lineage is interpreted, due to the shape of its premaxillae and muzzle, as generalist individuals, with unspecialized morphology but mainly grazer/intermediate feeders (McDonald, 2005).

Our paleoecological interpretations corroborate to the grazing diet expected for *Glossotherium* species in South America (*e.g.,* Bargo et al., 2006; Bargo & Vizcaíno, 2008). *G. robustum* has been interpreted as a bulk-feeder (*i.e.,* an effective technique to ingest a large amount of food from the source), potentially diggers, and builders of burrows (Vizcaíno et al., 2001; Bargo et al., 2006; Bargo & Vizcaíno, 2008; Oliveira & Santos 2018). Dantas & Santos (2022) also suggest a bulk-feeding behavior for *G. phoenesis* in tropical regions of Brazil. $\delta^{13}C$ and $\delta^{15}N$ isotopic analyses of *G. robustum* from the Argentinean Pampas indicate a diet preference for C_3 vegetation (Czerwonogora et al., 2011), which the authors interpreted as consistent for a bulk feeder in open environments.

Our data contrast with the diet preference for C_3 plants revealed for *Glossotherium* species from temperate regions. The broad niche breadth revealed for the tropical *Glossotherium* species from Santa Elina indicates a generalist behavior, which may have allowed them to consume a variety of food resources in arboreal savanna habitat and withstand possible ecological and environmental pressures through the glacial-interglacial periods, such as climate fluctuations and scarcity of food resources.

Our results show that the two ground sloth individuals of both the phases studied were mix-feeders with a preference for C_4 plants. We recognize two possible scenarios to interpret this data: 1) a C_4-dominated grassland may not have changed significantly in the region

between the phases of ~26,000 cal a BP to ~17,000 cal a BP; or 2) the vegetation may have changed over the 8 thousand years' time span, but it was a C_4-dominated grassland landscape in both moments of the studied phases.

We suggest that the first scenario is the most likely. Although climate shifts prevailed during the Pleistocene in South America, resulting in the alternation of glacial and interglacial periods and the expansion and contraction of forested vegetation through time, major ecological changes and dramatic vegetational reconfiguration during the Pleistocene had a larger time span than 9,000 years (Kern et al., 2023). We cannot assert any possible shrinkage and expansion of the forested environment during this time span with our data. Therefore, we suggest similar paleoenvironmental setting during the phases studied.

The slight difference between only two $\delta^{18}O$ values is insufficient for broader paleoenvironmental interpretation, but we can foster general hypotheses to explain our data. This difference represents the distinct oxygen isotope composition between the two individuals, and it can be related to paleoenvironmental conditions, as local water composition (e.g., leaves, drinking source) becomes more $\delta^{18}O$-enriched due to higher evaporation in arid environments (Luz & Kolodny, 1989; Kohn & Cerling, 2002). However, more data are needed to elucidate this interpretation.

Because the ground sloth from unit III4 exhibits a lower $\delta^{18}O$ value than the youngest ground sloth from unit II2, we might suggest a seasonal change in aridity in the local environment, becoming a bit drier over time. This increase of aridity could have affected the levels of ^{16}O evaporation in two distinct wetter/drier phases, and that could have been reflected in the oxygen isotopic incorporation of these individuals.

The narrow niche breath of the youngest individual (unit II), with an increase preference for C_4 grasses rather than C_3 plants, seems to agree with this presumed seasonality. However, this oxygen difference might also be explained if the different individuals may have incorporated water from distinct drinking sources, which is related to variable isotopic content and levels of oxygen enrichment (Kohn et al., 1996). Nonetheless, these are general suggestions as we cannot assert paleoclimate shifts with only two isotopic data. Exploring this paleoclimatic scenario requires further isotopic data on a larger isotopic dataset of megafauna and other proxies (*e.g.,* stalagmites; Novello et al., 2017; 2018; Azevedo et al., 2021) from Central Brazil.

From a paleoenvironmental point of view, our carbon isotopic data for *G. phoenesis* is congruent with the suggested past landscape configuration of Santa Elina, characterized by a mosaic of vegetation including forest and open savanna-like environments, similar to the

nowadays phytogeographical domain Cerrado (Scheel-Ybert & Bachelet, 2020). The Brazilian Cerrado is characterized as a moist savanna, including open savannas, savanna woodlands, grasslands, and forest formations, as well as their weathered, nutrient-poor soils (Cassino et al., 2020).

Scheel-Ybert & Bachelet (2020) show that unit III of Santa Elina has low plant diversity and is predominantly composed of the plant families Leguminosae, Rubiaceae (which is common in the current Cerrado), as well as Lauraceae and Sapotaceae. They are mainly represented by trees, shrubs, or herbs (C_3 plants). The authors highlight that the high frequency of Lauraceae, an arboreal plant of humid or semi-humid forests, associated with the presence of the riparian forest plant *Alchornea* (Euphorbiaceae), points to a past forested environment. The authors also demonstrate that the families Leguminosae, Rubiaceae, among other C_3 plants, still predominate in the local area in more recent layers dated between 11–10,000 cal a BP, including the presence of a taxa associated to the current Cerrado domain (e.g., *Anacardium* sp., *Prosopis* sp., *Sileroxylon* sp.).

Our oxygen isotopic data, although limited, agree with the suggestion for regional vegetation and climate change over time in Santa Elina (Scheel-Ybert & Bachelet, 2020). From a broader perspective, this is also in agreement with the moisture oscillation during the Late Pleistocene in Cerrado regions and the decrease of humidity in the Late Quaternary of Central Brazil from between ~22–18 thousand years ago (Salgado-Labouriau, 1997; Salgado-Labouriau et al., 1997).

Palynological records suggest a colder and humid climate in Central Brazil from ~27–22 thousand years ago; and drier climate conditions starting from ~22–18 thousand years ago, reaching maximum dryness around ~14–11 thousand years ago (Ferraz-Vicentini & Salgado-Labouriau, 1996; Salgado-Labouriau et al., 1997; 1998). Likewise, it is suggested that the current Brazilian Cerrado may have experienced water stress between ~19-9 thousand years ago (Salgado-Labouriau et al., 1998), which could also explain the variation of the oxygen isotopic content among the ground sloths from different periods in Santa Elina.

4.2. Chronology

Our radiocarbon data shed new light on the significance of the zooarchaeological site of Santa Elina in the discussion of peopling of the Americas and the human co-habitation with the Pleistocene megafauna in South America. We present new data, from fossil material (dentine) that endorses previous dating on bones of the ground sloths from Santa Elina. Previous U/Th

dating of their osteoderms present values of 27±2 thousand years ago for the ground sloth from unit III(4) and 13±1 thousand years ago for the ground sloth from unit II(2) (Vialou et al., 2017). In addition to bone dating, previous radiocarbon dating on microcharcoal from an ashy layer from the oldest unit (III4) was dated to 27,402 cal a BP. The dating of charcoal or wood material can give a more precise date of the stratigraphy of the site; because these materials are more resistant to isotopic exchange than bone bioapatite (Zazzo & Saliège, 2011).

Our team working at Santa Elina is constantly striving to improve the dating methods of the shelter, providing updated methodologies and dates over the decades. In this regard, Optically Stimulated Luminescence (OSL) dating of the sediments performed at the Luminescence Dating Lab of the University of Washington, previously published in Feathers (2005), has been reviewed recently after methodological revision using updated procedures (Vialou et al., 2017; J. Feathers, *pers. comm.*). OSL dating was performed in quartz grains material due to its high luminescence sensitivity and as they are dominant in the fine sediments of the rock shelter. The updated data are explained as follows: 1) sample UW464, from unit II3 and depth of 228 cm, updated from 23,7±1,2 to 18,7±0,9 thousand years ago; 2) sample UW465, from unit III4 and depth between of 296 and 300 cm and in association with osteoderms, updated from 27,6±1,5 thousand years ago to 25,1±2.5; and 3) sample UW609, from unit IV and depth of 385 cm, updated from 35,5±2,4 to 27,8±2,7 thousand years ago (Feathers, 2005; Vialou et al., 2017).

Bioapatite samples for stable isotope analyses are reliable for paleodietary reconstructions (Tieszen & Fagre, 1993; Kohn & Cerling, 2002; Passey et al., 2005). However, diagenetic effects may cause errors in their radiocarbon dating. Because of the quick degradation of collagen and other organic remains in bones, its preservation in fossils is rare and occurs generally in exceptional circumstances (e.g., Kuitems et al., 2015; Lee et al., 2017).

The absence of collagen due to the diagenetic process is remarkable in fossils from tropical regions, such as the Brazilian Intertropical Region (BIR) and Central Brazil (Dantas et al., 2020; Dantas & Cherkinsky, in press). Therefore, a common alternative for dating and for the paleoecological investigation of Quaternary fossils without collagen preservation relies on the extraction and measurements of hydroxyapatite (*e.g.,* Garrison et al., 2019; Pansani et al., 2019; Asevedo et al., 2021), which has been demonstrated to be a successful tool due to the resistance of the mineral phase of bone and teeth to diagenetic processes (Cherkinsky, 2009).

However, bioapatite is more susceptive to diagenetic alteration than bone collagen once ambient fluids can penetrate the bone structure and cause diagenesis (Fernandes et al., 2013). The carbonate in bioapatite may exchange isotopically with the carbon source from the

depositional environment, thus, resulting in younger ages of bone and tooth samples (Zazzo & Saliège, 2011). In this context, Zazzo (2014) proposes that dating on bioapatite should be interpreted as minimum ages, and Dantas & Cherkinsky (in press) propose a regression to convert the minimum ages of $^{14}C_{bioapatite}$ to $^{14}C_{collagen}$.

In this context, our radiocarbon dating presents minimal ages of ~15,000 cal a BP to unit II2; and ~22,000 cal a BP to unit III4, supporting the stratigraphy of this oldest unit to around the LGM interval. Taking into consideration that younger dates are likely due to bioapatite contamination (Zazzo, 2014), and therefore using the regression proposed by Dantas & Cherkinsky (in press), we suggest the ages of 17,450–17,906 cal a BP to unit II2 and 25,994–26,395 cal a BP to unit III4 (Figure 5). Our results agree with previous chronological data for Santa Elina (Vialou et al., 2017; Figure 5).

Our new radiocarbon dating reinforces the chronology of Santa Elina and highlights the zooarchaeological significance of Santa Elina's unit III4, whose association of giant sloth remains with material culture from the LGM contributes to the discussion on the peopling of the Americas and the co-habitation of humans with the Pleistocene megafauna in South America. We endorse the time span of giant sloths in Santa Elina during two moments in the Late Pleistocene: i) the Last Glacial Maximum (26,000–19,000 years ago; Clark et al., 2009) and ii) before the Younger Dryas (12,900–11,200 years ago; Broecker et al., 2010), and the time span for human presence in the site evidenced by the precise association of the fossil remains with rich lithic assemblage.

The Americas is known to have been the last continents settled by humans (Waters, 2019), but the timing and the migration routes are still hotly debated. A Pacific Coastal route is strongly suggested for early human migration before at least 16,000 years ago (Braje et al., 2020; Davis & Madsen, 2020). Despite growing evidence that humans were in the Americas before the LGM (*e.g.,* Guidon & Delibrias, 1986; Bourgeon et al., 2017; Ardelean et al., 2020; Becerra-Valdivia & Higham, 2020; Bennett et al., 2021; Boëda et al., 2021; Rowe et al., 2022), this is still a contentious topic in academia (*e.g.,* Waters, 2019; Potter et al., 2022). In light of this fervent discussion, we reinforce by our new radiocarbon dating on fossil teeth material that Santa Elina is chronologically consistent with other pre-LGM archaeological sites in the Americas.

When compared to North America, evidence of human-megafauna interaction in the southern continent is rare and controversial, but has increased recently (*e.g.,* human intervention in megamammal remains, Dantas et al., 2012; Fariña et al., 2014; 2021; Mothé et al., 2020; Domínguez-Rodrigo et al., 2022; Carlini et al., 2022; and artistic representation of

megamammals, including ground sloths, in rock art paintings in the Colombian Amazon, Iriarte et al., 2022). The increasing evidence for the co-habitation of humans and megafauna in South America has been valuable for elucidating the drives, and possible human role, in the Late Quaternary megafaunal extinction (Barnosky & Lindsey, 2010; Sandom et al., 2014). Santa Elina, more than archaeologically intriguing, is a remarkable zooarchaeological site that provides a fundamental contribution in this debate.

5. Conclusion

In this study, we provide new paleontological data of the ground sloth fossils from Santa Elina shelter, Central Brazil. We analyzed the isotopic paleoecology (δ^{13}C, δ^{18}O) and provided new radiocarbon dating for two ground sloth individuals from different chronostratigraphic units during the Late Pleistocene.

We update the species assignment of the mylodontid from Santa Elina to *Glossotherium phoenesis* Cartelle, De Iuliis, Boscaini & Pujos, 2019. Our contribution on isotopic paleoecology is the first for a tropical *Glossotherium*, contributing to the still scarce knowledge regarding the paleoecology of mylodontids in South America.

Our isotopic δ^{13}C data reveal a broad niche breadth and mixed feeder behavior with a slight preference for C_4-grasses for both individuals from two moments of the Late Pleistocene in Santa Elina: 25,994–26,395 cal a BP (unit III4) and 17,450–17,906 cal a BP (unit II2). We suggest that the diet behavior of this species did not change significantly over time, and that they lived in a predominant arboreal savanna habitat. Our isotopic δ^{18}O data shows differences in their isotopic content, which may be related to variations in the isotopic composition of water sources available in each period or to distinct conditions of humidity over time.

Finally, we provide new radiocarbon dating to contextualize our isotopic data as the minimum ages: 22,339–22,534 cal a BP (for the ground sloth from unit III4) and 14,944–15,239 cal a BP (for the ground sloth from unit II2). Because exogenous carbon contamination and exchange can affect the radiocarbon dating made in bioapatite (promoting younger ages), we correct these bioapatite ages based on a novel model that convert radiocarbon dates in collagen, and suggest the following corrected ages: 25,994–26,395 cal a BP (for the ground sloth from unit III4) and 17,450–17,906 cal a BP (for the ground sloth from unit II2).

Our results support the occurrence of two individuals of ground sloths, in association with material culture from past human occupations, in different periods during the Late Pleistocene in Santa Elina, with a time span of ~9,000 years. The radiocarbon dating for the

ground sloth from unit III4 endorses the chronology of this unit to the Last Glacial Maximum (LGM) and reinforces Santa Elina as a reference in the study of early human occupation of the Americas and their co-habitation with the Pleistocene megafauna.

CONFLICT OF INTEREST

We declare no competing of interest.

REFERENCES

Amson, E., Argot, C., McDonald, H.G., Muizon, C., 2015. Osteology and functional morphology of the axial postcranium of the marine sloth *Thalassocnus* (Mammalia, Tardigrada) with paleobiological implications. Journal of Mammalian Evolution. 22, 473-518.

Ardelean, C.F., Becerra-Valdivia, L., Pedersen, M.W., et al., 2020. Evidence of human occupation in Mexico around the Last Glacial Maximum. Nature. 584(7819), 87-92.

Asevedo, L., Ranzi, A., Kalliola, R., et al., 2021. Isotopic paleoecology (δ^{13}C, δ^{18}O) of late Quaternary herbivorous mammal assemblages from southwestern Amazon. Quaternary Science Reviews. 251, 106700.

Azevedo, V., Strikis, N.M., Novello, V.F., et al., 2021. Paleovegetation seesaw in Brazil since the Late Pleistocene: A multiproxy study of two biomes. Earth and Planetary Science Letters. 563, 116880.

Barbosa, F.H.D.S., Porpino, K.D.O., Araújo-Júnior, H.I.D., et al., 2019. Articular and vertebral lesions in the Pleistocene sloths (Xenarthra, Folivora) from the Brazilian Intertropical Region. Historical Biology. 31(5), 544-558.

Bargo, M.S., Vizcaíno, S.F., Archuby, F.M., et al., 2000. Limb bone proportions, strength and digging in some Lujanian (Late Pleistocene-Early Holocene) mylodontid ground sloths (Mammalia, Xenarthra). Journal of Vertebrate Paleontology. 20(3), 601-610.

Bargo, S.M., Toledo, N., Vizcaíno, S.F., 2006. Muzzle of South American Pleistocene ground sloths (Xenarthra, Tardigrada). Journal of Morphology. 267, 248-263.

Bargo, S.M., Vizcaíno, S.F., 2008. Paleobiology of Pleistocene ground sloths (Xenarthra, Tardigrada): biomechanics, morphogeometry and ecomorphology applied to the masticatory apparatus. Ameghiniana. 45, 175-96.

Barnosky, A.D., Lindsey, E.L., 2010. Timing of Quaternary megafaunal extinction in South America in relation to human arrival and climate change. Quaternary International. 217(1-2), 10-29.

Becerra-Valdivia, L., Higham, T., 2020. The timing and effect of the earliest human arrivals in North America. Nature. 584(7819), 93-97.

Ben-David, M., Flaherty, E., 2012. Stable isotopes in mammalian research: a beginner's guide. Journal of Mammalogy. 93, 312-328.

Benabdelhadi, M., 2005. Contribuição da sedimentologia e da microscopia para o conhecimento dos sítios pré-históricos: Métodos de pesquisa e resultados. In: Vialou, A.V. Pré-história do Mato Grosso: Santa Elina. EdUSP, São Paulo. 113-124.

Bennett, M.R., Bustos, D., Pigati, J.S., et al., 2021. Evidence of humans in North America during the last glacial maximum. Science. 373(6562), 1528-1531.

Blumenthal, S.A., Rothman, J.M., Chritz, K.L., Cerling, T.E., 2016. Stable isotopic variation in tropical forest plants for applications in primatology. American Journal of Primatology. 78(10), 1041-1054.

Bocherens, H., Drucker, D.G., 2013. Terrestrial teeth and bones. In: Elias S.A. The encyclopedia of quaternary science. Amsterdam: Elsevier, 304-314.

Bocherens, H., 2015. Isotopic tracking of large carnivore palaeoecology in the mammoth steppe. Quaternary Science Reviews. 117, 42-71.

Bocherens, H., Cotte, M., Bonini, R.A., et al., 2017. Isotopic insight on paleodiet of extinct Pleistocene megafaunal Xenarthrans from Argentina. Gondwana Research. 48, 7-14.

Boëda, E., Ramos, M., Pérez, A., et al., 2021. 24.0 kyr cal BP stone artefact from Vale da Pedra Furada, Piauí, 399 Brazil: Techno-functional analysis. PLoS ONE. 16(3), e0247965.

Boscaini, A., Iurino, D.A., Billet, G., et al., 2018. Phylogenetic and functional implications of the ear region anatomy of *Glossotherium robustum* (Xenarthra, Mylodontidae) from the Late Pleistocene of Argentina. The Science of Nature. 105, 1-18.

Boscaini, A., Pujos, F., Gaudin, T.J., 2019. A reappraisal of the phylogeny of Mylodontidae (Mammalia, Xenarthra) and the divergence of mylodontine and lestodontine sloths. Zoologica Scripta. 48(6), 691-710.

Boscaini, A., Toledo, N., Pérez, L.M., et al., 2022. New well-preserved materials of *Glossotherium chapadmalense* (Xenarthra, Mylodontidae) from the Pliocene of Argentina shed light on the origin and evolution of the genus. Journal of Vertebrate Paleontology. e2128688.

Bourgeon, L., Burke, A., Higham, T., 2017. Earliest human presence in North America dated to the last glacial maximum: new radiocarbon dates from Bluefish Caves, Canada. PLoS ONE. 12(1), e0169486.

Braje, T.J., Erlandson, J.M., Rick, T.C., et al., 2020. Fladmark+ 40: What have we learned about a potential Pacific Coast peopling of the Americas?. American Antiquity. 85(1), 1-21.

Broecker, W.S., Denton, G.H., Edwards, R.L., et al., 2010. Putting the Younger Dryas cold event into context. Quaternary Science Reviews. 29(9-10), 1078-1081.

Bryant, J.D., Froelich, P.N, 1995. A model of oxygen isotope fractionation in body water of large mammals. Geochimica et Cosmochimica Acta, 59(21). 4523-4537.

Bustos, D. Jakeway, J., Urban, T.M., et al., 2018. Footprints preserve terminal Pleistocene hunt? Human-sloth interactions in North America. Science Advances. 4(4), eaar7621.

Carlini, A.A., Carrilo-Briceño, J.D., Jaimes, A., et al., 2022. Damaged glyptodontid skulls from Late Pleistocene sites of northwestern Venezuela: evidence of hunting by humans?. Swiss Journal of Palaeontology. 141, 413 11.

Cartelle, C., 1991. Um novo Mylodontinae (Edentata, Xenarthra) do Pleistoceno final de região intertropical brasileira. Anais da Academia brasileira de Ciências. 63(2), 161-170.

Cartelle, C., 1992. Edentata e megamamíferos herbívoros extintos da Toca dos Ossos (Ourolândia, BA, Brasil). Ph.D. Thesis, Universidade Federal de Minas Gerais, Belo Horizonte. 700 p.

Cartelle, C., De Iuliis, G., 1995. *Eremotherium laurillardi*: the Panamerican late Pleistocene megatheriid sloth. Journal of Vertebrate Paleontology. 15(4), 830-841.

Cartelle, C., 2005. A Preguiça-terrícola de Santa Elina. In: Vialou, A.V. Pré-história do Mato Grosso: Santa Elina. EdUSP, São Paulo. 159-162.

Cartelle, C., De Iuliis, G., Ferreira, R.L., 2009. Systematic revision of tropical Brazilian scelidotheriine sloths (Xenarthra, Mylodontoidea). Journal of Vertebrate Paleontology. 29(2), 555-566.

Cartelle, C., De Iuliis, G., Boscaini, A., et al., 2019. Anatomy, possible sexual dimorphism, and phylogenetic affinities of a new mylodontine sloth from the late Pleistocene of intertropical Brazil. Journal of Systematic Palaeontology. 17(23), 1957-1988.

Cassino, R.F., Ledru, M.P., Santos, R.A, et al., 2020. Vegetation and fire variability in the central Cerrados (Brazil) during the Pleistocene-Holocene transition was influenced by oscillations in the SASM boundary belt. Quaternary Science Reviews 232, 106209.

Cherkinsky, A., 2009. Can we get a good radiocarbon age from "bad bone"? Determining the reliability of radiocarbon age from bioapatite. Radiocarbon. 51(2), 647-655.

Clark, P.U., Dyke, A.S., Shakun, J.D., et al., 2009. "The Last Glacial Maximum." Science. 325, 710-714.

Cerling, T.E., Harris, J.M., 1999. Carbon isotope fractionation between diet and bioapatite in ungulate mammals and implications for ecological and paleoecological studies. Oecologia. 120, 347-363.

Clementz, M.T., 2012. New insight from old bones: stable isotope analysis of fossil mammals. Journal of Mammalogy. 93-(2), 368-380.

Collatz, G.J., Berry, J.A., Clark, J.S., 1998. Effects of climate and atmospheric CO_2 partial pressure on the global distribution of C_4 grasses: present, past, and future. Oecologia. 114, 441-454.

Coplen, T.B., 1994. Reporting of stable hydrogen, carbon, and oxygen isotopic abundances. Pure and Applied Chemistry. 66, 273e276

Coplen, T.B., 1995. Discontinuance of SMOW and PDB. Nature. 375, 285-285.

Czerwonogora, A., Fariña, R.A., Tonni, E.P., 2011. Diet and isotopes of Late Pleistocene ground sloths: first results for *Lestodon* and *Glossotherium* (Xenarthra, Tardigrada). Neues Jahrbuch fur Geologie und Palaontologie-Abhandlungen. 262(3), 257-266.

Czerwonogora, A., Fariña., R.A., 2012. How many Pleistocene species of *Lestodon* (Mammalia, Xenarthra, Tardigrada)? Journal of Systematic Palaeontology. 11, 251-263.

Dantas, M.A.T., Queiroz, A.N., Santos, F.V., et al., 2012. An anthropogenic modification in an Eremotherium tooth from northeastern Brazil. Quaternary International. 253, 107-109.

Dantas, M.A.T., Cherkinsky, A., Bocherens, H., et al., 2017. Isotopic paleoecology of the Pleistocene megamammals from the Brazilian Intertropical Region: feeding ecology ($\delta^{13}C$), niche breadth and overlap. Quaternary Science Reviews. 170, 152-163.

Dantas, M.A.T., Cherkinsky, A., Lessa, C.M.B., et al., 2020. Isotopic paleoecology ($\delta^{13}C$, $\delta^{18}O$) of a late Pleistocene vertebrate community from the Brazilian Intertropical Region. Revista Brasileira de Paleontologia. 23(2), 138-152.

Dantas, M A.T, 2022. Estimating the body mass of the late Pleistocene megafauna from the South America Intertropical Region and a new regression to estimate the body mass of extinct xenarthrans. Journal of South American Earth Sciences. 103900.

Dantas, M.A.T, Santos, A.M., 2022. Inferring the paleoecology of the Late Pleistocene giant ground sloths from the Brazilian Intertropical Region. Journal of South American Earth Sciences,.117, 103899.

Dantas, M.A.T., Bernardes, C., Asevedo, L., et al., 2022. Isotopic palaeoecology ($\delta^{13}C$) of three faunivores from Late Pleistocene of the Brazilian intertropical region. Historical Biology. 34(3), 507-514.

Dantas, M.A.T, Cherkinsky, A. (in press). Interrelation of radiocarbon ages bone fractions in the Brazilian Intertropical Region. Quaternary Research.

Davis, L.G., Madsen, D.B., 2020. The coastal migration theory: Formulation and testable hypotheses. Quaternary Science Reviews. 249, 106605.

D'Errico, F., Dubreuil, L., 2005. A utilização dos corantes em Pré-História: O Exemplo de Santas Elina. In: Vialou, A.V. Pré-história do Mato Grosso. EdUSP, São Paulo. 177-188.

D'Errico, F., Vialou, A.V., 2007. Reduction sequences of colorant materials: the rock artsite of Santa Elina (Mato Grosso, Brazil). Rock Art Research, 24(2).

De Los Arcos, S., Partarrieu, D., Carrillo-Briceño, et al., 2017. The Southernmost occurrence of the aquatic sloth *Thalassocnus* (Mammalia, Tardigrada) in two new Pliocene localities in Chile. Ameghiniana. 54(4), 351-369.

De Iuliis, G., Cartelle, C., McDonald, H.G., et al., 2017. The mylodontine ground sloth *Glossotherium tropicorum* from the late Pleistocene of Ecuador and Peru. Papers in Palaeontology. 3(4), 613-636.

De Iuliis, G., Boscaini, A., Pujos, F.R.F., et al., 2020. On the status of the giant mylodontine sloth *Glossotherium wegneri* (Spillmann, 1931)(Xenarthra, Folivora) from the late Pleistocene of Ecuador. Comptes Rendus Palevol. 19 (12), 215-232.

DeSantis, L.R., Crites, J.M., Feranec, R.S., et al., 2019. Causes and consequences of Pleistocene megafaunal extinctions as revealed from Rancho La Brea mammals. Current Biology. 29(15), 2488-2495.

Domingo, L., Koch, P.L., Grimes, S.T., et al., 2012a. Isotopic paleoecology of mammals and the Middle Miocene Cooling event in the Madrid Basin (Spain). Palaeogeography, Palaeoclimatology, Palaeoecology. 339, 98-113.

Domingo, L., Prado, J.L., Alberdi, M.T., 2012b. The effect of paleoecology and paleobiogeography on stable isotopes of Quaternary mammals from South America. Quaternary Science Reviews. 55, 103-113.

Domínguez-Rodrigo, M., Baquedano, E., Varela, L., et al., 2021. Deep classification of cut-marks on bones from Arroyo del Vizcaíno (Uruguay). Proceedings of the Royal Society B. 288(1954), 20210711.

Fariña, R.A., Blanco, R.E., 1996. Megatherium, the stabber. Proceedings of the Royal Society B. 263(1377), 1725-1729.

Fariña, R.A., Vizcaíno, S.F., 2001. Carved teeth and strange jaws: how glyptodonts masticated. Acta Paleontologica Polonica. 46, 87-102.

Fariña, R.A., Tambusso, P.S., Varela, L., et al., 2014. Arroyo del Vizcaíno, Uruguay: a fossil-rich 30-ka-old megafaunal locality with cut-marked bones. Proceedings of the Royal Society B. 281, 20132211.

Feathers, J., 2005. Datação por luminescência óptica estimulada. In: Vialou, A.V. Pré-história do Mato Grosso: Santa Elina. EdUSP, São Paulo. 245-54.

Fernandes, R., Hüls, M., Nadeau, M., et al., 2013. Assessing screening criteria for the radiocarbon dating of bone mineral. Nuclear Instruments and Methods in Physics Research Section B: Beam Interactions with Materials and Atoms. 294, 226-232.

Ferraz-Vicentini, K.R., Salgado-Labouriau, M.L., 1996. Palynological analysis of a palm swamp in central Brazil. Journal of South American Earth Sciences. 9(3-4), 207-219.

Figueirido, B., Soibelzon, L.H., 2010. Inferring palaeoecology in extinct tremarctine bears (Carnivora, Ursidae) using geometric morphometrics. Lethaia. 43(2), 209-222.

Figuti, L., 2005a. A arqueofauna do sítio de Santa Elina: Nota preliminar. In: Vialou, A.V. Pré-história do Mato Grosso: Santa Elina. EdUSP, São Paulo. 155-158.

Figuti, L., 2005b. Considerações sobre a distribuição espacial da megafauna em Santa Elina. In: Vialou, A.V. Pré-história do Mato Grosso. EdUSP, São Paulo. 163-166.

Garrison, E.G., Morgan, G.S., McGrath, K., et al., 2019. Recent dating of extinct Atlantic gray whale fossils, (*Eschrichtius robustus*), Georgia Bight and Florida, western Atlantic Ocean. PeerJ. 7, e6381.

Guidon, N., Delibrias, G., 1986. Carbon-14 dates point to man in the Americas 32,000 years ago. Nature. 321(6072), 769-771.

Haro, J.A., Tauber, A.A., Krapovickas, J.M., 2016. The manus of *Mylodon darwinii* Owen (Tardigrada, Mylodontidae) and its phylogenetic implications. Journal of Vertebrate Paleontology. 36(5), e1188824.

Hogg, A.G., Heaton, T.J., Hua, Q., et al., 2020. SHCal20 Southern Hemisphere calibration, 0–55,000 years cal BP. Radiocarbon. 62(4), 759-778.

Iriarte, J., Ziegler, M.J., Outram, A.K., et al., 2022. Ice Age megafauna rock art in the Colombian Amazon?. Philosophical Transactions of the Royal Society B. 377(1849), 20200496.

Kern, A.K., Akabane, T.K., Ferreira, J.Q., et al., 2023. A 1.8 million year history of Amazon vegetation. Quaternary Science Reviews. 299, 107867.

Koch, P.L., 2007. Isotopic study of the biology of modern and fossil vertebrates. In: Michener, R., Lajtha, K. Stable Isotopes in Ecology and Environmental Science. Blackwell Publishing. 99-154.

Koch, P.L., Hoppe, K.A., Webb, D., 1998. The isotopic ecology of late Pleistocene mammals in North America, Part 1. Florida. Chemical Geology. 152, 119-138.

Kohn, M.J., 1996. Predicting animal δ^{18}O: accounting for diet and physiological adaptation. Geochimica et Cosmochimica Acta. 60(23), 4811-4829.

Kohn, M.J., Schoeninger, M.J., Valley, J.W., 1996. Herbivore tooth oxygen isotope compositions: effects of diet and physiology. Geochimica et Cosmochimica Acta. 60(20), 3889-3896.

Kohn, M.J., Cerling, T.E., 2002. Stable Isotope Compositions of Biological Apatite. Phosphates-Geochemical, Geobiological, and Materials Importance. Reviews in Mineralogy and Geochemistry. 48, 455-488.

Kuitems, M., van der Plicht, J., Drucker, D.G., et al., 2015. Carbon and nitrogen stable isotopes of well-preserved Middle Pleistocene bone collagen from Schöningen (Germany) and their paleoecological implications. Journal of Human Evolution. 89, 105-113.

Lee, Y.C., Chiang, C.C, Huang, P.Y., et al., 2017. Evidence of preserved collagen in an Early Jurassic sauropodomorph dinosaur revealed by synchrotron FTIR microspectroscopy. Nature communications. 8(1), 14220.

Luz, B., Kolodny, Y., 1989. Oxygen isotope variation in bone phosphate. Applied Geochemistry. 4(3), 317-323.

Ma, J., Wang, Y., Baryshnikov, G.F., et al., 2021. The Mammuthus-Coelodonta Faunal Complex at its southeastern limit: A biogeochemical paleoecology investigation in Northeast Asia. Quaternary International. 591, 93-106.

MacFadden, B.J., Wang, Y., Cerling, T.E., Anaya, F., 1994. South American fossil mammals and carbon isotopes: a 25 million-year sequence from the Bolivian Andes. Palaeogeography, Palaeoclimatology, Palaeoecology. 107(3-4), 257-268.

MacFadden, B.J., 2005. Diet and habitat of toxodont megaherbivores (Mammalia, Notoungulata) from the late Quaternary of South and Central America. Quatermary Research. 64(2), 113-124.

Marshall, L.G., 1988. Land mammals and the great American interchange. American Scientist. 76(4), 380-388.

McDonald, H.G., 2005. Paleoecology of extinct xenarthrans and the Great American Biotic Interchange. Bulletin of the Florida Museum of Natural History. 45(4), 313-333.

McDonald, H.G., De Iuliis, G., 2008. Fossil history of sloths. In: Vizcaíno, S.F., Loughry, W.J. The Biology of the Xenarthra. The University of Florida Press, Gainesville. 39-55.

McDonald, H.G., 2018. An Overview of the Presence of Osteoderms in Sloths: Implications for Osteoderms as a Plesiomorphic Character of the Xenarthra. Journal of Mammalian Evolution. 25(4), 485-493.

McDonald, H.G., 2021. Yukon to the Yucatan: Habitat partitioning in North American Late Pleistocene Ground Sloths (Xenarthra, Pilosa). Journal of Palaeosciences. 70(1-2), 237-252.

Mendoza, P.L., Cartajena, I., Carabias, D., et al., 2018. Reconstructing drowned terrestrial landscapes. Isotopic paleoecology of a late Pleistocene extinct faunal assemblage: Site GNL Quintero 1 (GNLQ1)(32 S, Central Chile). Quaternary International. 463, 153-160.

Mothé, D., Avilla, L.S., Araújo-Júnior, H.I., et al., 2020. An artifact embedded in an extinct proboscidean sheds new light on human-megafaunal interactions in the Quaternary of South America. Quaternary Science Reviews. 229, 106125.

Novello, V.F., Cruz, F.W., Vuille, M., et al., 2017. A high-resolution history of the South American Monsoon from Last Glacial Maximum to the Holocene. Scientific Reports. 7(1), 44267.

Novello, V.F., Cruz, F.W., Moquet, J.S., et al., 2018. Two millennia of South Atlantic Convergence Zone variability reconstructed from isotopic proxies. Geophysical Research Letters. 45(10), 5045-5051.

O'Dea, A., Lessios, H.A., Coates, A.G., et al., 2016. Formation of the Isthmus of Panama. Science Advances. 2, e1600883.

Oelze, V.M., Fuller, B.T., Richards, M.P., et al., 2011. Exploring the contribution and significance of animal protein in the diet of bonobos by stable isotope ratio analysis of hair. Proceedings of the National Academy of Sciences. 108(24), 9792-9797.

Oliveira, A.M., Santos, C.M.D., 2018. Functional morphology and paleoecology of Pilosa (Xenarthra, Mammalia) based on a two-dimensional geometric Morphometrics study of the Humerus. Journal of Morphology. 279(10), 1455-1467.

Oliveira, J.F., Asevedo, L., Cherkinsky, A., et al., 2020. Radiocarbon dating and integrative paleoecology (δ^{13}C, stereomicrowear) of *Eremotherium laurillardi* (LUND, 1842) from midwest region of the Brazilian intertropical region. Journal of South American Earth Sciences. 102, 102653.

Pacheco, M.L.A.F., 2009. Zooarqueologia dos sítios arqueológicos Maracaju 1, MS e Santa Elina, MT. Master's Dissertation, Museu de Arqueologia e Etnologia, Universidade de São Paulo, São Paulo.

Pansani, T.R., Muniz, F.P., Cherkinsky, A., et al., 2019. Isotopic paleoecology (δ^{13}C, δ^{18}O) of late Quaternary megafauna from Mato Grosso do Sul and Bahia states, Brazil. Quaternary Science Reviews. 221, 105864.

Passey, B.H., Robinson, T.F., Ayliffe, L.K., et al., 2005. Carbon isotope fractionation between diet, breath CO_2, and bioapatite in different mammals. Journal of Archaeological Science. 32(10), 1459-1470.

Pitana, V.G., Esteban, G.I., Ribeiro, A.M., et al., 2013. Cranial and dental studies of *Glossotherium robustum* (Owen, 1842) (Xenarthra: Pilosa: Mylodontidae) from the Pleistocene of southern Brazil. Alcheringa: An Australasian Journal of Palaeontology. 37(2), 147-162.

Politis, G.G., Messineo, P.G., Stafford Jr, T.W., et al., 2019. Campo Laborde: a Late Pleistocene giant ground sloth kill and butchering site in the Pampas. Science Advances. 5(3), eaau4546.

Potter, B.A., Chatters, J.C., Prentiss, A.M., et al., 2022. Current Understanding of the Earliest Human Occupations in the Americas: Evaluation of Becerra-Valdivia and Higham (2020). PaleoAmerica. 8(1), 62-76.

Prevosti, F.J., Martin, F.M., 2013. Paleoecology of the mammalian predator guild of Southern Patagonia during the latest Pleistocene: ecomorphology, stable isotopes, and taphonomy. Quaternary International. 305, 74-84.

Pujos, F., De Iuliis, G., Argot, C., et al., 2007. A peculiar climbing Megalonychidae from the Pleistocene of Peru and its implication for sloth history. Zoological Journal of the Linnean Society. 149, 179-235.

Pujos, F., Gaudin, T.J., De Iuliis, G., et al., 2012. Recent advances on variability, morpho-functional adaptations, dental terminology, and evolution of sloths. Journal of Mammalian Evolution. 19, 159-69.

Pujos, F., Ciancio, M.R., Forasiepi, A.M., et al., 2021. The late Oligocene xenarthran fauna of Quebrada Fiera (Mendoza, Argentina) and its implications for sloth origins and the diversity of Palaeogene cingulates. Papers in Palaeontology. 7(3), 1613-1656.

Pushkina, D., Saarinen, J., Zeigler, R., et al., 2020. Stable isotopic and mesowear reconstructions of paleodiet and habitat of the Middle and Late Pleistocene mammals in south-western Germany. Quaternary Science Reviews. 227, 106026.

Redmond, B.G., McDonald, H.G., Greenfield, H.J., et al., 2012. New evidence for Late Pleistocene human exploitation of Jefferson's Ground Sloth (*Megalonyx jeffersonii*) from northern Ohio, USA. World Archaeology. 44(1), 75-101.

Reimer, P.J., Austin, W., Bard, E., et al., 2020. The IntCal20 Northern Hemisphere radiocarbon age calibration curve (0–55 cal kBP). Radiocarbon. 62(4), 725-757.

Ribeiro, M.S.L., Varela, S., Nogués-Bravo, D., et al., 2012. Potential suitable areas of giant ground sloths dropped before its extinction in South America: the evidences from bioclimatic envelope modeling. Natureza & Conservação.10(2), 145-151.

Rowe, T.B., Stafford Jr., T.W., Fisher, D., et al., 2022. Human Occupation of the North American Colorado Plateau ～37,000 Years Ago. Frontiers in Ecology and Evolution. 10:903795.

Salgado-Labouriau, M.L., 1997. Late Quaternary palaeoclimate in the savannas of South America. Journal of Quaternary Science. 12(5), 371-379.

Salgado-Labouriau, M.L., Casseti, V., Ferraz-Vicentini, K.R., et al., 1997. Late Quaternary vegetational and climatic changes in cerrado and palm swamp from central Brazil. Palaeogeography, Palaeoclimatology, Palaeoecology. 128, 215-226.

Salgado-Labouriau, M.L., Barberi, M., Ferraz-Vicentini, K.R., et al., 1998. A dry climatic event during the late Quaternary of tropical Brazil. Review of Palaeobotany and Palynology. 99, 115-129.

Sandom, C., Faurby, S., Sandel, B., et al., 2014. Global late Quaternary megafauna extinctions linked to humans, not climate change. Proceedings of the Royal Society B: Biological Sciences. 281(1787), 20133254.

Shockey, B.J., Anaya, F., 2011. Grazing in a new late Oligocene mylodontid sloth and a mylodontid radiation as a component of the Eocene-Oligocene faunal turnover and the early spread of grasslands/savannas in South America. Journal of Mammalian Evolution. 18(2), 101-115.

Sponheimer, M., Lee-Thorp, J.A., 1999. Oxygen isotopes in enamel carbonate and their ecological significance. Journal of Archaeological Science. 26(6), 723-728.

Szabó, P., Kovács, J., Kocsis, et al., 2022. Pliocene-Early Pleistocene continental climate and vegetation in Europe based on stable isotope compositions of mammal tooth enamel. Quaternary Science Reviews. 288, 107572.

Sánz-Pérez, D., Fernández, M.H., Tomassini, R.L., et al., 2022. The Pampean region (Argentina) underwent larger variation in aridity than in temperature during the late Pleistocene: New evidence from the isotopic analysis of mammalian taxa. Quaternary Science Reviews. 286, 107555.

Tejada, J.V., Flynn, J.J., MacPhee, R., et al., 2021. Isotope data from amino acids indicate Darwin's ground sloth was not an herbivore. Scientific Reports. 11:18944.

Tieszen, L.L., Fagre, T., 1993. Effect of diet quality and composition on the isotopic composition of respiratory CO_2, bone collagen, bioapatite, and soft tissues. In: Lambert, J.B., Grupe, G. Prehistoric human bone: archaeology at the molecular level. Springer, Berlin, Heidelberg. 121-155.

Tomassini, R.L., Montalvo, C.I., Garrone, M.C., et al., 2020. Gregariousness in the giant sloth *Lestodon* (Xenarthra): multi-proxy approach of a bonebed from the Last Maximum Glacial of Argentine Pampas. Scientific Reports. 10(1), 1-16.

Varela, L., McDonald, H.G., Fariña, R., 2021. Sexual dimorphism in the fossil ground sloth *Lestodon armatus* (Xenarthra, Folivora). Historical Biology. 1-13.

Vargas-Peixoto, D., Colusso, C.S., Da-Rosa, Á.A.S., et al., 2021. A new record of *Lestodon armatus* Gervais 1855 (Xenarthra, Mylodontidae) from the Quaternary of southern Brazil and remarks on its postcranial anatomy. Historical Biology. 33(2), 159-175.

Vialou, A.V., Vialou, D., 1994. Les premiers peuplements préhistoriques du Mato Grosso. In: Le peuplement préhistorique de l'Amérique. Bulletin de la Société préhistorique française. 91, 257-263.

Vialou, A.V., Aubry, T., Benabdelhadi, M., et al., 1995. Découverte de Mylodontinae dans un habitat préhistorique daté du Mato Grosso (Brésil): l'abri rupestre de Santa Elina. Comptes rendus de l'Académie des sciences. Série 2. Sciences de la terre et des planètes. 320(7), 655-661.

Vialou, A.V., 2003. Santa Elina rockshelter, Brazil: evidence of the coexistence of man and *Glossotherium*. In: L. Miotti, M. Salemme, N. Flegenheimer. Where the south winds blow: ancient evidence of Paleo South Americans. College Station: Center for the Study of the First Americans, Texas A&M University. 21-28.

Vialou, D., 2005. Representações rupestres. In: Vialou, A.V. Pré-história do Mato Grosso: Santa Elina. EdUSP, São Paulo. 245-54.

Vialou, D., Benabdelhadi, M., Feathers, J., et al., 2017. Peopling South America's centre: the late Pleistocene site of Santa Elina. Antiquity. 91(358), 865-884.

Vialou, A.V., Vialou, D., 2019. Symbolic expressions in the Santa Elina shelter, Mato Grosso, Brazil: rock art images, artifacts, and adornments from the Pleistocene to the late Holocene. Boletim do Museu Paraense Emílio Goeldi. Ciências Humanas. 14, 343-366.

Vizcaíno, S.F., Bargo M.S., Fariña, R.A., 2008. Form, function and paleobiology in xenarthrans. In: Vizcaíno, S.F., Loughry, W.L. The Biology of the Xenarthra. University Press of Florida, Florida, 86-99.

Waters, M.R., 2019. Late Pleistocene exploration and settlement of the Americas by modern humans. Science. 365(6449), eaat5447.

Webb, S.D., 1976. Mammalian faunal dynamics of the great American interchange. Paleobiology. 2(3), 220-234.

Woodburne, M.O., 2010. The Great American Biotic Interchange: dispersals, tectonics, climate, sea level and holding pens. Journal of mammalian evolution. 17, 245-264.

Zazzo, A., 2014. Bone and enamel carbonate diagenesis: a radiocarbon prospective. Palaeogeography, Palaeoclimatology, Palaeoecology. 416, 168-178.

Zazzo, A., Saliège, J.F., 2011. Radiocarbon dating of biological apatites: a review. Palaeogeography, Palaeoclimatology, Palaeoecology. 310(1-2), 52-61.

Table 1. Measurements of the angle between the C1 and M1 to the medial part of the skull and the diastema between the C1 to M1 in several taxa of Mylodontidae from the Late Pleistocene of South America.

	Angle between C1-M1 (º)			Diastema C1-M1 (mm)		
	left	right	mean	left	right	mean
O. giganteum						
MCL 4346	19.5	30.0	24.7	41.6	38.7	40.1
L. armatus						
MPRSC 807	36.3	33.5	34.9	91.4	96.5	93.9
M. ibseni						
MCL 4353	-	22.6	22.6	-	5.2	5.2
G. phoenesis						
St Elina/MT	-	13.8	13.8	-	5.6	5.6
MCL 4303	17.6	19.7		14.1	-	
			15.7			10.8
MCL 4027[*]	17.3	8.2		8.9	9.5	
G. tropicorum						
ROM 3146	15.5	4.6	8.2	8.8	2.0	6.7

MNHN LAR 237	4.6	-		9.3	-	
G. wegneri						
MECN 505	25.0	-		15.2	-	
			33.2			14.3
MECN 356	42.6	32.1		13.5	14.2	
G. robustum						
MN 3944-V[*]	20.9	23.8		6.5	11.6	
			23.0			8.3
MAR-SUL 974	22.4	25.0		7.1	8.2	

Table 2. Data for two teeth samples (UGAMS) of *G. phoenesis* from Santa Elina, Central Brazil. Radiocarbon dating in bioapatite ($^{14}C_{bioapatite}$) and converted to collagen ($^{14}C_{collagen}$), calibrated ages, carbon isotopic signature ($\delta^{13}C_{vPDB}$, ‰), proportion of C_3 (piC_3) and C_4 (piC_4) plants consumed, standard niche breadth (B_A), and oxygen isotopic signature ($\delta^{18}O_{vSMOW}$, , ‰).

Sample	Material	Unit	Location	$^{14}C_{bioapatite}$	$^{14}C_{collagen}$	Age cal a BP	$\delta^{13}C$	p_iC_3	p_iC_4	B_A	$\delta^{18}O$
51687	Bioapatite	II2	25C, z = 200 cm	12,690±40	14,547±40	17,450–17,906	−1.8	0.21	0.79	0.50	27.9
51688	Bioapatite	III4	27B, z = 327 cm	18,580±45	22,042±45	25,994–26,395	−3.3	0.31	0.69	0.74	26.2
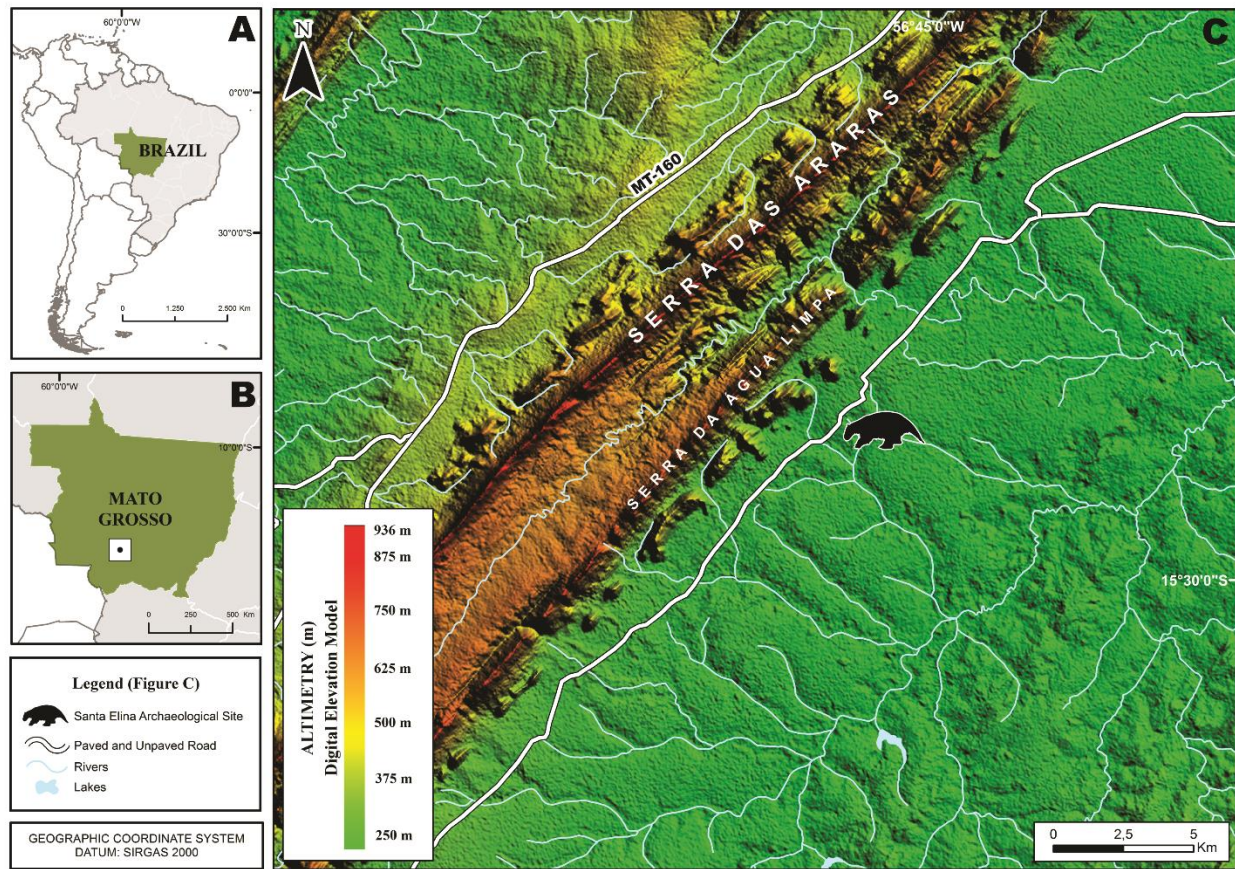
Figure 1. Maps of A) South America, B) Mato Grosso state, Brazil, and C) the Santa Elina archaeological site (15°27′28″S, 56°46′93″W) highlighted before. Graphic figure by Felipe Waldherr, through ArcGIS 10.1 software.
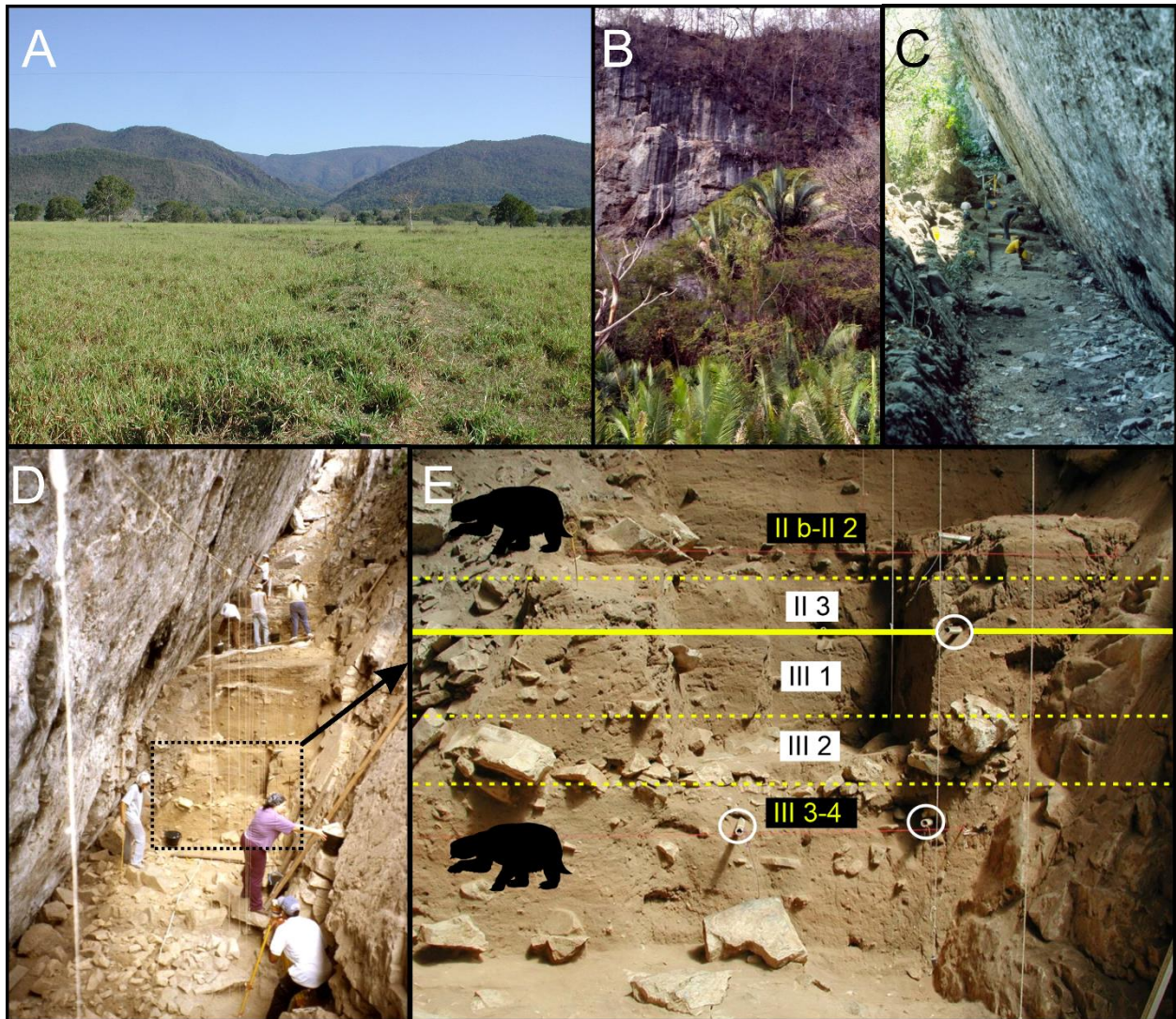
Figure 2. Geographical and stratigraphical context of Santa Elina. A) Serra das Araras landscape. B) Limestone outcrop where the Santa Elina rock shelter is inserted. C–D) Panoramic view of the human occupation and excavation area. E) Zoomed of the stratigraphy of units II and III. The ground sloth silhouettes indicate the archaeological layers (units) where there are remains of ground sloth. All other layers display lithic industry. The white circles indicate the location of instruments where sediments were OSL-dated.
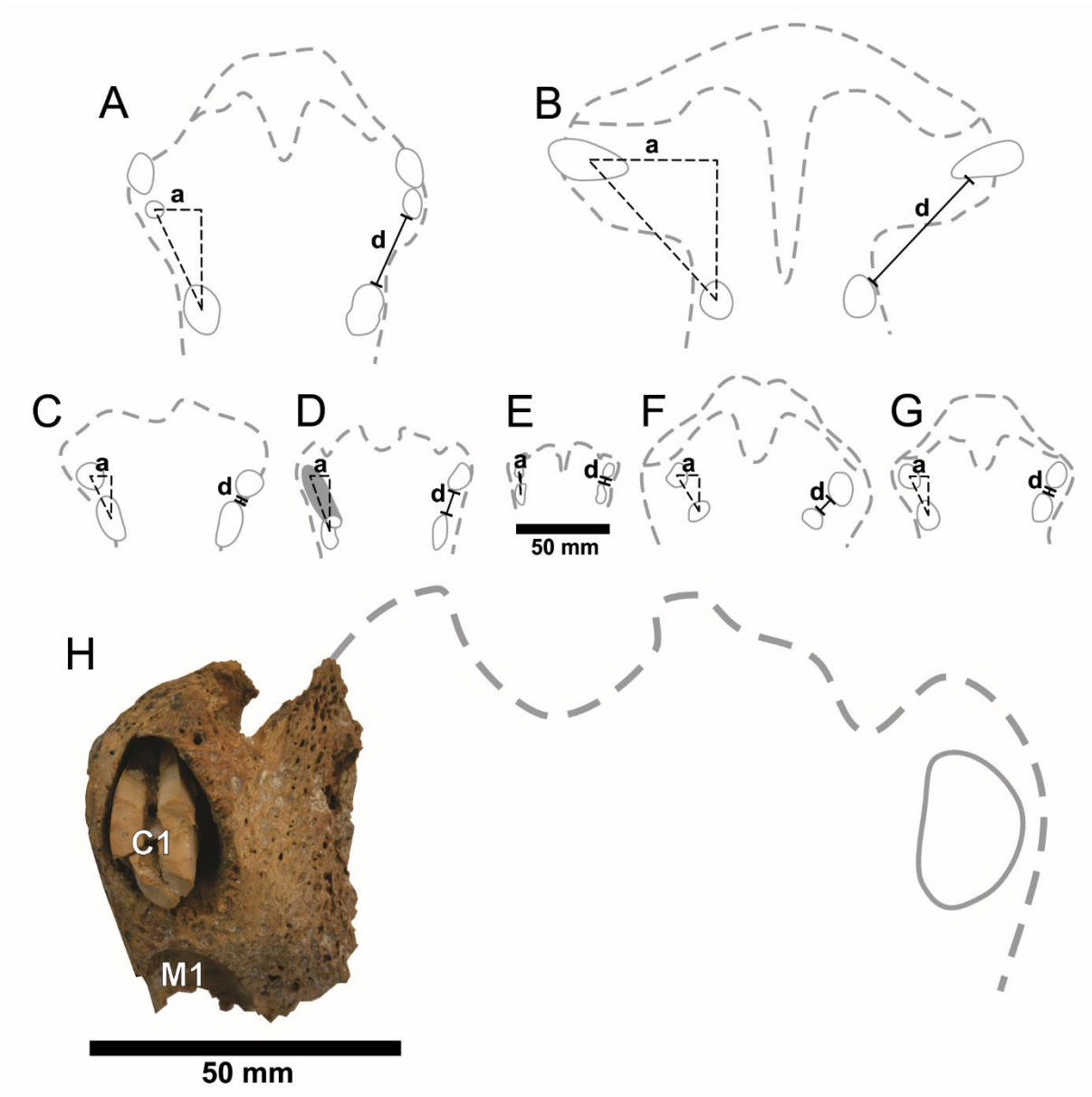
Figure 3. Ventral view of the maxilla, showing the C1 and M1 of (A) *Ocnotherium giganteum*, angle between C1 to M1 (a) = ~24.7º, diastema between C1 and M1 (d) = ~40.1 mm; (B) *Lestodon armatus*, a = ~34.9º, d = ~93.9 mm; (C) *Mylodonopsis ibseni*, a = ~22.6º, d = ~5.2 mm; (D) *Glossotherium phoenesis*, a = ~15.7º, d = ~10.8 mm; (E) *Glosssotherium tropicorum*, a = ~8.2º, d = ~6.7 mm; (F) *Glosssotherium wegneri*, a = ~33.2º, d = ~14.3 mm; (G) *Glosssotherium robustum*, a = ~23.0º, d = ~8.3 mm; and, (H) *Glossotherium phoenesis* from Santa Elina/MT, a = 13.8º, d = 5.6 mm.

33
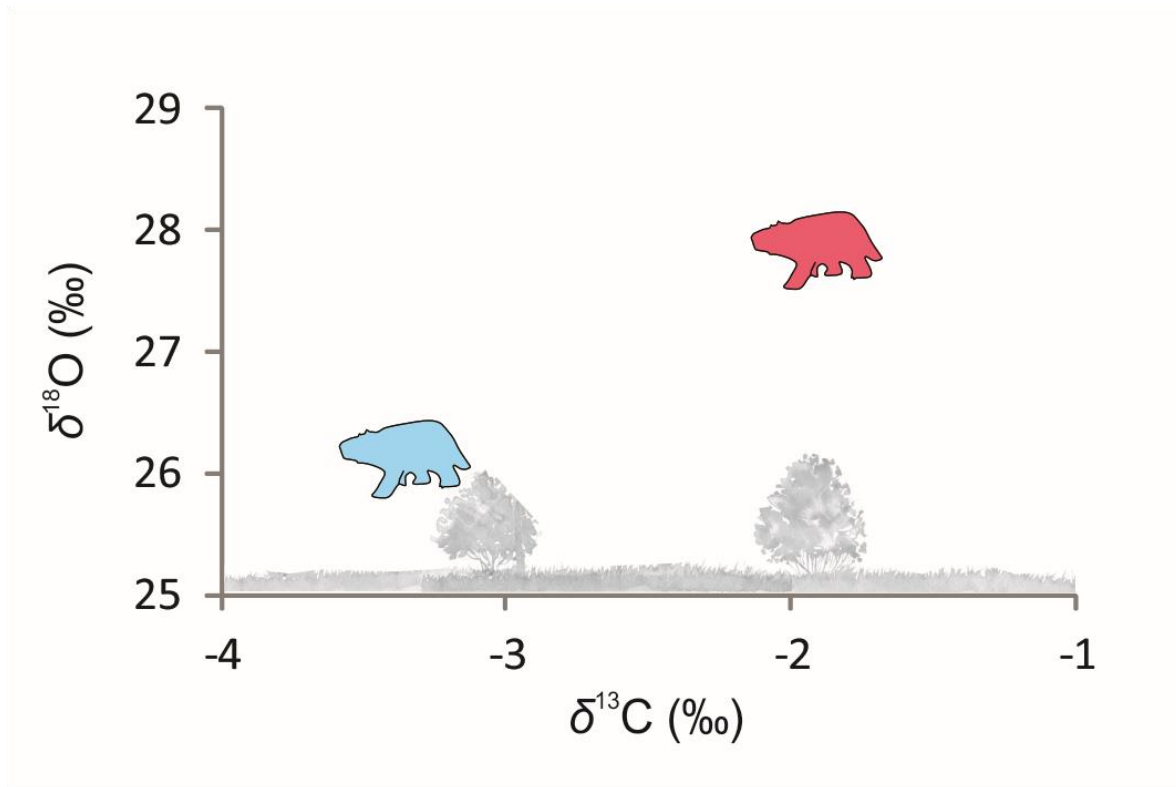
Figure 4. Bivariate plot with $\delta^{13}C_{vPDB}$ and $\delta^{18}O_{vSMOW}$ values of both *G. phoenesis* from Santa Elina, Mato Grosso state, Brazil. The red silhouette indicates the ground sloth from unit II (17,450–17,906 cal a BP), and the blue silhouette indicates the one from unit III (25,994–26,395 cal a BP). Both lived in arboreal savanna habitats.
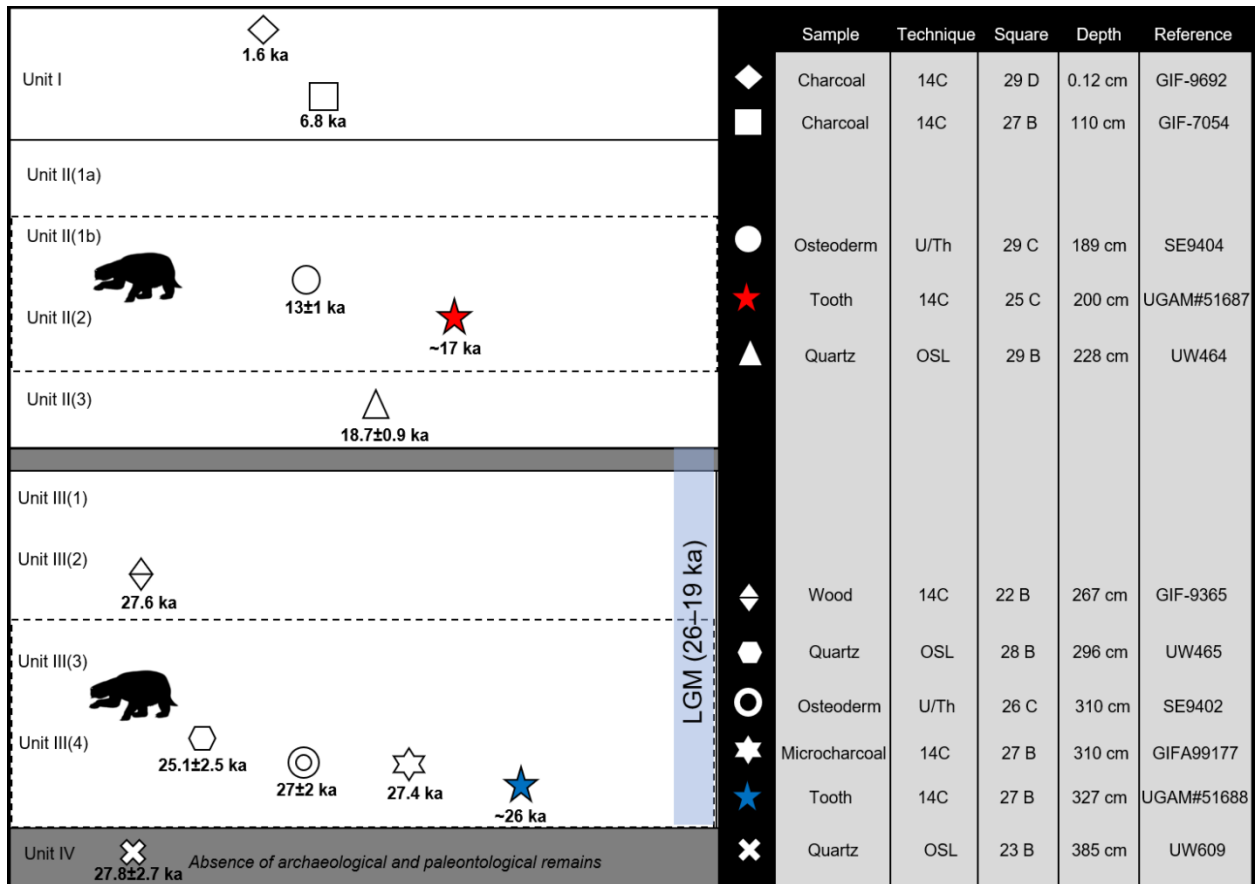
Figure 5. Simplified illustrative scheme of the chronostratigraphy of Santa Elina with main dates of each unit (I-IV). Approximate calibrated ages. Distinct symbols represent dates whose techniques, material, stratigraphic origin (meters and depth), and reference number are detailed in the table to the right (adapted by Vialou et al., 2017). Red and blue stars refer to the new dates resulting from this work. The silhouette of a giant sloth indicates the archaeological layers where there are fossil remains of *G. phoenesis*, both in association with lithic assemblage from human occupations.

3. CHAPTER 3: PAPER 2- HUMAN-MEGAFAUNA INTERACTION
Manuscript submitted to *Proceedings of the Royal Society B: Biological Sciences*.

Evidence of artefacts made of giant sloth bones in Central Brazil around the last glacial maximum

Thaís R. Pansani[a b c], Briana Pobiner[d], Pierre Gueriau[e], Mathieu Thoury[e], Paul Tafforeau[f], Emmanuel Baranger[g], Águeda V. Vialou[h i], Denis Vialou[h], Cormac McSparron[j], Mariela C. de Castro[k], Mário A. T. Dantas[l], Loïc Bertrand[e], Mírian L. A. F. Pacheco[b] *

[a]Programa de Pós-Graduação em Ecologia e Recursos Naturais, Universidade Federal de São Carlos, 13565-905 São Carlos, SP, Brazil
[b]Laboratório de Paleontologia e Astrobiologia, Departamento de Biologia, Universidade Federal de São Carlos, 18052-780 Sorocaba, SP, Brazil
[c]Université Paris-Saclay, ENS Paris-Saclay, CNRS, PPSM, 91190 Gif-sur-Yvette, France
[d]Department of Anthropology, National Museum of Natural History, Smithsonian Institution, 20560 Washington DC, USA
[e]Université Paris-Saclay, CNRS, ministère de la Culture, UVSQ, MNHN, Institut photonique d'analyse non-destructive européen des matériaux anciens, 91192 Saint-Aubin, France
[f]European Synchrotron Radiation Facility, 38043 Grenoble, France
[g]Université Paris-Saclay, ENS Paris-Saclay, CNRS, LMPS, 91190 Gif-sur-Yvette, France
[h]Muséum National d'Histoire Naturelle, 75005 Paris, France
[i]Universidade de São Paulo, 05508-900 São Paulo, SP, Brazil
[j]School of Natural and Built Environment, Queen's University Belfast BT9 5AG, UK
[k]Laboratório de Biologia Integrativa e Conservação, Departamento de Ciências Biológicas, IBiotec, Universidade Federal de Catalão, 75704-020 Catalão, GO, Brazil
[l]Laboratório de Ecologia e Geociências, Instituto Multidisciplinar em Saúde, Universidade Federal da Bahia - Campus Anísio Teixeira, 45029-094 Vitória da Conquista, BA, Brazil

*Mírian Liza Alves Forancelli Pacheco

Email: forancelli@ufscar.br

Abstract

The peopling of the Americas and the human interaction with the Pleistocene megafauna in South America remain hotly debated. The Santa Elina rock shelter in Central Brazil shows evidence of successive human settlements from around the last glacial maximum (LGM) to the early Holocene. Two Pleistocene archaeological layers display rich lithic industry associated with remains of extinct giant ground sloth *Glossotherium phoenesis*. The remains include thousands of osteoderms (i.e., dermal bones), three of which were human-modified. In this study, we perform a traceological analysis of these artefacts by optical microscopy, non-destructive scanning electron microscopy, UV/visible photoluminescence, and synchrotron-based microtomography. We also describe the spatial association between the giant sloth bone remains and stone tools, and provide a Bayesian age model that confirms the timing of this association in stratigraphic successions in Santa Elina. The conclusion that the three giant sloth osteoderms were intentionally modified into artefacts from a fresh carcass by a detailed profilometric study provides evidence

for the contemporaneity of humans and megafauna, and for the human manufacturing of personal artefacts on remains of ground sloths around the LGM in central Brazil.

1. Introduction

(a) Background

Most Pleistocene megafauna (here defined as mammals with body mass > 44 kg (1)) became extinct worldwide by the Pleistocene-Holocene transition. The causes of the decline and eventual extinction of these megamammals in South America are still debated (1). Recent studies have raised new perspectives about human arrival in South America, as well as on its impact on the megafauna (e.g., 2, 3, 4, 5, 6, 7, 8). However, while records for early peopling and hunting megafauna in North America receive broad attention (e.g., (9, 10, 11, 12), scepticism about an earlier human occupation in South America still persists (13). Whereas it is currently well-accepted that peopling of the Americas happened earlier than the Clovis culture (14, 15), the timing and routes of *Homo sapiens* into the continent remain open to debate, likely following multiple routes and time frames, including Pacific coastal and an inland (ice-free corridor) routes (14, 16). In this scenario, late Pleistocene sites containing evidence of early human occupation in South America should be closely scrutinised with interest.

The evidence of human occupation at Santa Elina rock shelter (Mato Grosso State, Brazil) includes a rock panel rich in paintings, including anthropomorphs (e.g., "men with ornaments"), and zoomorphs such as birds, deer, monkeys, and tapir. Dated mineral pigments and bonfire structures associated with stone tools and megafaunal remains found on the shelter provided late Pleistocene to the Holocene ages (7, 17). The only representative of the Pleistocene megafauna present in the shelter are two extinct giant ground sloths of the species *Glossotherium phoenesis* Cartelle, De Iuliis, Boscaini & Pujos, 2019 (18), in two different archaeological layers. Their bone remains are found in a poor state of preservation, and we cannot macroscopically observe any carnivore or cut marks. Along with the giant sloth bones, there are thousands of osteoderms, which are dermal bones embedded within the skin of the animal (19). Three osteoderms from the oldest layer of the shelter have previously been reported to have shapes consistent with anthropogenic modification (7, 17, 20). However, no deep investigation on the nature of these osteoderms has been performed to date.

Human modification of bone, teeth, and shells for ornamentation purposes may reflect social identity, and are commonly found in archaeological contexts from the Paleolithic worldwide (e.g., 21, 22, 23, 24). However, these records are rare in the late Quaternary of South America. Previous publications on Santa Elina have demonstrated the relevance of this archaeological site for documenting human settlement in South America. Here, we provide maps of the spatial and temporal distribution of megafaunal artefacts and bones at Santa Elina and conduct the first detailed macroscopic and microscopic study of the anthropogenically modified osteoderms from this site in order to test the following hypotheses: (1) humans and megafauna cohabitated around the last glacial maximum (LGM) in South America; (2) humans modified giant sloth bones for cultural purposes other than subsistence. We provide a detailed investigation using advanced non-destructive techniques. Our results offer new insights into human-megafaunal interactions in Pleistocene South America and the cultural behaviour of some of the continent's earliest inhabitants.

(b) Archaeological context

The Santa Elina rock shelter in Central Brazil (15°27′28″S, 56°46′93″W) is located in Serra das Araras, a Precambrian geomorphological unit (7) (Figure 1A). Excavations at the site have revealed successive human occupations, layered in four main units (Figure 1B). Three methods (radiocarbon, U/Th, and optical stimulated luminescence (OSL) have been used to date bone, charcoal, wood, and quartz samples of Santa Elina. Detailed information about the archaeological layers and dating methods used to determine the age of the deposits can be found in previous publications (e.g., (7)) and in our electronic supplementary material (Text S1). Fossil bones of ground sloths occur only in two layers (Units II2 and III4; Figure 1C), both in clear

association with archaeological material, including stone tools and other mineral and rock artefacts. The modified osteoderms discussed here were recovered in Unit III4, at depths of 306 cm, 319 cm, and 323 cm. OSL dating of quartz (z = 296 cm) dates this Unit to 25.1±2 thousand years ago, whereas U/Th dating of osteoderm (z = 310 cm) dates the same Unit to 27.0±2 thousand years ago, and radiocarbon dating of microcharcoal from the same depth to 27,402 BP (7). Unit III is separated from Unit II by a layer of limestone blocks and the absence of fireplace structures, lithics, or faunal remains (Figure 1B). The only difference between Units III1 and III2 to III3 and III4 is based on sediment characteristics and archaeological content, and on that the two latter Units bear traces of illuviation (7), but do not present vertical contamination. The rich and diverse archaeological assemblage of Santa Elina includes human-made flakes of limestone bearing evident micro-retouch (Figure 1D), calcite flakes, and quartz and silex items, some of which could have been used by humans to perform bone surface alterations (Figure 1D; (7)).

2. Results and Discussion

(a) Antiquity and human-megafauna association in Santa Elina

An OxCal 4.4 was built to calibrate and model the radiocarbon, OLS and U/Th dates from Santa Elina using the chronological information obtained from the site stratification (see Tables S1-3 and Text S2; electronic supplementary material). The acceptable threshold in OxCal4.4 for an agreement index is 60%. The OxCal 4.4 model for Santa Elina has an agreement index of 101.9%, which shows that the stratigraphic model and the dating evidence are compatible with each other (Figure 2). The model considers that the units from Santa Elina represent successive stratigraphic phases, with one ending before another begins. Bayesian analysis in OxCal estimates that the human activity at Santa Elina started before the LGM. The beginning of Unit III dates to between 28,743–26,536 BP (Unit III; 95.4% probability), with Unit II commencing sometime between 24,922–16,880 BP (95.4% probability), likely between 21,473–17,778 BP (68.3% probability) and extending through the end of the Pleistocene into the Holocene, ending between 7,947 and 7,714 BP (95.4% probability). Deposition of the youngest Unit (I) started between 7,901 and 7,656 BP, and possibly continued into the modern era with two samples samples dated as recent, which are likely only a very few centuries old (see Text S3, Tables S2-3; electronic supplementary material). 2D and 3D georeferenced maps of elements from Santa Elina support the human activity, in the form of stone tools and other lithic artefacts, associated with remains of *G. phoenesis* in the two distinct periods of occupation during the late Pleistocene (see Text S1 and Figure S3, electronic supplementary material). Through the 2D spatial distribution of the osteoderms, it is possible to observe unusual accumulation of osteoderms in specific loci that might be related to intentional disposal (> 1,000 elements in per m^2; Figure S4; electronic supplementary material). However, more efforts are needed to elucidate the taphonomic history of Santa Elina, including studies on the weathering stages of the ground sloth bones, which has not yet been undertaken. The lack of meticulous investigation of the sedimentary context of Santa also demands further efforts.

(b) Human and rodent modification of giant sloth osteoderms

Here we provide evidence that the three giant ground sloth osteoderms from Unit III4 of Santa Elina (SEI6059, SEI6557, and SEI6386) were anthropogenically modified. The combination of different magnification and imaging techniques allows observation of the polished appearance and use-wear traces around the bone surfaces and hole perforations. The presence of several marks from human modification, including drilled perforations, polishing, multi-directional scratches, and use-wear traces (Figures 3-5, Figures S11-13; electronic supplementary material) suggests their anthropic nature and extensive use. We document the smoothing of the surface; traces of stone tool interaction with bone, including incisions and scars, scraping marks, scratches, percussion notches, polish, and gloss; use-wear smoothing of the rim and the attachment systems; and animal-inflicted modifications on the three osteoderms (Figures 3-5 Figures S11-S13; electronic supplementary material). These observations show that these three osteoderms were modified by humans into artefacts, probably personal ornaments. Two osteoderms (SEI6557 and SEI6386) present a circular perforation that goes through the bone, with a well-defined and

regular rim and scars along the edges showing the development of a deliberate human manufacturing process. One osteoderm (SEI6059) has two broken holes on its borders; this osteoderm appears polished and flattened on its whole surface and has been modified and shaped to be thinner than others with one side more polished and smoothed than the other, and one hole larger than the other in opposite and symmetric portions of the bone (Figure 3, Figure S13; electronic supplementary material). The osteoderm SEI6386 presents a remarkable concave area on one of the sides of its perforation hole. SEI6557 presents a similar pattern. We attribute these deformations to use-wear, possibly due to string interaction or suspension in the attachment system. Osteoderm SEI6557 has a unique shape, with the hole perforation connected to an elongated structure that we interpret as probably deformed ancient grooves of the natural osteoderm. These grooves may naturally intersect with foramina on both sides of the bone (see microscopic images of FR3B in Figure S5; electronic supplementary material). The morphological difference between natural foramina and intentionally perforated holes can be seen both macroscopically and microscopically (Figure S5-8; electronic supplementary material).

Unmodified mylodontid osteoderms show a naturally rough external surface (18, 19), notably different from the smooth polished surfaces of the human-modified osteoderms. Within the thousands of fossil osteoderms on the site, the perforated and polished state of the three osteoderms studied here is exceptional (see Text S5, Table S11; electronic supplementary material). Superficial pits and vascular foramina are present on the external surface of some, but not all, osteoderms of *G. phoenesis* from Santa Elina. When present, they penetrate the bone tissue and appear significantly smaller than the human perforated holes (see Figure S5-6; Table S12; electronic supplementary material). We hypothesise that the natural foramina may have been used as a starting point for the perforation process operated by humans. Analyses of the perforation morphology allow us to exclude natural processes as possible agents of modification. Bioerosion traces generally produce shallow circular holes and chambers with eroded morphology and deformed or coarse rims, and mainly reach the internal spongy structure (25). They are significantly different from the smooth, well-delimited rim of the perforations here described (see Text S5; electronic supplementary material). Armadillo osteoderms perforated by flea parasites present a conic section of their irregularly shaped hole morphology, and have a heterogeneous and corroded appearance (26). The osteoderm artefacts from Santa Elina also do not present the cracked surface and 'torn-like' appearance resulting from digestion or regurgitation (27). We also note that the osteoderm SEI6059 presents one side more polished than the other (which is not expected in the case of a digestion product). In addition, the well-preserved and distinguishable features of scraping and incision marks would likely have been erased with acidic corrosion, as can occur with cut marks on bones reported in previous studies (28, 29). Thus, we reject the possibility of natural or non-human causes of modification of these osteoderms.

The human-made perforation holes of osteoderms SEI6386 and SEI6557 are polished and worn (Figures 4-5, Figures S11-13; electronic supplementary material). While it is still possible to identify remaining traces from scraping and intentional drilling, they are in general extremely worn, which has erased most of the rough internal damage that was likely induced by the perforation process; still, the use-wear traces are visible. This smoothing could be explained by the osteoderms being suspended as pendants, or a substantially long period of use (e.g., contact with solid or softer organic material, other ornament beads, clothes, skin, etc.), which has been documented in previous experiments (30) and for other ancient ornaments (e.g., 31, 32, 33, 34). The holes exhibit the same homogenous colour as the rest of the osteoderms' outer surfaces (Figures S10-12; electronic supplementary material), suggesting that the modifications occurred prior to the final burial of the osteoderms, rather than being created afterwards on already fossilised bones.

Bone damage and human modification marks on the surface of highly modified osteoderms were studied in detail from 3D reconstructions generated from SR-μCT (Figures 3G-J, Figures 4O-S, Figures 5O-R, and videos in electronic supplementary material). Direct visualisation of the retouched and sharp edges in SEI6557, and intensive deformation of the rim evidenced by the concave surface in osteoderm SEI6386 (Figure 4R), are possible on the 3D volumes of SR-μCT, thus overcoming the limitations of conventional surface profilometry. The concave use-wear traces observed in the osteoderms SEI6386 and SEI6557, although less intense in the latter, may be attributed to interaction with strings, clothes, or pressure against other pieces (31, 32, 33). The double perforated osteoderm (SEI6059) and the single perforated osteoderm (SEI6386) were found in a broken state, which may be related to having been lost or

discarded after being worn (35). Indeed, experiments show that only months are enough for wearning, deformation, and breakage of attached ornaments (e.g., 36). All the characteristics meticulously observed in the modified osteoderms from Santa Elina suggest that they were used as ornaments. However, further technological and ethnographical studies of these artefacts are encouraged to allow a more precise interpretation of their exact function.

We tested another, rarely exploited property of fossil bone materials: the UV/visible photoluminescence (PL) response of their constitutive minerals. The composition of altered apatite minerals such as those found in bones and soft tissue remains (e.g., fossilised collagen and muscle fibres) is modified during weathering or diagenesis. Substitutions by elements from percolating fluids (e.g., by rare earth elements, F, Mn, Fe or Sr), as well as structural defects formed in the crystallites, can be mapped and studied by photoluminescence (see (37,38) and references therein). While biological apatites generally show a weak PL signal, these defects can result in intense and specific PL emissions in ancient apatites. PL contrasts in a sample can be tested to recover information about its taphonomic history. False colour PL images (see *Methods*) highlight the differences between osteoderms (Figure 6). To further explore the contemporaneity of the perforation, we experimentally modified an ancient osteoderm (SEI8004, perforated and polished by our team). PL shows a high contrast between the low luminescent osteoderm surface and the new perforation, which emits strongly at 514±15 nm under excitation at 385 nm (Figure 6, Text S6; electronic supplementary material). This demonstrates a significant difference between the chemical composition of the patina formed over a very long period of time and the subsurface revealed by experimental modification. In contrast, the two modified osteoderms SEI6557 (Figures 4A-B) and SEI6386 (Figures 5A-B) show uniform luminescence along the hole and anthropogenic marks with little or no detectable difference in hue. In SEI6386, the only variation observed in the PL signal occurs in the area consolidated with glue. These observations indicate that, while recent human perforations expose a less altered internal bone structure and mineralogy than the osteoderm surface, anthropogenically modified osteoderms display a homogenous composition of surface defects. This suggests a homogenous history of the surface of anthropogenically modified osteoderms, i.e., ancient modifications and marks that were made before fossilisation, most likely before burial, while the osteoderms were in a "fresh state" according to the definition of (39). Most interestingly, PL imaging of the flat, smooth human-modified osteoderm SEI6059 reveals that its most intensively scraped and polished flat surface exposes histological features, such as the networks of over-crossing mineralised fibre bundles in variable orientation and vascular foramina pits (Figure 3, Figure S13M; electronic supplementary material). This is direct evidence that human intervention and ancient use of this osteoderm abraded the osteoderm material down to deep histological levels, the detailed morphology of which has been preserved to this day.

Traces of non-human ecological interaction, such as rodent gnawing marks, are commonly found on osteoderms from Santa Elina. These marks are visible even macroscopically along the edges of osteoderm FR10 from Santa Elina, in two sets along the edges of the ornament SEI6059 (Figure 3B, Figure 3H), and on the surface of SEI6386 (Figure 5L). Broad, shallow, flat-bottomed, elongated parallel pairs of grooves of rodent gnawing, consistent in size and shape along the bone edges, also exhibiting internal but shallow microstriations, were observed in osteoderm FR10 using macroscopic and microscopic visualisation with SEM (Figure S14; electronic supplementary material). Repeated rodent gnawing in a restricted area may result in deep and wider grooves (40; Figure 5L). The presence of morphological features, such as foramina pits and natural depressions, surrounded by rodent gnawing marks, led to a uniform luminescence in PL imaging in FR10 (Figure S14B; electronic supplementary material). Rodents tend to gnaw on carcasses in fresh/dry state, mainly to obtain minerals from the bone and wear their teeth (41). The rodent gnawing on the edges of a flat artefact (SEI6059) indicates pre-burial modification of fresh bone. The uniform pattern observed using PL supports the hypothesis that osteoderm FR10 was gnawed by rodents in a fresh state and corroborates our interpretation that the human-induced modifications were created on osteoderms in a fresh state, due to similar PL behaviour. The PL behaviour in osteoderm SEI6386 (Figures 5A-B, Figure 6C) revealed a uniform chemical contrast in the hole perforation, rodent marks (Figure 5L), and other marks here identified as anthropogenic modifications. The uniform chemical contrast observed in the anthropic marks, hole perforation, and mineralized bone surface of the osteoderm SEI6557 provides a similar interpretation (Figure 4A-B).

3. Final Remarks

Detailed imaging and traceological analyses on three anthropogenically-modified osteoderms of the giant ground sloth from layers dated to around the LGM in Santa Elina show direct evidence for human modification of these bones and personal use of them. The different techniques and magnifications applied, as well as the combination of the criteria analysed (the morphology of the perforation holes and bone surface modifications, the environmental/archaeological context with a rich lithic industry, and the absence of other large faunal remains such as carnivores that might have inflicted bone surface modifications) all support our identification of human modification of three giant sloth osteoderms. These are, so far, the only record of presumably personal artefacts from the LGM in the Americas. Their unique and diverse shapes, hole perforation sizes, and presence of diverse anthropogenic traces suggest that different tools and techniques could have been employed during the production and finishing process of the final artefacts. The worn hole perforations and deformed surfaces, as well as attachment systems and use-wear traces, suggest their extensive use, probably as suspended ornaments. Their rarity (three artefacts among thousands of osteoderms) and the broken condition of two of them suggest that they may have been lost or intentionally discarded because of breakage. This rarity is also explained as personal items are generally taken along when people leave their settlements (42). Based on the zooarchaeological context of Santa Elina, we conclude that the most parsimonious scenario is that humans collected and modified the osteoderms of the ground sloth exposed on the shelter floor, used the artefacts during their occupation and/or use of the shelter, and subsequently lost or discarded the artefacts in the shelter. However, we recognise the possibility that these three osteoderms could have been obtained and modified from a different ground sloth individual elsewhere, transported to Santa Elina, and then lost or discarded there. In this scenario, the human modification of these three osteoderms would bear no relationship with the ground sloth skeleton found in Unit III4 of Santa Elina. However, this scenario would still have ramifications regarding the complex symbolic behaviour of early human populations of the region. The movement of cultural artefacts over long distances suggests potential exchange networks and the symbolic value of these objects in their communities (43, 44). We cannot evaluate whether this alternative scenario is accurate for the three modified osteoderms found at Santa Elina with the evidence we provide in this study. Additional evidence and research, such as use-wear and residue analyses on the stone tools from Unit III4, still absent for Santa Elina, would be needed to elucidate if the production of these bone artefacts was made locally.

This study contributes to discussions on the peopling of the Americas and possible human interaction with the Pleistocene megafauna in South America (e.g., (5, 8, 45)). It is widely accepted that the humans' dispersal in the Americas occurred earlier than the Clovis culture expansion (46). Evidence of human occupation before 15,000 BP in South America is discussed in light of sites such as Monte Verde in Chile (8), Arroyo Seco 2 and Campo Laborde in Argentina (47), Huaca Prieta in Peru (48), and Taima-Taima in Venezuela (49). Although peopling of the Americas prior to the LGM (~19–26 ka, (50)) has been contested (e.g., 46), recent discoveries suggest human occupation and megafauna butchery in the Americas before 30,000 BP, such as at the Hartly mammoth locality in New Mexico, USA (51) and Arroyo del Vizcaíno in Uruguay (5). However, the proposed pre-LGM human presence in Arroyo del Vizcaíno has been disputed (52). The Cerutti Mastodon site in California, USA, stands out as an even more controversial site which has been suggested to present evidence for human presence and megafauna butchery during an interglacial period (~130,000 BP; (53)), but this evidence has been also contested by several authors (e.g., 54, 55, 56).

Santa Elina challenges mainstream claims on peopling of the Americas, in favour of a model in which people first reached out to the American continent during, or even earlier than, the LGM. It agrees with other pre-LGM sites in North America, such as the Bluefish Caves in Canada (9, 10), the White Sands National Park in New Mexico, USA (11, 57), and the Chiquihuite Cave in Mexico (12), which has retouched artefacts similar to the ones found in Unit III of Santa Elina (58). It also agrees with the suggested early human presence in other sites in South America, such as localities at the Serra da Capivara National Park in northeast Brazil (3, 4, 59, 60, 61). It agrees with the interpretation of some authors that the scarcity of archaeological evidence of pre-LGM sites in the Americas may be explained by an initial settlement occurring earlier than the introduction of elaborate stone technology in the continent (51), and that pre-LGM hunter/gatherers populations were probably affected by climate pressures and remained at low densities until their wide dispersal after the deglaciation (62).

The evidence of the anthropic modification of giant sloth osteoderms during the LGM supports the hypothesis that humans were in South America thousands of years before the extinction of the Pleistocene megafauna in the continent. Together with the presence of another giant sloth individual in a more recent level of the site (Unit II2), this evidence might suggest that the human presence in South America likely was not the main agent responsible for the megafauna extinction. It agrees with (62), which claims that it would have taken thousands of years for hunter/gatherers populations to expand and dominate this vast and diverse continent. Further investigations, including a detailed taphonomic study on the ground sloth bone assemblage from Santa Elina, should clarify this palaeoecological discussion.

Our contribution reinforces Santa Elina as a pivotal site in the scientific debate on human occupation and megafaunal bone modification in the late Pleistocene of South America. The human intervention on giant sloth fresh bones at Santa Elina can be summarized as: i) the archaeological context and association of giant sloth remains with cultural elements from human occupations in two periods of the late Pleistocene (7); ii) the anthropic modification of giant sloth' osteoderms from a layer dated to the early LGM, evidenced by intentional shaping and perforation of these bones; iii) the interpretation of these modified osteoderms as artefacts due to use-wear traces and smooth deformations, likely used as personal ornaments; and iv) evidence that these modifications were performed on fresh or semi-fresh osteoderms, prior to the burial and fossilisation of the giant sloth bone remains, during the last glacial period.

4. Materials and Methods

(a) Bayesian age model

35 radiocarbon, OSL, and U/Th dates from Santa Elina, spread through four stratigraphic units (I-IV) (Table S1; electronic supplementary material), were modelled and calibrated with OxCal 4.4, using the SHCal20 calibration curve (63) (see Text S2; electronic supplementary material). The clear and well-understood stratigraphy of Santa Elina (7) allows the model of this site to be easily created in OxCal. OxCal cannot *prove* that a model is correct, more than one possible model can fit the data, but it can reject models which are incompatible with the radiocarbon evidence. In addition to being able to tell which models are compatible with the radiocarbon evidence, OxCal has a number of tools for estimating the start, end, or span of defined phases (Text S2; electronic supplementary material).

(b) Taphonomic aspects of giant sloth osteoderms

We provide, for knowledge and comparison, images of the morphology of 19 osteoderms from Santa Elina without intentionally modified marks (Figure S5-6; electronic supplementary material). We compare the three fossil osteoderms that we confirm as human-modified (specimens SEI6059, SEI6557, and SEI6386) with one natural osteoderm (specimen FR3A), one osteoderm exhibiting rodent tooth marks (specimen FR10), one osteoderm with bioerosion damage (specimen FR6), and one osteoderm experimentally modified into an ornament (specimen SEI8004, see details in Text S5; electronic supplementary material), at micro- and macroscales using scanning electron microscopy (SEM), photoluminescence (PL) multispectral imaging, and synchrotron-based X-ray microtomography (SR-µCT). Identification of the agent of bone surface modifications (e.g., bioerosion, rodent gnawing, trampling marks, anthropogenic marks, and use-wear traces) relied on established signature criteria following in particular references (31, 32, 33, 40, 41, 64, 65).

Microscopic images were taken using optical microscopes (Leica), a stereomicroscope Nikon SMZ-25, and a scanning electron microscope. SEM images were collected using two microscopes: (1) low vacuum (~50–70 Pa) with an acceleration voltage of 15 kV, using the Zeiss supra 55VP FEG-SEM at the IPANEMA laboratory, with a Variable Pressure Secondary Electron detector (VPSE, default) or an Angle Selective beam detector (AsB, where noted); and (2) low vacuum with an acceleration voltage of 15 kV using the TM3000 Tabletop microscope Hitachi at the Laboratório de Pesquisa em Bioenergia e Materiais Lignocelulósicos, UFSCar.

PL multispectral macro- and micro-imaging were performed using a prototype setup developed by IPANEMA, allowing for the collection of reflection and luminescence images in the UV, visible and near-infrared spectral ranges (66). We collected luminescence emissions in the blue (472 nm), green (514 nm), yellow (571 nm), and red (685 nm) domains under UV (385 nm) illumination. The resulting greyscale images were combined into false colour RGB images using ImageJ. False colour RGB images presented here were produced using two settings: red—emission at 685 ± 20 nm, green—emission at 571 ± 36 nm, blue—emission at 514 ± 15 nm for SEI6557, SEI6386, and SEI8004 (Figure 4A-B, Figure 5A-B, Figure 6A and Figure 6C), and red—emission at 685 ± 20 nm , green—emission at 571 ± 36 nm, blue—emission at 472 ± 15 nm for SEI6059, FR3A, and FR10 (Figure 3A-B, Figure S6B, Figure S14B; electronic supplementary material).

Synchrotron-based X-ray μCT was performed on the three modified fossil osteoderms at the BM05 beamline of the European Synchrotron Radiation Facility synchrotron using a polychromatic beam with a detected average energy of 75 keV. This energy was obtained by filtering the white beam from the 0.85 T dipole wiggler source with 50 mm of SiO_2 (as a series of 10 bars of 5 mm of diameter used to homogenise vertically the beam power profile) and 2.3 mm Al. Scans were performed using 6,000 projections over 360° using a detector configuration giving a pixel size of 3.9 μm (500-μm thick LuAg:Ce scintillator coupled to a PCO edge 4.2 CLHS sCMOS camera using a zoom optic based on a Canon 65 mm MP-E f/2.8 supermacro objective). The sample-to-detector distance was fixed at 1.4 m in order to have propagation phase contrast effect to reveal fine internal and external details. The available field of view was extended horizontally by positioning the rotation axis off-centre and extended vertically by recording a series of acquisitions with vertical movement of the sample. The volume (3.9 μm isotropic voxel size) was reconstructed from the radiographs by using a filtered back-projection algorithm implemented in PyHST2 software (67), with a single distance phase retrieval algorithm (68). 3D rendering was performed using 3DSlicer (https://www.slicer.org/). We generated a false colour overlay of the median and standard deviation projections of 40 tomograms using ImageJ, displayed as levels of green and blue respectively (Figure 3K).

Acknowledgments

References

1. Koch PL, Barnosky AD. 2006 Late Quaternary extinctions: state of the debate. *Annu. Rev. Ecol. Evol. Syst.* 37, 215–250. (doi:10.1146/annurev.ecolsys.34.011802.132415)
2. Prado JL, Martinez-Maza C, Alberdi MT. 2015 Megafauna extinction in South America: A new chronology for the Argentine Pampas. *Palaeogeogr. Palaeoclimatol. Palaeoecol.* 425, 41–49. (doi: 10.1016/j.palaeo.2015.02.026)
3. Lahaye C *et al.* 2013 Human occupation in South America by 20,000 BC: the Toca da Tira Peia site, Piauí, Brazil. *J. Archaeol. Sci.* 40(6), 2840–2847. (doi:10.1016/j.jas.2013.02.019)
4. Boëda E *et al.* 2014. A new late Pleistocene archaeological sequence in South America: the Vale da Pedra Furada (Piauí, Brazil). *Antiquity* 88(341), 927–941. (doi:10.1017/S0003598X00050845)
5. Fariña RA *et al.* 2014 Arroyo del Vizcaíno, Uruguay: a fossil-rich 30-ka-old megafaunal locality with cut-marked bones. *Proc. R. Soc. B: Biol. Sci.* 281(1774), 20132211. (doi:10.1098/rspb.2013.2211)
6. Dillehay TD *et al.* 2015 New archaeological evidence for an early human presence at Monte Verde, Chile. *PLoS One* 10(11), e0141923. (doi:10.1371/journal.pone.0145471)
7. Vialou D, Benabdelhadi M, Feathers J, Fontugne M, Vialou AV. 2017 Peopling South America's centre: the late Pleistocene site of Santa Elina. *Antiquity* 91(358), 865–884. (doi:10.15184/aqy.2017.101)
8. Politis GG, Messineo PG, Stafford Jr TW, Lindsey EL. 2019 Campo Laborde: a Late Pleistocene giant ground sloth kill and butchering site in the Pampas. *Sci. Adv.* 5(3), eaau4546. (doi: 10.1126/sciadv.aau4546)
9. Bourgeon L, Burke A, Higham T. 2017 Earliest human presence in North America dated to the last glacial maximum: new radiocarbon dates from Bluefish Caves, Canada. *PLoS One* 12(1), e0169486. (doi:10.1371/journal.pone.0169486)
10. Bourgeon L. 2021 Revisiting the mammoth bone modifications from Bluefish Caves (YT, Canada). *J. Archaeol. Sci. Rep.* 37, 102969. (doi:10.1016/j.jasrep.2021.102969)
11. Bustos D *et al.* 2018 Footprints preserve terminal Pleistocene hunt? Human-sloth interactions in North America. *Sci. Adv.* 4(4), eaar7621. (doi:10.1126/sciadv.aar7621)
12. Ardelean CF *et al.* 2020 Evidence of human occupation in Mexico around the Last Glacial Maximum. *Nature* 584(7819), 87–92. (doi:10.1038/s41586-020-2509-0)
13. Boëda E, Pérez-Balarezo A, Ramos MP. 2022 Another "Critique," Same Old Song: A Brief Rebuttal to Gómez Coutouly. *PaleoAmerica* 8(1), 53–61. (doi:10.1080/20555563.2021.1985051)
14. Braje TJ *et al.* 2019 Fladmark + 40: What Have We Learned about a Potential Pacific Coast Peopling of the Americas? *Am. Antiq.* 85(1), 1–21. (doi:10.1017/aaq.2019.80)
15. Politis G, Prates L. 2019 The pre-clovis peopling of South America. *The SAA Archaeol. Rec.* 19(3), 40–44. (ISSN:1532-7299)
16. Potter BA *et al.* 2018 Current evidence allows multiple models for the peopling of the Americas. *Sci. Adv.* 4(8), eaat5473. (doi:10.1126/sciadv.aat5473)
17. Vialou AV, Vialou D. 2019 Manifestações simbólicas em Santa Elina, Mato Grosso, Brasil: representações rupestres, objetos e adornos desde o Pleistoceno ao Holoceno recente. *Bol. Mus. Para. Emílio Goeldi,* sér. Ciências Humanas 14, 343–366. (doi:10.1590/1981.81222019000200006)

18. Cartelle C, De Iuliis G, Boscaini A, Pujos F. 2019 Anatomy, possible sexual dimorphism, and phylogenetic affinities of a new mylodontine sloth from the late Pleistocene of intertropical Brazil. *J. Syst. Palaeotol.* 17(23), 1957–1988. (doi:10.1080/14772019.2019.1574406)

19. McDonald HG. 2018 An overview of the presence of osteoderms in sloths: implications for osteoderms as a plesiomorphic character of the Xenarthra. *J. Mamm. Evol.* 25(4), 485–493. (doi:10.1007/s10914-017-9415-8)

20. Vialou AV. 1998 Une pendeloque taillée dans un os de *Glossotherium*. Universalis. In: Encyclopaedia Universalis Paris, 267.

21. Hublin JJ *et al.* 2020 Initial upper palaeolithic Homo sapiens from Bacho Kiro cave, Bulgaria. *Nature* 581(7808), 299-302. (doi:10.1038/s41586-020-2259-z)

22. Shunkov MV, Fedorchenko AY, Kozlikin MB, Derevianko AP. 2020 Initial Upper Palaeolithic ornaments and formal bone tools from the East Chamber of Denisova Cave in the Russian Altai. *Quat. Int.* 559, 47–67. (doi:10.1016/j.quaint.2020.07.027)

23. Mannermaa K, Rainio R, Girya EY, Gerasimov DV. 2021 Let's groove: attachment techniques of Eurasian elk (Alces alces) tooth pendants at the Late Mesolithic cemetery Yuzhniy Oleniy Ostrov (Lake Onega, Russia). *Archaeol. Anthropol. Sci.* 13(1), 1–22. (doi:10.1007/s12520-020-01237-5)

24. D'Errico F, Martí AP, Wei Y, Gao X, Vanhaeren M, Doyon L. 2021 Zhoukoudian Upper Cave personal ornaments and ochre: Rediscovery and reevaluation. *J. Hum. Evol.* 161, 103088. (doi:org/10.1016/j.jhevol.2021.103088)

25. Moura JF, Nascimento CSI, de Barros GE, Robbi B, Fernandes MA. 2021 Damaged armour: Ichnotaxonomy and paleoparasitology of bioerosion lesions in osteoderms of Quaternary extinct armadillos. *J. South Am. Earth Sci.* 109, 103255. (doi:10.1016/j.jsames.2021.103255)

26. Hammond H, Lareschi M, Zilio L, Ezquiaga MC, Castro AS. 2014 Placas óseas perforadas de *Zaedyus pichiy* en un contexto arqueológico: ¿Elementos confeccionados antrópicamente o generados por agentes biológicos? Un abordaje interdisciplinario. *Atek Na [En La Tierra]* 4, 9–36.

27. Fernandez-Jalvo Y, Andrews P, Sevilla P, Requejo V. 2014 Digestion versus abrasion features in rodent bones. *Lethaia* 47(3), 323–336. (doi:10.1111/let.12061)

28. Pineda A, Saldié P, Verges JM, Huguet R, Cáceres I, Vallverdú J. 2014 Trampling versus cut marks on chemically altered surfaces: an experimental approach and archaeological application at the Barranc de la Boella site (la Canonja, Tarragona, Spain). *J. Archaeol. Sci.* 50, 84–93. (doi:10.1016/j.jas.2014.06.018)

29. Amadasi A, Camici A, Sironi L, Profumo A, Merli D, Mazzarelli D, Porta D, Duday H, Cattaneo C. 2015 The effects of acid and alkaline solutions on cut marks and on the structure of bone: An experimental study on porcine ribs. *Leg. Med.* 17(6), 503–508. (doi:10.1016/j.legalmed.2015.10.006)

30. D'Errico F. 1993 La vie sociale de l'art mobilier paléolithique. Manipulation, transport, suspension des objets en os, bois de cervidés, ivoire. *Oxf. J. of Archaeol.* 12(2), 145–174. (doi:10.1111/j.1468-0092.1993.tb00289.x)

31. Falci CG, Cuisin J, Delpuech A, Van Gijn A, Hofman CL. 2019 New insights into use-wear development in bodily ornaments through the study of ethnographic collections. *J. Archaeol. Method Theory.* 26(2), 755–805. (doi:org/10.1007/s10816-018-9389-8)

32. Osipowicz G, Piličiauskienė G, Orłowska J, Piličiauskas G. 2020 An occasional ornament, part of clothes or just a gift for ancestors? The results of traceological studies of teeth pendants from the Subneolithic sites in Šventoji, Lithuania. *J. Archaeol. Sci. Rep.* 29, 102130. (doi:10.1016/j.jasrep.2019.102130)

33. Tejero TM, Bar-Oz g, Bar-Yosef O, Meshveliani T, Jakeli N, Matskevich Z, Pinhasi R, Belfer-Cohen A. 2021 New insights into the Upper Palaeolithic of the Caucasus through the study of personal ornaments. Teeth and bones pendants from Satsurblia and Dzudzuana caves (Imereti, Georgia). *PLoS One* 16(11), e0258974. (doi:10.1371/journal.pone.0258974)

34. Vercoutère C, Patou-Mathis M, Giacobini G. 2007 The importance of the paleontological and taphonomical analyses for the study of bone industries. In: St-Pierre CG, Walker RB (Eds). Bones as Tools: Current Methods and Interpretations in Worked Bone Studies, BAR S (1622), 23–34.

35. Gravel-Miguel C. 2011 Exoticism of Portable Art and Ornaments: A Study of Social Networks Around the Last Glacial Maximum. Doctoral Dissertation, University of Victoria.

36. Mărgărit M. 2016 Testing the endurance of prehistoric adornments: raw materials from the aquatic environment. *J. Archaeol. Sci.* 70, 66–81. (doi:10.1016/j.jas.2016.04.009)
37. Waychunas GA. 2012 Apatite Luminescence. *Rev. Mineral. Geochem.* 48(1), 701–742. (doi:10.2138/rmg.2002.48.19)
38. Gueriau P, Mocuta C, Dutheil DB, Cohen SX, Thiaudière D, Charbonnier S, Clément G, Bertrand B. 2014 Trace elemental imaging of rare earth elements discriminates tissues at microscale in flat fossils. *PLoS One 9*(1), e86946. (doi:10.1371/journal.pone.0086946)
39. Knüsel CJ. 2005 The physical evidence of warfare-subtle stigmata? In: Parker-Pearson M, Thorpe IJN (Eds). Warfare, Violence and Slavery in Prehistory. BAR International Series. Archaeopress, Oxford, UK. (1374), 49–65.
40. Shipman P, Rose J. 1983 Early hominid hunting, butchering, and carcass-processing behaviors: approaches to the fossil record. *J. Anthropol. Archaeol.* 2(1), 57–98. (doi:10.1016/0278-4165(83)90008-9)
41. Fernandez-Jalvo Y, Andrews P. 2016 Atlas of taphonomic identifications: 1001+ images of fossil and recent mammal bone modification. (Springer, Dordrecht, The Netherlands) (ISBN:978-94-017-7432-1)
42. Van Gijn AL. 2017 Bead biographies from Neolithic burial contexts: contributions from the microscope. In: Mayer DBY, Choyke AM (Eds). Not just for show: the archaeology of beads, beadwork, and personal ornaments, Oxbow Books, 103–14.
43. d'Errico F, Vanhaeren M, Barton N, Bouzouggar A, Mienis H, Richter D, Hublin JJ, McPherron SP, Lozouet P. 2009 Additional evidence on the use of personal ornaments in the Middle Paleolithic of North Africa. *Proc. Natl. Acad. Sci.* 106(38), 16051–16056. (doi:10.1073/pnas.0903532106)
44. Brooks AS. 2010 What does it mean to be human? A behavioral perspective. *Anthronotes* 31, 1–10.
45. Carlini AA, Carrillo- Briceño JD, Jamines A, Aguilera O, Zurita AE, Iriarte J, Sánchez-Villagra MR. 2022 Damaged glyptodontid skulls from Late Pleistocene sites of northwestern Venezuela: evidence of hunting by humans?. *Swiss J. Palaeontol.* 141(1), 1–14. (doi:10.1186/s13358-022-00253-3)
46. Waters MR. 2019 Late Pleistocene exploration and settlement of the Americas by modern humans. *Science* 365(6449), eaat5447. (doi:10.1126/science.aat5447)
47. Politis GG, Gutiérrez MA, Rafuse DJ, Blasi A. 2016 The arrival of *Homo sapiens* into the Southern Cone at 14,000 years ago. *PLoS One* 11(9), e0162870. (doi:10.1371/journal.pone.0162870)
48. Dillehay TD, Bonavia D, Goodbred SL, Pino M, Vásquez V, Tham TR. 2012 A late Pleistocene human presence at Huaca Prieta, Peru, and early Pacific Coastal adaptations. *Quat. Res.* 77, 418–23. (doi:10.1016/j.yqres.2012.02.003)
49. Bryan A, Casamiquela R, Cruxent JM, Gruhn R, Ochsenius C. 1978 An El Jobo mastodon kill at Taima-Taima, Venezuela. *Science* 200, 1275–1277 (doi:10.1126/science.200.4347.1275)
50. Clark PU *et al.* 2019 The Last Glacial Maximum. *Science* 325(5941), 710–714. (doi:10.1126/science.1172873)
51. Rowe TB, Stafford Jr TW, Fisher DC, Enghild JJ, Quigg JM, Ketcham RA, Sagebiel JC, Hanna R, Colbert MW. 2022 Human Occupation of the North American Colorado Plateau~ 37,000 Years Ago. *Front. Ecol. Evol.* 10, 534. (doi:10.3389/fevo.2022.903795)
52. Suárez R, Borrero LA, Borrazzo K, Ubilla M, Martínez S, Perea D. 2014 Archaeological evidences are still missing: a comment on Fariña et al. Arroyo del Vizcaíno site, Uruguay. *Proc. Royal Soc. B.* 281(1795), 20140449. (doi: 10.1098/rspb.2014.0449)
53. Holen SR *et al.* 2017. A 130,000-year-old archaeological site in southern California, USA. *Nature.* 544(7651), 479–483. (doi:10.1038/nature22065)
54. Braje TJ, Dillehay TD, Erlandson JM, Fitzpatrick SM, Grayson DK, Holliday VT, Kelly RL, Klein RG, Meltzer DJ, Rick TC. 2017. Were hominins in California~ 130,000 years ago?. *PaleoAmerica* 3(3), 200–202. (doi:10.1080/20555563.2017.1348091)
55. Haynes G. 2017 The Cerutti mastodon. *PaleoAmerica* 3(3), 196–199. (doi: 10.1080/20555563.2017.1330103)
56. Sutton MQ, Parkinson J, Rosen MD. 2019 Observations regarding the Cerutti mastodon. *PaleoAmerica* 5(1), 8–15. (doi:10.1080/20555563.2019.1589409)
57. Bennett MR *et al.* 2021 Evidence of humans in North America during the last glacial maximum. *Science* 373(6562), 1528–1531. (doi:10.1126/science.abg7586)

58. Boëda E, Gruhn R, Vialou AV, Aschero C, Vialou D, Pino M, Gluchy M, Pérez A, Ramos MP. 2021 The Chiquihuite Cave, a Real Novelty? Observations about the Still-ignored South American Prehistory. *PaleoAmerica* 7(1), 1–7. (doi:10.1080/20555563.2020.1851500)

59. Boëda E *et al.* 2016 New Data on a Pleistocene Archaeological Sequence in South America: Toca do Sítio do Meio, Piauí, Brazil. *PaleoAmerica* 2(4), 286–302. (doi:10.1080/20555563.2016.1237828)

60. Boëda E *et al.* 2021 24.0 kyr cal BP stone artefact from Vale da Pedra Furada, Piauí, Brazil: Techno-functional analysis. *PLoS One* 16(3), e0247965. (doi:10.1371/journal.pone.0247965)

61. C. Lahaye *et al.* 2019 Another Site, Same Old Song: The Pleistocene-Holocene Archaeological Sequence of Toca da Janela da Barra do Antonião-North, Piauí, Brazil. *Quat. Geochronol.* 49, 223–229. (doi:10.1016/j.quageo.2018.03.006)

62. Gruhn R. 2022 To the end of the world: southern Patagonia in models of the initial peopling of the western hemisphere. In: Miotti L, Salemme M, Hermo D (Eds). Archaeology of Piedra Museo Locality. The Latin American Studies Book Series. Springer, Cham. 449–456. (doi:10.1007/978-3-030-92503-1_16)

63. Hogg AG *et al.* 2020 SHCal20 Southern Hemisphere calibration, 0–55,000 years cal BP. *Radiocarbon* 62(4), 759–778. (doi:10.1017/RDC.2020.59)

64. Olsen SL, Shipman P. 1988 Surface modification on bone: trampling versus butchery. *J. Archaeol. Sci.* 15(5), 535–553. (doi:10.1016/0305-4403(88)90081-7)

65. Blumenschine RJ, Selvaggio MM. 1988 Percussion marks on bone surfaces as a new diagnostic of hominid behaviour. *Nature* 333(6175), 763–765. (doi:10.1038/333763a0)

66. Brayard A, Gueriau P, Thoury M, Escarguel G. 2019 Glow in the dark: use of synchrotron µXRF trace elemental mapping and multispectral macro- imaging on fossils from the Paris Biota (Bear Lake County, Idaho, USA). *Geobios* 54, 71–79. (doi:10.1016/j.geobios.2019.04.008)

67. Mirone A, Gouillart E, Brun E, Tafforeau P, Kieffer J. 2014 The PyHST2 hybrid distributed code for high speed tomographic reconstruction with iterative reconstruction and a priori knowledge capabilities. *Nucl. Instrum. Methods Phys. Res., Sect. B.* 324, 41–48. (doi: 10.1016/j.nimb.2013.09.030)

68. Paganin D, Mayo SC, Gureyev TE, Miller PR, Wilkins SW. 2002 Simultaneous phase and amplitude extraction from a single defocused image of a homogeneous object. *J. Microsci.* 206, 33–40. (doi: 10.1046/j.1365-2818.2002.01010.x)
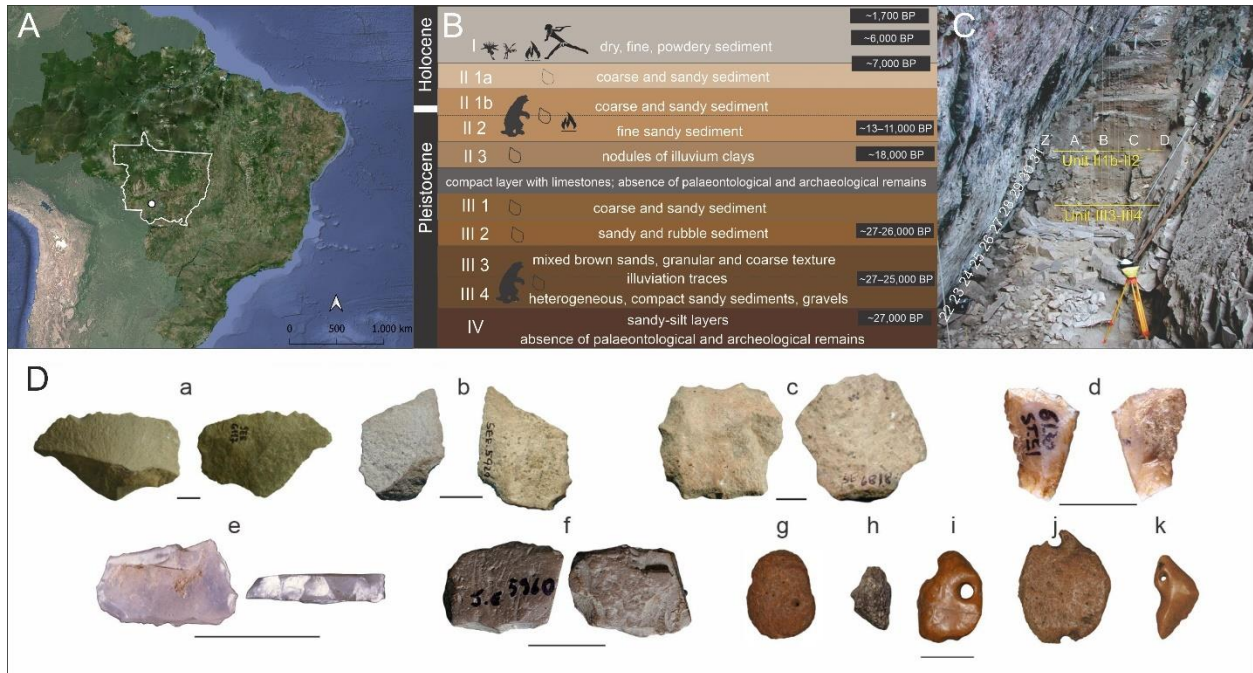
Figure 1. Geological setting and zooarchaeological context of Santa Elina. (*a*) Satellite image of Brazil highlighted in South America showing the location of Santa Elina rock shelter (white dot) in Mato Grosso state (delimited in white). (*b*) Schematic representation of the archaeological layers at the site, indicating the presence of stone tools, ground sloth remains, fire structures, fruit macrofossils, and wall paintings. (*c*) Excavation area. Credit: Águeda Vialou. (*d*) Objects found in association in Unit III4: limestone flakes (*a,b*) and microblade cores (*c*) with micro-retouch, retouched siliceous blade cores (*d,e*), hematite with microwear evidence (*f*), giant sloth osteoderms (*g–k*), including unmodified osteoderm (*g*), possibly burnt bone fragment (*h*) and three osteoderms modified into artefacts (*i–k*). Scale bars: 1 cm.
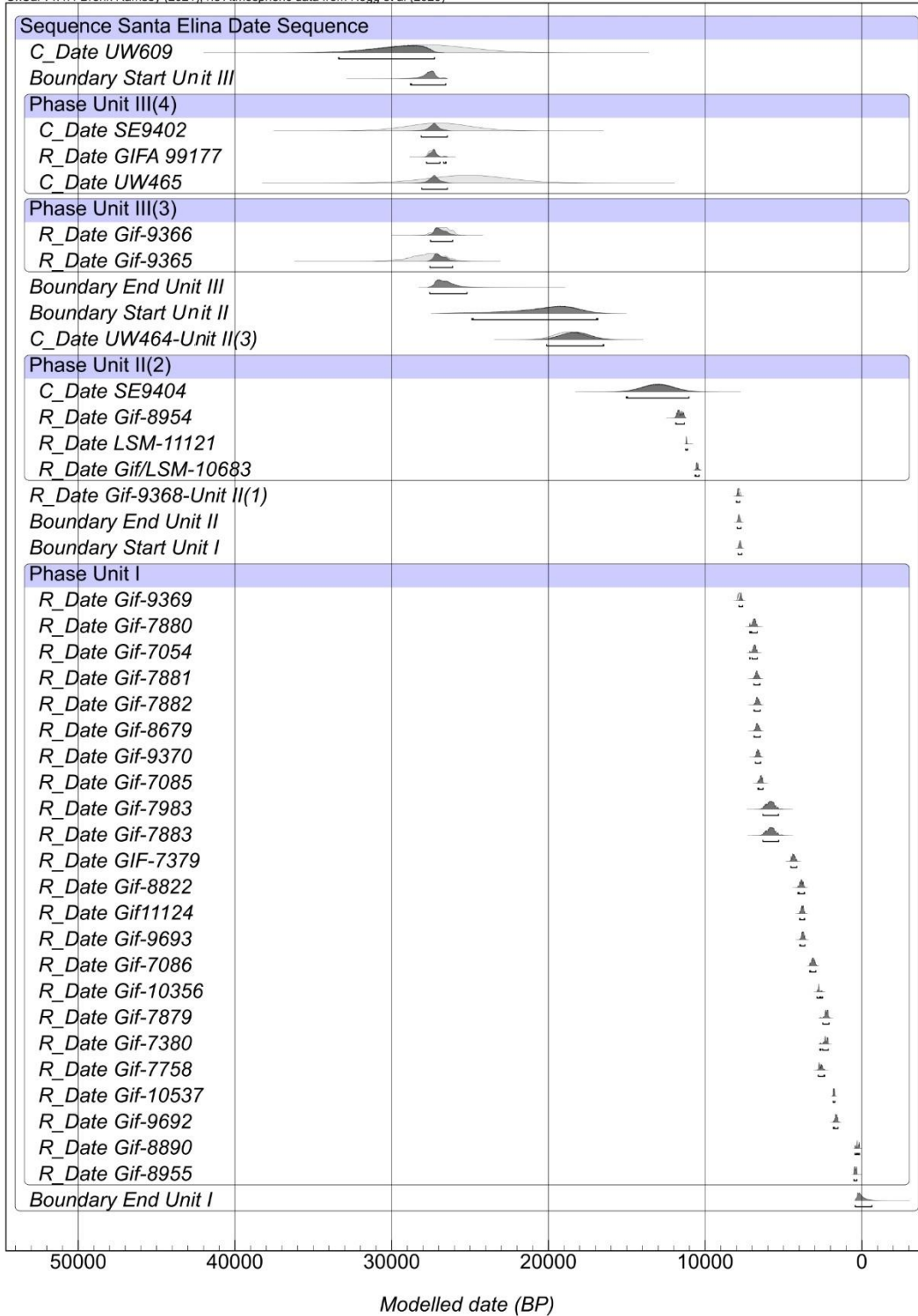
Figure 2. Bayesian age model of Santa Elina.
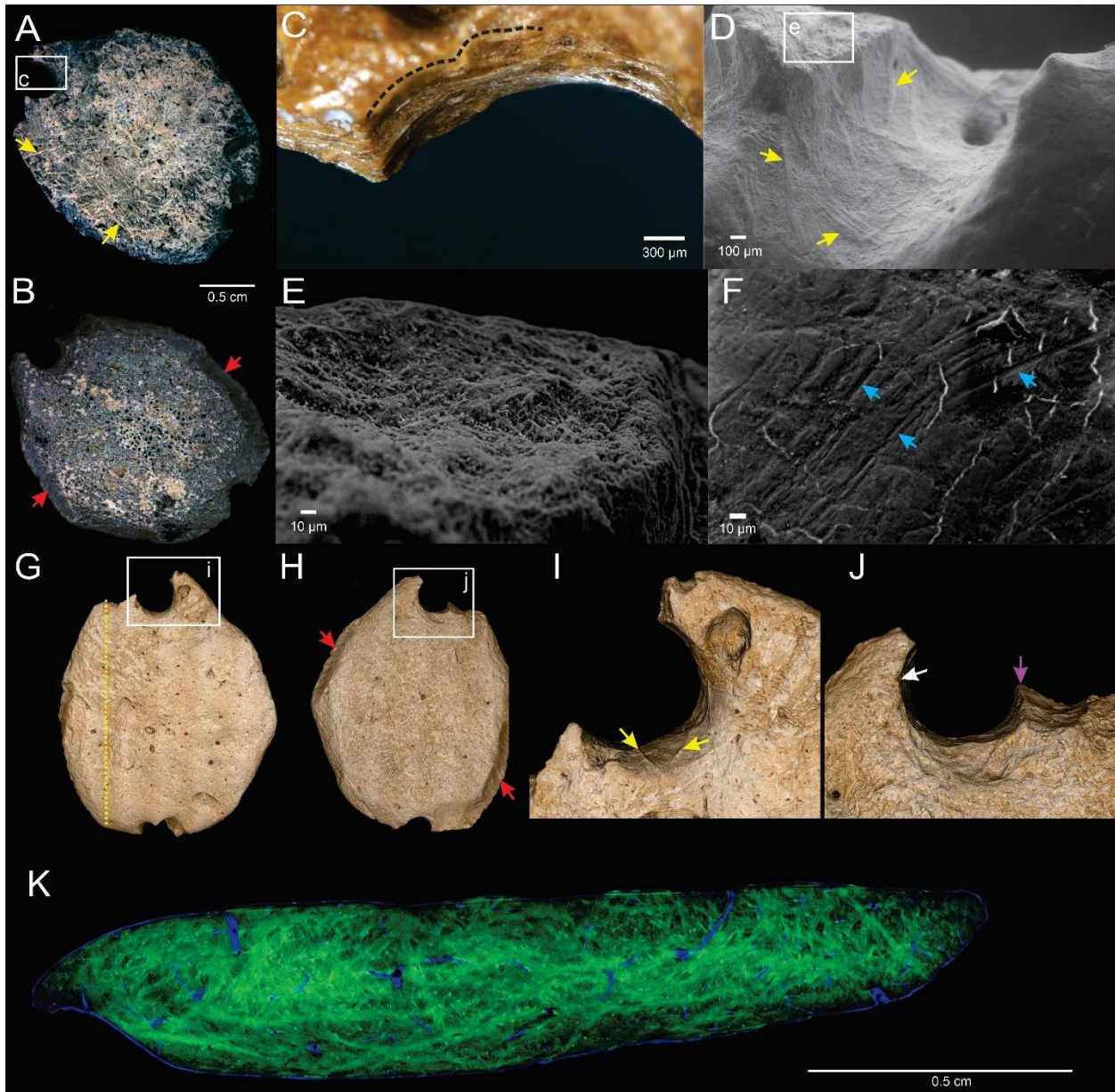
Figure 3. Anthropically modified giant sloth osteoderm (SEI6059). (*a–b*) Macroscopic view using photoluminescence, side 1 and 2, respectively. (*c*) Microscopic and (*d*) Scanning electron microscopy images of a hole drilled into the osteoderm (zoomed broken perforation area in *c*, notice drilling traces and smooth deformation). (*e–f*) SEM images. (*e*) Fracture surface exposing internal bone tissue. (*f*) Scraping marks on the polished surface. (*g–j*) SR-µCT reconstructed images, see main text for discussion. (*k*) False-colour image of the virtual cross section SR-µCT along the yellow dotted line in *g* highlighting collagen fibre bundles (green) and vascular channels (blue). In all figures: yellow arrows point to fibre bundles exposed by intentional and intensive polishing or extensive use-wear, red arrows to sets of likely rodent gnawing, blue arrows to scraping marks, white arrow to deformation of the perforation wall probably due to use-wear, and purple arrow to the well-delimited wall of the broken deliberate perforation.
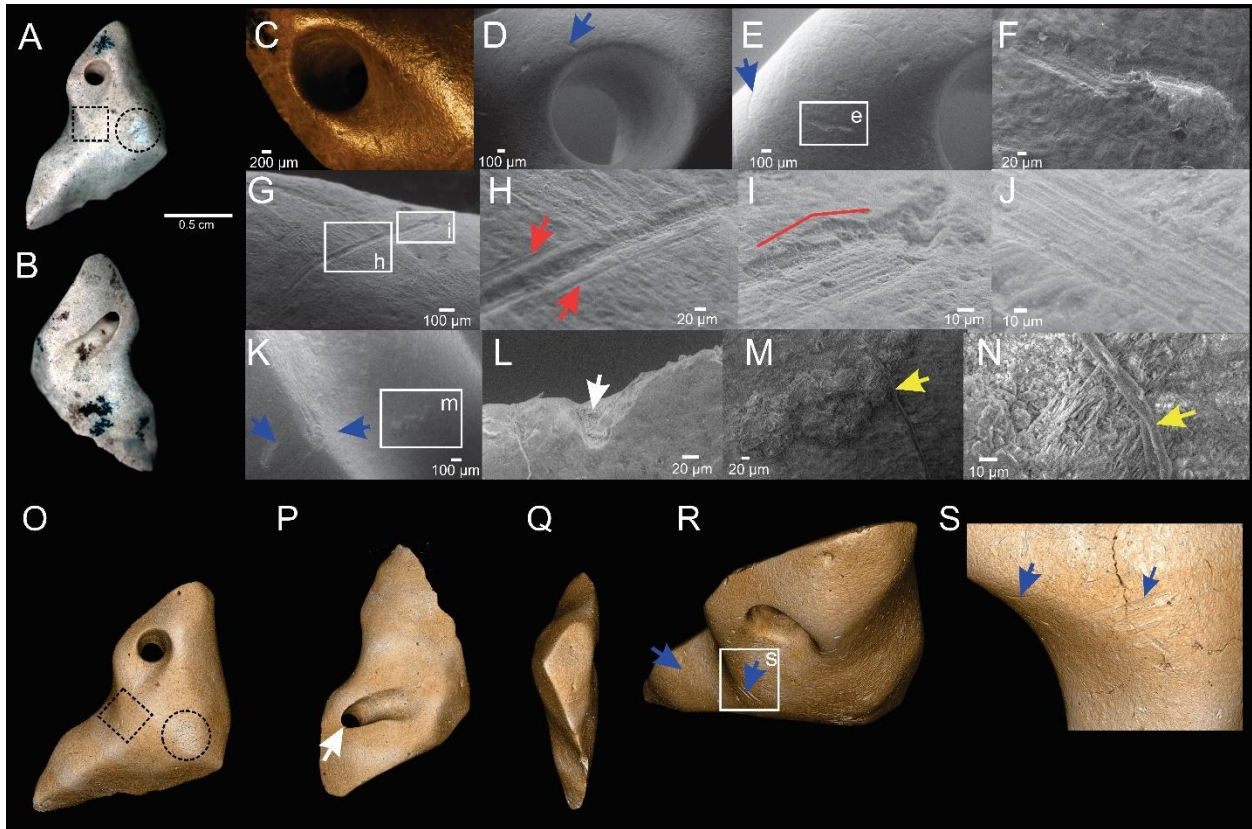
Figure 4. Anthropically modified giant sloth osteoderm (SEI6557). (*a–b*) Macroscopic photoluminescence images. Notice human-manufactured curvature and retouched edges showing intentional shaping of the bone, sides 1 and 2, respectively. Notice the uniform PL contrast along the bone. An area of possible trampling damage with distinctive brighter PL contrast (black dotted circle), can be compared with an area where ancient marks are uniform to the bone surface and perforation (black dotted square; see detailed morphology in the 3D image in *o*). Incisions and other multiple fine parallel striations from scraping over a broad area are frequent along this osteoderm. (*c*) Notice polish aspect and worn and deformed perforation, likely result of use-wear of the attached system. (*d–n*) Scanning electron microscopy images. Blue arrows indicate several scars around the drilled hole on side 1 (*d, e*), and side 2 (*k*). (*g*) Elongated and deep curve-shaped groove with regular internal microstriations located in a concave area of the bone. Shoulder effect is indicated by red arrows (*h*), and Hertzian cone highlighted in the red line (*i*). (*j*) Straight-walled scrape mark with multiple internal striations. (*l*) One of the micro-breakages present on the top of the enlarged perforation on side 2 (*b, p*). Notice the exposure of internal bone tissue indicated by the white arrow. (*m–n*) Yellow arrows indicate probable collagen fibre residue, trapped in a translucent gelatinous matrix inside the concave hole area of side 2 (zoom in *m* and *n*). (*o–s*) 3D SR-μCT images. Blue arrows indicate parallel deep marks in curvature areas, unlikely to be produced by trampling.
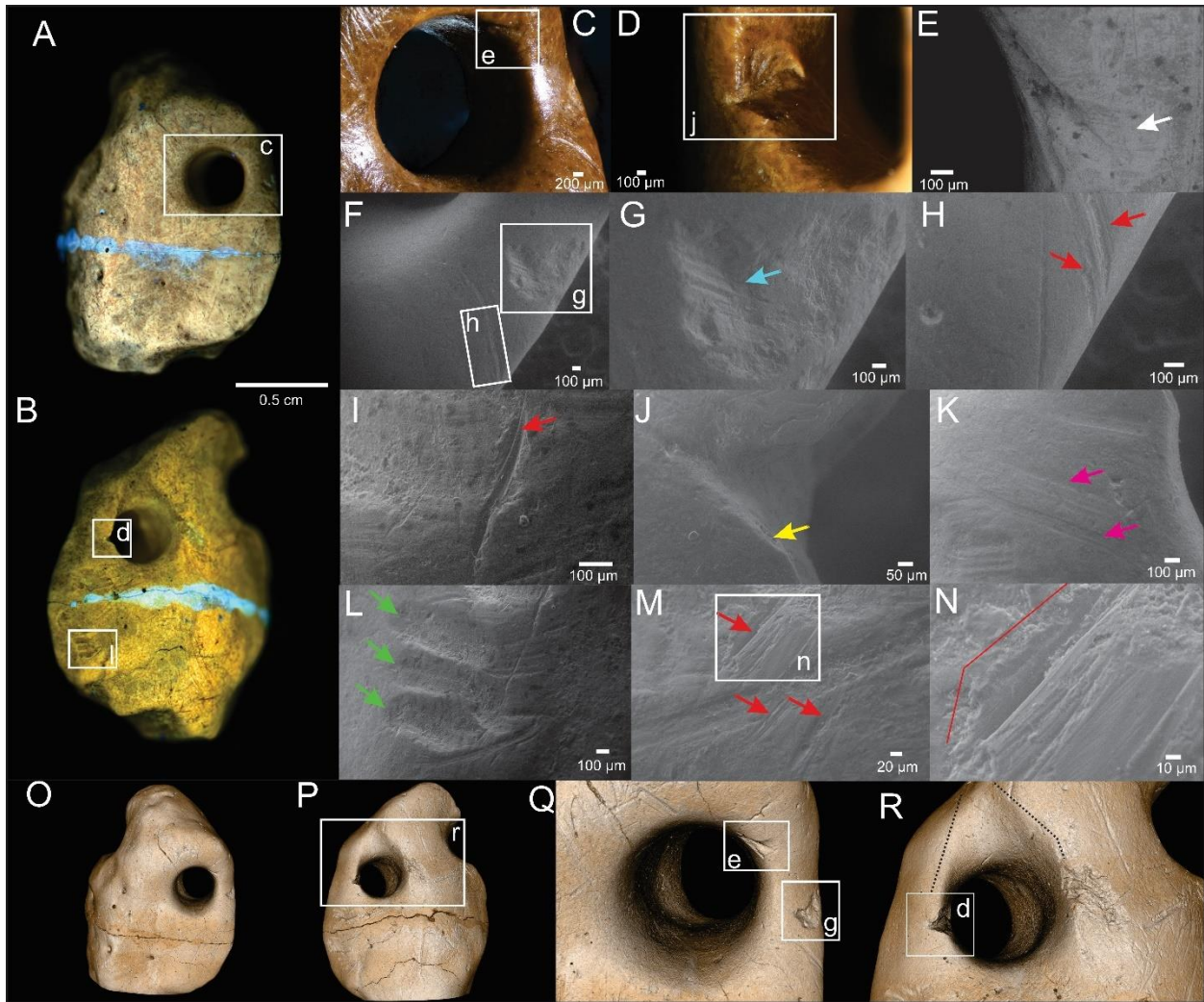
Figure 5. Anthropically modified giant sloth osteoderm (SEI6386). (*a–b*) Macroscopic photoluminescence images, sides 1 and 2, respectively. Blue-ish horizontal line across the sample corresponds to glued-area. (*c–d*) Microscopic images. Notice use-wear traces around the perforation hole on side 1 (*c*), and human modification scar on the lateral of the perforation hole on side 2 (*d*). (*e–n*) Scanning electron microscopy images, (*e*) AsB detector, (*f–n*) VPSE detector. (*d, j*) Anthropic scar, probably accidentally produced by stone tools during the process of drilling the hole. (*e*) V-shaped scar incision, also probably produced during the drilling of the hole. White arrows indicate 'barbs' features on the terminal of the stone tool incision. (*f, h*) Two elongated incision marks (red arrows), following the curvature of the bone, with internal microstriations and shoulder effects, and accompanied by a single mark. (*g*) Percussion notch associated with internal microstriation (blue arrow), probably from slippage. (*i*) Single incision mark (red arrows) accompanied by Hertzian cone formations. (*j*) SEM image of stone tool-inflicted0 scar. Yellow arrow indicates exposure of periosteum. (*k*) Scraping marks lateral to the perforation hole (pink arrows). (*l*) Small deep grooves, probably resulting from repeated gnawing in the same area made by a small rodent (green arrows). (*m*) Incisions likely inflicted by a series of single strokes made by a stone tool (red arrows), overlapping a linear mark. (*n*) Zoomed in image in which a red delimitation indicates the area of Hertzian cone formation. (*o–r*) SR-μCT images highlight natural bone structures, such as small foramen, and anthropogenically-caused modifications, including circular depressions, on both sides of the osteoderm and around the perforated hole. (*r*) Use-wear deformation in V-shape above the hole (black dotted lines), probably resulted from the suspension of the object or interaction with string.

52
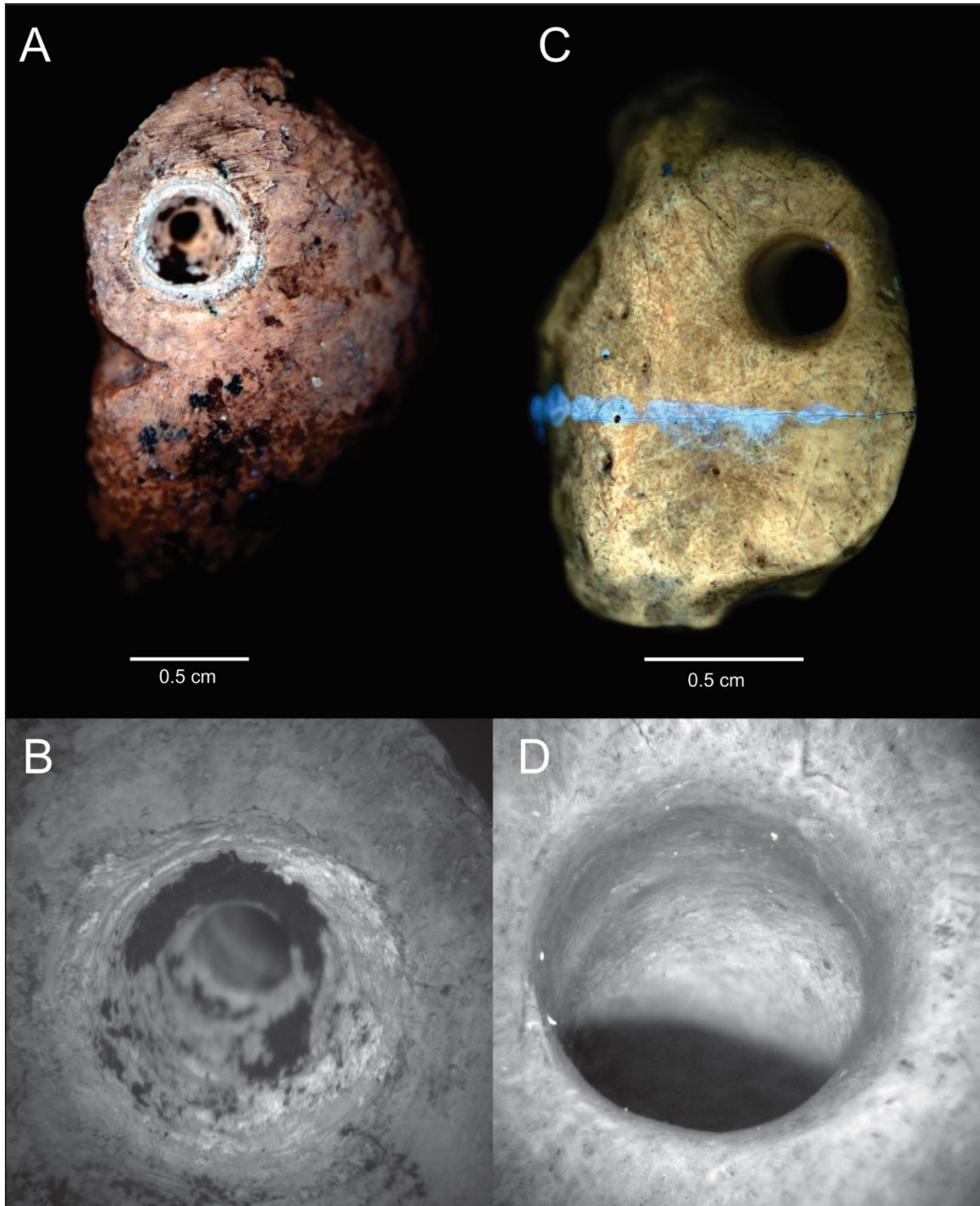
Figure 6. Comparison of modification between an experimentally modified fossil osteoderm and one of the ancient anthropically modified osteoderms. (*a*) PL image of experimentally modified osteoderm SEI8004 and (*b*) microscopic view of its perforated hole. (*c*) PL image of archaeological osteoderm SEI6386 and (*d*) microscopic view of its perforated hole. Notice the brighter and grooved hole in the experimentally modified osteoderm and the worn rim perforation in the ancient anthropically modified osteoderm. Blue contrast in the osteoderm SEI6386 (*c*) corresponds to glued area.

Electronic supplementary material

Evidence of artefacts made of giant sloth bones in Central Brazil around the last glacial maximum

Thaís Rabito Pansani, Briana Pobiner, Pierre Gueriau, Mathieu Thoury, Paul Tafforeau, Emmanuel Baranger, Agueda Vilhena Vialou, Denis Vialou, Cormac McSparron, Mariela Cordeiro de Castro, Mário André Trindade Dantas, Loïc Bertrand, Mírian Liza Alves Forancelli Pacheco

Other supplementary materials for this manuscript include the Movies S1 to S3 and scripts of the Oxcal and RStudio codes.

Text S1. Background of Santa Elina's geological context. Santa Elina is located in a warm tropical/seasonal environment, in the phytogeographical domain *Cerrado*, characterised by a mosaic of vegetation of forested formations and savanna-like open fragments (1). The biodiversity present in the Serra das Araras, where Santa Elina is geographically inserted, was probably attractive to humans and animals due to the favourable weather conditions and vegetation diversity (1).

The excavations in Santa Elina followed standard archaeological methods, especially concerning the collection of samples for dating. Santa Elina is an open-air shelter. Two dolomitic limestone walls protect the shelter, but do not fully protect it from meteorological conditions. The tropical warm climate, seasonal rains, and the carbonate content (from the shelter) in the bones contribute to a process of diagenesis/weathering that modifies the structure of bone remains. Indeed, long bones and teeth of *G. phoenesis* are found in a poor state of preservation (Figure S1). Giant sloth bones are mainly in fragmentary pieces and are weathered. As earlier described in (2), "*All of the bones had had their periosteum biochemically altered*". That is one of the reasons that we cannot observe cut marks, as well as carnivore tooth marks, or any other possible bone surface modifications on these bones. Only forelimbs, vertebrae, skull, and jaw bones were identified for the giant sloth from Unit III4, which may indicate the transport and selection of the animal's body parts by humans. The thousands of osteoderms are an exception due to their high fossilisation potential. They present diverse taphonomic traits, varying degrees of manganese/iron oxides and carbonate incrustations (Figure S1).

The coexistence of humans and giant sloths in Santa Elina is demonstrated by the evidence of culture material (rich lithic industry) and ground sloth bones in clear spatial and temporal context, as well as by the human modification of the osteoderms. The dates of the site further contextualise the time in which this cohabitation happened. Unit III4 is dated by U/Th, OSL and radiocarbon techniques, in different materials, such as bone, quartz, and microcharcoal, and all of them present similar results back to the last glacial maximum (LGM), around 25,000–27,000 years ago. Unit III4 presents charcoal structures and a thin film of ash in clear association with lithics and bones, dated to 27,818–26,887 cal ka BP (2). The referred microcharcoal was found in the excavation area, together with bones and lithic materials. We did not find any evidence of charcoal in levels above Unit III4 until Unit II2 (depth 205 cm, dated to 12,007–11,404 cal ka BP; (2)). It is unlikely that older ashes would be carried to the shelter and deposited into an already compacted and structured archaeological layer. In sum, whether if this charcoal results from natural fires or anthropic activity, it is a solid dating evidence for the age of Unit III4 in Santa Elina.

Text S2. Antiquity of Santa Elina. There were 35 radiocarbon, OSL, and U/Th dates obtained from the excavations at Santa Elina (Table S1), spread through four stratigraphic Units (I-IV). Unit I was dated by 23 dates from the most recent stratigraphic phase (Unit I). Of these, 25 were obtained from charcoal, one from a wooden stake, and one from a corn cob. Unit II was dated by five radiocarbon dates on charcoal and one U/Th date on a *Glossotherium* osteoderm, with the radiocarbon dates in the later sub-units Unit II(1) and Unit II(2). Unit III was dated by five dates: three radiocarbon dates, two on wood and one on micro-charcoal, an OSL date on quartz, and a U/Th date on a *Glossotherium* osteoderm. Unit IV was dated by a single OSL date obtained from a sample of quartz.

OxCal 4.4 (3) contains a number of powerful statistical tools for analysing radiocarbon dates. It is possible in OxCal 4.4 to build models using additional, non-radiocarbon information, such as stratigraphy from an excavation, a known calendrical date, or a supposed sequence of events. OxCal can estimate how possible these models are when compared to the actual radiocarbon dates available. A brief description of the basic OxCal 4.4 program structures and commands implemented in the models is presented below.

A *Sequence* is an OxCal 4.4 program structure, which orders events or groups of events. A *Phase* is an OxCal 4.4 structure for grouping a series of radiocarbon dates together, which are believed to belong to the same era, but which have no stratigraphical or other information that can be used to further order them relative to each other. Internally therefore the Phase is unordered, but externally each Phase can be ordered relative to other Phases, radiocarbon dates, or calendrical events. A *Boundary* is an OxCal4.4 command which estimates the beginning and end of Phases and Sequences. The *Agreement Index* is OxCal 4.4's estimation of how well the radiocarbon dates fit the model. An Agreement Index of less than 60% is usually thought of as denoting a model which does not agree well with the available radiocarbon dates. An Agreement Index of more than 60% is thought of as compatible with the radiocarbon dates. A high Agreement Index does not prove a model is correct, just that it is possible. It is always conceivable that another model could be constructed to fit the radiocarbon dates just as well, or even better. In this respect, it is like other, less quantitative, archaeological evidence. Due to an artifact of the OxCal agreement index algorithm models which closely match the dating evidence may on occasion have agreement indices over 100%.

Text S3. Modelling the Santa Elina sequence. The stratigraphy of the site is clear and well understood, allowing a model of the sequence at Santa Elina to be easily created in OxCal. The model considers that each of the Units from Santa Elina is contiguous stratigraphic phases, with one ending before another begins. This is called the Contiguous Model (4). This model creates a number of *Phases* ordered in a *Sequence*. The contiguous nature of this model is represented in the OxCal 4.4 code using the *Boundary* command. Boundary commands are placed at the commencement and end of Unit III and Unit III. These make estimations of the age ranges of the beginning and end of each of these Units. Because Unit IV consists of only a single OSL date, it is not treated as a phase, and it is not enclosed by boundaries.

The OxCal 4.4 code replicates the stratigraphic sequence of the excavated strata. Unit IV did not have evidence of human activity, but an OSL date (UW690), from the accumulation of Unit IV strata is included in the model because it provides a terminus post quem for the succeeding stratigraphic Units. Unit III and II are bracketed by the boundary command which estimates the commencement and end of the Units. Where the sub-units have multiple dates, they are modelled using the phase command. Because of the relatively small number of dates in each sub-unit, boundary commands were not used to model them because the Boundary function in phases with small numbers of dates may produce *very* wide start or end date ranges (5). The OxCal 4.4 model has an agreement index of 101.9%, which shows that the stratigraphic model and the dating evidence are compatible with each other. The boundary commands also have provided reliable estimations of the commencement, and end, of each of the main stratigraphic Units.

Unit III, the first strata with clear evidence for human activity, had five dates spread across two broad stratigraphic sub-divisions (III4 and III3). The beginning of Unit III dates to between 28743–26536 BP (95.4% probability) and likely between 27942–27185 BP (68.3% probability) (Tables S2 and S3, Figure 2 in the main text). Unit III ended between 27225–25225 BP (95.4% probability) and likely between 26230–26230 BP (68.3% probability). Unit II had five dates spread across two stratigraphic sub-divisions. Of these five dates, three are radiocarbon dates, one is a U/Th date, and one is an OSL date. Unit II commenced between 24922–16850 BP (95.4% probability) and likely between 21473–17778 BP (68.3% probability). It ended between 7714–7714 BP (95.4% probability), likely between 7785–7785BP (68.3% probability). Unit I had 23 dates, which gave a modelled range commencing between 7901–7656 BP, likely between 7833–7709 BP. A number of samples from Unit I are relatively recent and the model estimate that Unit I ends between 422 BP and the present day (95.4% probability), and likely between 323 BP and the present day (68.3% probability).

Text S4. Human-megafauna association in Santa Elina. Archaeological and palaeontological data from Santa Elina comes from samples uncovered in excavations during 1980–1994. All distribution data were collected through digital access to the excavation inventory. All osteoderms (n=7,069) were accessed and carefully analysed by TRP at the Museu de Arqueologia e Etnologia of the University of São Paulo (USP), São Paulo, Brazil, where the material is housed. Here, we update the detailed information on stone objects and *Glossotherium* bones and osteoderms from Units II (II1b+II2) and III (III3+III4) (Tables S4-9). We generated maps of distribution and frequency (Figure S2) and distribution and association (Figure S3) of these elements using scripts in the R environment (v3.5.1; R Core Team 2018). In this study, we did not include excavated material with uncertain or absent information concerning Unit, square, and/or z (depth). Also, particularly in Unit II, there is an area of block falling from z = 235 around the squares 22-24/A-Z. Thus, all the data relating to these coordinates were not included in this study to avoid misjudgement and ensure the inclusion of data only from undisturbed geological contexts. Some osteoderms are labelled with approximately x, y (square coordinates), and z (depth) values, so we calculated the average of the values range available in the collection labels. Because of the prevalence of osteoderms with only approximate x, y, and z information, we did not include osteoderms in the association maps of stone tools and ground sloth remains (Figure S3), and generated another simplified map showing the distribution of the osteoderms (Figure S4). To better visualise the data in the 2D and 3D association maps, we converted the original x and y values in agreement to (6): by adding an increasing set of hundreds in the x and y axis on related squares; for x values (North to South) we added +100 in each letter related (A to D), and for y values (East to West) we added +100 in each number related (19 to 31). In this approach, nothing changed in the z and 18 metres.

2D grid maps includes only lithic artefacts and fossils undisputedly from Units II and III (within 1-m-wide squares). The generated maps clarify the distribution pattern of these objects, including localised areas with higher frequencies of objects. In Unit III, particularly, areas of higher concentration of giant sloth bones overlap with the lithic artefacts (e.g., square 26B, Figure S2).

2D and 3D georeferenced maps were generated for only stone tools and megafauna bones (excluding osteoderms) with precise X (D-Z notating metre increments North to South respectively), Y (18–31 metres notating metre increments East to West respectively), and Z (depth) coordinates, showing their distribution for both Units simultaneously. This dataset consists of 48 stone tools and 90 fossil bones from Unit II and 85 stone tools and 309 fossil bones from Unit III (Table S10).

The 3D georeferenced distribution map of giant sloth bones and stone tools reveals a distinct distribution and association in both Units (Figure S3B). This corroborates that there are no significant stratigraphical disturbances in these excavated areas. While Unit II appears to have a lower association between stone tools and megafaunal bones than Unit III, both show a clustered pattern of remains. In Unit III, the strongest association between stone tools and megafaunal bones occurs at 26–28 x A–C, ~150–

300 cm (z = depth), especially in 26A, 26B, 27A, 27B, 28A and 28B. The three anthropogenically modified osteoderms were found in Unit III, specifically in 23A (z=323 cm), 27A (z=319 cm) and 28A (z=306 cm). Their locations correspond to some of the areas of highest concentration of stone tools (27A and 28A) (Figure S3A).

Besides the spatial relationship of ground sloth bones and material culture, we provide a simplified 2D map of the spatial distribution of the ground sloth osteoderms (Units II and III) and compare their location and abundance with other previously identified bones (6). In the superior level (Unit II), the distribution range of the osteoderms is mainly through metres 28-30 x A-D. The higher frequency of these elements is found in metres 30B (n = 782) and 29C (n = 616). In the lower level (Unit III), the distribution range of the osteoderms is mainly through metres 23-26 x Z-C. The higher frequency of these elements is in 24A (n = 1,051), which represents approximately 23% of the total osteoderms distributed in this layer. 25A, 25B, and 26B also present a high frequency of osteoderms (n= 998, 328, and 339, respectively).

We can observe that in Unit III there is a higher frequency of loci with higher density of osteoderms than in Unit II. Also, the higher concentration of these elements in Unit II is close to the skull remains, and mainly closer to the ribs, vertebrae, and scapula in Unit III. The other bone elements do not follow an exact anatomical arrangement with the osteoderms (notice the distance from the scapula and skull in Unit II, for example). There is no evidence of soft tissue or articulated osteoderms preserved in either of these layers.

The spatial concentration of osteoderms close to the location of thoracic vertebrae and ribs (Units II and III; Figure S4) agrees with the previously inferred arrangement of osteoderms on ground sloths' integument, which is mainly on the animal's dorsum (e.g., (9)). However, due to the poor preservation of other bones, it is hard to assert their original disposition in Santa Elina. The high amount of osteoderms (concentrated in specific squares) without other bones that might suggest anatomical connections; the accumulation of more than 1,000 osteoderms in one square (24A, Unit III); the three anthropically perforated modified osteoderms in the squares 23A, 27A, and 28A; as well as their association with lithic assemblage (*e.g.,* limestone flakes, haematite, and quartz in 23A; retouched limestone tools and limestone flakes in 27A; and retouched limestone tools, limestone flakes, platelets, and limestone cores in 28A), might indicate intentional disposal. This interpretation would agree with the previous suggestion that the osteoderms were probably not fossilised *in situ* right after the animal's death but were transported by humans to the shelter and intentionally disposed ((2), (6)). However, further taphonomic studies are needed to determine if humans were the main agent of transport of the ground sloth remains to the shelter and intentionally disposed of some specific parts of these remains in areas of interest.

Text S5. Natural and taphonomic aspects of ground sloth osteoderms from Santa Elina. Approximately 7,069 osteoderms of *Glossotherium phoenesis* were analysed under stereomicroscope to investigate taphonomic and/or anthropogenic traces. A small set (n=18) of natural (unmodified) osteoderms of *G. phoenesis* was photographed using a digital camera (Canon EOS). We can observe and compare the difference between pits and vascular foramina present in the natural surfaces (Figure S5) and the human perforation on the modified osteoderms. Even the biggest vascular foramina that are present in the unmodified osteoderms still have a compact and rough structure, surrounded by small depressions, and show a distinct pattern of penetrating into the bone tissue rather than through it. These foramina are different from the polished hole perforations created by humans. We do not find holes of the size and consistent shape like the ones present in the anthropically modified osteoderms analysed in this study in any of the other thousands of osteoderms of Santa Elina. Holes of this size and shape are also not recorded on other Megatheriidae osteoderms reported in previous studies (e.g., (7, 8, 9)). Thus, in addition to the presence of stone tool marks and wear traces revealed in this work, we reject the possibility of the perforated holes being natural structures of the osteoderms. We provide macro and microscopic image data of a non-

modified osteoderm (FR3A, Figure S6) and a damaged osteoderm by bioerosion (FR6, Figure S7) for comparison with the three modified osteoderms (Figure S8, main text and Figures S11-13). In addition, we provide a folder where it is possible to access and compare images of these two samples and the three human-modified osteoderms with a wider range of SEM magnifications (~30x to 600x), available on our ESM zipped folder.

Other possible processes we considered that could have created the holes are non-human modification of bones by natural agents, such as bioerosion by living organisms, and abrasion or digestion corrosion resulting in the rounding and polishing of the bones. However, we excluded these scenarios after distinguishing the features observed in the ornaments of Santa Elina from the established signature criteria of these other processes. The published characteristics of holes produced by insects or ectoparasites (i.e., fleas) in bones, specifically osteoderms, do not match the perforation of the ornaments. Here we provide an example of a damaged osteoderm from Santa Elina (Figure S7) for comparison. The non-human damaged osteoderm has bigger chambers starting from the superficial bone layer and reaching the internal spongy structure with smaller perforations, similar to what has been described in Cingulata osteoderms with insect traces (10, 11). Perforations in armadillo osteoderms caused by fleas also display a shallow circular shape that penetrates the bone tissue but does not go through the entire bone and may present small cavities inside (12). Other studies have also shown that common features of bioerosion borings that do not penetrate through the entire bone (13). Although some ichnotaxa may penetrate the bone, their morphology is remarkable different from the modified osteoderms of Santa Elina, which present manufacturing traces, regular shape, polish, and worn aspects and associated use-wear traces.

Digestion by predators and natural abrasion may produce rounding and polishing of small mammal bones (14), but their macroscopic and SEM characterisation are distinct from what we found in the Santa Elina modified osteoderms. Armadillo osteoderms altered by digestion might present modification on their ornamentation, as well as present several degrees of degradation of their compact bone surfaces, generating partial or complete perforations. These perforations, however, are irregularly shaped, and often numerous (15). The cracked surface and torn appearance of the bone structure resulting from digestion or regurgitation (14) are also distinct from what we observe in the ornaments. This scenario also does not explain osteoderm SEI6059 having one side more polished than the other, or the concave feature above the perforation in osteoderm SEI6386, identified by us as a use-wear trace, possibly due to string interaction in the attachment system. In addition, the well-preserved and distinguishable features of scraping and incision marks that we document in this study would probably have been erased with acidic corrosion, as is noted to happen with cut marks on bones (16, 17). In the case of human modification made over a bone corroded by gastric acid, we would also expect to see different PL contrasts displayed on the marks along the bone surfaces due to different pH conditions of the corroded bone and the internal bone uncovered by the anthropic marks or rodent gnawing marks.

Drilling holes mainly relies on the rotational movement of a tool whose edges will generate a surface of revolution. In Figure S9A, the section of the hole of the SEI6386 osteoderm can be observed. Cylindrical surfaces are described by couples of straight parallel lines (green and white). This shows that several operations were needed to create a single hole. The distance between these parallel lines is not constant, indicating the use of different tools. In figures S9B and S9C, a first hole drilled from the left side of the image can be observed. It is not going through the sample (a sharp edge is not totally removed). In Figure S9B, an open hole on the left side of the image intersecting the first one can clearly be observed. This creates the sharp edges indicated by white arrows that are not present on other entry points. This shows the ability of the humans who modified this osteoderm to perform rather complex manufacturing strategies.

The artefacts from Santa Elina undoubtedly represented the cultural activity of the people of Santa Elina, due to human-manufacturing and use, evidenced by the traces of diverse techniques employed during the *chaîne opératoire* of the raw material (e.g., perforation, shaping and finishing), technical marks (e.g., incision marks, scraping marks, micro-breakages), and use-wear traces (e.g., deformation of the rim and bone edges, erased manufacturing marks of the perforation holes, attachment system, sunken areas close to the hole perforation, smoothed and worn surface). The worm rim perforations (SEI6386 and SEI6557); deformation of the rim, including the formation of attachment systems (SEI6386); sunken appearance close to the hole perforation (SEI6557); one side more worn/polished than the other (SEI6059); the symmetric position of the double holes (SEI6059); the deformation and smoothing of the surfaces, and mainly the **worn areas and use-wear traces** (all three osteoderms) are solid evidence that these objects were modified and used, expressing the cultural symbolic behaviour of population from Santa Elina and therefore suggested as "ornaments". We interpret this modification and use as the creation of "ornaments". See examples below of archaeological ornaments worldwide made from different materials, such as shells, bones, teeth, and jet to contextualise how their perforations and surfaces can be worn and deformed, especially due to string interaction and suspension, contact with other beads, and extensive use (Figure S10; (18), (19), (20), (21)). Still, further technological and ethnographic studies will be fundamental to elucidate how these cultural objects were used and what their functions were, if there were any besides stylistic ones.

We notice in the SEM images of the ornaments the presence of shallow microstriations and pitting that may result from sedimentary abrasion (14), as well as trampling marks; these can make it difficult to identify stone tool traces (16). However, the presence of damage signs on the ornaments from the depositional environment does not exclude the presence of other anthropic marks and/or marks from animal interactions that we identified. Indeed, their superimposition may indicate the timing of each activity that occurred during the taphonomic history of these bones. Several traces and scars from manufacturing and use-wear can be observed in figures S11-S13. Photoluminescence and SEM characterisation of a rodent modified osteoderm demonstrate the zooarchaeological aspect of rodent gnawing in fresh bones (Figure S14).

A dataset of 80 randomly selected osteoderms from Santa Elina observed under a portable digital microscope (50—1,000X magnification) registers the presence or absence of holes or grooves, colouration, and types of bone surface alterations present on each sample (Table S11). To identify the presence of "holes or grooves", we considered only circular holes that penetrate through the whole bone. We are not considering foramina pits and circular depressions mainly present on the external surface of the bone, since these are common anatomic traits of the osteoderms (7). We identified four types of modifications of bone surface modifications, categorised as 1) abiotic taphonomic modifications, including all, some, or one of the following features: cracks and sediment incrustations (carbonate, dendrites, oxides); 2) rodent marks; 3) trampling marks; 4) indistinguishable marks, either because the bone is not well preserve enough to identify mark features or because it would require investigation at a higher level of magnification. This dataset, which presents some of the thousands of osteoderms from Santa Elina, documents the most frequent characteristics of non-human taphonomic modifications on osteoderms and reinforces the perforated holes and polished surfaces of the modified osteoderms as rare modifications.

We calculated the size of each foramen (big chambers, bioerosion, and small pits) in six unmodified samples, one bioeroded sample, and the three modified osteoderms using ImageJ software by freehand selections to catch the exact area of each one (Table S12). We performed an ANOVA test (F = -100.4, p < 0.05), and observed that the size of the area of the natural foramina in the unmodified (specimens FR1, FR3A, FR3B, FR7, FR12, and FR14) and bioeroded osteoderms (FR6), are significantly different from the area of the human-created perforation holes in the modified osteoderms (SEI6059, SEI6557, and SEI6386).

The mean value of the area of the natural foramina is 0.19 ± 0.36 mm, while the mean values of the bioerosions is 0.47±0.72 mm, and the mean value of the perforated holes is 5.56 ± 2.53 mm.

Text S6. Information on experimentally modified osteoderm. The experimentally modified fossil osteoderm (sample SEI8004) was perforated by our team in the 2000s, in situ, at the archaeological site of Santa Elina (Figure S15). To try to reproduce the ornament manufacturing with the possible stone tools utilised by the early humans of Santa Elina, the experiment was conducted using small limestone flakes and quartz grains from the site (Unit III4). First, the sample osteoderms were selected after a careful consideration of finding osteoderms of similar sizes and shapes to the modified osteoderms, and two were completely modified with hole perforation and polishing (Figure S14C). The experiment consisted of the techniques of scraping, tapering (bevel-shaping), smoothing, and hole perforation. The hole perforation was made by reworking both faces. Finally, a thorn of the palm *Bactris setosa* (Arecaceae) was used to polish the hole perforation, and cattle leather from the region was used for the general polishing of the piece. Our team realised that after polishing the bone with leather the rough traces of the manufacturing process were erased (*personal communication from D.V. and A.V.*).
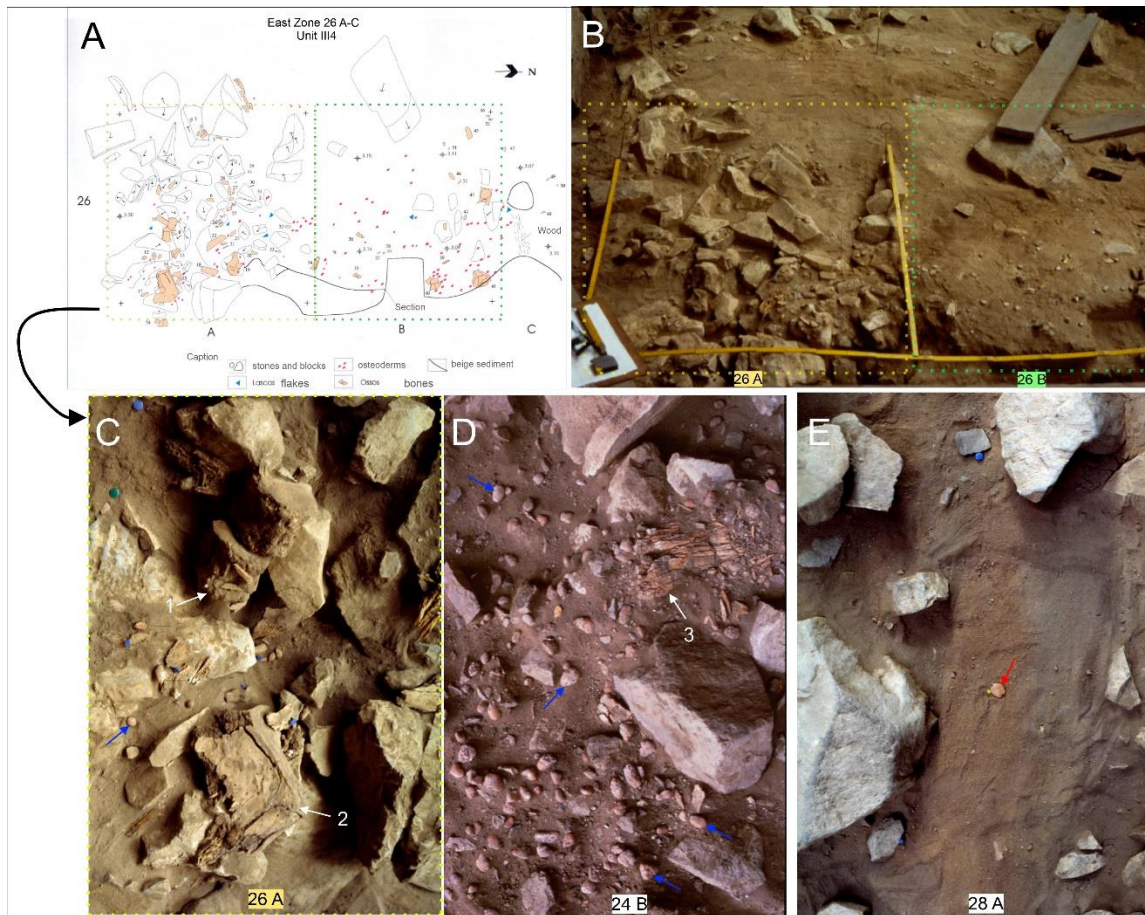
Figure S1. In situ giant sloth bones from Unit III4. Excavation was conducted following rigorous methods standards, carefully subdivided into zones (squares, e.g., *a-b*). (*c, d*) Notice weathering of bones (white arrows), as well as carbonate and oxides traces visible on several osteoderms in (*d*) (blue arrows). (*e*) In situ anthropic modified osteoderm SEI6059 (red arrow). Bone captions: 1) vertebrae (*c*), 2) tooth fragment (*c*), and 3) unidentified long bone (*d*).
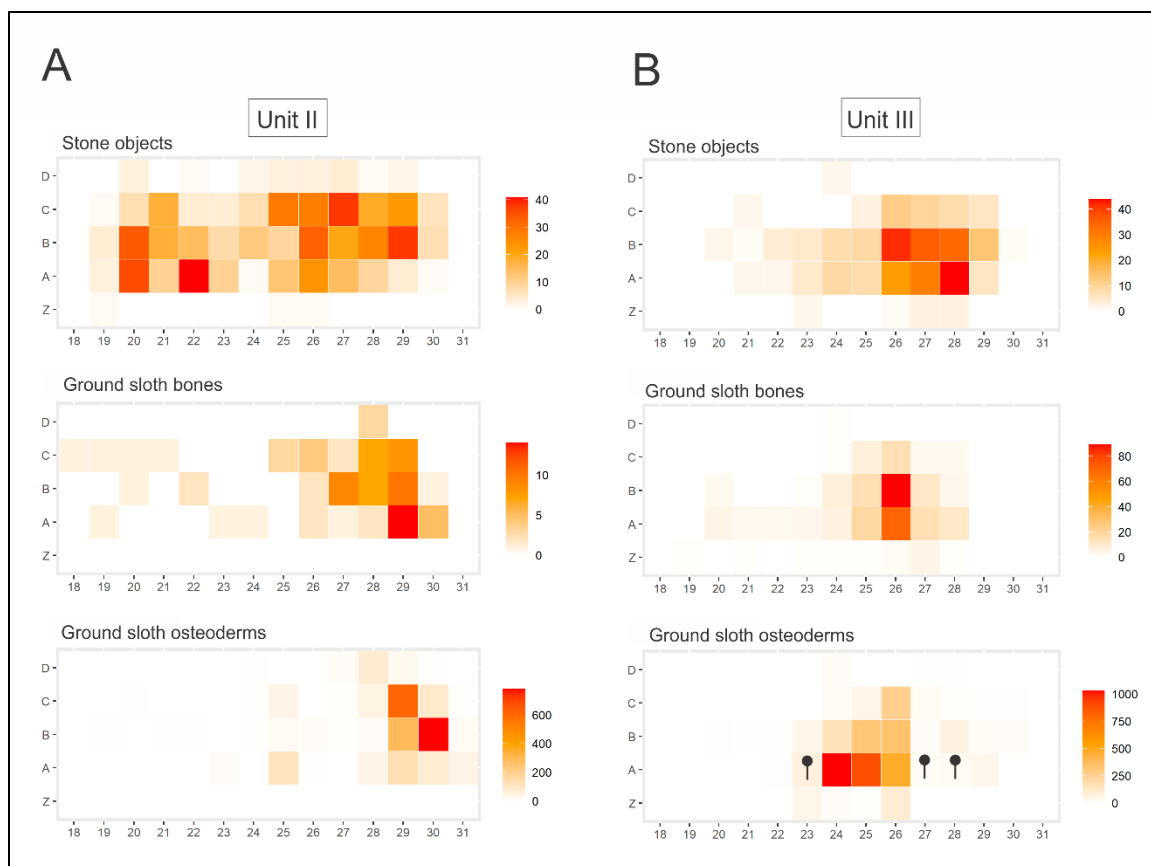
Figure S2. 2D map of spatial distribution of stone tool objects, ground sloth bones, and ground sloth osteoderms in (*a*) Unit II and (*b*) Unit III. X coordinates are represented by letters (Z–D) and Y coordinates are represented by numbers (18–31). Squares from the archaeological excavation are divided by 100 cm². Black pins indicate the location where the three human-modified osteoderms were found. This dataset consists of 598 stone objects (including stone tools and others), 90 ground sloth bones, and 2,564 ground sloth osteoderms from Unit II; and 338 stone objects (among stone tools and others), 309 ground sloth bones, and 4,505 ground sloth osteoderms from Unit III (Tables S4–S9).
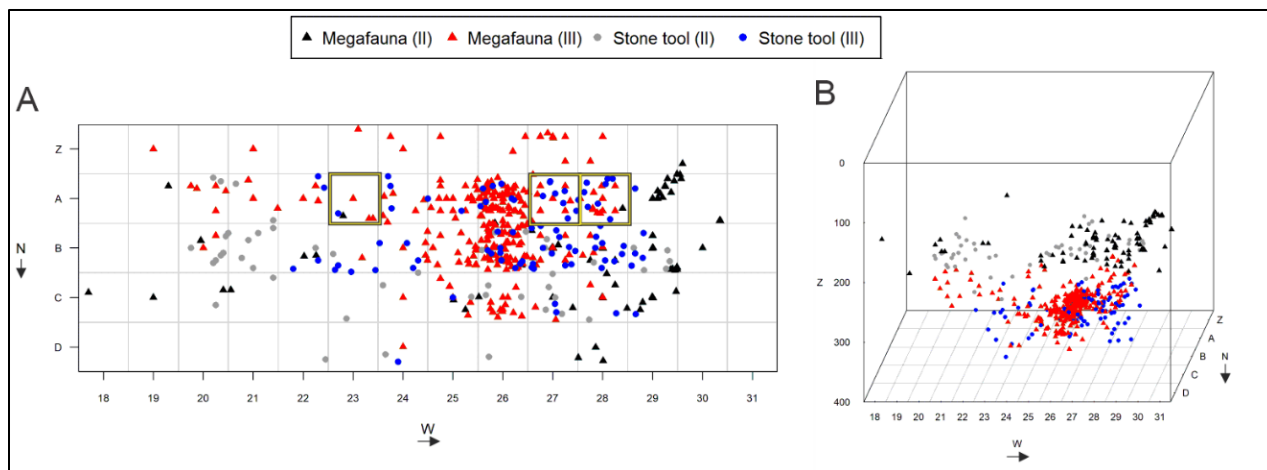
Figure S3. Association maps of stone tools and ground sloth remains in Santa Elina. (*a*) 2D and (*b*) 3D maps showing spatial distribution and association of stone tools and megafauna bones from both Units II2 and III4. Colour grid squares indicate the location where the three modified osteoderms were found (23A, 27A, 28A). Grid squares represent 100 cm². Depth in Z coordinate is indicated in cm. Dataset available in Table S10.
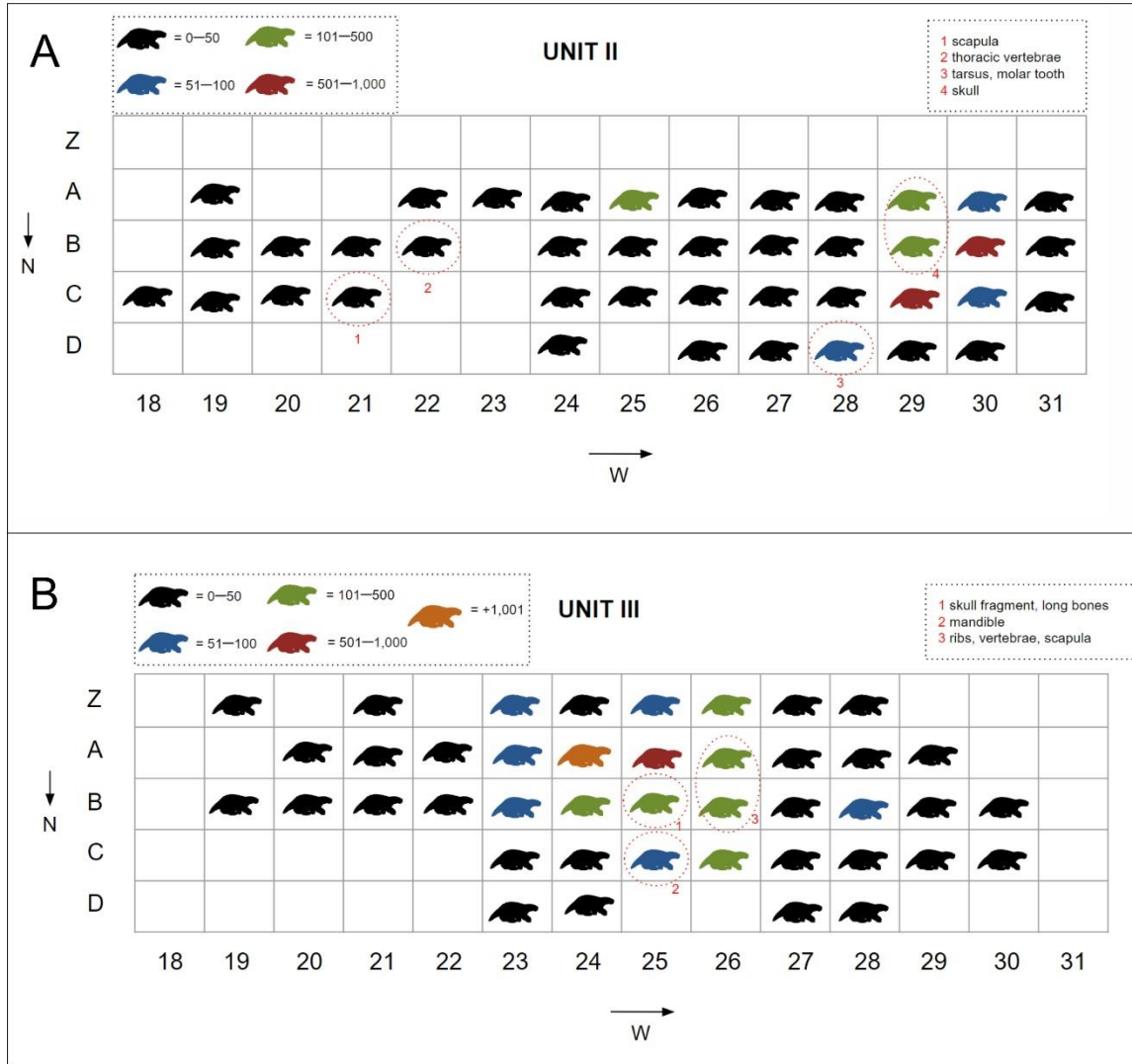
Figure S4. Simplified spatial map of osteoderms' distribution and skeletal element frequency in Santa Elina. (*a*) Unit II, 2,564 elements. (*b*) Unit III, 4,505 elements. Colours represent the frequency of osteoderms in each square: black = 01-50; blue = 51-100; green = 101-500; red = 501-1,000; orange = +1,000. Numbered circles indicate the location of previously identified skeletal elements (6), as detailed in the legend on top right of each figure.
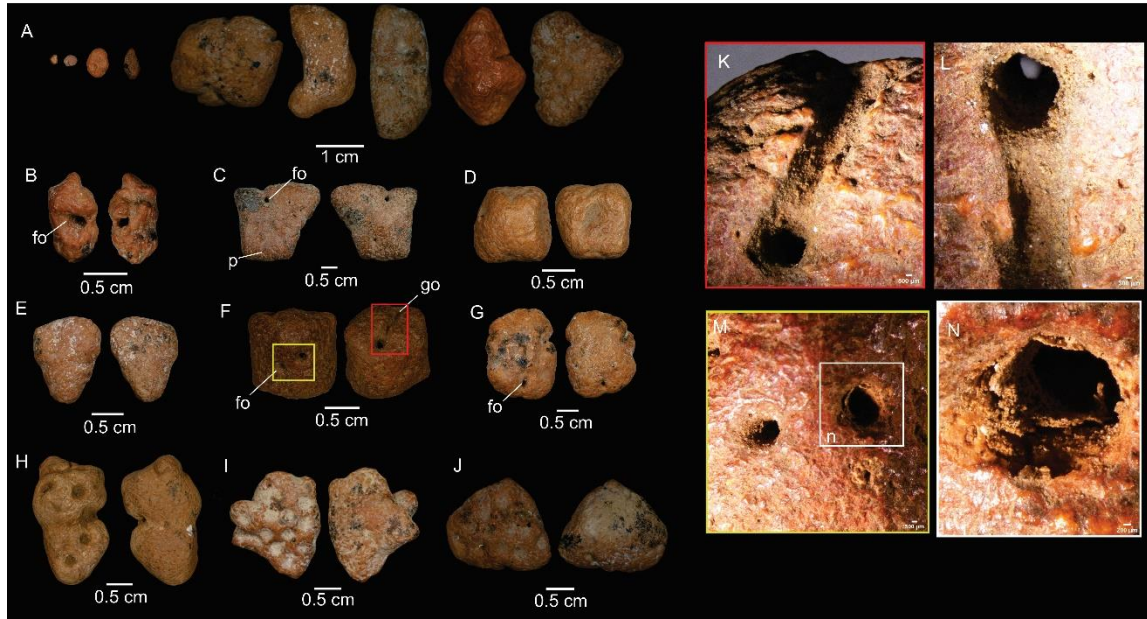
Figure S5. Set of 18 non-modified osteoderms of *G. phoenesis* from Santa Elina. (*a*) 9 specimens in scale to demonstrate their diverse morphology and sizes. (*b-j*) Specimens showing both sides. Notice irregularly pitted surface with depressions, and sometimes one side presenting vascular foramina whereas the opposite side is smoother (*h-j*). (k-n) Microscopic images of zoomed in areas of osteoderm FR3B (Unit II, 29C, z= 195-200 cm), delineated with yellow and red squares, using stereomicroscope Nikon SMZ-25. Notice that the natural groove structure intersects with a foramen (*k*), that is connected with another foramen in the other side of the bone (*n*). This connection is observed in (*l*) where we can see the foramen in specific perspective. Abbreviations: *fo*: foramina, *go*: groove, *p*: pit.
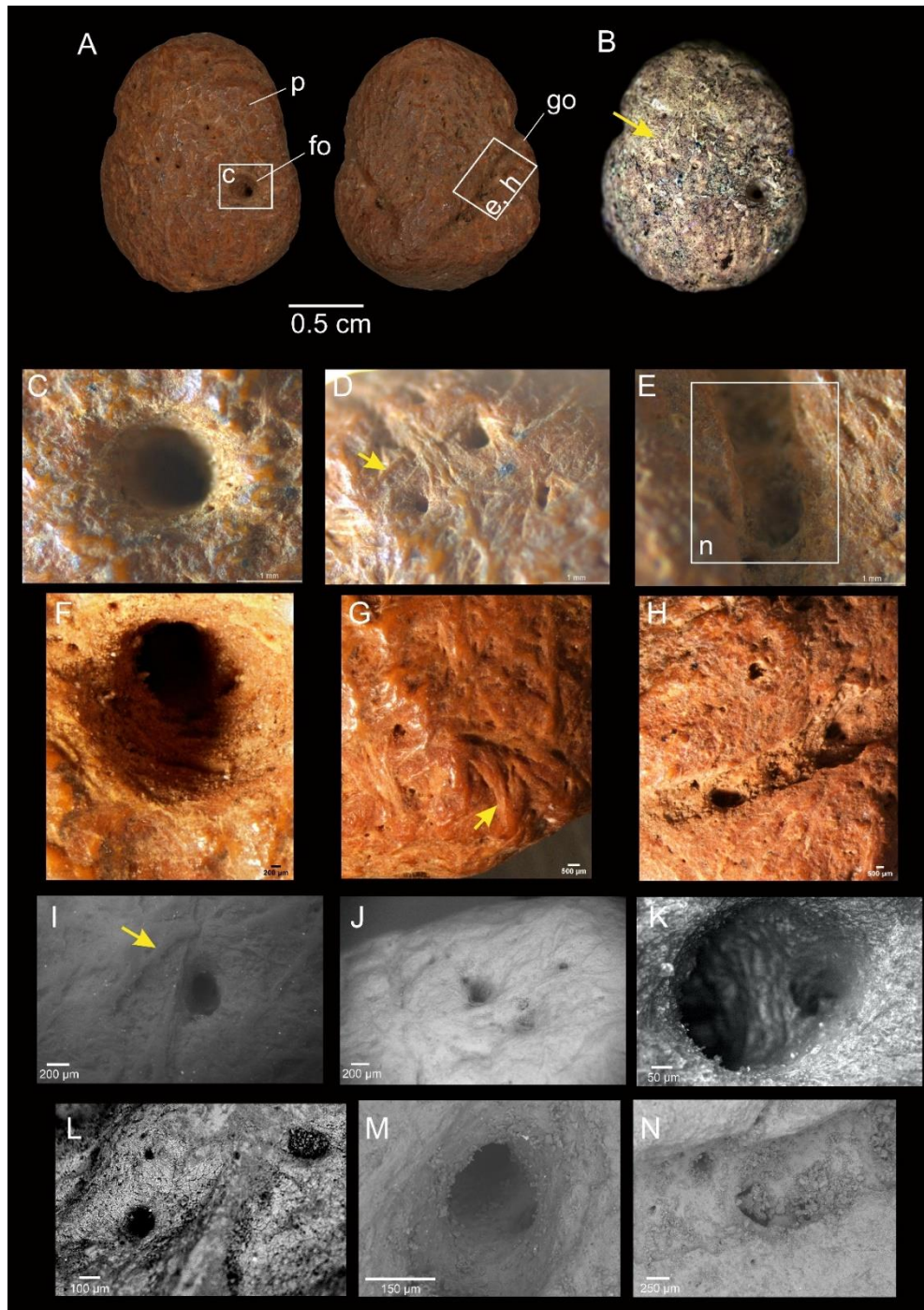
Figure S6. Osteoderm FR3A, Unit II, 29C, z= 195-200 cm. (*a*) Macroscopic images of both sides were taken using a digital camera. *(b)* Photoluminescence macroscopic image. (*c-e*) Microscopic images taken using an optical microscope (Leica 2700P) under reflected light illumination. Notice foramina penetrating the internal bone tissue. (*f-h*) Microscopic images using stereomicroscope Nikon SMZ-25. (*i-n*) Scanning electron microscopy images using VPSE (*i-k; m-n*) and AsB detectors (*l*). Yellow arrows indicate fibre bundles with topographic aspects that characterise its naturally rough compact surface. This aspect is also remarkably apparently in (*g*).
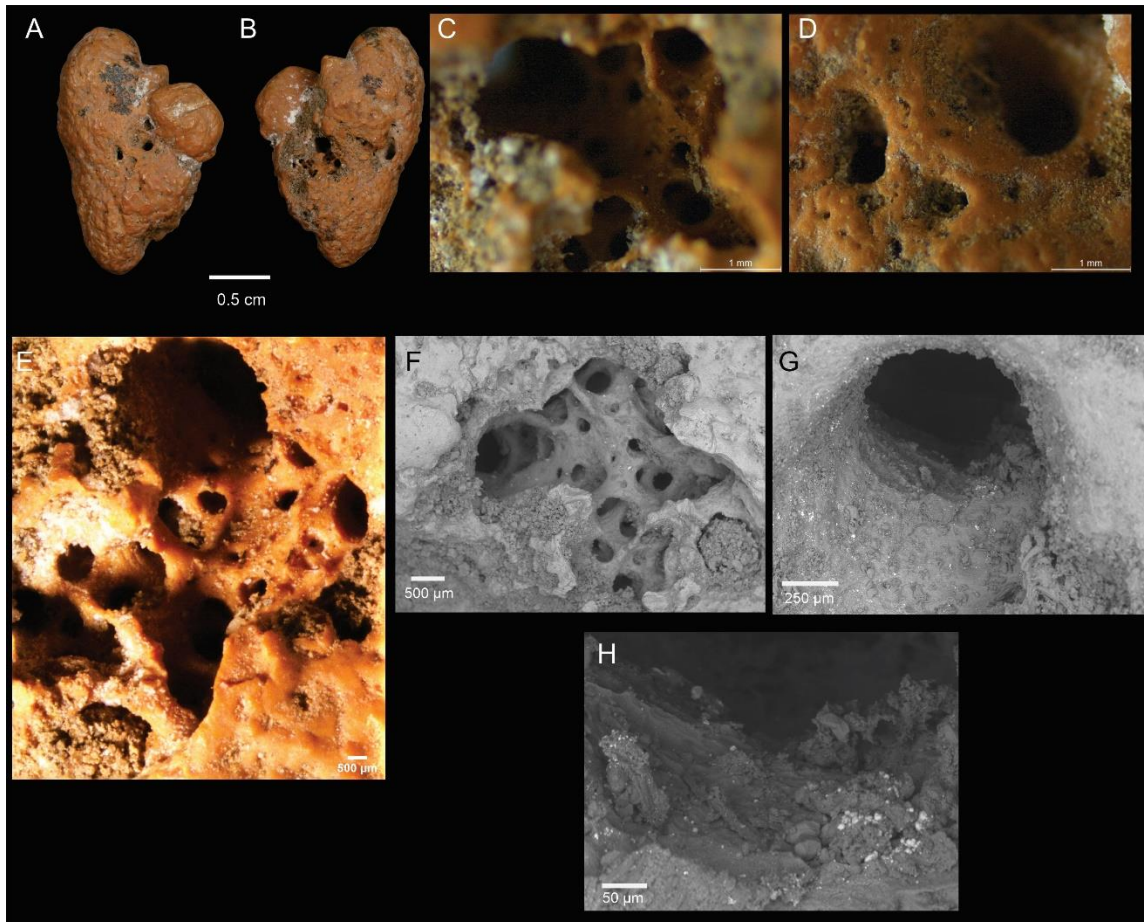
Figure S7. FR6, Unit III, 25A, z= 330-350 cm. Example of an osteoderm likely damaged by bioerosion (undetermined ichnotaxonomy). (*a-b*) Images of sides 1 and 2 taken using a digital camera. (*c,d*) Microscopic images using optical microscope (Leica 2700P) under reflected light illumination. (*e*) Microscopic image using stereomicroscope Nikon SMZ-25. (*f-h*) Scanning electron microscopy images. Notice that the big chambers expose the internal structures of the bone, including small internal intertwined cavities (*e* and *f*), and present irregular and damaged aspects of their walls.
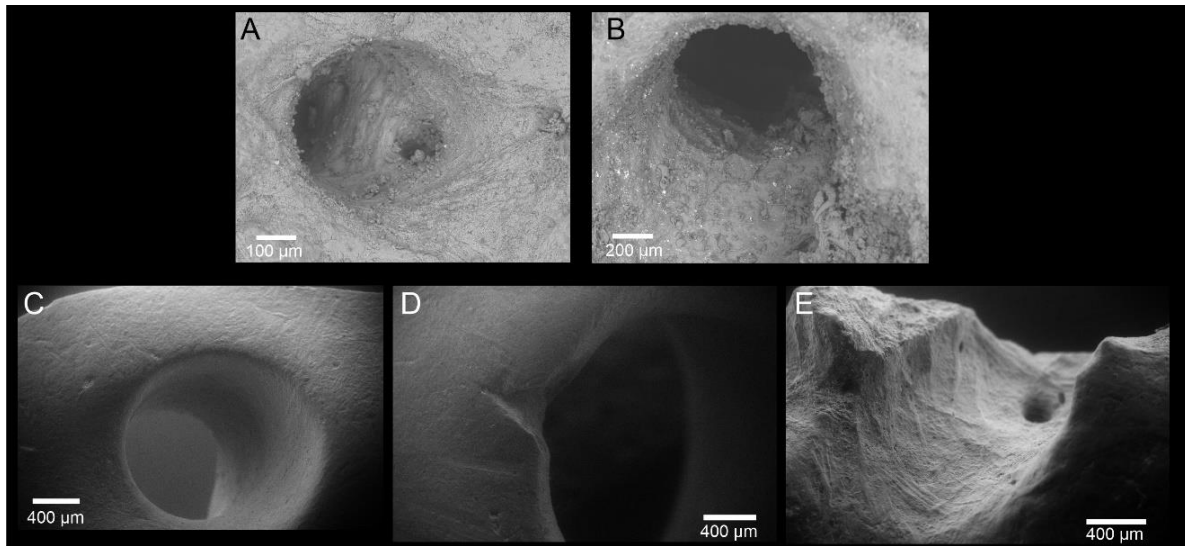
Figure S8. SEM images of (*a*) FR3A, (*b*) FR6, and (*c-e*) anthropic modified osteoderms SEI6557, SEI6386, and SEI6059, respectively. Notice different sizes of natural foramina (*a*) and bioeroded (*b*) samples in comparison with the regular rim accompanied by scars and micro-breakages on the anthropic modified osteoderms. Notice natural rough aspects in (*a*) and damaged aspects in (*b*), in contrast with the polished aspects and worn characteristics of the artefacts (*c-e*).
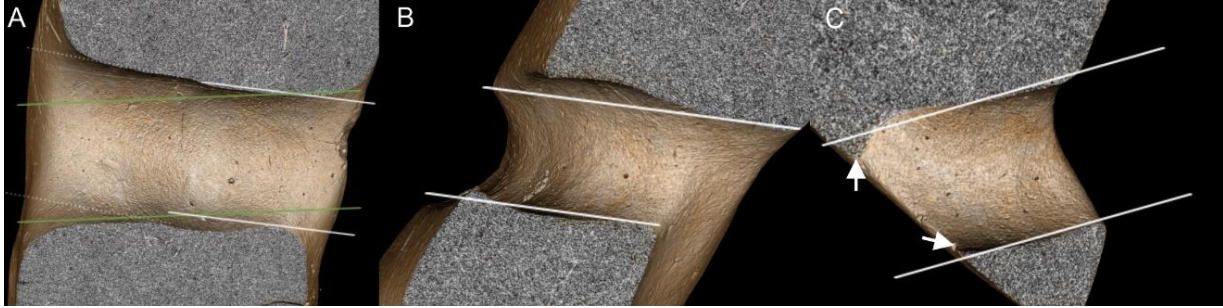
Figure S9. Potential cylindrical envelopes of a tool edge during drilling are sketched by pairs of straight lines on SEI6386 and SEI6557. (*a*) Two cylindrical shapes are needed to approximate the internal surface of the hole of SEI6386. (*b-c*) The drilling of a part of this hole (SEI6557) starts from the right side and does not go through the osteoderm; other manufacturing steps are needed to complete the complex geometry of this hole.
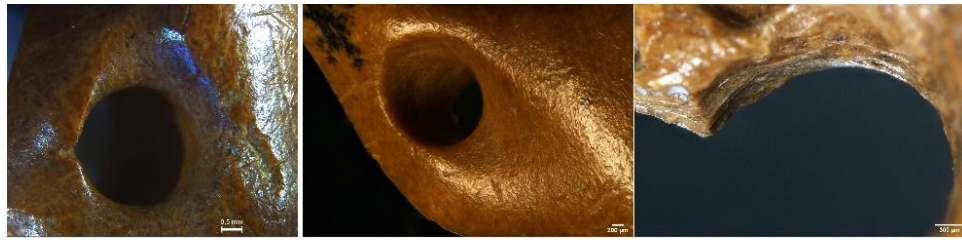
Bone osteoderms from Santa Elina: SEI6368, SEI6557, and SEI6059 (this study)

Shells (Falci et al., 2019)   Jet (Falci, 2015)   Shell (Falci, 2015)

Teeth (Falci et al., 2019)   Tooth (Vercoutère et al., 2007)   Bone (Mărgărit et al., 2018)

Figure S10. Comparison of modified osteoderms from Santa Elina and other ornaments made from bone, shells, and teeth worldwide presenting worn aspects and use-wear traces. Notice similarities with the samples from Santa Elina. Figures from Falci et al. (2019), and Mărgărit et al. (2018) are licensed under a Creative Commons Attribution 4.0 International License. To view a copy of this license, visit: http://creativecommons.org/licences/by/4.0. Figure by Vercoutére et al., (2007) reproduced with permission of BAR Publishing, www.barpublishing.com.
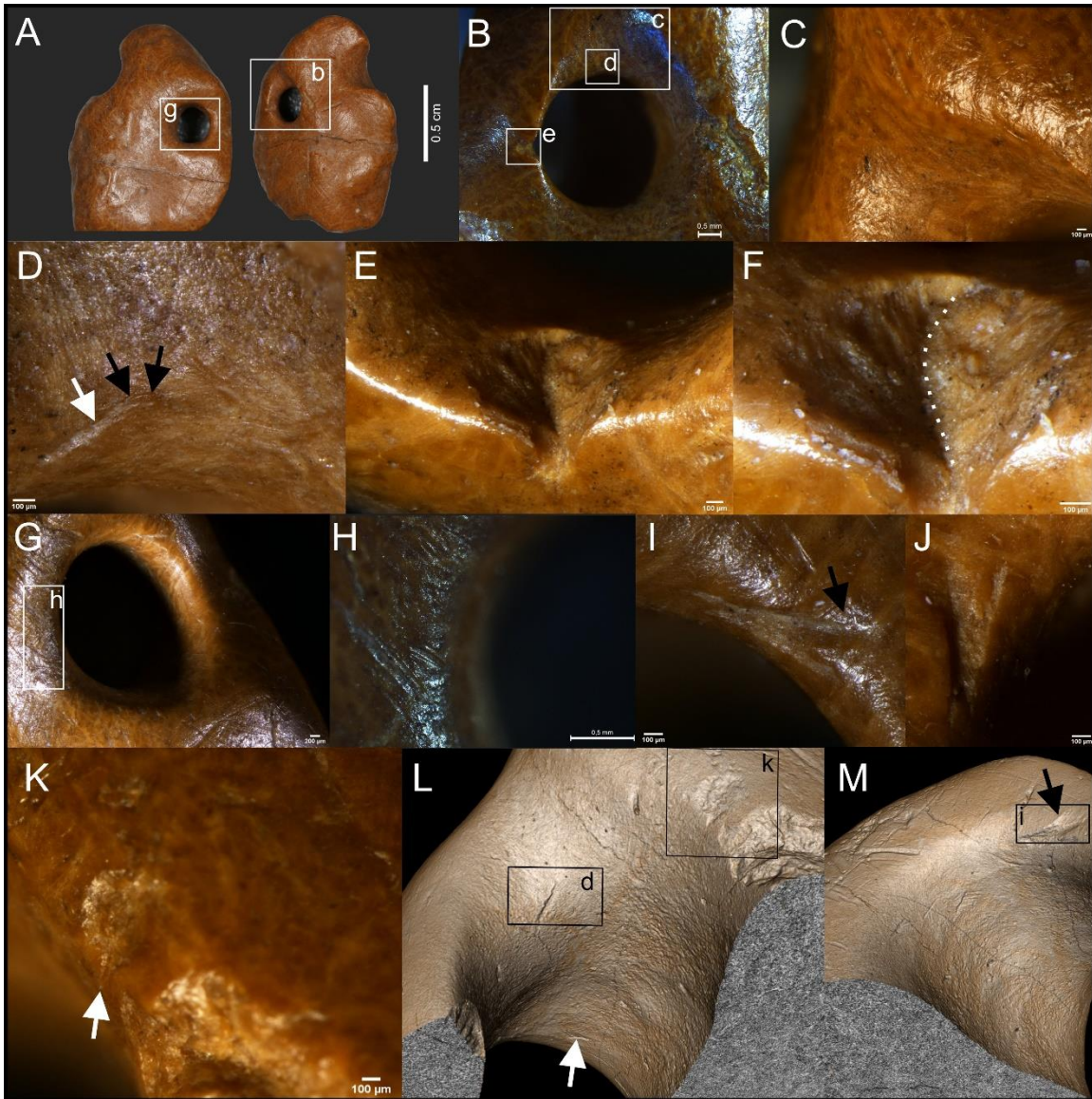
Figure S11. Additional images of the anthropic modified osteoderm SEI6386. (*a*) Macroscopic images using a digital camera. (*b-k*) Microscopic images using microscopes (Leica 2700P, *b-h*) and stereomicroscope (Nikon SMZ-25, *c-g, i-k*). (*l-m*) 3D images around the hole perforations, made using 3D Slicer software. Notice the smoothing, polish, and lustrous aspect of the bone and hole perforation. The presence of use-wear traces around the hole perforation and the attachement system is remarkable, including multiple directional shallow scratches (*c, g*). Notice anthropic traces from stone tools (white arrows), some with barbs (black arrows). Notice the curvature central striation of the anthropic scar (possible notch) with the dotted white line (*f*).
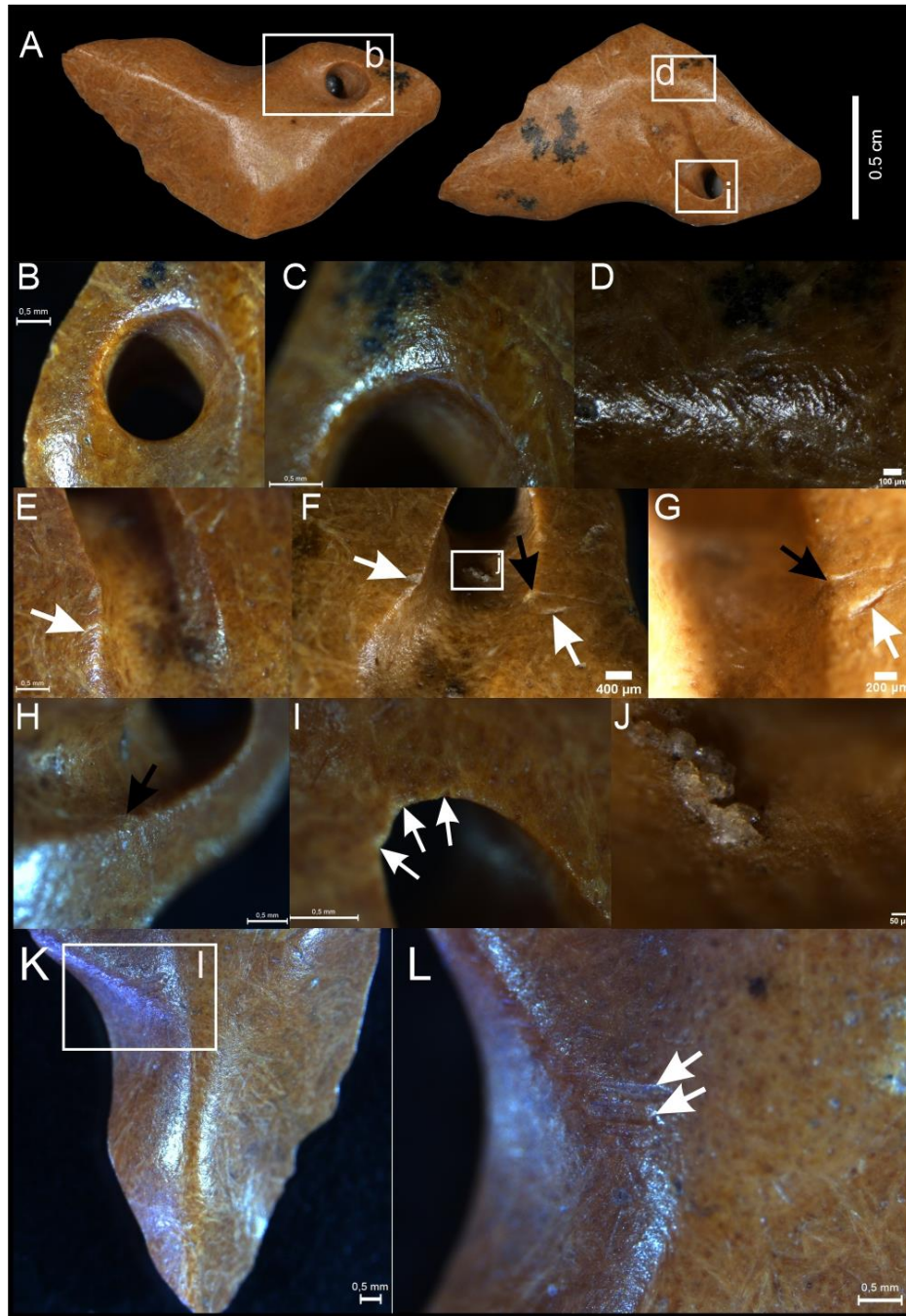
Figure S12. Additional images of the anthropic modified osteoderm SEI6557. (*a*) Macroscopic images using a digital camera. *(b-m)* Microscopic images using a microscope (Leica 2700P *c-e, h-i, k-l)* and stereomicroscope (Nikon SMZ-25, *b, f-g, j, m*). Notice the smoothing and polished aspect of the bone surface and hole perforation, including use-wear traces along the whole bone surface (*b-d*) and widened perforation (*b*). White arrows indicate diverse manufacturing marks, characterised by multiple directional fine and deep striations. Black arrows indicate a scar (possibly anthropic) that goes through the wall of the elongated hole on side 2. (*i*) Damaged areas, probable from pressure technique during the drilled perforation or intensive use-wear. (*j*) amorphous and greasy bone residue. (*l*) Set of parallel scratches on the transformed surface of the ornament.
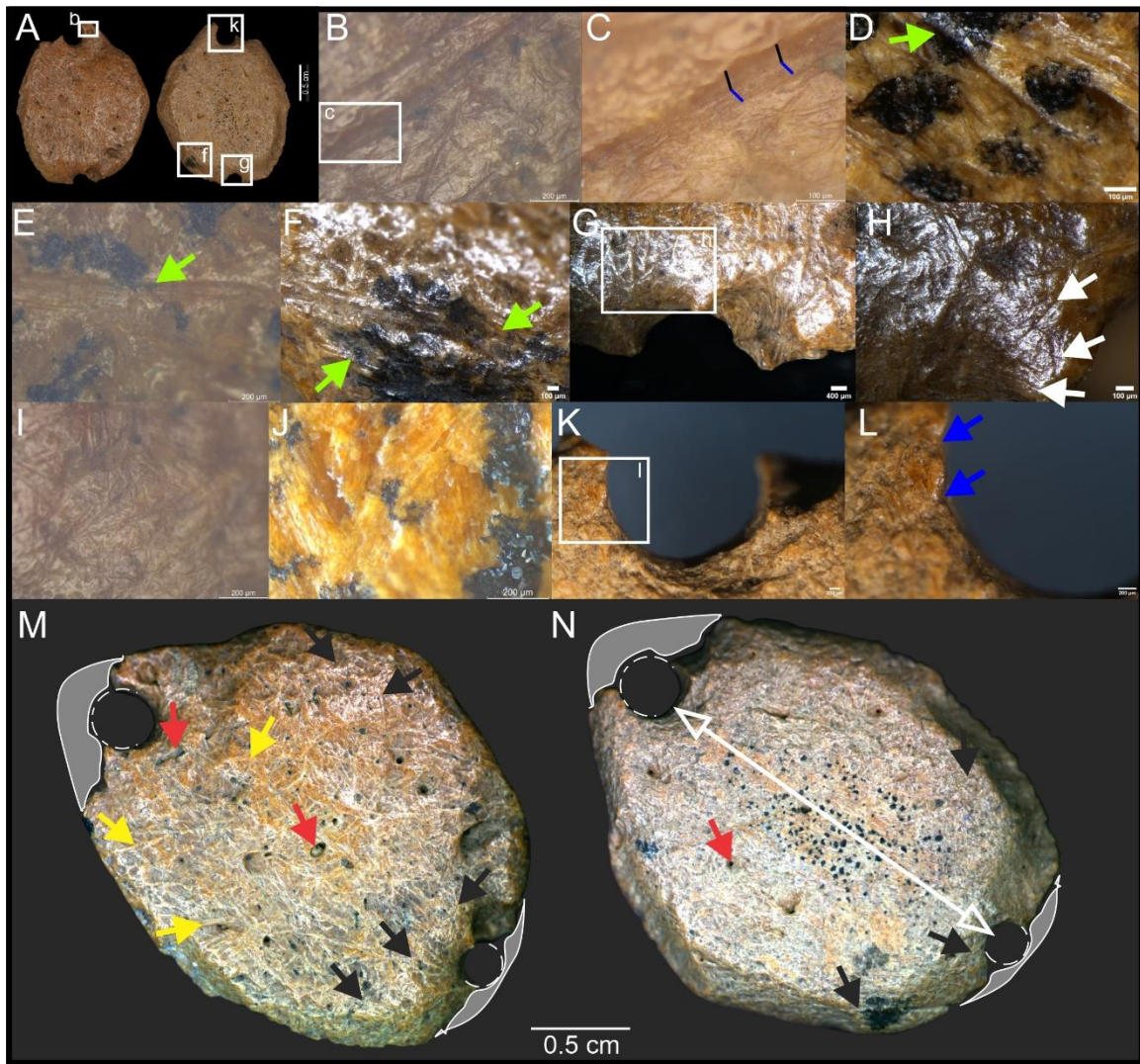
Figure S13. Additional images of the anthropic modified osteoderm SEI6059. (*a*) Macroscopic images of side 1 and 2, respectively, taken by digital camera. (*b,c*) Images taken using microscope (Leica 2700P) on side 1. *(d-l)* Images taken using microscope Leica (*e, i-j*) and stereomicroscope Nikon SMZ-25 (*d, f-h, k-l*) on side 2. (*m,n*) Macroscopic view by photoluminescence on side 1 and 2, respectively. The polished surface with use-wear traces all over the surface (*b-j*) and around the hole perforation (*h*) is remarkable. Notice the internal microstriations (*c,e*), characteristic of stone tool marks. (*d-f*) Notice taphonomic traits (oxides) overlapping marks, indicating their development before diagenesis. Notice the polish aspect of the collagen fibres (*j*), and a different aspect when compared with other unmodified osteoderm surfaces. (*h*) White arrow highlights drilling marks following the internal wall of one of the hole's perforations. (*l*) Blue arrows indicate deformed areas on the hole perforation, probably due to use-wear. Notice the polished aspect of the ornament, predominantly more on one of its sides (*m*) and consequently greater exposure of histological features than on the other side (*n*). Yellow arrows indicate exposed collagen fibre bundles, red arrows indicate vascular foramina, black arrows indicate anthropic marks, white arrows indicate use-wear traces, and green arrows indicate ancient marks overlapped by diagenetic traits. False colour RGB images were produced using reflection and red—emission at 685 ± 20 nm, green—emission at 571 ± 36 nm, and blue—emission at 472 ± 15 nm. (*m-n*) Reconstitution of the ancient ornament before breakage, likely an oval shape ornament. Probable ancient perforations (white dotted circles) and lost fragments of the bone

(grey areas). It is possible to observe different sizes of these perforations. Double-arrow line in white highlights its symmetry of the holes on the edges and in half potion of the bone, clearly intentional, probably for regular orientation of the suspension material.
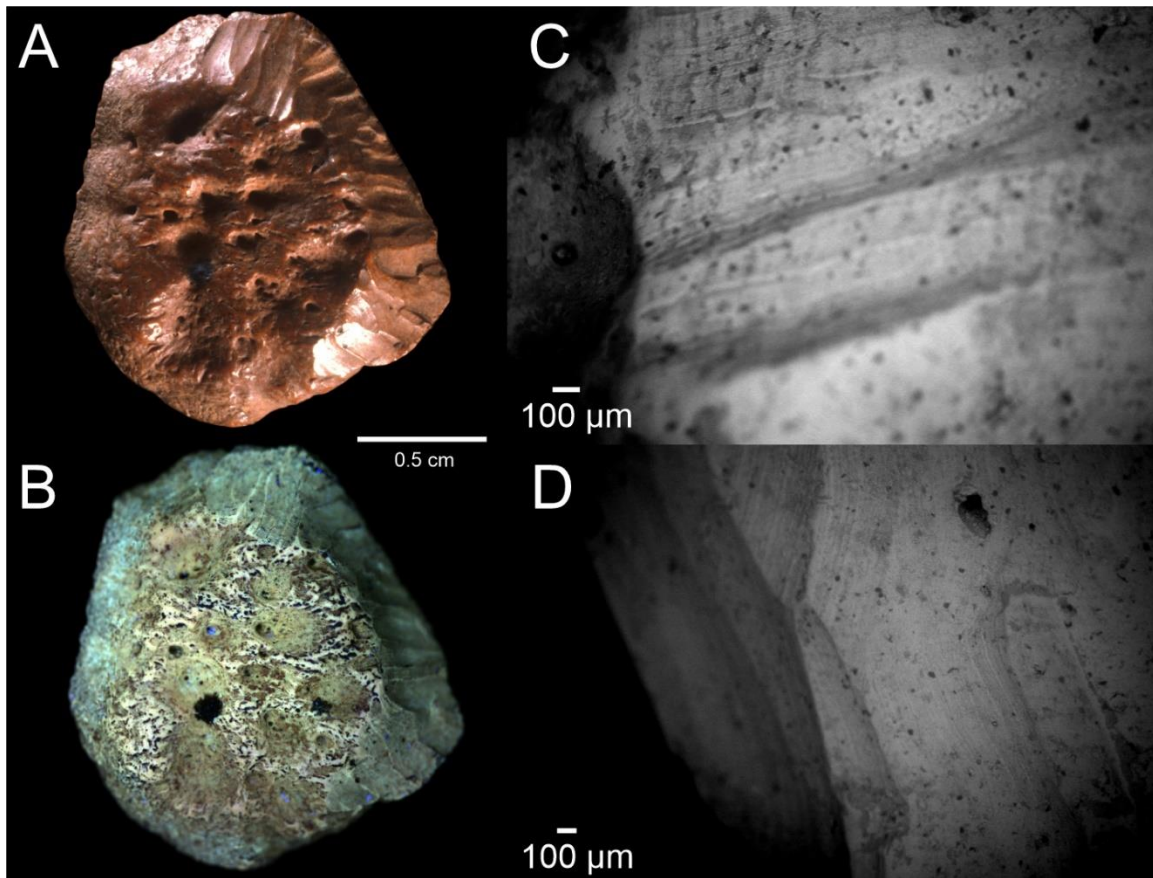
Figure S14. FR10, Unit II, 28D, z= 119 cm. Example of an osteoderm modified by rodent gnawing. (*a*) Macroscopic view with natural light. Notice homogenous colouration of the bone surface and the gnawed areas, which confirms fresh/pre-burial modification. (*b*) Macroscopic view using photoluminescence (PL). Notice the nature of the bone with superficial topographic depressions, natural foramina and pits, and rodent gnawing marks on the edges of the bone. Each set of rodent gnawing marks have a similar size and width. We highlight the uniform luminescence pattern of this freshly modified bone, which is similar to the PL behaviour observed in the anthropic modified osteoderms in this study. (*c-d*) Microscopic view by scanning electron microscope images using AsB detector. Notice the set of shallow internal microstriations in each groove, and U-shape of the end of these marks.
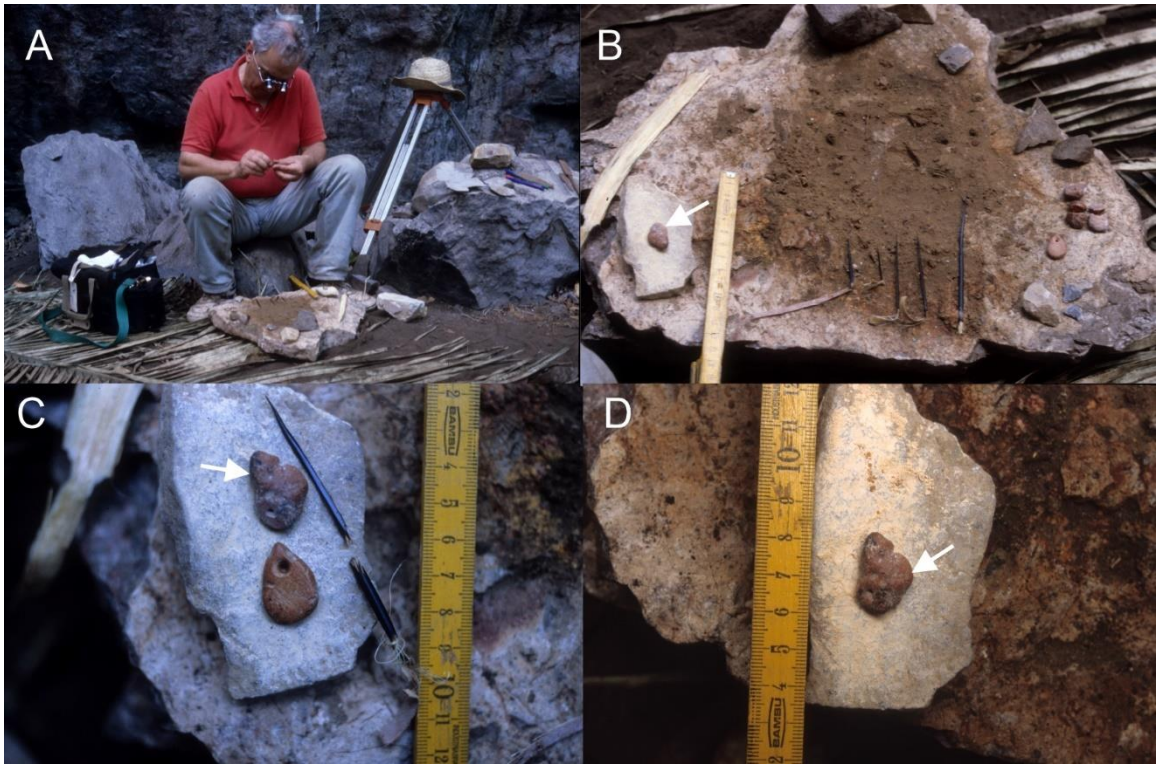
Figure S15. Images show the experiment conducted by Denis Vialou (*a*), in which fossil ground sloth osteoderms were perforated and shaped in Santa Elina using natural material from the site (Unit III4). (*b-d*) White arrows indicate specimen SEI8004 studied in this work. Credit: Águeda Vialou.

Table S1. Compiled dates from Santa Elina.

Table S2. Modelled commencement and end dates of Unit III-I, as estimated by OxCal boundary command.

Table S3. OxCal 4.4 Santa Elina Model.

Table S4. Detailed data of stone objects (n=598) from Unit II of Santa Elina. Blank spaces correspond to absent information.

Table S5. Detailed data of stone objects (n=338) from Unit III of Santa Elina. Blank spaces correspond to absent information.

Table S6. Detailed data of *G. phoenesis* bones (n=90), excluding osteoderms, from Unit II of Santa Elina.

Table S7. Detailed data of *G. phoenesis* bones (n=309), excluding osteoderms, from Unit III of Santa Elina.

Table S8. Detailed data of *G. phoenesis* osteoderms (n=2564), from Unit II of Santa Elina.

Table S9. Detailed data of *G. phoenesis* osteoderms (n=4505), from Unit III of Santa Elina.

Table S10. Coordinates of stone tools and ground sloth bones (excluding osteoderms) from Units II and III of Santa Elina used to generate 2D and 3D association maps.

Table S11. Dataset of the features observed in the fossil osteoderms. BSM: Bone Surface Modifications, 1: taphonomic aspects; 2: rodent gnawing marks; 3: trampling marks; 4: indistinguishable marks (see criteria details in Text S1).

Table S12. Size of natural foramina, bioerosion, and the anthropic perforation holes present in unmodified and modified osteoderms.

(Supplementary tables are found in the Appendix I).

Movie S1 (separate file). Short video in 3D of the ornament SEI6059 in rotation movement enables observation of the modified surfaces and marks distributed along the bone in different views.

Movie S2 (separate file). Short video in 3D of the ornament SEI6557 in rotation movement enables observation of the modified surfaces and marks distributed along the bone in different views.

Movie S3 (separate file). Short video in 3D of the ornament SEI6386 in rotation movement enables observation of the modified surfaces and marks distributed along the bone in different views.

References

1. Scheel‑Ybert R, Bachelet C. 2020 A good place to live: Plants and people at the Santa Elina rock shelter (Central Brazil) from Late Pleistocene to the Holocene. *Lat. Am. Antiq.* 31(2), 273–291. (doi:10.1017/laq.2020.3)

2. Vialou D, Benabdelhadi M, Feathers J, Fontugne M, Vialou AV. 2017 Peopling South America's centre: the late Pleistocene site of Santa Elina. *Antiquity* 91(358), 865–884. (doi:10.15184/aqy.2017.101)

3. Ramsey CB. 2021 OxCal 4.4.4 calibration program.

4. Ramsey CB. 2009 Bayesian analysis of radiocarbon dates. *Radiocarbon* 51(1), 337–360. (doi:10.1017/S0033822200033865)

5. Ramsey CB. 2000 Comment on 'The Use of Bayesian Statistics for 14C dates of chronologically ordered samples: a critical analysis', *Radiocarbon* 42 (2), 199–202. (doi:10.1017/S0033822200059002)

6. Figuti, L. 2005 Considerações sobre a distribuição espacial da megafauna em Santa Elina. In: Vialou, AV.. Pré-história do Mato Grosso: Santa Elina (1), EdUSP, 163-166. (ISBN:85-3140861-X)

7. Brambilla L, Toledo MJ, Haro JA, Aguilar JL. 2019 New osteoderm morphotype (Xenarthra, Mylodontidae) from the middle Pleistocene of Argentina. *J. S. Am.* 95, 102298. (doi:10.1016/j.jsames.2019.102298)

8. Cartelle C, De Iuliis G, Boscaini A, Pujos F. 2019 Anatomy, possible sexual dimorphism, and phylogenetic affinities of a new mylodontine sloth from the late Pleistocene of intertropical Brazil. *J. Syst. Palaeontol.* 17(23), 1957–1988. (doi:10.1080/14772019.2019.1574406)

9. Toledo N, Boscaini A, Pérez LM. 2021 The dermal armor of mylodontid sloths (Mammalia, Xenarthra) from Cueva del Milodon (Última Esperanza, Chile). *J. Morphol.* 282(4), 612–627. (doi: 10.1002/jmor.21333)

10. Tomassini RL, Montalvo CI, Ezquiaga MC. 2016 The oldest record of flea/armadillos interaction as example of bioerosion on osteoderms from the late Miocene of the Argentine Pampas. *Int. J. Paleopathol.* 15, 65–68. (doi:10.1016/j.ijpp.2016.08.004)

11. Perea D, Verde M, Montenegro F, Toriño P, Manzuetti A, Roland G. 2019 Insect trace fossils in glyptodonts from Uruguay. *Ichnos* 27(1), 70–79. (doi:10.1080/10420940.2019.1584562)

12. de Lima FCG, Porpino KDO. 2018 Ectoparasitism and infections in the exoskeletons of large fossil cingulates. *PLoS One* 13(10), e0205656. (doi:10.1371/journal.pone.0205656)

13. Xing L, Parkinson AH, Ran H, Pirrone CA, Roberts EM, Zhang J, Burns ME, Wang T, Choiniere J. 2016 The earliest fossil evidence of bone boring by terrestrial invertebrates, examples from China and South Africa. *Hist. Biol.* 28(8), 1108–1117. (doi:10.1080/08912963.2015.1111884)

14. Fernandez-Jalvo Y, Andrews P, Sevilla P, Requejo V. 2014 Digestion versus abrasion features in rodent bones. *Lethaia* 47(3), 323–336. (doi:10.1111/let.12061)

15. Montalvo CI et al. 2023. Armadillo osteoderms altered by digestion and how taphonomy can help taxonomy. *Palaios* 38(1), 31–42. (doi:10.2110/palo.2022.040)

16. Pineda A, Saladié P, Vergès JM, Huguet R, Cáceres I, Vallverdú J. 2014 Trampling versus cut marks on chemically altered surfaces: an experimental approach and archaeological application at the Barranc de la Boella site (la Canonja, Tarragona, Spain). *J. Archaeol. Sci.* 50, 84–93. (doi:org/10.1016/j.jas.2014.06.018)

17. Amadasi A, Camici A, Sironi L, Profumo A, Merli D, Mazzarelli D, Porta D, Duday H, Cattaneo C. 2015 The effects of acid and alkaline solutions on cut marks and on the structure of bone: An experimental study on porcine ribs. *Leg. Med.* 17(6), 503–508. (doi: 10.1016/j.legalmed.2015.10.006)

18. Falci CG, Cuisin J, Delpuech A, Van Gijn A, Hofman CL. 2019 New Insights into Use-Wear Development in Bodily Ornaments Through the Study of Ethnographic Collections. *J. Archaeol. Method Theory*. 26(2), 755–805. (doi.org/10.1007/s10816-018-9389-8)

19. Falci CG. 2015 Stringing Beads Together: A Microwear Study of Bodily Ornaments in the Late PreColonial North-Central Venezuela and North-Western Dominican Republic. M.A. thesis. Faculty of Archaeology, Leiden University.

20. Vercoutère C, Patou-Mathis M, Giacobini G. 2007 The importance of the paleontological and taphonomical analyses for the study of bone industries. In: Bones as Tools: Current Methods and Interpretations in Worked Bone Studies, BAR S (1622), 23–34.

21. Mărgărit M, Radu V, Boroneanț A, Bonsall C. 2018 Experimental studies of personal ornaments from the Iron Gates Mesolithic. *Archaeol Anthropol Sci.* 10(8), 2095–2122. (doi:10.1007/s12520-017-0522-5)

4. CHAPTER 4: ABSTRACT - PALEOBIOLOGY

Synchrotron-based XRF applied to the paleohistological study of giant sloths' osteoderms

Thaís R Pansani, Mariela C de Castro, Sebastian Schöder, Mírian LAF Pacheco, Loïc Bertrand

The Santa Elina archaeological site (MT, Brazil) has a paradigmatic importance due to the possibility of one of the oldest human/fauna interactions. The shelter features an expressive rock art panel and a rich archaeological record containing lithic tools, bonfire structures, materials worked with plant fibers, and faunal remains attributed to human's culture. Among the most important records are the Pleistocene giant sloth (*Glossotherium* sp.) osteoderms (~ 7,000), displaying distinct shapes and sizes, and including some with surface modifications and fusions. Here, we investigate the chemical and histological features of two fossil osteoderms by synchrotron-based X-Ray Fluorescence (XRF) that resulted in unprecedented elemental imaging maps for this mylodontid species. Besides the detailed microstructure revealed by the cross-sections, we were able to observe a compact histological structure, composed predominantly by Zn-rich phases which we interpreted as collagen fiber bundles and growth lines parallel to the external surface. Our results also show conspicuous vascular channels filled by diagenetic traits corroborated by Sr, Ba, Ni and Eu enrichment and Ca and K depletion. Another sample analyzed represents two fused elements. Its imaging maps show distinct directions of the growth lines along the two centers of ossification, highlighted by Zn. Our team is still performing other synchrotron-based analyses in order to investigate if some of the distinct shape and fused osteoderms are related to a bone disease in this animal, as well as the taphonomic history of these fossils.

APPENDIX I – CHAPTER 2

Supplementary Table S1. Compiled dates from Santa Elina.

Lab no.	Material	Dating Technique	Unit	Date BP	Lab error	Reference
UW609	quartz	OSL	IV	27800	2700	Vialou et al., 2017
Th/U SE9402	bone(osteoderm)	U/Th	III (4)	27000	2000	Vialou et al., 2017
UW465	quartz	OSL	III (4)	25100	2500	Vialou et al., 2017
Gif-9365	wood	C14	III (2)	23320	1000	Vialou et al., 2017
GIFA 99177	microcharcoal	C14	III (4)	23120	260	Vialou et al., 2017
Gif-9366	wood	C14	III (2)	22500	500	Vialou et al., 2017
UW464	quartz	OSL	II (3)	18700	900	Vialou et al., 2017
Th/U SE 9404	bone(osteoderm)	U/Th	II (2)	13000	1000	Vialou et al., 2017
Gif-8954	charcoal	C14	II (2)	10120	60	Vialou et al., 2017
Gif/LSM-11121	charcoal	C14	II (2)	9790	20	Vialou et al., 2017
Gif/LSM-10683	charcoal	C14	II (2)	9340	20	Vialou et al., 2017
Gif-9368	charcoal	C14	II (1)	7050	55	Vialou et al., 2017
Gif-9369	charcoal	C14	II	7010	70	Vialou et al., 1995
Gif-7880	charcoal	C14	I	6060	80	Vialou et al., 1995
Gif-7054	charcoal	C14	I	6040	70	Vialou et al., 2017
Gif-7881	charcoal	C14	I	5920	70	Vialou et al., 1995
Gif-7882	charcoal	C14	I	5890	70	Vialou et al., 1995
Gif-8679	charcoal	C14	I	5890	70	Vialou et al., 1995
Gif-9370	charcoal	C14	I	5860	60	Vialou et al., 1995
Gif-7085	charcoal	C14	I	5660	60	Vialou et al., 1995
Gif-7983	charcoal	C14	I	5110	230	Vialou et al., 1995
Gif-7883	charcoal	C14	I	5080	230	Vialou et al., 1995
GIF-7379	charcoal	C14	I	3970	60	Vialou et al., 1995
Gif-8822	charcoal	C14	I	3600	60	Vialou et al., 1995
Gif11124	charcoal	C14	I	3560	50	Vialou, 2005
Gif-9693	charcoal	C14	I	3530	50	Vialou, 2005
Gif-7086	charcoal	C14	I	2990	60	Vialou et al., 1995
Gif-10356	charcoal	C14	I	2660	50	Vialou, 2005
Gif-7758	charcoal	C14	I	2600	60	Vialou et al., 1995
Gif-7380	charcoal	C14	I	2350	60	Vialou et al., 1995
Gif-7879	charcoal	C14	I	2310	70	Vialou et al., 1995
Gif-10537	charcoal	C14	I	1890	20	Vialou, 2005
Gif-9692	charcoal	C14	I	1770	60	Vialou et al., 2017
Gif-8955	corn cob	C14	I	400	50	Vialou et al., 1995

| Gif-8890 | stake | C14 | I | 275 | 40 | Vialou et al., 1995 |

Supplementary Table S2. Modelled commencement and end dates of Unit III-I, as estimated by OxCal boundary command.

Unit	1 sigma (68.3% probability) BP	2 sigma (95.4% probability) BP
Unit III commences	27942-27185	28743-26536
Unit III ends by	26230-26230	27225-25225
Unit II commences	21473-17778	24922-16880
Unit II ends by	7785-7785	7947-7714
Unit I commences	7832-7709	7901-7656
Unit I ends by	323-	422-

Supplementary Table S3. OxCal 4.4 Santa Elina Model.

Name	Unmodelled (BP)						Modelled (BP)						Indices Amodel 92.9 Aoverall 92.8				
	from	to	%	from	to	%	from	to	%	from	to	%	Acomb	A	L	P	C
Sequence Santa Elina Date Sequence																	
C_Date UW609	30502	25100	68.26895	33201	22401	95.45	31499	28279	68.268949	33727	27614	95.44997		89.3			97.1
Boundary Start Unit III							28832	27408	68.268949	30329	27136	95.44997					99.2
Phase Unit III(4)																	
C_Date SE9402	29002	25000	68.26895	31001	23001	95.45	27969	26772	68.268949	28917	26294	95.44997		130.9			99.8
R_Date GIFA 99177	27639	27215	68.26895	27831	26919	95.45	27621	27214	68.268949	27793	26974	95.44997		102.3			99.8
C_Date UW465	27602	22600	68.26895	30101	20101	95.45	27896	26727	68.268949	28821	26253	95.44997		90.8			99.7
Phase Unit III(3)																	
R_Date Gif-9366	27262	26297	68.26895	27691	25898	95.45	26865	26039	68.268949	27273	25842	95.44997		102.5			99.6
R_Date Gif-9365	28632	26475	68.26895	29941	25860	95.45	27019	26012	68.268949	27511	25574	95.44997		81.9			99.4
Boundary End Unit III							22462	21273	68.268949	22524	19640	95.44997					99.5
Boundary Start Unit II							20364	17819	68.268948	21689	16958	95.44997					99.1
C_Date UW464-Unit II(3)	19602	17800	68.26895	20501	16901	95.45	18982	17184	68.26895	19820	16312	95.44997		89.4			98.9
Phase Unit II(2)																	
C_Date SE9404	14002	12000	68.26895	15001	11001	95.45	14035	11975	68.268948	14982	11013	95.44997		100			98.8
R_Date Gif-8954	11834	11353	68.26895	11871	11318	95.45	11833	11353	68.26895	11871	11318	95.44997		99.8			99.9
R_Date LSM-11121	11217	11176	68.26895	11240	11116	95.45	11217	11176	68.268949	11240	11117	95.44997		99.4			99.9
R_Date Gif/LSM-10683	10567	10439	68.26895	10645	10380	95.45	10567	10439	68.268949	10645	10380	95.44997		99.6			99.9
R_Date Gif-9368-Unit II(1)	7932	7786	68.26895	7956	7699	95.45	7941	7845	68.268949	8006	7787	95.44997		101.5			99.9
Boundary End Unit II							7907	7785	68.268949	7948	7714	95.44997					100
Boundary Start Unit I							7833	7709	68.268949	7901	7655	95.44997					100
Phase Unit I																	
R_Date Gif-9369	7922	7725	68.26895	7943	7671	95.45	7773	7672	68.268949	7838	7611	95.44997		83.8			99.9
R_Date Gif-7880	6975	6747	68.26895	7157	6669	95.45	6975	6747	68.268949	7157	6669	95.44997		99.9			99.8
R_Date Gif-7054	6941	6747	68.26895	7154	6663	95.45	6940	6747	68.268949	7154	6662	95.44997		100			99.9
R_Date Gif-7881	6795	6568	68.26895	6886	6499	95.45	6795	6568	68.26895	6886	6500	95.44997		99.9			99.9

R_Date Gif-7882	6776	6561	68.26895	6881	6485	95.45	6776	6561	68.268949	6879	6485	95.44997	99.9	99.9
R_Date Gif-8679	6776	6561	68.26895	6881	6485	95.45	6776	6561	68.268949	6879	6484	95.44997	99.9	99.8
R_Date Gif-9370	6732	6553	68.26895	6787	6455	95.45	6732	6552	68.268949	6787	6455	95.44997	100	99.9
R_Date Gif-7085	6499	6314	68.26895	6627	6300	95.45	6527	6314	68.268949	6627	6300	95.44997	99.9	99.8
R_Date Gif-7983	6175	5588	68.26895	6310	5318	95.45	6175	5588	68.268949	6311	5318	95.44997	99.9	99.6
R_Date Gif-7883	6172	5488	68.26895	6310	5306	95.45	6171	5488	68.268949	6311	5306	95.44997	99.9	99.5
R_Date GIF-7379	4510	4255	68.26895	4530	4153	95.45	4510	4254	68.26895	4530	4153	95.44997	99.8	99.9
R_Date Gif-8822	3970	3725	68.26895	4080	3650	95.45	3970	3725	68.268949	4080	3651	95.44997	99.9	99.8
R_Date Gif11124	3881	3718	68.26895	3970	3644	95.45	3881	3718	68.268949	3970	3644	95.44997	99.9	99.9
R_Date Gif-9693	3835	3695	68.26895	3958	3627	95.45	3836	3695	68.268949	3957	3627	95.44997	100	99.9
R_Date Gif-7086	3209	3003	68.26895	3337	2934	95.45	3208	3004	68.268949	3337	2934	95.44997	100	99.8
R_Date Gif-10356	2845	2713	68.26895	2860	2499	95.45	2845	2713	68.268949	2860	2500	95.44997	99.8	99.9
R_Date Gif-7879	2345	2146	68.26895	2489	2090	95.45	2345	2145	68.26895	2488	2090	95.44997	99.9	99.9
R_Date Gif-7380	2363	2148	68.26895	2676	2136	95.45	2363	2148	68.268949	2678	2136	95.44997	99.8	99.9
R_Date Gif-7758	2755	2500	68.26895	2779	2370	95.45	2756	2501	68.268949	2779	2370	95.44997	99.7	99.9
R_Date Gif-10537	1822	1744	68.26895	1834	1720	95.45	1822	1744	68.268949	1834	1719	95.44997	99.6	99.9
R_Date Gif-9692	1704	1568	68.26895	1821	1520	95.45	1705	1568	68.268949	1821	1520	95.44997	99.9	99.9
R_Date Gif-8890	321	151	68.26895	442	144	95.45	437	154	68.268949	445	146	95.44997	96	99.9
R_Date Gif-8955	493	327	68.26895	500	314	95.45	493	328	68.268949	500	315	95.44997	100	99.9
Boundary End Unit I							320	-119	68.268949	425	-677	95.44997		98.8

Supplementary Table S4. Detailed data of stone objects (n=598) from Unit II of Santa Elina. Blank spaces correspond to absent information.

Nº	Square	X	Y	Z	Artifact	Material	Association with charcoal?
4133	29 C	-	-	124	Stone tool	Limestone	
4271	29 C	-	-	124	Pigment	Hematite	
4996	28 D	35	5	130	Flake	Limestone	
3404 a	29 C	-	-	131	Pigment	Hematite	
3339	26 D	-	-	135	Fragment	Limestone	
3329	27 D	-	-	138	Smaller flakes	Limestone	
3330	27 D	-	-	138	Smaller flakes	Limestone	
3331	27 D	-	-	138	Smaller flakes	Limestone	
3300	27 C	4	30	139	Flake	Quartz	
3306	27 C	-	-	142	Platelet	Silex	
3337	27 C	-	-	142	Crystal	Quartz	Yes
3324	29 C	-	-	144	Smaller flakes	Limestone	
3325	29 C	-	-	144	Smaller flakes	Limestone	
3326	29 C	-	-	144	Smaller flakes	Limestone	
3327	29 C	-	-	144	Smaller flakes	Limestone	
3328	29 C	-	-	144	Smaller flakes	Limestone	
3342	30 C	-	-	144	Fragment	Limestone	
3343	30 C	-	-	144	Fragment	Limestone	
3344	30 C	-	-	144	Fragment	Limestone	
3301	27 C	54	70	145	Flake	Limestone	
3302	27 C	13	86	145	Flake	Limestone	
3332	27 C	-	-	146	Smaller flakes	Limestone	
3333	27 C	-	-	146	Smaller flakes	Limestone	
3334	27 C	-	-	146	Smaller flakes	Limestone	
3412	28 C	98	15	146	Pigment	Hematite	
3585	26 D	30	22	148	Stone tool?	Silex	
4404	26 D	-	-	150	Smaller flakes	Calcite	
3549	27 C	-	-	150	Pigment	Hematite	
3799	27 C	98	50	151	Stone tool	Limestone	
3345	28 C	-	-	152	Flake	Limestone	

3346	28 C	-	-	152	Flake	Limestone	
3347	28 C	-	-	152	Flake	Limestone	
3348	28 C	-	-	152	Smaller flakes	Silex	
3349	28 C	-	-	152	Smaller flakes	Silex	
3318	29 B	65	60	152	Flake	Limestone	
3547	27 B	-	-	153	Flake	Limestone	
3566	27 C	-	-	153	Stone tool	Limestone	
3575	28 C	85	54	153	Painted block	Limestone	
3319	29 B	60	10	153	Flake	Limestone	
3648	26 C	-	-	155	Flake	Silex	
3637	27 C	-	-	157	Flake	Calcite	
4289	28 B	-	-	157	Pigment	Hematite	
4213	29 B	-	-	158	Stone tool	Limestone	
3450	29 B	-	-	160	Painted block	Limestone	
3663 a	29 C	-	-	160	Flake	Limestone	
3663 b	29 C	-	-	160	Smaller flakes	Limestone	
3451	30 A	-	-	160	Painted block	Limestone	
3658	26 C	-	-	161	Fragment	Sandstone	
3662 a	29 B	-	-	161	Stone tool?	Limestone	
3661	26 C	56	20	162	Flake	Limestone	
3602 a	29 C	25	31	162	Flake	Limestone	
3340	25 C	-	-	163	Flake	Limestone	
3341	25 C	-	-	163	Flake	Limestone	
4372	28 C	-	-	163	Fragment	Calcite	
3680	29 C	-	-	163	Stone tool?	Limestone	
3679	26 B	83	96	164	Stone tool	Limestone	
3707	27 C	-	-	164	Flake	Limestone	Yes
3708	27 C	-	-	164	Flake	Limestone	Yes
3709	27 C	-	-	164	Flake	Limestone	Yes
3743	27 C	-	-	164	Flake	Silex	
3726	27 C	-	-	164	Fragment	Calcite	
3793	27 C	-	-	164	Stone tool?	Quartz	
4373	28 C	-	-	164	Stone tool	Quartz	
3335	25 D	-	-	165	Flake	Limestone	
3336	25 D	-	-	165	Flake	Limestone	
3818	29 D	-	-	165	Flake	Limestone	
3706	26 B	-	-	167	Stone tool	Limestone	
3725	26 C	-	-	167	Flake	Limestone	
3723	26 C	42	82	167	Flake	Limestone	

3623 b	26 A	-	-	168	Flake	Calcite	
3623 a	26 A	-	-	168	Flake	Quartz	
3624	26 A	-	-	168	Flake	Limestone	
3861 a	27 B	68	38	168	Stone tool	Limestone	
3861 b	27 B	68	38	168	Smaller flakes	Limestone	
3751	27 C	-	-	168	?	Limestone	
3752	27 C	-	-	168	Fragment	Calcite	
3754 a	27 C	-	-	168	Fragment	Calcite	
3754 b	27 C	-	-	168	Fragment	Calcite	
3778	29 C	-	-	168	Smaller flakes	Calcite	
3775 a	24 C	-	-	169	Flake	Limestone	
3775 b	24 C	-	-	169	Fragment	Calcite	
3667	26 A	90	30	169	Flake	Limestone	
3868 b	26 A	95	35	169	Flake	Limestone	
6975	30 C	60	10	169	?	Sandstone	Yes
3749	26 B	-	-	169	Pigment	Hematite	
4798	19 B	80	50	170	Painted block	Limestone	
3943	23 A	-	-	170	Flake	Limestone	
3510	25 C	-	-	170	Flake	Silex/Calcite	
3669	26 A	-	-	170	Flake	Quartz	
3671	26 A	-	-	170	Flake	Limestone	
3773	27 B	-	-	170	Fragment	Silex	
3774	27 B	-	-	170	Smaller flakes	Limestone	
4409	27 C	25	87	170	Block	Limestone	
3920	28 C	-	-	170	Fragment	Calcite	
3779	29 B	-	-	170	Fragment	Calcite	
3748	26 B	-	-	171	Pigment	Hematite	
4248	26 B	-	-	171	Pigment	Hematite	
3879	27 C	25	36	171	Stone tool	Limestone	
2307	24 C	48	63	172	Block	Limestone	
3769	26 B	-	-	172	Pigment	Hematite	
4189	27 C	10	75	172	Block	Limestone	
4274	27 C	5	5	172	Pigment	Hematite	
4288	27 C	56	7	172	Pigment	Hematite	
6493	29 A	90	87	172	Block	Silex	
3913	27 A	93	94	173	Flake	Silica	

3869	27 C	-	-	173	Flake	Limestone	
3908	27 C	-	-	173	Smaller flakes	Limestone	
3847	27 B	38	30	174	Flake	Limestone	
3914	28 A	-	-	174	Smaller flakes	Limestone	
3915	28 A	-	-	174	Smaller flakes	Limestone	
3916	28 A	-	-	174	Smaller flakes	Limestone	
3871	28 B	-	-	174	Flake	Limestone	
2308	24 C	-	-	175	?	Limestone	
4340	25 C	32	84	175	Fragment	Limestone	
3917	26 B	-	-	175	Smaller flakes	Limestone	
4356	26 C	-	-	175	Smaller flakes	Calcite	
4935	27 D	-	-	175	Flake	Limestone	
3940	26 C	55	16	176	Stone tool	Limestone	
4361	27 A	-	-	176	Pigment	Hematite	
4362	27 A	-	-	176	Fragment	Calcite	
3971	27 C	-	-	176	Pigment	Hematite	
3996	27 C	-	-	176	Pigment	Hematite	
3791 b	29 B	-	-	176	Crystal	Quartz	
3833	29 B	-	-	176	Smaller flakes	Limestone	
1821	21 B	95	53	177	Flake	Limestone	Yes
1911	22 A	73	48	177	Platelet	Hematite	
2343	24 C	-	-	177	Pigment	Hematite	
4343	26 B	-	-	177	Smaller flakes	Crystal	
4344	26 B	-	-	177	Fragment	Quartz	
3789	26 C	-	-	177	Pigment	Hematite	
3790	26 C	-	-	177	Flake	Quartz	
4039	26 C	-	-	177	Flake	Limestone	
4302	27 A	-	-	177	Pigment	Hematite	
1904	22 A	-	-	178	Flake	Silex	
1905	22 A	-	-	178	Flake	Limestone	
1906	22 A	-	-	178	Flake	Limestone	
4778	24 B	-	-	178	Flake	Limestone	Yes
4779	24 B	-	-	178	Flake	Limestone	Yes
4003	26 B	-	-	178	Fragment	Calcite	
4004	26 B	-	-	178	Smaller flakes	Limestone	
4341	26 C	-	-	178	Fragment	Calcite	
4377	26 C	-	-	178	Smaller flakes	Calcite	

4032	27 C	71	42	178	Stone tool	Quartz	
4020	28 B	21	32	178	Stone tool	Limestone	
4033	29 B	-	-	178	Smaller flakes	Calcite	
3918	29 C	-	-	178	Smaller flakes	Clay	
4331	25 C	-	-	179	Smaller flakes	Limestone	
4363	26 C	-	-	179	Fragment	Quartz	
1802	22 B	20	48	180	Flake	Silex	
1828	22 C	59	59	180	Pigment	Hematite	
1940	23 C	50	30	180	Flake	?	
4381	25 C	-	-	180	Smaller flakes	Limestone	
4292	26 A	-	-	180	Pigment	Hematite	
4378	26 B	-	-	180	Smaller flakes	Limestone	
4383	27 B	-	-	180	Smaller flakes	Calcite	
4384	27 B	-	-	180	Flake	?	
4385	27 B	-	-	180	Fragment	Calcite	
4386	27 B	-	-	180	Smaller flakes	Calcite	
4022	28 B	-	-	180	Stone tool	Limestone	
4023	28 B	-	-	180	Flake	Limestone	
4293	28 B	-	-	180	Pigment	Hematite	
4294	28 B	-	-	180	Pigment	Hematite	
4295	28 B	-	-	180	Pigment	Hematite	
6498	29 A	70-80	70-80	180	Block	Silex	
4019	29 B	5	33	180	Stone tool?	Limestone	
4290	29 B	-	-	180	Pigment	Hematite	
1820	21 C	20	75	181	Smaller flakes	?	Yes
4025 a	26 C	-	-	181	Flake	Limestone	
4025 b	26 C	-	-	181	Fragment	Calcite	
4318	28 A	-	-	181	Smaller flakes	Calcite	
4279	22 A	-	-	182	Pigment	Hematite	
4278	25 A	-	-	182	Pigment	Hematite	
3639	26 A	-	-	182	Fragment	Quartz	
3645	26 A	-	-	182	Flake	Limestone	
3647	26 A	-	-	182	Flake	Limestone	
3665	26 A	-	-	182	Smaller flakes	Limestone	
3670	26 A	-	-	182	Smaller flakes	Calcite	

4419	26 A	-	-	182	Fragment	Calcite	
4420	26 A	-	-	182	Smaller flakes	Calcite	
4421	26 A	-	-	182	Pigment	Hematite	
4068	26 C	-	-	182	Smaller flakes	Limestone	
4188	27 C	-	-	182	Block	Limestone	
6494	29 A	95	86	182	Block	Silex	
1813	21 C	50	40	183	Smaller flakes	Limestone	Yes
1816	21 C	99	76	183	Flake	Limestone	
1817	21 C	95	74	183	Flake	Limestone	
1818	21 C	93	78	183	Smaller flakes	Limestone	
1819	21 C	60	75	183	Flake	Limestone	
4001	25 B	21/30	70/80	183	Core	Sandstone	
4379	25 C	80	67	183	Smaller flakes	Limestone	
4281	26 B	-	-	183	Pigment	Hematite	
4336	26 B	-	-	183	Fragment	Calcite	
4005	26 C	-	-	183	Pigment	Hematite	
4007	26 C	-	-	183	Smaller flakes	Limestone	
4010	26 C	-	-	183	Pigment	Hematite	
4014	26 C	74	21	183	Stone tool	Limestone	
4015	26 C	-	-	183	Pigment	Hematite	
4021	26 C	-	-	183	Pigment	Hematite	
4016	26 C	-	-	183	Smaller flakes	Limestone	
4017 a	26 C	-	-	183	Flake	Limestone	
4017 b	26 C	-	-	183	Flake	Limestone	
4067	28 C	5	23	183	Stone tool	Limestone	
4013	29 A	-	-	183	Stone tool	Limestone	
4034	29 B	-	-	183	Flake	Calcite	
4035	29 B	-	-	183	Fragment	Calcite	
4037	29 B	-	-	183	Pigment	Hematite	
4040	29 B	-	-	183	Pigment	Hematite	
4050	29 B	-	-	183	Pigment	Hematite	
4114 a	29 B	-	-	183	Smaller flakes	Calcite	
4114 b	29 B	-	-	183	Flake	Silica	
4114 c	29 B	-	-	183	Fragment	Calcite	
4332	29 B	-	-	183	Fragment	Crystal	

4056 b	29 C	-	-	183	Flake	Calcite	
4057 b	29 C	-	-	183	Flake	Limestone	
4059	29 C	-	-	183	Smaller flakes	Calcite	
1814	21 C	42	47	184	Smaller flakes	Limestone	Yes
1815	21 C	35	47	184	Flake	Limestone	Yes
4132	25 A	-	-	184	Smaller flakes	Limestone	
4243	25 A	-	-	184	Flake	Limestone	
4131	26 A	60	32	184	Flake	Limestone	
4358	26 A	-	-	184	Fragment	Limestone	
7064	30 C	76	83	184	Flake	?	
2650	20 A	-	-	185	Flake	Silex	
1944	22 A	80	85	185	Painted block	Limestone	
1947	22 A	-	-	185	Flake	Limestone	
4113	25 C	-	-	185	Smaller flakes	Calcite	
4249	25 C	93	53	185	Pigment	Hematite	
3766	26 A	-	-	185	Flake	Limestone	
3756	26 A	-	-	185	Flake	Limestone	
3757	26 A	-	-	185	Flake	Limestone	
3758	26 A	-	-	185	Fragment	Limestone	
3760	26 A	-	-	185	Pigment	Hematite	
4234	26 C	-	-	185	Smaller flakes	Limestone	
4053	27 C	-	-	185	Pigment	Hematite	
4094	27 C	50	55	185	Stone tool	Limestone	
4235	28 B	-	-	185	Fragment	Calcite	
4287 a	28 B	-	-	185	Smaller flakes	Limestone	
4287 b	28 B	-	-	185	Pigment	Hematite	
4121 a	29 B	-	-	185	Smaller flakes	Calcite	
4121 b	29 B	-	-	185	Fragment	Calcite	
4047	29 B	-	-	185	Flake	Limestone	
1812	21 C	85	37	186	Flake	Limestone	
1931	22 A	45	45	186	Flake	Limestone	
2071	21 C	2	10	187	Painted block	Limestone	
2541	24 B	20	20	187	Flake	Limestone	Yes
4093	25 A	61	30	187	Painted block	Limestone	
4128	25 D	2	85	187	Flake	Limestone	
4230	26 B	-	-	187	Smaller flakes	Limestone	

4231	26 B	-	-	187	Flake	Limestone	
4232	26 B	-	-	187	Smaller flakes	Limestone	
4233	26 B	-	-	187	Smaller flakes	Limestone	
4251	26 B	-	-	187	Pigment	Hematite	
5654	29 B	23	84	187	Stone tool	Limestone	
1822	21 C	61	30	188	Blade	Limestone	Yes
4054	25 C	51	87	188	Flake	Limestone	
4055	25 C	51	87	188	Flake	Limestone	
4055 a	25 C	51	87	188	Stone tool	Limestone	
4282	25 C	-	-	188	Pigment	Hematite	
4283	25 C	-	-	188	Pigment	Hematite	
4284	25 C	-	-	188	Pigment	Hematite	
4285	25 C	-	-	188	Pigment	Hematite	
4055 a	26 C	51	87	188	Stone tool	Sandstone	
5157	29 C	50	45	188	?	Silex	
3834	23 A	-	-	189	Painted block	Limestone	Yes
3848	23 A	-	-	189	Pebble	Limestone	Yes
4257	23 A	-	-	189	Pigment	Hematite	Yes
4280	25 C	86	55	189	Pigment	Hematite	
1862	20 C	35	75	190	Stone tool	Limestone	
3886	22 A	-	-	190	Flake	Limestone	Yes
3892	22 A	-	-	190	Flake	Limestone	Yes
3893	22 A	-	-	190	Flake	Limestone	Yes
3862	23 A	80	20	190	Painted block	Limestone	
4275	28 C	-	-	190	Pigment	Hematite	
4276	28 C	-	-	190	Pigment	Hematite	
4306	28 C	-	-	190	Pigment	Hematite	
4900	19 B	70	97	191	Flake	Limestone	
4130	25 B	45	31	191	Flake	Limestone	
4118	27 B	-	-	191	Flake	Calcite	
4118 b	27 B	-	-	191	Smaller flakes	Calcite	
4299	27 B	-	-	191	Pigment	Hematite	
4300	27 B	-	-	191	Pigment	Hematite	
4301	27 B	-	-	191	Pigment	Hematite	
4100	29 B	35	50	191	Flake	Limestone	
4115 a	29 B	-	-	191	Fragment	Calcite	
2731	20 B	20	15	192	Flake	Limestone	
2670	21 A	90	85	192	Flake	Sandstone	
1827	22 B	23	74	192	Flake	Limestone	
4256	25 A	64	80	192	Pigment	Hematite	

4382	25 B	-	-	192	Fragment	Calcite	
4305	25 C	-	-	192	Pigment	Hematite	
4222	27 A	-	-	192	Smaller flakes	Limestone	
4226	27 A	-	-	192	Fragment	Calcite	
4296	27 A	-	-	192	Fragment	Calcite	
4297	27 A	-	-	192	Pigment	Hematite	
4298	27 A	-	-	192	Pigment	Hematite	
5154	27 C	77	55	192	Flake	Limestone	
4134 a	28 B	-	-	192	Smaller flakes	Calcite	
4134 b	28 B	-	-	192	Smaller flakes	Calcite	
4122 b	29 B	-	-	192	Flake	Calcite	
4122 a	29 B	-	-	192	Fragment	Calcite	
4109	29 B	-	-	192	Flake	Limestone	
4304	29 C	-	-	192	Pigment	Hematite	
2702	20 A	90	20	193	Flake	Limestone	
2710	20 A	40	90	193	Flake	Sandstone	
4110	25 A	80	53	193	Painted block	Limestone	
4406	25 A	-	-	193	Smaller flakes	Limestone	
2701	20 B	30	10	194	Painted block	Limestone	
3030	20 B	-	-	194	Pigment	Hematite	
4223	26 B	26	59	194	Smaller flakes	Limestone	
4224	27 B	-	-	194	Fragment	Quartz	
4400	26 Z	67	42	194	Fragment	Silicified sandstone	
2752	20 B	-	-	195	Flake	Limestone	
2017	20 B	-	-	195	?	Hematite	
3933	22 A	-	-	195	Flake	Limestone	
3934	22 A	-	-	195	Flake	Limestone	
3935	22 A	-	-	195	Flake	Limestone	
3942	23 A	90	15	195	Painted block	Limestone	
4342	26 C	-	-	195	?	Quartz	
4228	28 A	-	-	195	Smaller flakes	Calcite	
5663	29 B	9	77	195	Fragment	Silex	
1975	20 C	40	50	196	Fragment	Limestone	
1976	20 C	35	45	196	Fragment	Limestone	
1977	20 C	20	25	196	Fragment	Limestone	
1978	20 C	50	55	196	Fragment	Limestone	
2729	21 A	80	60	196	?	Sandstone	
4286	25 C	27	76	196	Pigment	Hematite	

2730	21 A	80	15	197	Stone tool	Limestone	
4216	26 B	86	93	197	Flake	Limestone	
4267	26 B	-	-	197	Pigment	Hematite	
4268	26 B	-	-	197	Pigment	Hematite	
4269	26 B	-	-	197	Pigment	Hematite	
4270	26 B	-	-	197	Pigment	Hematite	
2736	26 B	90	10	197	Painted block	Limestone	
7003	30 B	26	87	197	Platelet	Limestone	
6152	19 A	50	20	198	Flake	Silex	
6160	19 B	90	20	198	Painted block	Limestone	Yes
2759	22 A	-	-	198	Flake	Quartz	
2760	22 A	-	-	198	Pigment	Hematite	
4291	25 B	-	-	198	Pigment	Hematite	
4117	28 B	-	-	198	Fragment	Calcite	
4333	29 B	-	-	198	Smaller flakes	Limestone	
4334	29 B	-	-	198	Fragment	Calcite	
5605	29 B	45	80	198	Stone tool	Limestone	
5662	29 B	8	77	198	Stone tool	Limestone	
2783	20 A	64	80	199	Flake	Limestone	
3896	22 A	65	85	200	Block	Limestone	
1974	22 B	40	76	200	Flake	Limestone	
2791	22 B	-	-	200	Flake	Silex	
3225	26 B	-	-	200	Pigment	Hematite	
3226	26 B	-	-	200	Flake	Limestone	
3227	26 B	-	-	200	Flake	Limestone	
3228	26 B	-	-	200	Flake	Limestone	
5155	28 C	82	45	200	Flake	Limestone	
4210 a	29 B	50	12	200	Stone tool	Limestone	
4210 b	29 B	50	12	200	Flake	Limestone	
6731	29 C	30/80	60/100	200	Flake	Limestone	
6732	29 C	30/80	60/100	200	Flake	Hematite	
6733	29 C	30/80	60/100	200	Flake	Limestone	
7400	29 D	-	-	200	Pigment	Hematite	
7307	30 B	42/10	40/100	200	Stone tool?	Quartz	
7215	30 B	80/95		200	Platelet	Hematite	
7216	30 B	80/95		200	Grain	Hematite	
2936	22 C	13	47	201	Flake	Limestone	
4119	25 A	-	-	201	Fragment	Quartz	

4241	26 B	46	8	201	Stone tool	Limestone	
4111	25 A	-	-	202	Smaller flakes	Limestone	
4112	25 A	85	90	202	Flake	Limestone	
4307	25 B	-	-	202	Pigment	Hematite	Yes
4308	25 B	-	-	202	Pigment	Hematite	Yes
4319	25 B	-	-	202	Flake	Silex	
4320	28 B	-	-	202	Fragment	Calcite	
4321	28 B	-	-	202	Smaller flakes	Calcite	
4322	28 B	-	-	202	Fragment	Silex	
4323	28 B	-	-	202	Fragment	Calcite	
4324	28 B	-	-	202	Fragment	Calcite	
4325	28 B	-	-	202	Fragment	Calcite	
4326	28 B	-	-	202	Fragment	Calcite	
4327	28 B	-	-	202	Fragment	Calcite	
4328	28 B	-	-	202	Smaller flakes	Limestone	
4329	28 B	-	-	202	Fragment	Calcite	
4330	28 B	-	-	202	Fragment	Calcite	
2784	20 A	70	70	203	Flake	Limestone	
2003	20 C	95	5	203	Platelet	Limestone	
2938	21 B	80	60	203	Stone tool	Limestone	
2939	21 B	10	50	203	Stone tool	Limestone	
2919	21 B	-	-	203	Stone tool	Limestone	
2920	21 B	-	-	203	Flake	Silex	
3407	22 B	-	-	203	Pigment	Hematite	
5655	29 B	12	68	203	Flake	Limestone	
7002	30 B	80	33	203	?	Hematite	
2937	21 C	12	78	204	Flake	Limestone	
3922	23 B	10	5	204	Pigment	Hematite	
4239	25 C	-	-	204	Smaller flakes	Limestone	
4348	25 C	-	-	204	Fragment	Calcite	
4349	25 C	93	53	204	Fragment	Calcite	
4350	25 C	-	-	204	Fragment	Calcite	
4351	25 C	-	-	204	Fragment	Calcite	
4352	25 C	-	-	204	Fragment	Calcite	
4353	25 C	-	-	204	Smaller flakes	Limestone	
4354 a	25 C	-	-	204	Fragment	Calcite	
4355	25 C	-	-	204	Fragment	Calcite	
4240	27 B	50	35	204	Stone tool	Limestone	
4214	28 C	-	-	204	Flake	Limestone	
4337	28 C	-	-	204	Fragment	Calcite	

4338	28 C	-	-	204	Smaller flakes	Calcite	
4339	28 C	-	-	204	Fragment	Calcite	
2800	20 A	-	-	205	Pigment	Hematite	
2914	20 B	15	99	205	Flake	Limestone	
2915	20 B	20	98	205	Flake	Limestone	
2762	21 B	-	-	205	Flake	Limestone	
2941	21 B	10	40	205	Flake	Limestone	
3900	22 A	78	75	205	Fragment	Quartz	
3907	22 A	90	75	205	Painted block	Limestone	
3899	23 A	70	5	205	Fragment	Quartz	
2626	24 B	25	10	205	Flake	Limestone	
3953	23 A	70-10	40-50	206	Blade	Sandstone	Yes
2846	20 A	63	80	207	Painted block	Limestone	
2847	20 A	70	90	207	Pigment	Hematite	
2844	20 B	10	90	207	Painted block	Limestone	
2845	20 B	10	80	207	Painted block	Limestone	
2932	20 B	55	80	207	Painted block	Limestone	
2882	20 B	20	70	207	Stone tool	Limestone	
2883	20 B	25	75	207	Stone tool	Limestone	
3901	22 A	80	98	207	Painted block	Limestone	
4221	28 B	-	-	207	Fragment	Calcite	
2934	20 B	57	80	208	Smaller flakes	Limestone	
2940	21 B	66	40	208	Stone tool	Limestone	
2072	21 C	90	90	208	Stone tool	?	
4198	25 B	-	-	208	Smaller flakes	Calcite	
3029	20 A	-	-	210	Flake	Limestone	
3047	20 B	60	15	210	Flake	Limestone	
2972	22 A	-	-	210	Fragment	Quartz	
2973	22 A	-	-	210	Fragment	Quartz	
3126	22 B	-	-	210	Stone tool	Limestone	
3127	22 B	-	-	210	Stone tool	Limestone	
3128	22 B	-	-	210	Flake	Limestone	
3129	22 B	-	-	210	Stone tool	Limestone	
3130	22 B	-	-	210	Stone tool	Limestone	
3963	23 A	-	-	210	Flake	Limestone	
3964	23 A	-	-	210	Flake	Limestone	Yes
4476	25 A	-	-	210	Flake	?	Yes
3636	24 B	79	53	211	Flake	Silex	
4471	25 C	10	5	211	Flake	?	
2927	20 A	99	60	212	Flake	?	
2923	20 B	8	75	212	Flake	Silex	

2951	20 B	25	55	212	Flake	Quartz	
2880	21 B	-	-	212	Stone tool	Limestone	
2891	21 B	20	20	212	Smaller flakes	?	
2884	21 B	90	90	212	Stone tool	Limestone	
2885	21 B	-	-	212	Stone tool	Limestone	
2995	21 C	-	-	212	Painted block	Limestone	
2996	21 C	-	-	212	Block	Limestone	
3149	22 B	-	-	212	Flake	Limestone	
3181	22 C	-	-	212	Stone tool	Limestone	
3631	22 D	25	95	212	Stone tool	Limestone	
3630	23 B	25	2	212	Painted block	Limestone	Yes
3146	23 C	-	-	212	Pigment	Hematite	
4212	28 B	-	-	212	Smaller flakes	Limestone	
2817	22 B	-	-	213	Fragment	Silex	
3147	23 C	7	37	213	Stone tool	Limestone	
4193	26 B	11	20	213	Flake	Calcite	
3473	24 B	-	-	214	Pebble	Quartz	
3615	24 B	50	75	214	Platelet	Limestone	
3474	24 B	-	-	214	Flake	Sandstone	
3469	24 B	-	-	214	Pigment	Hematite	
3470	24 B	-	-	214	Pigment	Hematite	
3471	24 B	-	-	214	Pigment	Hematite	
3015	20 A	50	60	215	Platelet	Limestone	
3016	20 A	50	60	215	Flake	Limestone	
3017	20 A	50	60	215	Flake	Limestone	
3018	20 A	50	60	215	Flake	Limestone	
3045	20 A	-	-	215	Flake	Limestone	
3046	20 A	-	-	215	Flake	Limestone	
3019	21 A	-	-	215	Flake	Limestone	
2992	21 A	-	-	215	Pigment	Hematite	
3938	22 A	-	-	215	Stone tool	Limestone	
4364	22 A	-	-	215	Fragment	Quartz	
4365	22 A	-	-	215	Fragment	Quartz	
4366	22 A	-	-	215	Fragment	Quartz	
4367	22 A	-	-	215	Fragment	Quartz	
4368	22 A	-	-	215	Fragment	Crystal	
4428	26 A	41	81	215	Flake	Limestone	
2878	19 B	-	-	216	Flake	Limestone	
2977	22 A	-	-	216	Flake	Silex	
3297	23 B	25	80	216	Painted block	Limestone	
3613	23 B	38	10	216	Painted block	Limestone	

3612	23 B	38	10	216	Stone tool	Limestone fino	
4346	27 B	-	-	216	Grain	Quartz	
4277	29 C	-	-	216	Pigment	Hematite	
3298	23 C	15	55	217	Flake	Limestone	
2955	22 A	-	-	218	Stone tool	Limestone	
4569	26 B	82	34	218	Stone tool	Limestone	
4170	27 B	-	-	218	Smaller flakes	Limestone	
4155	27 C	17	68	218	Stone tool	Limestone	
4156	27 C	17	68	218	Stone tool	Limestone	
3569	19 C	18	15	219	Pigment	Hematite	
3498	20 A	-	-	219	Stone tool	Quartz	
3499	20 A	-	-	219	Stone tool	Silex	
3113	20 A	60	80	219	Painted block	Limestone	
3221	20 A	78	29	219	Flake	Limestone	
3222	20 A	68	32	219	Flake	Limestone	
3223	20 A	89	34	219	Flake	Limestone	
5656	29 B	35	81	219	Core	Limestone	
3551	20 B	50	25	220	Stone tool	Limestone	
3555	20 B	50	35	220	Flake	Limestone	
4422	20 B	55	40	220	Flake	Limestone	
4423	20 B	55	40	220	Flake	Limestone	
2956	22 A	-	-	220	Painted block	Limestone	
3937	22 A	-	-	220	Flake	Limestone	
3941	22 A	-	-	220	Stone tool	Limestone	Yes
3012	22 A	40	35	220	Painted block	Limestone	
3538	22 B	-	-	220	Pigment	Hematite	
4686	24 B	0	80	220	Stone tool	Limestone	
4485	25 B	-	-	220	Smaller flakes	Limestone	
1117 W	30 B	-	-	220	Platelet	Hematite	
3618	20 B	10	0	221	Painted block	Limestone	
2900	21 B	75	20	222	Flake	Limestone	
4303	27 B	-	-	222	Pigment	Hematite	
3282	20 A	-	-	223	Flake	Limestone	
3567	22 B	-	-	223	Flake	Limestone	
3672	22 B	50	75	223	Stone tool	Limestone	
7067	30 C	-	-	223	Platelet	Silex	
3224	20 A	70	16	224	Burnt flake	Limestone	
3245	20 A	46	29	224	Burnt Flake	Limestone	
3616	23 B	40	29	224	Painted block	Limestone	
3246	20 A	63	35	225	Block	Limestone	

3248	20 A	-	-	225	Flake	Limestone	
1153 W	30 B	-	-	225	Stone tool	Limestone	
3571	20 A	92	70	227	Stone tool	Limestone	Yes
3570	20 A	94	77	227	Core	Limestone	Yes
3519	20 B	10	35	227	Flake	Silex	
3518	20 B	10	35	227	?	Hematite	
3676	20 B	80	100	227	Stone tool	Limestone	
3516	20 B	10	35	227	?	Calcite	
3141	21 A	6	90	227	Stone tool	Limestone	
4389	24 D	35	15	227	Stone tool	Limestone	
4390	24 D	35	15	227	Smaller flakes	Calcite	
3114	20 A	75	90	228	Smaller flakes	Quartz	
5253	27 A	-	-	228	Flake	Limestone	
5254	27 A	-	-	228	Platelet	Limestone	
5255	27 A	-	-	228	Platelet	Limestone	
5256	27 A	-	-	228	Flake	Limestone	
5257	27 A	-	-	228	Flake	Limestone	
5258	27 A	-	-	228	Stone tool	Limestone	
5251	28 A	-	-	228	Flake	Limestone	
5252	28 A	-	-	228	Platelet	Limestone	
3261	22 A	-	-	229	Smaller flakes	Limestone	
3577	20 A	85	85	230	Stone tool	Silex	
3581	20 A	85	60	230	Core	Silex	
4272	20 A	-	-	230	Pigment	Hematite	
4273	20 A	-	-	230	Pigment	Hematite	
4370	20 C	-	-	230	Flake	Limestone	
3579	21 A	-	-	230	Flake	Calcite	
3194	21 A	60	91	230	Painted block	Limestone	
3196	21 A	15	50	230	Painted block	Limestone	
3199	21 A	80	81	230	Flake	Silex	
3021	22 A	-	-	230	Fragment	Silex	
3856	22 A	-	-	230	Stone tool	Limestone	
4388	22 A	-	-	230	Stone tool	Limestone	
4803	24 A	54	56	230	Flake	Silex	
5274	28 A	-	-	230	Platelet	Limestone	
5275	28 A	-	-	230	Flake	Limestone	
4399	20 B	74	95	231	Stone tool	Limestone	
4394	20 B	35	85	231	Stone tool	Limestone	
3724	21 B	30	27	232	Stone tool	Limestone	
3854	22 A	70	15	232	Crystal	Quartz	
3995	22 A	-	-	232	Flake	Limestone	

4401	24 C	75	10	232	Stone tool	Limestone	
5059	20 A	35	55	233	Painted block	Limestone	
5478	20 A	58	18	233	Flake	Limestone	
4392	21 C	-	-	233	Flake	Limestone	
4395	21 C	-	-	233	Flake	Limestone	
4393	21 C	-	-	233	Flake	Limestone	
4483	22 A	-	-	234	Fragment	Quartz	
4403	20 B	40	90	236	Stone tool	Limestone	
3699	22 C	-	-	242	Pigment	Hematite	
5492	20 B	-	-	247	Flake	Silex	
6429	19 A	95	75	250	Block	Limestone	
4906	20 D	-	-	250	Flake	Limestone	
4907	20 D	-	-	250	Flake	Limestone	
4908	20 D	-	-	250	Flake	Limestone	
4795	23 B	-	-	250	Smaller flakes	Limestone	
4796	23 B	-	-	250	Flake	Limestone	
5324	25 A	-	-	255	Flake	Limestone	
5325	25 A	-	-	255	Flake	Limestone	
5678	21 B	-	-	268	Flake	Limestone	
6141	21 B	-	-	276	Small Flake	Calcite	
6142	21 B	-	-	276	Fragment	Quartz	
6217	19 A	-	-	283	Fragment	Quartz	Yes
3998	24 C	-	-	283	Pigment	Hematite	
6951	20 B	-	-	285	Flake	Quartz	
6952	20 B	-	-	285	Flake	Quartz	
6954	20 B	-	-	285	Pebble	Quartz	
6955	20 B	-	-	285	Stone tool	Limestone	
6956	20 B	-	-	285	Flake	Sandstone	
6435	21 B	55	5	290	Block	Limestone	Yes
6225	19 Z	30/40	53/98	295	Painted block	Hematite	Yes
6781	25 Z	0/50	12/80	340	Stone tool	Limestone	Yes

Supplementary Table S5. Detailed data of stone objects (n=338) from Unit III of Santa Elina. Blank spaces correspond to absent information.

Nº	Square	X	Y	Z	Artifact	Material	Association with charcoal?
6139	20 B	-	-	272	Stone tool	Quartz	
5601	27 A	-	-	272	Stone tool	Limestone	
6243	20 B	-	-	275	Stone tool	Calcite	

5720	26 B	82	70	278	Stone tool	Limestone	
5924	28 A	-	-	280	Smaller flakes	Quartz	
5925	28 A	-	-	280	Flake	Silex	
5923	28 A	-	-	280	Flake	Limestone	
5926	28 A	-	-	280	Smaller flakes	Quartz	
5928	28 A	-	-	280	Stone tool	Limestone	
5927	28 A	-	-	280	Stone tool	Calcite	
6068	28 C	-	-	280	Fragment	Limestone	
5893	28 Z	-	-	280	Stone tool	Limestone	
7127	30 B	-	-	280	Stone tool	Quartz	
5736	26 B	-	-	282	Stone tool	Limestone	
5911	28 A	8	65	284	Stone tool	Limestone	
4676	24 D	-	-	285	Flake	Limestone	
5847	28 A	-	-	285	Flake	Quartz	
5849	28 A	-	-	285	Stone tool	Limestone	
5852	28 A	-	-	285	Stone tool	Limestone	
5848	28 A	-	-	285	Pigment	Hematite	
5850	28 A	-	-	285	Flake	Limestone	
5851	28 A	-	-	285	Stone tool	Limestone	
5934	29 B	80	32	286	Stone tool	Limestone	
5935	28 B	95	45	287	Stone tool?	Limestone	
5914	29 C	-	-	288	Platelet	Limestone	
5936	27 B	86	57	289	Stone tool	Limestone	
5941	26 C	-	-	290	Stone tool	Limestone	
5929	27 B	39	48	290	Stone tool	Limestone	
5931	27 B	17	87	290	Stone tool	Limestone	
5937	27 C	20	57	290	Stone tool	Limestone	
5957	28 B	54	92	290	Stone tool	Limestone	
5945	26 B	-	-	291	Smaller flakes	Limestone	
5682	26 C	-	-	291	Stone tool	Limestone	
5955	27 B	50	30	291	Stone tool	Limestone	
5956	27 B	72	63	291	Stone tool?	Limestone	
5946	27 C	-	-	291	Flake	Limestone	
5953	27 C	-	-	293	Flake	Limestone	
5977	28 A	-	-	292	Stone tool	Limestone	Yes
5978	28 A	-	-	292	Smaller flakes	Limestone	Yes
5952	28 C	-	-	293	Smaller flakes	Limestone	
5960	27 A	-	-	295	Stone tool	Hematite	

7221	27 B	-	-	294	Smaller flakes	Silica	
7217	27 B	-	-	294	Blade	Quartz (silica)	
5999	27 C	37	54	295	Stone tool	Limestone	
5951	28 A	-	-	296	Flake	Limestone	
5947	26 B	-	-	297	Stone tool	Limestone	
5948	26 B	-	-	297	Stone tool	Limestone	
5949	26 B	-	-	297	Stone tool	Limestone	
5950	26 B	-	-	297	Smaller flakes	Limestone	
5942	27 A	-	-	297	Flake	Limestone	
5943	27 A	-	-	297	Smaller flakes	Limestone	
5944	27 A	-	-	297	Stone tool	Limestone	
6058	28 A	40	40	297	Stone tool	Limestone	
5959	28 A	33	20	297	Stone tool	Limestone	
6351	22 B	8	30	298	Stone tool	Limestone	
5979	27 B	-	-	298	Stone tool	Hematite	
5983	28 C	-	-	298	Stone tool	Limestone	
5984	28 C	-	-	298	Stone tool	Limestone	
5972	27 A	-	-	299	Stone tool	Limestone	
5991	27 B	15	75	299	Stone tool	Limestone	
5998	28 B	38	89	299	Stone tool	Limestone	
6344	23 B	2	46	300	Stone tool	Limestone	
4682	25 C	50	99	300	Flake	Limestone	
6144	27 A	-	-	300	Stone tool?	Quartz	
7212	27 C	-	-	300	Stone tool	Limestone	
7211	27 C	-	-	300	Stone tool	Hematite	
5993	28 A	13	3	300	Flake	Limestone	
6007	28 B	-	-	300	Stone tool	Limestone	
5994	28 A	90	60	301	Stone tool	Limestone	
6342	23 B	6	14	302	Stone tool	Limestone	
6368	24 A	65	25	302	Block?	Limestone	
5940	26 A	-	-	302	Flake	Limestone	
5965	27 C	40-6	0-80	302	Stone tool	Limestone	
5967	27 C	40-6	0-80	302	Stone tool	Limestone	
5966	27 C	40-6	0-80	302	Flake	Limestone	
5992	28 A	47	1	302	Stone tool	Limestone	
6062	29 A	90	5	302	Flake	Limestone	
7379	23 A	-	-	303	Stone tool	Hematite	
4727	25 C	-	-	303	Stone tool	Limestone	
6063	28 B	60	49	303	Stone tool	Limestone	
6343	22 A	72	92	304	Stone tool	Limestone	

5985	26 A	80	47	304	Stone tool	Limestone	
6040	26 C	-	-	304	Flake	Limestone	
6061	28 B	10	48	304	Stone tool	Limestone	
6026	26 B	-	-	305	Stone tool?	Quartz	
6057	27 A	35	87	305	Flake	Limestone	
7205	28 C	-	-	305	Fragment	Hematite	
6455	22 B	20	80	306	Painted block	Limestone	
6306	24 B	60	58	306	Stone tool	Limestone	
4721	25 C	50	50	306	Stone tool	Limestone	
6201	26 B	19	18	306	Flake	Limestone	
6053	26 B	78	1	307	Smaller flakes	Limestone	
7291	26 B	-	-	307	Stone tool	Limestone	
7287b	26 B	-	-	307	Flake	Limestone	
6134	26 C	8	46	307	Flake	Limestone	
5987	26 C	80	63	307	Flake	Limestone	
6049	26 B	39	27	307	Stone tool	Limestone	
6052	26 B	25	47	307	Stone tool	Limestone	
7290	26 B	-	-	307	Stone tool	Limestone	
7292	26 B	-	-	307	Flake	Limestone	
6067	26 B	45	20	307	Stone tool	Limestone	
7270	27 B	-	-	307	Stone tool?	Quartz	
6035	27 B	-	-	307	Stone tool	Limestone	
6108	28 B	25	55	307	Stone tool	Limestone	
6116	28 B	-	-	307	Stone tool	Limestone	
6117	28 B	-	-	307	Stone tool	Limestone	
6460	21 B	50	10	308	Block	Limestone	
6027	26 B	-	-	308	Stone tool	Limestone	
6024	27 B	-	-	308	Stone tool	Limestone	
6025	27 B	-	-	308	Flake	Limestone	
7371	28 A	40/6	40/6	308	Stone tool	Limestone	Yes
6008	28 A	50/6	40/6	308	Flake	Limestone	Yes
6129	28 B	72	99	308	Pigment	Hematite	
6017	29 C	-	-	308	Flake?	Limestone	
6015	29 C	-	-	308	Flake	Limestone	
6042	26 B	-	-	309	Flake	Limestone	
6055	27 B	95	26	309	Stone tool	Limestone	
6128	28 A	90	70	309	Stone tool	Calcite	
6328	24 B	60	3	310	Stone tool	Limestone	
4698	25 B	-	-	310	Smaller flakes	Limestone	
6044	26 A	50	68	310	Stone tool	Limestone	

4722	26 A	-	-	310	Fragment	Quartz	
6054	26 B	23	89	310	Stone tool	Limestone	
6013	27 A	-	-	310	Flake	Limestone	
6110	27 B	30	92	310	Flake	Limestone	
6111	27 B	44	95	310	Stone tool	Limestone	
6112	27 B	42	84	310	Smaller flakes	Limestone	
6099	28 A	-	-	310	Flake	Silex	
6098	28 A	1	33	310	Flake	Limestone	
6120	28 A	34	28	310	Smaller flakes	Limestone	
6121	28 A	40	25	310	Flake	Limestone	
6135	26 B	60	48	311	Flake	Limestone	
6136	26 B	90	61	311	Fragment	Limestone	
6208	26 B	83	40	311	Stone tool	Limestone	
6123	27 A	42	11	311	Flake	Limestone	
6124	27 A	50	10	311	Flake	Limestone	
6087	27 B	8	12	312	Stone tool	Limestone	
6090	27 B	11	8	312	Stone tool	Limestone	
7229a	29 A	50-1	10	312	Crystal	Quartz	
7229b	29 A	50-1	10	312	Crystal	Quartz	
6076	26 B	-	-	313	Smaller flakes	Limestone	
6086	26 B	10	75	313	Stone tool	Limestone	
6296	26 B	55	64	313	Flake	Limestone	
6126	27 A	25	97	313	Stone tool	Limestone	
6080	27 A	-	-	314	Stone tool	Limestone	
6081	27 A	-	-	314	Flake	Limestone	
6078	27 A	-	-	314	Platelet	Calcite	
6453	23 B	5	95	315	Block	Limestone	
6030	26 A	-	-	315	Flake	Limestone	
6031	26 A	-	-	315	Flake	Limestone	
6302	28 B	5	77	315	Flake	Limestone	Yes
6362	22 B	13	30	316	Flake	Limestone	Yes
6355	24 A	75	25	316	Stone tool	Limestone	
6439	28 A	-	-	316	Flake	Limestone	
6440	28 B	-	-	316	Flake	Limestone	
6293	27 B	97	1	317	Flake	Limestone	
6203	26 B	18	85	318	Stone tool	Limestone	
6364	24 D	20	40	319	Stone tool	Limestone	Yes
6133	26 A	78	33	319	Smaller flakes	Limestone	
7219	28 B	-	-	319	Flake	Limestone	
7220	28 B	-	-	319	Flake	Limestone	
7125	28 B	-	-	319	Flake	Hematite	

6367	24 A	30	50	320	Flake	Limestone	
6046	26 A	47	72	320	Stone tool	Limestone	
4743	26 B	-	-	320	Stone tool?	Calcite	
4744	26 B	-	-	320	Stone tool	Calcite	
6119	27 A	-	-	320	Flake	Quartz	
6294	27 A	82	15	320	Flake	Limestone	
7123	28 A	-	-	320	Smaller flakes	Quartz	
7097	28 A	-	-	320	Flake	Limestone	
7098	28 A	-	-	320	Stone tool	Limestone	
7096	28 A	-	-	320	Platelet	Limestone	
7099	28 A	-	-	320	Stone tool	Hematite	
7124	28 A	-	-	320	Grain	Quartz	
7200	28 B	-	-	320	Stone tool	Limestone	
7126	28 B	-	-	320		Limestone	
6747	29 A	-	-	320	Stone tool	Limestone	
6383	24 A	95	20	321	Stone tool	Limestone	
6647	26 B	-	-	321	Flake	Limestone	
6298	26 B	44	39	321	Flake	Limestone	
6683	29 C	9	5	321	Flake	Limestone	
6685	29 C	16	16	321	Stone tool	Limestone	
6690	29 B	39	15	321	Stone tool	Silica	
6132	26 A	80	45	322	Flake	Quartz	
6698	28 B	71	92	322	Smaller flakes	Limestone	
6686	29 B	14	8	322	Stone tool	Limestone	
6689	29 B	76	10	322	Flake	Limestone	
4345a	21 C	-	-	323	Stone flake	Limestone	
4345b	21 C	-	-	323	Flake	Limestone	
6374	24 A	95	20	323	Block	Limestone	Yes
6691	28 C	18	77	323	Stone tool	Limestone	
6687	29 B	30	28	323	Flake	Limestone	
6688	29 B	45	25	323	Flake	Limestone	
6385	24 A	30	27	324	Stone tool	Limestone	
6319	26 C	5	70	324	Flake	Limestone	
6442	26 C	-	-	325	Flake	Calcite	
6295	27 A	74	17	325	Flake	Limestone	
6700	28 A	79	56	325	Stone tool	Limestone	
6699	28 A	89	28	325	Smaller flakes	Limestone	
6692	28 B	13	31	325	Flake	Limestone	
6694	28 B	62	30	325	Flake	Limestone	
6695b	28 B	23	73	325	Stone tool	Limestone	

6696	28 B	27	83	325	Flake	Limestone	
6369	24 A	25	40	326	Flake	Limestone	
6701	27 B	52	83	326	Stone tool	Limestone	
6301	26 A	27	100	327	Flake	Limestone	
6702	27 B	18	10	327	Stone tool	Limestone	
6299	26 A	44	58	328	Flake	Limestone	
6300	26 A	38	82	328	Flake	Limestone	
7302	29 A	-	-	328	Crystal	Quartz	
6703	27 A	65	74	329	Stone tool	Limestone	
6130	26 A	43	16	330	Stone tool	Calcite	
4742	26 A	-	-	330	Smaller flakes	Limestone	
6695ª	26 C	-	-	330	Stone tool	Limestone	
6723	26 C	-	-	330	Smaller flakes	Limestone	
6724	26 C	-	-	330	Smaller flakes	Limestone	
6725	26 C	-	-	330	Flake	Limestone	
6726	26 C	-	-	330	Stone tool?	Silica	
6800	27 A	55	30	330	Stone tool	Limestone	
6802	27 A	60	55	330	Stone tool	Limestone	
6801	28 A	51	10	330	Core	Limestone	
7395	28 B	-	-	330	Crystal	Quartz	
7394	28 B	-	-	330	Smaller flakes	Quartz	
6783	28 C	-	-	330	Flake	Limestone	
6782	29 C	12	80	330	Flake	Limestone	
6784	28 B	-	-	331	Smaller flakes	Limestone	
6785	28 B	-	-	331	Stone tool	Limestone	
6566	24 B	-	-	332	Flake	Limestone	
6719	26 A	35	5	332	Stone tool	Limestone	
6704	27 A	47	57	332	Flake	Limestone	
7104	26 A	-	-	334	Fragment	Quartz	
5865	25 A	60	70	335	Crystal	Quartz	
7214	22 B	25	80	336	Stone tool	Limestone	
6809	26 B	-	-	337	Stone tool	Limestone	
6815	28 A	63	13	337	Stone tool	Limestone	Yes
5864	25 A	80	70	340	Flake	Limestone	
4756	25 B	-	-	340	Flake	Limestone	
6816	26 A	75	30	340	Stone tool	Limestone	Yes
4749	26 B	-	-	340	Stone tool	Limestone	
6831	27 Z	-	-	340	Stone tool	Limestone	
6823	27 A	85	45	340	Stone tool	Limestone	
6825	27 A	41	71	340	Stone tool	Limestone	

6829	27 A	-	-	340	Stone tool	Limestone	
6830	27 A	-	-	340	Stone tool	Limestone	
6818	27 B	-	-	340	Stone tool	Limestone	Yes
6811	27 B	-	-	340	Flake	Limestone	
6812	27 B	-	-	340	Flake	Limestone	
6813	27 B	-	-	340	Flake	Limestone	
6817	27 B	-	-	340	Flake	Limestone	Yes
6820	27 B	-	-	340	Smaller flakes	Limestone	Yes
6877	27 B	-	-	340	Flake	Limestone	
6810	28 B	-	-	340	Flake	Limestone	
6807	28 C	-	-	340	Flake	Limestone	
6990	29 A	70	15	340	Stone tool	Limestone	
6746	24 A	50	100	341	Stone tool	Limestone	
6832	28 Z	90/100	-	341	Stone tool	Limestone	
6837	23 A	-	-	342	Flake	Quartz	
6822	27 A	10	80	342	Stone tool	Limestone	
6806	23 A	14	7	343	Flake	Limestone	
6992	25 B	-	-	343	Flake	Silex	Yes
6774	26 Z	-	-	343	Smaller flakes	Quartz	
6649	23 A	20	20	344	Stone tool	Limestone	Yes
6637	24 B	25	80	344	Stone tool	Limestone	
6824	27 A	83	44	344	Stone tool	Limestone	
6841	28 A	-	-	344	Smaller flakes	Limestone	
6842	28 A	-	-	344	Flake	Limestone	
6848	28 A	65	35	344	Flake	Limestone	
6849	28 A	82	18	344	Stone tool	Silica?	
6840	24 A	-	-	345	Platelet	Quartz	
6827	26 B	-	-	345	Flake	Limestone	
6826	26 B	-	-	345	Flake	Limestone	
6828	26 B	-	-	345	Pebble	Limestone	
6854	27 A	-	-	345	Stone tool	Limestone	
6845	28 A	-	-	345	Crystal	Quartz	
6775	21 A	-	-	346	Stone tool	Limestone	
6777	21 A	30	10	346	Pebble	Limestone	Yes
6635	24 B	10	70	346	Stone tool	Limestone	
7280	24 B	-	-	346	Flake	Limestone	
6833	26 A	-	-	346	Stone tool	Limestone	
6821	26 B	50	80	346	Flake	Limestone	
6835	29 B	0-40	0-45	346	Flake	Limestone	
6836	29 B	0-40	0-45	346	Stone tool	Limestone	
6715	25 B	45	2	347	Smaller flakes	Limestone	

6838	27 B	-	-	347	Flake	Limestone	
6839	27 B	90	8	347	Stone tool	Limestone	
6834	28 Z	55/7	0/55	347	Flake	Limestone	
6846	28 B	-	-	347	Flake	Limestone	
6847	28 B	-	-	347	Flake	Limestone	
6850	23 Z	-	-	348	Flake	Limestone	
6851a	23 Z	-	-	348	Flake	Limestone	
6438	25 A	-	-	348	Flake	Limestone	
7305	28 B	-	-	348	Flake	Quartz	
7304	28 B	-	-	348	Crystal	Quartz	
6728	24 B	40	25	349	Flake	Limestone	
6716	25 A	25	67	349	Stone tool	Limestone	
6717	25 A	30	75	349	Flake	Limestone	
6814	27 B	-	-	349	Flake	Limestone	
6657	23 B	15	20	350	Stone tool	Limestone	Yes
6988	26 A	-	-	350		Hematite	
7001	26 A	0	25	350	Flake	Limestone	
4701	26 A	84	50	350	Flake	Limestone	
6995	26 A	97	88	350	Platelet	Limestone	
6844	26 B	-	-	350	Block	Limestone	
6843	26 B	-	-	350	Flake	Limestone	
7009	27 A	18	77	350	Flake	Limestone	
7012	27 B	20	93	350	Platelet	Limestone	
7228a	27 B	0/50	0/75	350	Fragments	Quartz	
7228b	27 B	0/50	0/75	350	Fragments	Quartz	
7013	27 B	29	88	350	Platelet	Limestone	
7276	27 C	20	80	350	Platelet	Limestone	
7080	28 B	-	-	350	Platelet	Limestone	
7010	28 B	50	35	350	Stone tool	Limestone	
7011	28 B	73	37	350	Stone tool	Limestone	
7259	29 B	-	-	350	Fragment	Quartz	
7259	29 B	-	-	350		Hematite	
7327	23 A	-	-	351	Fragment	Quartz	
6997	26 B	50	45	351	Stone tool	Limestone	
6998	26 B	40	45	352	Stone tool	Limestone	
7106	24 B	-	-	353	Stone tool	Limestone	
7303	25 A	67/9	50/80	353	Stone tool	Hematite	
6994	26 A	85	23	353	Flake	Limestone	
6996	26 A	70	10	353	Stone tool	Limestone	
7000	26 B	35	15	353	Flake	Limestone	
6710	23 B	5	95	354	Stone tool	Limestone	
7070	29 B	30	30	354	Stone tool	Limestone	
7071	29 B	-	-	354	Flake	Limestone	

7072	29 B	-	-	354	Platelet	Silica	
7073	29 B	-	-	354	Platelet	Silica	
6656	22 A	95	80	355	Stone tool	Limestone	
7014	25 B	4	54	355	Flake	Limestone	
7393	25 B	26/02	97/100	358	Flake	Limestone	Yes
8000	25 B	-	-	358	Flake	Limestone	
7077	25 A	15/04	25/70	359	Flake	Limestone	
6986	27 Z	-	-	359	Block	Iron	
6987	27 Z	-	-	359	Stone tool	Limestone	
4766	25 B	-	-	360	Smaller flakes	Limestone	
7083	25 A	5	60	361	Flake	Limestone	
7392	25 B	26/02.	52/55	362	Stone tool	Limestone	Yes

Supplementary Table S6. Detailed data of *G. phoenesis* bones (n=90), excluding osteoderms, from Unit II of Santa Elina.

Square	X	Y	Z
28 D	49	36	120
28 D	22	51	120
28 D	28	1	133
23 A	15	30	139
18 C	60	20	165
28 C	28	99	166
29 C	62	97	175
28 C	50	50	180
28 C	98	58	180
29 C	50	50	181
28 C	50	50	181
29 A	62	87	181
29 C	40	30	182
29 B	50	50	183
28 B	25	75	183
28 C	75	75	183
28 B	25	25	185
26 C	50	50	185
28 B	50	50	186
26 A	0	34	186
21 C	65	5	187
26 B	50	50	187
27 C	29	90	187
29 C	49	51	187
20 C	65	90	187
27 B	85	8	188
25 C	45	51	188
27 B	50	50	188
26 C	51	2	189
28 A	30	90	190
29 A	75	75	190
27 B	25	25	191
27 B	51	49	191
29 B	49	49	191
29 A	90	80	191
27 A	50	50	192
29 C	25	25	192
29 B	50	51	192
28 A	50	50	193

29 A	50	50	193
29 A	75	75	193
29 A	74	76	193
29 A	85	93	193
29 A	50	60	193
30 A	5	85	193
30 A	5	86	193
30 A	5	84	193
22 B	33	52	194
29 A	60	65	194
29 A	65	60	194
22 B	35	76	195
29 C	50	50	195
28 C	51	49	195
29 B	5	95	195
27 B	56	61	196
29 B	8	90	196
29 A	52	70	196
30 A	90	7	196
29 B	6	86	197
29 B	7	99	197
30 A	98	5	197
20 B	65	45	198
27 C	50	50	198
29 B	75	50	198
25 C	50	50	198
26 C	50	50	198
29 B	11	99	199
29 A	99	99	199
29 A	99	99	199
29 B	50	50	200
29 C	25	25	200
25 C	25	75	200
26 C	50	50	200
29 A	50	50	200
26 A	50	50	202
28 B	51	49	202
28 C	49	51	204
27 B	49	51	207
28 B	50	50	207
28 B	49	51	207
26 B	15	88	213
27 B	51	49	216

29 C	51	49	216
27 B	50	51	218
19 C	50	50	219
27 B	49	50	220
28 B	50	49	238
19 A	75	80	240
30 B	50	50	245
24 A	120	610	257

Supplementary Table S7. Detailed data of *G. phoenesis* bones (n=309), excluding osteoderms, from Unit III of Santa Elina.

Square	X	Y	Z
28 A	25	75	272
20 B	75	75	273
20 B	50	50	275
20 B	50	50	275
20 A	75	75	282
20 A	75	25	285
24 A	54	12	287
27 Z	75	50	290
27 Z	72	51	290
21 A	87	40	291
21 A	50	50	291
27 B	15	17	292
27 B	25	75	293
26 B	75	25	295
24 A	25	75	295
27 B	30	10	296
26 B	75	75	297
26 B	25	75	297
27 A	50	50	297
27 Z	75	75	297
28 A	50	50	297
26 C	50	60	298
27 B	25	75	298
27 B	50	50	299
25 A	67	99	300
25 B	15	95	300
25 C	50	50	300
25 B	17	82	300
26 B	25	75	300

26 B	75	25	300
27 A	75	75	300
27 B	25	25	300
26 B	99	99	301
26 B	88	20	303
26 B	75	25	303
26 B	99	23	304
26 C	50	50	304
25 C	50	50	305
25 B	50	10	305
26 B	25	75	305
26 B	95	60	305
28 Z	75	50	305
27 C	325	75	305
28 C	325	25	305
24 B	250	50	305
24 Z	75	25	305
24 B	50	50	305
26 B	82	27	306
26 B	82	27	306
25 C	88	25	307
25 B	25	80	307
25 C	40	85	307
26 B	27	47	307
26 B	30	65	307
26 B	85	30	307
26 B	35	35	307
27 B	75	75	307
28 A	75	75	307
28 B	51	50	307
26 C	12	88	307
26 C	20	30	307
26 B	84	22	308
26 A	75	25	308
26 B	82	27	308
26 C	26	50	308
27 A	75	25	308
26 B	74	20	309
26 B	81	68	309
26 B	50	50	309
26 A	25	75	309
26 C	25	45	309
28 B	35	10	309

28 B	75	25	309
25 B	45	95	310
25 B	33	91	310
25 B	40	60	310
24 D	50	50	310
25 C	72	43	310
25 C	72	44	310
25 C	14	80	310
26 B	65	7	310
26 B	95	12	310
26 B	95	51	310
26 B	8	76	310
26 A	50	50	310
26 B	30	20	310
26 B	94	87	310
26 C	50	50	310
26 Z	75	95	310
27 A	25	25	310
27 B	50	50	310
27 B	36	83	310
28 A	30	30	310
28 C	75	25	310
26 B	62	60	310
26 B	99	30	310
26 B	50	38	310
26 B	77	46	310
28 A	25	50	310
28 B	40	32	310
28 C	50	50	310
21 A	30	99	310
25 B	21	62	311
25 B	53	95	311
26 B	81	48	311
26 B	94	90	311
26 B	76	80	311
26 B	76	80	311
26 B	99	99	311
26 B	80	64	311
28 A	50	5	311
26 C	22	49	311
26 C	19	71	311
26 B	77	68	311
26 B	98	22	311

26 B	96	35	311
26 B	75	25	311
25 B	80	66	312
26 B	50	47	312
27 B	75	25	312
26 B	60	87	312
26 B	81	54	312
26 B	75	75	312
26 B	25	75	312
25 B	62	83	313
26 B	30	20	313
27 A	45	85	313
27 Z	75	25	313
26 B	32	98	313
26 B	97	98	313
26 C	70	76	313
26 B	24	42	313
22 A	50	50	313
26 A	75	25	314
27 A	25	75	314
27 A	75	25	314
27 A	75	25	314
26 B	35	22	314
26 B	35	22	314
26 B	67	19	314
28 A	62	32	314
25 B	15	95	315
25 B	15	19	315
26 A	44	87	315
26 B	6	20	315
26 B	36	25	315
26 B	42	25	315
26 A	75	75	315
26 B	30	20	315
26 Z	45	70	315
26 B	31	59	315
26 B	15	39	315
27 C	30	15	315
26 B	56	83	315
26 B	56	83	315
26 B	56	83	315
26 A	30	36	316
26 A	30	40	316

26 B	29	13	316
26 B	28	40	316
27 B	75	75	316
26 B	20	63	316
26 B	90	80	316
26 B	31	55	316
28 A	20	45	316
27 C	5	56	316
22 A	75	75	316
26 A	50	5	317
26 A	75	75	317
26 B	50	17	317
26 B	33	93	317
26 B	60	71	317
26 C	40	26	317
28 A	75	48	317
26 B	33	98	317
26 C	35	55	317
26 C	50	50	317
27 A	58	19	317
26 A	60	70	318
26 A	25	25	318
26 C	27	25	318
26 B	62	57	318
26 B	59	59	318
26 B	55	32	318
26 A	82	20	319
26 B	15	82	319
26 B	22	57	319
26 B	47	55	319
26 A	50	2	320
26 A	22	85	320
26 A	36	94	320
26 A	51	81	320
26 A	30	64	320
26 A	34	30	320
26 A	31	36	320
26 A	25	23	320
26 A	62	20	320
26 A	56	29	320
26 A	50	32	320
26 A	62	35	320
26 A	55	43	320

26 A	58	49	320
26 A	60	55	320
26 A	60	60	320
26 A	70	70	320
26 A	71	60	320
26 A	75	53	320
26 A	92	40	320
26 A	84	27	320
26 A	25	50	320
27 A	25	25	320
27 A	75	25	320
26 B	16	82	320
19 Z	50	50	320
26 B	75	75	320
25 A	50	50	320
26 B	18	90	320
24 B	50	50	320
27 A	63	1	320
28 A	21	39	320
26 B	11	80	320
27 A	50	50	320
23 Z	90	60	320
26 A	26	45	321
26 A	65	13	321
26 B	45	2	321
26 A	49	50	321
26 A	50	51	321
26 A	75	25	321
26 A	66	92	321
26 B	65	18	321
26 A	50	15	322
26 A	57	63	322
26 B	12	67	322
26 A	14	91	322
28 A	27	30	322
22 A	45	80	322
26 A	60	12	323
26 A	80	20	323
25 A	75	75	323
26 C	10	40	323
26 B	25	25	323
20 A	65	95	323
23 A	50	50	323

27 A	98	10	323
26 A	32	27	324
26 A	42	13	324
26 A	33	61	324
26 A	56	81	324
26 A	72	71	324
27 A	3	9	324
24 A	60	30	324
25 A	53	87	325
25 A	50	80	325
26 A	42	50	325
26 A	70	25	325
25 A	88	99	325
25 A	75	95	325
25 B	16	97	325
26 A	25	25	325
26 A	65	15	325
26 B	50	30	325
24 B	35	95	325
20 A	70	37	325
25 A	50	37	325
26 A	50	50	325
23 B	30	68	325
26 A	18	62	326
26 A	24	72	326
25 A	10	55	327
25 A	50	22	327
20 A	25	75	327
25 A	45	90	327
24 B	60	95	327
27 Z	82	40	328
26 A	28	23	329
26 A	27	15	329
26 B	18	88	329
26 A	68	17	330
26 A	75	75	330
26 A	75	25	330
26 A	75	25	330
25 A	87	25	331
26 A	15	5	331
23 A	50	50	332
21 Z	50	50	332
24 A	47	92	332

26 A	5	50	333
26 A	50	50	333
25 A	31	6	333
25 A	25	25	333
25 A	75	75	334
26 A	25	25	335
24 B	25	99	336
23 A	9	82	336
23 A	9	90	336
26 A	32	15	337
26 A	14	8	337
24 B	83	99	337
25 A	25	75	338
24 A	2	19	338
24 A	15	10	338
24 C	50	50	340
25 Z	75	25	340
25 A	25	25	340
25 A	75	25	340
25 A	25	50	345
25 B	75	25	350
26 B	6	57	363

Supplementary Table S8. Detailed data of *G. phoenesis* osteoderms (n=2564), from Unit II of Santa Elina.

Square	X	Y	Z	Quantity
31 B	-	-	74	1
30 D	-	-	80	4
23 A	-	-	87	15
30 A	40	15	89	2
30 A	90	85	91	4
31 C	50	25	98	1
30 B	-	-	100	47
31 B	90	25	100	2
30 C	-	-	110	2
31 C	54	26	110	1
31 C	50	35	111	1
28 D	-	-	114	45
30 C	50	30	114	3
30 A	-	-	114	1
28 D	-	-	115	30
30 C	-	-	115	2
31 A	-	-	115	2
30 A	-	-	116	6
30 B	-	-	118	55
28 D	-	-	119	1
28 D	-	-	120	6
31 C	50	25	120	1
30 C	-	-	120	1
31 C	50	20	121	1
31 A	-	-	128	1
30 A	35	85	130	1
30 C	-	-	139	2
30 B	32	80	140	1
27 C	-	-	140	1
30 B	0	95	142	1
30 C	25	95	142	2
31 B	-	-	147	1
29 C	-	-	150	8
27 B	-	-	150	1
29 C	-	-	152	5
30 B	98	98	153	1
29 B	62	85	154	17
30 B	-	-	154	1
30 C	90	35	154	3

27 D	-	-	155	3
30 B	-	-	155	1
31 B	5	5	158	4
30 B	90	10	160	3
30 B	-	-	160	3
30 C	-	-	160	3
30 C	62	35	160	3
30 C	62	35	164	2
19 B	-	-	165	3
19 B	-	-	165	2
27 B	-	-	165	3
30 C	-	-	166	2
30 C	-	-	166	1
30 A	-	-	169	2
27 D	-	-	170	3
30 B	85	85	170	2
30 C	45	20	170	2
31 B	-	-	171	4
27 D	-	-	172	3
30 B	33	90	173	3
27 D	-	-	175	4
30 B	75	93	175	3
30 D	-	-	175	1
30 B	-	-	175	3
30 C	-	-	175	2
30 C	70	80	175	2
30 A	16	99	175	5
29 C	-	-	176	8
25 C	58	75	176	1
30 B	20	75	176	8
29 C	-	-	177	37
29 B	-	-	178	12
19 A	-	-	180	1
29 A	-	-	180	6
22 A	-	-	180	1
25 C	23	87	180	1
29 C	-	-	180	6
28 C	-	-	180	44
27 C	-	-	180	3
30 B	-	-	180	4
29 C	-	-	181	6
29 C	-	-	181	14
30 C	-	-	181	10

29 C	-	-	181	83
30 B	25	85	182	3
21 B	-	-	183	2
29 B	-	-	183	1
29 C	-	-	184	24
29 A	-	-	185	2
30 A	-	-	185	5
30 C	-	-	186	8
30 B	20	75	186	4
30 B	20	84	187	1
29 B	62	80	187	10
29 C	-	-	187	42
31 A	-	-	188	43
28 A	-	-	188	21
29 C	-	-	188	9
30 C	-	-	188	14
29 B	24	82	189	3
30 B	12	75	189	1
30 B	92	90	189	6
29 A	-	-	189	2
27 D	-	-	189	1
29 C	-	-	189	81
30 B	21	82	190	1
30 B	-	-	190	1
29 A	-	-	190	6
29 A	-	-	190	2
22 A	-	-	190	1
29 B	55	70	190	2
30 B	-	-	190	2
29 C	67	60	190	19
29 C	39	53	190	16
29 B	-	-	191	1
29 A	-	-	192	6
30 A	-	-	192	28
30 B	90	89	192	18
30 C	-	-	192	5
29 C	-	-	192	8
30 A	5	85	193	2
30 A	0,5	85	193	13
30 B	-	-	193	5
29 B	22	84	194	2
29 B	-	-	194	4
29 C	-	-	195	13

30 B	45	80	195	1
29 B	-	-	195	1
30 B	-	-	195	1
30 B	-	-	196	42
29 A	50	60	197	12
30 A	95	5	197	9
29 A	-	-	197	32
30 B	26	87	197	4
29 D	-	-	197	26
30 C	-	-	197	3
29 C	-	-	197	137
30 B	22	67	197	5
30 B	12	95	198	1
29 B	-	-	198	20
30 B	-	-	198	12
30 B	65	85	198	17
29 A	99	99	199	4
29 B	-	-	200	25
29 A	47	40	200	1
27 C	-	-	200	6
29 A	-	-	200	5
29 B	-	-	200	1
29 B	37	92	200	9
29 B	-	-	200	16
29 A	-	-	200	24
29 C	-	-	200	85
30 A	85	10	200	2
30 B	75	25	200	10
30 B	-	-	200	44
30 B	-	-	200	80
29 B	-	-	201	10
29 B	8	79	202	4
30 B	-	-	202	10
29 B	-	-	202	15
29 C	-	-	202	2
26 C	-	-	202	2
22 B	-	-	203	3
24 B	-	-	205	4
28 A	-	-	205	2
29 B	-	-	205	10
29 A	75	52	205	1
30 B	-	-	205	17
30 C	-	-	206	4

29 C	-	-	206	1
30 B	75	65	207	4
30 B	-	-	207	11
29 B	-	-	209	20
29 B	-	-	209	1
29 B	-	-	209	10
29 B	-	-	210	1
30 B	10	47	210	8
25 C	-	-	210	42
29 B	62	85	210	41
29 B	5	75	211	1
28 A	-	-	211	2
28 A	-	-	211	2
30 B	-	-	212	20
30 B	-	-	212	3
26 B	-	-	213	1
28 C	-	-	213	3
30 C	-	-	214	4
29 C	-	-	214	6
29 B	65	110	214	5
29 B	-	-	215	4
30 B	-	-	215	31
30 B	-	-	217	4
29 B	-	-	217	14
30 B	-	-	217	18
25 A	-	-	218	3
29 B	-	-	218	19
30 C	-	-	218	8
25 B	-	-	218	2
30 B	-	-	220	3
30 B	57	70	220	1
26 B	-	-	220	15
25 B	-	-	220	8
29 B	85	75	220	4
29 C	-	-	220	6
26 D	-	-	220	1
30 B	87	70	220	15
30 B	71	70	220	18
30 B	-	-	220	19
30 B	30	50	220	46
29 B	-	-	221	5
29 A	-	-	221	22
30 B	15	15	222	3

28 A	-	-	222	15
28 B	-	-	222	4
28 B	-	-	222	5
30 C	-	-	223	3
27 B	-	-	224	1
30 B	20	15	225	3
25 B	-	-	225	8
30 B	-	-	225	9
30 B	57	70	225	16
30 B	-	-	227	6
30 B	87	70	227	11
25 B	-	-	228	1
30 B	75	87	230	1
30 B	65	55	231	4
29 B	85	75	232	3
30 B	-	-	232	5
30 B	57	70	235	14
30 B	20	15	235	3
25 A	-	-	235	8
28 B	-	-	235	1
30 B	87	70	235	6
30 B	75	35	236	3
25 A	-	-	236	10
30 B	70	70	236	5
26 A	-	-	238	6
28 C	-	-	238	1
29 A	75	35	240	4
30 B	70	17	240	18
25 A	-	-	240	72
27 B	-	-	240	3
31 B	-	-	240	9
30 B	20	15	240	1
30 B	55	85	240	4
30 B	57	70	240	4
30 B	-	-	241	5
30 B	-	-	242	31
28 B	-	-	242	2
30 B	-	-	242	2
25 A	-	-	244	22
20 C	-	-	246	2
27 A	-	-	247	1
30 B	-	-	250	5
24 C	-	-	250	3

30 B	-	-	251	3
25 A	-	-	255	1
30 B	-	-	255	1
29 A	-	-	260	3
24 D	-	-	270	6
19 B	10	87	281	1

Supplementary Table S9. Detailed data of *G. phoenesis* osteoderms (n=4505), from Unit III of Santa Elina.

Square	X	Y	Z	Quantity
28 B	-	-	244	5
29 C	-	-	264	2
28 C	-	-	266	1
29 B	-	-	272	1
20 B	-	-	273	1
29 A	75	30	273	2
24 A	-	-	273	1
29 B	-	-	274	4
20 B	-	-	275	2
24 B	-	-	275	1
29 C	-	-	275	1
30 B	95	35	275	5
30 B	55	15	275	6
21 B	-	-	276	1
20 B	-	-	277	1
26 C	-	-	277	8
20 B	-	-	278	5
30 B	50	15	280	6
19 B	20	35	281	1
25 B	25	10	283	1
29 C	-	-	285	3
21 B	44	18	285	1
27 D	-	-	285	3
24 D	-	-	285	8
24 A	-	-	287	4
23 A	82	80	287	1
24 B	-	-	287	1
22 B	-	-	290	2
28 D	-	-	290	4
28 B	90	41	291	1
28 B	-	-	293	1

30 C	60	45	293	4
24 B	-	-	294	23
25 B	0,36	0,2	295	7
26 C	-	-	295	3
28 A	-	-	296	1
26 B	100	70	298	1
28 A	4	6	299	1
29 A	24	26	300	1
28 B	-	-	300	3
27 B	-	-	300	1
26 C	-	-	300	3
25 C	-	-	300	11
25 B	-	-	300	27
25 A	95	85	300	8
25 B	-	-	300	19
25 B	25	25	300	4
25 B	15	85	300	19
24 A	-	-	300	1
29 A	20	25	300	2
25 C	-	-	300	5
24 B	-	-	300	3
25 B	-	-	301	13
21 B	-	-	301	1
29 B	-	-	301	3
23 C	-	-	301	1
25 C	-	-	301	2
25 B	-	-	303	1
24 B	-	-	304	53
24 B	36	85	304	1
28 B	-	-	304	1
28 A	-	-	304	1
26 C	60	25	304	3
24 B	-	-	305	8
22 B	-	-	305	2
27 C	-	-	305	2
24 B	-	-	305	9
23 B	50	25	305	1
25 B	-	-	305	13
24 B	-	-	305	17
26 B	-	-	305	40
26 B	95	20	305	8
24 B	9	95	306	2
26 B	82	27	306	11

26 B	-	-	307	14
28 A	-	-	307	3
23 A	-	-	307	1
23 B	15	15	307	1
24 A	-	-	307	2
26 C	30	85	307	2
26 C	16	90	307	1
26 C	20	35	307	1
26 C	90	16	307	1
26 C	3	33	307	1
26 C	69	43	308	16
28 A	57	51	308	4
27 A	-	-	308	3
27 A	-	-	308	3
26 B	87	36	308	5
26 B	-	-	308	1
26 C	-	-	309	32
26 B	72	10	309	14
26 B	93	35	309	5
26 B	53	32	309	5
26 B	70	35	309	7
25 B	-	-	310	10
28 B	-	-	310	1
23 B	-	-	310	16
27 B	-	-	310	1
27 B	-	-	310	1
27 C	-	-	310	2
24 B	-	-	310	10
26 B	-	-	310	6
25 C	75	91	310	7
25 B	-	-	310	80
25 C	-	-	310	15
24 D	-	-	310	10
25 A	-	-	310	2
25 B	-	-	310	20
26 B	99	32	310	2
28 C	40	54	310	3
26 C	10	45	310	5
26 C	55	55	310	1
26 C	20	24	310	1
26 B	32	15	310	4
23 B			310	7
26 B	40	40	310	8

26 A	80	40	310	4
28 A	-	-	311	2
27 B	-	-	311	1
27 A	-	-	311	1
27 C	-	-	311	1
26 B	-	-	311	21
26 B	98	90	311	2
21 B	-	-	312	1
26 C	-	-	312	41
26 C	-	-	312	10
26 B	-	-	312	5
25 B	-	-	312	7
25 C	-	-	313	10
28 C	-	-	313	1
23 B	5	40	313	1
26 C	-	-	313	7
27 A	40	92	313	1
27 A	-	-	313	3
24 A	-	-	313	1
24 B	-	-	313	6
27 C	45	80	313	4
26 C	40	52	314	30
23 B	-	-	314	1
27 A	-	-	314	3
26 A	-	-	314	1
28 C	35	26	315	2
28 A	97	99	315	1
28 A	80	97	315	1
28 A	-	-	315	2
26 C	-	-	315	39
28 C	-	-	315	1
26 B	-	-	315	3
26 B	-	-	315	13
26 B	-	-	315	45
26 B	52	75	315	2
26 B	60	70	315	1
26 B	59	62	315	1
26 B	20	50	315	1
22 A	-	-	316	1
26 B	-	-	316	10
22 A	60	5	316	1
23 B	7	58	316	1
23 B	-	-	316	20

26 C	5	30	316	2
27 C	40	10	316	1
26 B	-	-	316	5
27 C	-	-	316	6
26 B	-	-	316	9
26 B	28	45	316	2
26 B	2	42	316	4
26 B	59	45	316	2
26 B	43	48	316	3
26 B	15	40	316	1
26 B	11	18	316	4
26 B	15	20	316	4
29 A	5	10	317	5
27 B	-	-	317	2
26 A	81	55	317	2
26 A	96	41	317	5
22 A	36	42	318	1
22 A	45	50	318	1
27 B	31	95	318	1
25 A	-	-	318	8
24 B	-	-	318	6
27 A	-	-	318	1
21 A	30	100	319	1
22 A	40	31	319	1
24 A	-	-	319	5
24 D	-	-	319	1
26 A	-	-	319	1
26 A	-	-	319	2
26 A	50	70	319	5
24 B	-	-	320	8
25 A	-	-	320	1
26 B	-	-	320	6
28 A	-	-	320	1
23 A	70	55	320	1
26 B	4	68	320	1
27 A	-	-	320	1
28 A	-	-	320	2
25 A	-	-	320	1
25 B	-	-	320	40
26 B	-	-	320	47
23 D	-	-	320	1
25 B	-	-	320	2
26 A	-	-	320	4

26 B	-	-	320	1
23 A	54	36	321	1
23 B	-	-	321	4
26 B	14	81	321	1
26 C	18	50	321	4
26 B	20	100	321	2
26 A	-	-	321	10
23 A	80	50	322	5
26 B	-	-	322	2
24 A	10	95	322	5
22 A	45	80	322	1
25 B	-	-	322	26
26 A			322	3
26 A	65	40	322	2
23 A	-	-	323	1
26 B	-	-	323	7
26 C	10	40	323	3
22 A	36	34	323	1
23 A	22	20	323	2
23 A	86	85	323	1
26 A	12	90	323	1
26 A	62	95	323	1
26 B	10	49	323	1
26 C	46	32	323	17
27 A	-	-	323	1
27 B	-	-	323	1
26 A	65	85	323	2
27 C	90	90	323	9
26 C	35	82	323	3
26 B	-	-	323	1
25 A	-	-	323	52
25 B	5	50	323	6
26 A	44	71	324	1
26 A	49	84	324	2
26 A	15	86	324	1
26 C	17	50	324	7
26 A	81	58	324	5
25 A	-	-	324	9
24 B	-	-	324	5
24 A	-	-	324	1
28 C	40	60	324	2
22 A	-	-	325	1
23 B	30	60	325	1

24 A	-	-	325	40
25 A	50	22	325	67
25 B	50	30	325	3
29 A	85	70	325	30
26 C	-	-	325	1
26 A	-	-	325	4
28 B	-	-	325	2
25 B	-	-	325	1
24 A	-	-	326	1
28 A	76	3	326	2
25 A	-	-	326	7
24 A	60	5	326	20
27 B	-	-	326	1
23 B	20	99	327	1
25 A	45	90	327	6
25 A	50	22	327	56
26 A	50	27	327	1
22 A	42	42	327	1
23 A	97	97	327	1
23 A	-	-	327	1
26 A	58	66	327	1
25 A	-	-	327	10
24 B	2	2	327	1
27 C	-	-	327	3
28 B	-	-	327	3
28 B	-	-	327	3
26 A	-	-	327	5
26 A	28	38	328	1
28 B	-	-	328	1
27 Z	82	40	328	1
29 A	-	-	328	3
24 A	75	100	328	20
25 A	49	4	328	20
24 A	-	-	328	1
24 B	-	-	328	8
28 A	-	-	328	5
24 A	-	-	328	44
24 A	-	-	329	20
24 A	-	-	329	85
24 A	-	-	329	1
24 A	-	-	329	5
24 A	-	-	329	95
27 B	-	-	329	5

28 B	-	-	329	1
24 A	-	-	330	6
25 A	25	90	330	9
25 A	-	-	330	4
25 A	-	-	330	1
25 A	-	-	330	20
24 A	65	85	330	9
24 A	60	60	330	11
24 A	-	-	330	12
26 A	13	37	330	2
28 A	-	-	330	1
26 A	-	-	330	12
25 B	-	-	330	2
26 A	-	-	330	48
26 c	30	80	330	7
27 C	15	75	330	2
28 B	-	-	330	41
28 C	-	-	330	1
29 C	13	12	330	2
26 A	17	6	331	10
24 A	-	-	331	5
28 D	77	70	331	1
23 A	-	-	332	1
26 A	15	10	332	11
24 A	-	-	332	46
25 A	-	-	332	24
27 A	-	-	332	1
28 D	76	37	332	1
23 A	-	-	333	3
24 A	-	-	333	76
23 A	61	85	333	1
24 A	35	60	333	9
24 A	75	35	333	4
24 A	-	-	333	3
24 A	35	85	333	8
26 A	-	-	333	140
27 B	-	-	333	1
23 A	-	-	334	3
25 A	-	-	334	262
26 A	-	-	334	8
24 A	-	-	334	9
27 B	-	-	334	1
27 B	60	50	334	1

26 A	5	40	335	10
24 A	-	-	335	16
26 C	-	-	335	18
24 A	-	-	335	78
26 A	-	-	335	93
24 A	-	100	336	40
24 A	-	-	336	36
24 A	-	-	336	4
24 A	-	-	336	7
24 A	67	65	336	5
27 A	-	-	336	1
27 Z	60	60	336	1
24 A	-	-	337	27
24 A	62	100	337	76
25 A	-	-	337	100
24 A	87	100	337	20
26 A	-	-	337	12
28 B	10	85	337	1
27 B	-	-	338	1
23 Z	-	-	338	8
24 A	-	-	339	3
25 A	0,4	-	339	40
25 A	-	-	339	29
23 A	-	-	340	4
23 Z	-	-	340	4
25 A	-	-	340	56
24 A	-	-	340	7
25 B	-	-	340	6
28 B	-	-	340	5
23 Z	-	-	341	2
23 A	-	-	341	10
24 A	-	-	341	32
28 A	95	2	341	1
26 A	18	13	341	6
23 A	5	90	342	16
23 A	-	-	342	6
24 B	63	93	342	2
24 A	-	-	342	11
24 A	-	-	342	5
24 A	20	37	342	10
24 A	28	83	342	6
24 A	17	23	342	9
25 A	-	-	342	1

26 A	7	42	342	50
28 A	73	70	342	1
23 A	-	-	343	5
25 A	-	-	343	5
28 B	20	20	343	1
23 Z	82	18	344	9
23 Z	-	-	344	7
23 A	-	-	344	5
24 A	65	25	344	4
24 A	17	5	344	11
28 B	13	77	344	1
24 A	-	-	345	4
24 A	87	15	345	3
24 Z	88	63	345	1
25 A	-	-	345	1
25 A	3	2	345	10
25 A	-	-	345	2
25 B	-	-	345	2
26 Z	90	75	345	2
26 A	20	10	345	1
24 C	-	-	345	26
25 A	30	47	345	6
28 B	35	30	345	1
23 Z	90	41	346	18
23 A	-	-	346	2
24 A	-	-	346	5
24 A	6	70	346	13
25 A	7	5	346	3
25 A	-	-	346	4
29 B	-	-	346	2
25 A	-	-	347	12
23 A	-	-	347	1
24 Z	94	37	347	14
24 A	8	47	347	10
24 A	15	59	347	20
26 Z	94	72	347	70
25 A	-	-	348	16
25 A	4	87	348	14
24 A	90	80	348	7
24 A	68	90	348	1
28 C	20	80	349	1
24 A	3	96	349	10
24 A	3	93	349	1

25 A	-	-	349	10
23 A	-	-	349	6
28 B	80	80	349	1
28 B	35	69	349	1
25 Z	-	-	350	12
25 B	-	-	350	3
26 Z	91	34	350	30
26 A	0	0	350	4
28 B	40	35	350	1
27 B	25	37	350	1
24 Z	98	46	350	1
26 A	-	-	350	1
26 A	10	10	350	3
29 B	-	-	350	12
24 A	-	-	350	2
24 Z	-	-	350	5
25 B	-	-	350	8
25 A	15	40	350	12
25 A	-	-	350	1
23 A	-	-	351	3
25 A	-	-	351	11
25 A	7	95	351	22
26 A	44	0	351	1
25 Z	-	-	352	16
26 Z	90	30	352	15
26 Z	-	-	352	20
25 A	66	39	353	9
24 Z	90	85	353	6
25 B	-	-	353	1
26 Z	-	-	353	5
25 A	-	-	353	16
25 A	-	-	353	3
27 C	-	-	353	1
25 A	50	65	354	1
25 A	67	36	354	2
26 A	-	-	354	1
28 A	-	-	354	2
25 A	-	-	354	12
25 A	2	62	354	2
25 A	65	75	354	3
25 A	35	58	354	6
25 B	-	-	354	3
25 C	-	-	355	1

25 A	-	-	355	3
24 A	-	-	355	4
26 B	24	57	355	1
24 A	15	25	355	15
25 A	19	44	356	20
26 Z	76	44	357	21
26 Z	81	49	357	1
26 Z	82	40	357	1
23 Z	100	56	358	2
25 Z	96	33	358	8
25 A	-	-	358	3
25 Z	95	35	359	12
25 A	20	49	359	2
23 Z	-	-	359	1
25 C	-	-	360	8
25 Z	97	53	360	2
26 Z	95	3	360	4
25 B	-	-	360	3
25 A	-	-	364	5
23 Z	-	-	364	1
23 B	-	-	365	1
25 B	-	-	365	1
22 B	23	55	375	1
25 Z	75	30	375	5
28 C	-	-	380	1
23 B	-	-	410	2

Supplementary Table S10. *Coordinates of stone tools and ground sloth bones (excluding osteoderms) from Units II and III of Santa Elina used to generate 2D and 3D association maps.*

Square	X	Y	Z	Material
26 D	430	822	148	Stone tool (II)
27 C	398	950	151	Stone tool (II)
26 B	283	896	164	Stone tool (II)
27 B	268	938	168	Stone tool (II)
27 C	325	936	171	Stone tool (II)
26 C	355	816	176	Stone tool (II)
27 C	371	942	178	Stone tool (II)
28 B	221	1032	178	Stone tool (II)
29 B	205	1133	180	Stone tool (II)
26 C	374	821	183	Stone tool (II)
28 C	305	1023	183	Stone tool (II)
27 C	350	955	185	Stone tool (II)
29 B	223	1184	187	Stone tool (II)
25 C	351	787	188	Stone tool (II)
26 C	351	887	188	Stone tool (II)
20 C	335	275	190	Stone tool (II)
21 A	180	315	197	Stone tool (II)
29 B	245	1180	198	Stone tool (II)
29 B	208	1177	198	Stone tool (II)
29 B	250	1112	200	Stone tool (II)
26 B	246	808	201	Stone tool (II)
21 B	280	360	203	Stone tool (II)
21 B	210	350	203	Stone tool (II)
27 B	250	935	204	Stone tool (II)
20 B	220	270	207	Stone tool (II)
20 B	225	275	207	Stone tool (II)
21 B	266	340	208	Stone tool (II)
21 C	390	390	208	Stone tool (II)
21 B	290	390	212	Stone tool (II)
22 D	425	495	212	Stone tool (II)
23 C	307	537	213	Stone tool (II)
23 B	238	510	216	Stone tool (II)
26 B	282	834	218	Stone tool (II)
27 C	317	968	218	Stone tool (II)
27 C	317	968	218	Stone tool (II)
20 B	250	225	220	Stone tool (II)
24 B	200	680	220	Stone tool (II)
22 B	250	475	223	Stone tool (II)

20 A	192	270	227	Stone tool (II)
20 B	280	300	227	Stone tool (II)
21 A	106	390	227	Stone tool (II)
24 D	435	615	227	Stone tool (II)
20 A	185	285	230	Stone tool (II)
20 B	274	295	231	Stone tool (II)
20 B	235	285	231	Stone tool (II)
21 B	230	327	232	Stone tool (II)
24 C	375	610	232	Stone tool (II)
20 B	240	290	236	Stone tool (II)
26 B	282	870	278	Stone tool (III)
28 A	108	1065	284	Stone tool (III)
29 B	280	1132	286	Stone tool (III)
28 B	295	1045	287	Stone tool (III)
27 B	286	957	289	Stone tool (III)
27 B	239	948	290	Stone tool (III)
27 B	217	987	290	Stone tool (III)
27 C	320	957	290	Stone tool (III)
28 B	254	1092	290	Stone tool (III)
27 B	250	930	291	Stone tool (III)
27 B	272	963	291	Stone tool (III)
27 C	337	954	295	Stone tool (III)
28 A	140	1040	297	Stone tool (III)
28 A	133	1020	297	Stone tool (III)
22 B	208	430	298	Stone tool (III)
27 B	215	975	299	Stone tool (III)
28 B	238	1089	299	Stone tool (III)
23 B	202	546	300	Stone tool (III)
28 A	190	1060	301	Stone tool (III)
23 B	206	514	302	Stone tool (III)
28 A	147	1001	302	Stone tool (III)
28 B	260	1049	303	Stone tool (III)
22 A	172	492	304	Stone tool (III)
26 A	180	847	304	Stone tool (III)
28 B	210	1048	304	Stone tool (III)
24 B	260	658	306	Stone tool (III)
25 C	350	750	306	Stone tool (III)
26 B	239	827	307	Stone tool (III)
26 B	225	847	307	Stone tool (III)
26 B	245	820	307	Stone tool (III)
28 B	225	1055	307	Stone tool (III)
27 B	295	926	309	Stone tool (III)
28 A	190	1070	309	Stone tool (III)

24 B	260	603	310	Stone tool (III)
26 A	150	868	310	Stone tool (III)
26 B	223	889	310	Stone tool (III)
27 B	244	995	310	Stone tool (III)
26 B	283	840	311	Stone tool (III)
27 B	208	912	312	Stone tool (III)
27 B	211	908	312	Stone tool (III)
26 B	210	875	313	Stone tool (III)
27 A	125	997	313	Stone tool (III)
24 A	175	625	316	Stone tool (III)
26 B	218	885	318	Stone tool (III)
24 D	420	640	319	Stone tool (III)
26 A	147	872	320	Stone tool (III)
24 A	195	620	321	Stone tool (III)
29 C	316	1116	321	Stone tool (III)
29 B	239	1115	321	Stone tool (III)
29 B	214	1108	322	Stone tool (III)
28 C	318	1077	323	Stone tool (III)
24 A	130	627	324	Stone tool (III)
28 A	179	1056	325	Stone tool (III)
28 B	223	1073	325	Stone tool (III)
27 B	252	983	326	Stone tool (III)
27 B	218	910	327	Stone tool (III)
27 A	165	974	329	Stone tool (III)
26 A	143	816	330	Stone tool (III)
27 A	155	930	330	Stone tool (III)
27 A	160	955	330	Stone tool (III)
26 A	135	805	332	Stone tool (III)
22 B	225	480	336	Stone tool (III)
28 A	163	1013	337	Stone tool (III)
26 A	175	830	340	Stone tool (III)
27 A	185	945	340	Stone tool (III)
27 A	141	971	340	Stone tool (III)
29 A	170	1115	340	Stone tool (III)
24 A	150	700	341	Stone tool (III)
27 A	110	980	342	Stone tool (III)
23 A	120	520	344	Stone tool (III)
24 B	225	680	344	Stone tool (III)
27 A	183	944	344	Stone tool (III)
28 A	182	1018	344	Stone tool (III)
24 B	210	670	346	Stone tool (III)
27 B	290	908	347	Stone tool (III)
25 A	125	767	349	Stone tool (III)

23 B	215	520	350	Stone tool (III)
28 B	250	1035	350	Stone tool (III)
28 B	273	1037	350	Stone tool (III)
26 B	250	845	351	Stone tool (III)
26 B	240	845	352	Stone tool (III)
26 A	170	810	353	Stone tool (III)
23 B	205	595	354	Stone tool (III)
29 B	230	1130	354	Stone tool (III)
22 A	195	480	355	Stone tool (III)
28 D	449	1036	120	Megafauna (II)
28 D	422	1051	120	Megafauna (II)
28 D	428	1001	133	Megafauna (II)
23 A	115	530	139	Megafauna (II)
18 C	360	20	165	Megafauna (II)
28 C	328	1099	166	Megafauna (II)
29 C	362	1197	175	Megafauna (II)
28 C	350	1050	180	Megafauna (II)
28 C	398	1058	180	Megafauna (II)
29 C	350	1150	181	Megafauna (II)
28 C	350	1050	181	Megafauna (II)
29 A	162	1187	181	Megafauna (II)
29 C	340	1130	182	Megafauna (II)
29 B	250	1150	183	Megafauna (II)
28 B	225	1075	183	Megafauna (II)
28 C	375	1075	183	Megafauna (II)
28 B	225	1025	185	Megafauna (II)
26 C	350	850	185	Megafauna (II)
28 B	250	1050	186	Megafauna (II)
26 A	100	834	186	Megafauna (II)
21 C	365	305	187	Megafauna (II)
26 B	250	850	187	Megafauna (II)
27 C	329	990	187	Megafauna (II)
29 C	349	1151	187	Megafauna (II)
20 C	365	290	187	Megafauna (II)
27 B	285	908	188	Megafauna (II)
25 C	345	751	188	Megafauna (II)
27 B	250	950	188	Megafauna (II)
26 C	351	802	189	Megafauna (II)
28 A	130	1090	190	Megafauna (II)
29 A	175	1175	190	Megafauna (II)
27 B	225	925	191	Megafauna (II)
27 B	251	949	191	Megafauna (II)
29 B	249	1149	191	Megafauna (II)

29 A	190	1180	191	Megafauna (II)
27 A	150	950	192	Megafauna (II)
29 C	325	1125	192	Megafauna (II)
29 B	250	1151	192	Megafauna (II)
28 A	150	1050	193	Megafauna (II)
29 A	150	1150	193	Megafauna (II)
29 A	175	1175	193	Megafauna (II)
29 A	174	1176	193	Megafauna (II)
29 A	185	1193	193	Megafauna (II)
29 A	150	1160	193	Megafauna (II)
30 A	105	1285	193	Megafauna (II)
30 A	105	1286	193	Megafauna (II)
30 A	105	1284	193	Megafauna (II)
22 B	233	452	194	Megafauna (II)
29 A	160	1165	194	Megafauna (II)
29 A	165	1160	194	Megafauna (II)
22 B	235	476	195	Megafauna (II)
29 C	350	1150	195	Megafauna (II)
28 C	351	1049	195	Megafauna (II)
29 B	205	1195	195	Megafauna (II)
27 B	256	961	196	Megafauna (II)
29 B	208	1190	196	Megafauna (II)
29 A	152	1170	196	Megafauna (II)
30 A	190	1207	196	Megafauna (II)
29 B	206	1186	197	Megafauna (II)
29 B	207	1199	197	Megafauna (II)
30 A	198	1205	197	Megafauna (II)
20 B	265	245	198	Megafauna (II)
27 C	350	950	198	Megafauna (II)
29 B	275	1150	198	Megafauna (II)
25 C	350	750	198	Megafauna (II)
26 C	350	850	198	Megafauna (II)
29 B	211	1199	199	Megafauna (II)
29 A	199	1199	199	Megafauna (II)
29 A	199	1199	199	Megafauna (II)
29 B	250	1150	200	Megafauna (II)
29 C	325	1125	200	Megafauna (II)
25 C	325	775	200	Megafauna (II)
26 C	350	850	200	Megafauna (II)
29 A	150	1150	200	Megafauna (II)
26 A	150	850	202	Megafauna (II)
28 B	251	1049	202	Megafauna (II)
28 C	349	1051	204	Megafauna (II)

27 B	249	951	207	Megafauna (II)
28 B	250	1050	207	Megafauna (II)
28 B	249	1051	207	Megafauna (II)
26 B	215	888	213	Megafauna (II)
27 B	251	949	216	Megafauna (II)
29 C	351	1149	216	Megafauna (II)
27 B	250	951	218	Megafauna (II)
19 C	350	150	219	Megafauna (II)
27 B	249	950	220	Megafauna (II)
28 B	250	1049	238	Megafauna (II)
19 A	175	180	240	Megafauna (II)
30 B	250	1250	245	Megafauna (II)
24 A	220	1210	257	Megafauna (II)
28 A	125	1075	272	Megafauna (III)
20 B	275	275	273	Megafauna (III)
20 B	250	250	275	Megafauna (III)
20 B	250	250	275	Megafauna (III)
20 A	175	275	282	Megafauna (III)
20 A	175	225	285	Megafauna (III)
24 A	154	612	287	Megafauna (III)
27 Z	75	950	290	Megafauna (III)
27 Z	72	951	290	Megafauna (III)
21 A	187	340	291	Megafauna (III)
21 A	150	350	291	Megafauna (III)
27 B	215	917	292	Megafauna (III)
27 B	225	975	293	Megafauna (III)
26 B	275	825	295	Megafauna (III)
24 A	125	675	295	Megafauna (III)
27 B	230	910	296	Megafauna (III)
26 B	275	875	297	Megafauna (III)
26 B	225	875	297	Megafauna (III)
27 A	150	950	297	Megafauna (III)
27 Z	75	975	297	Megafauna (III)
28 A	150	1050	297	Megafauna (III)
26 C	350	860	298	Megafauna (III)
27 B	225	975	298	Megafauna (III)
27 B	250	950	299	Megafauna (III)
25 A	167	799	300	Megafauna (III)
25 B	215	795	300	Megafauna (III)
25 C	350	750	300	Megafauna (III)
25 B	217	782	300	Megafauna (III)
26 B	225	875	300	Megafauna (III)
26 B	275	825	300	Megafauna (III)

27 A	175	975	300	Megafauna (III)
27 B	225	925	300	Megafauna (III)
26 B	299	899	301	Megafauna (III)
26 B	288	820	303	Megafauna (III)
26 B	275	825	303	Megafauna (III)
26 B	299	823	304	Megafauna (III)
26 C	350	850	304	Megafauna (III)
25 C	350	750	305	Megafauna (III)
25 B	250	710	305	Megafauna (III)
26 B	225	875	305	Megafauna (III)
26 B	295	860	305	Megafauna (III)
28 Z	75	1050	305	Megafauna (III)
27 C	625	975	305	Megafauna (III)
28 C	625	1025	305	Megafauna (III)
24 B	450	650	305	Megafauna (III)
24 Z	75	625	305	Megafauna (III)
24 B	250	650	305	Megafauna (III)
26 B	282	827	306	Megafauna (III)
26 B	282	827	306	Megafauna (III)
25 C	388	725	307	Megafauna (III)
25 B	225	780	307	Megafauna (III)
25 C	340	785	307	Megafauna (III)
26 B	227	847	307	Megafauna (III)
26 B	230	865	307	Megafauna (III)
26 B	285	830	307	Megafauna (III)
26 B	235	835	307	Megafauna (III)
27 B	275	975	307	Megafauna (III)
28 A	175	1075	307	Megafauna (III)
28 B	251	1050	307	Megafauna (III)
26 C	312	888	307	Megafauna (III)
26 C	320	830	307	Megafauna (III)
26 B	284	822	308	Megafauna (III)
26 A	175	825	308	Megafauna (III)
26 B	282	827	308	Megafauna (III)
26 C	326	850	308	Megafauna (III)
27 A	175	925	308	Megafauna (III)
26 B	274	820	309	Megafauna (III)
26 B	281	868	309	Megafauna (III)
26 B	250	850	309	Megafauna (III)
26 A	125	875	309	Megafauna (III)
26 C	325	845	309	Megafauna (III)
28 B	235	1010	309	Megafauna (III)
28 B	275	1025	309	Megafauna (III)

25 B	245	795	310	Megafauna (III)
25 B	233	791	310	Megafauna (III)
25 B	240	760	310	Megafauna (III)
24 D	450	650	310	Megafauna (III)
25 C	372	743	310	Megafauna (III)
25 C	372	744	310	Megafauna (III)
25 C	314	780	310	Megafauna (III)
26 B	265	807	310	Megafauna (III)
26 B	295	812	310	Megafauna (III)
26 B	295	851	310	Megafauna (III)
26 B	208	876	310	Megafauna (III)
26 A	150	850	310	Megafauna (III)
26 B	230	820	310	Megafauna (III)
26 B	294	887	310	Megafauna (III)
26 C	350	850	310	Megafauna (III)
26 Z	75	895	310	Megafauna (III)
27 A	125	925	310	Megafauna (III)
27 B	250	950	310	Megafauna (III)
27 B	236	983	310	Megafauna (III)
28 A	130	1030	310	Megafauna (III)
28 C	375	1025	310	Megafauna (III)
26 B	262	860	310	Megafauna (III)
26 B	299	830	310	Megafauna (III)
26 B	250	838	310	Megafauna (III)
26 B	277	846	310	Megafauna (III)
28 A	125	1050	310	Megafauna (III)
28 B	240	1032	310	Megafauna (III)
28 C	350	1050	310	Megafauna (III)
21 A	130	399	310	Megafauna (III)
25 B	221	762	311	Megafauna (III)
25 B	253	795	311	Megafauna (III)
26 B	281	848	311	Megafauna (III)
26 B	294	890	311	Megafauna (III)
26 B	276	880	311	Megafauna (III)
26 B	276	880	311	Megafauna (III)
26 B	299	899	311	Megafauna (III)
26 B	280	864	311	Megafauna (III)
28 A	150	1005	311	Megafauna (III)
26 C	322	849	311	Megafauna (III)
26 C	319	871	311	Megafauna (III)
26 B	277	868	311	Megafauna (III)
26 B	298	822	311	Megafauna (III)
26 B	296	835	311	Megafauna (III)

26 B	275	825	311	Megafauna (III)
25 B	280	766	312	Megafauna (III)
26 B	250	847	312	Megafauna (III)
27 B	275	925	312	Megafauna (III)
26 B	260	887	312	Megafauna (III)
26 B	281	854	312	Megafauna (III)
26 B	275	875	312	Megafauna (III)
26 B	225	875	312	Megafauna (III)
25 B	262	783	313	Megafauna (III)
26 B	230	820	313	Megafauna (III)
27 A	145	985	313	Megafauna (III)
27 Z	75	925	313	Megafauna (III)
26 B	232	898	313	Megafauna (III)
26 B	297	898	313	Megafauna (III)
26 C	370	876	313	Megafauna (III)
26 B	224	842	313	Megafauna (III)
22 A	150	450	313	Megafauna (III)
26 A	175	825	314	Megafauna (III)
27 A	125	975	314	Megafauna (III)
27 A	175	925	314	Megafauna (III)
27 A	175	925	314	Megafauna (III)
26 B	235	822	314	Megafauna (III)
26 B	235	822	314	Megafauna (III)
26 B	267	819	314	Megafauna (III)
28 A	162	1032	314	Megafauna (III)
25 B	215	795	315	Megafauna (III)
25 B	215	719	315	Megafauna (III)
26 A	144	887	315	Megafauna (III)
26 B	206	820	315	Megafauna (III)
26 B	236	825	315	Megafauna (III)
26 B	242	825	315	Megafauna (III)
26 A	175	875	315	Megafauna (III)
26 B	230	820	315	Megafauna (III)
26 Z	45	870	315	Megafauna (III)
26 B	231	859	315	Megafauna (III)
26 B	215	839	315	Megafauna (III)
27 C	330	915	315	Megafauna (III)
26 B	256	883	315	Megafauna (III)
26 B	256	883	315	Megafauna (III)
26 B	256	883	315	Megafauna (III)
26 A	130	836	316	Megafauna (III)
26 A	130	840	316	Megafauna (III)
26 B	229	813	316	Megafauna (III)

26 B	228	840	316	Megafauna (III)
27 B	275	975	316	Megafauna (III)
26 B	220	863	316	Megafauna (III)
26 B	290	880	316	Megafauna (III)
26 B	231	855	316	Megafauna (III)
28 A	120	1045	316	Megafauna (III)
27 C	305	956	316	Megafauna (III)
22 A	175	475	316	Megafauna (III)
26 A	150	805	317	Megafauna (III)
26 A	175	875	317	Megafauna (III)
26 B	250	817	317	Megafauna (III)
26 B	233	893	317	Megafauna (III)
26 B	260	871	317	Megafauna (III)
26 C	340	826	317	Megafauna (III)
28 A	175	1048	317	Megafauna (III)
26 B	233	898	317	Megafauna (III)
26 C	335	855	317	Megafauna (III)
26 C	350	850	317	Megafauna (III)
27 A	158	919	317	Megafauna (III)
26 A	160	870	318	Megafauna (III)
26 A	125	825	318	Megafauna (III)
26 C	327	825	318	Megafauna (III)
26 B	262	857	318	Megafauna (III)
26 B	259	859	318	Megafauna (III)
26 B	255	832	318	Megafauna (III)
26 A	182	820	319	Megafauna (III)
26 B	215	882	319	Megafauna (III)
26 B	222	857	319	Megafauna (III)
26 B	247	855	319	Megafauna (III)
26 A	150	802	320	Megafauna (III)
26 A	122	885	320	Megafauna (III)
26 A	136	894	320	Megafauna (III)
26 A	151	881	320	Megafauna (III)
26 A	130	864	320	Megafauna (III)
26 A	134	830	320	Megafauna (III)
26 A	131	836	320	Megafauna (III)
26 A	125	823	320	Megafauna (III)
26 A	162	820	320	Megafauna (III)
26 A	156	829	320	Megafauna (III)
26 A	150	832	320	Megafauna (III)
26 A	162	835	320	Megafauna (III)
26 A	155	843	320	Megafauna (III)
26 A	158	849	320	Megafauna (III)

26 A	160	855	320	Megafauna (III)
26 A	160	860	320	Megafauna (III)
26 A	170	870	320	Megafauna (III)
26 A	171	860	320	Megafauna (III)
26 A	175	853	320	Megafauna (III)
26 A	192	840	320	Megafauna (III)
26 A	184	827	320	Megafauna (III)
26 A	125	850	320	Megafauna (III)
27 A	125	925	320	Megafauna (III)
27 A	175	925	320	Megafauna (III)
26 B	216	882	320	Megafauna (III)
19 Z	50	150	320	Megafauna (III)
26 B	275	875	320	Megafauna (III)
25 A	150	750	320	Megafauna (III)
26 B	218	890	320	Megafauna (III)
24 B	250	650	320	Megafauna (III)
27 A	163	901	320	Megafauna (III)
28 A	121	1039	320	Megafauna (III)
26 B	211	880	320	Megafauna (III)
27 A	150	950	320	Megafauna (III)
23 Z	90	560	320	Megafauna (III)
26 A	126	845	321	Megafauna (III)
26 A	165	813	321	Megafauna (III)
26 B	245	802	321	Megafauna (III)
26 A	149	850	321	Megafauna (III)
26 A	150	851	321	Megafauna (III)
26 A	175	825	321	Megafauna (III)
26 A	166	892	321	Megafauna (III)
26 B	265	818	321	Megafauna (III)
26 A	150	815	322	Megafauna (III)
26 A	157	863	322	Megafauna (III)
26 B	212	867	322	Megafauna (III)
26 A	114	891	322	Megafauna (III)
28 A	127	1030	322	Megafauna (III)
22 A	145	480	322	Megafauna (III)
26 A	160	812	323	Megafauna (III)
26 A	180	820	323	Megafauna (III)
25 A	175	775	323	Megafauna (III)
26 C	310	840	323	Megafauna (III)
26 B	225	825	323	Megafauna (III)
20 A	165	295	323	Megafauna (III)
23 A	150	550	323	Megafauna (III)
27 A	198	910	323	Megafauna (III)

26 A	132	827	324	Megafauna (III)
26 A	142	813	324	Megafauna (III)
26 A	133	861	324	Megafauna (III)
26 A	156	881	324	Megafauna (III)
26 A	172	871	324	Megafauna (III)
27 A	103	909	324	Megafauna (III)
24 A	160	630	324	Megafauna (III)
25 A	153	787	325	Megafauna (III)
25 A	150	780	325	Megafauna (III)
26 A	142	850	325	Megafauna (III)
26 A	170	825	325	Megafauna (III)
25 A	188	799	325	Megafauna (III)
25 A	175	795	325	Megafauna (III)
25 B	216	797	325	Megafauna (III)
26 A	125	825	325	Megafauna (III)
26 A	165	815	325	Megafauna (III)
26 B	250	830	325	Megafauna (III)
24 B	235	695	325	Megafauna (III)
20 A	170	237	325	Megafauna (III)
25 A	150	737	325	Megafauna (III)
26 A	150	850	325	Megafauna (III)
23 B	230	568	325	Megafauna (III)
26 A	118	862	326	Megafauna (III)
26 A	124	872	326	Megafauna (III)
25 A	110	755	327	Megafauna (III)
25 A	150	722	327	Megafauna (III)
20 A	125	275	327	Megafauna (III)
25 A	145	790	327	Megafauna (III)
24 B	260	695	327	Megafauna (III)
27 Z	82	940	328	Megafauna (III)
26 A	128	823	329	Megafauna (III)
26 A	127	815	329	Megafauna (III)
26 B	218	888	329	Megafauna (III)
26 A	168	817	330	Megafauna (III)
26 A	175	875	330	Megafauna (III)
26 A	175	825	330	Megafauna (III)
26 A	175	825	330	Megafauna (III)
25 A	187	725	331	Megafauna (III)
26 A	115	805	331	Megafauna (III)
23 A	150	550	332	Megafauna (III)
21 Z	50	350	332	Megafauna (III)
24 A	147	692	332	Megafauna (III)
26 A	105	850	333	Megafauna (III)

26 A	150	850	333	Megafauna (III)
25 A	131	706	333	Megafauna (III)
25 A	125	725	333	Megafauna (III)
25 A	175	775	334	Megafauna (III)
26 A	125	825	335	Megafauna (III)
24 B	225	699	336	Megafauna (III)
23 A	109	582	336	Megafauna (III)
23 A	109	590	336	Megafauna (III)
26 A	132	815	337	Megafauna (III)
26 A	114	808	337	Megafauna (III)
24 B	283	699	337	Megafauna (III)
25 A	125	775	338	Megafauna (III)
24 A	102	619	338	Megafauna (III)
24 A	115	610	338	Megafauna (III)
24 C	350	650	340	Megafauna (III)
25 Z	75	725	340	Megafauna (III)
25 A	125	725	340	Megafauna (III)
25 A	175	725	340	Megafauna (III)
25 A	125	750	345	Megafauna (III)
25 B	275	725	350	Megafauna (III)
26 B	206	857	363	Megafauna (III)

Supplementary Table S11. Dataset of the features observed in the fossil osteoderms. BSM: Bone Surface Modifications, 1: taphonomic aspects; 2: rodent gnawing marks; 3: trampling marks; 4: indistinguishable marks (see criteria details in Text S1).

Number	Origin	Size (cm)	Color	Hole perforation?	Polished?	BSM
1	unknown	2	light brown	no	no	1
2	unknown	2,2	light brown	no	no	1
3	unknown	1,7	light brown	no	no	1
4	unknown	2,3	light brown	no	no	1
5	unknown	1,8	light brown	no	no	1
6	unknown	2	light brown	no	no	1
7	unknown	2,2	light brown	no	no	1
8	unknown	2	light brown	no	no	1
9	unknown	1,7	light brown	no	no	1

10	unit III (25 A, z = 324-344)	1,2	light brown	no	no	1
11	unit III (25 A, z = 324-344)	1,4	brown	no	no	1
12	unit III (25 A, z = 324-344)	1,1	brown	no	no	1, 2
13	unit III (25 A, z = 324-344)	1,4	brown	no	no	1
14	unit III (25 A, z = 324-344)	1,2	brown	no	no	1, 4
15	unit III (25 A, z = 324-344)	1,1	brown	no	no	1, 2
16	unit III (25 A, z = 324-344)	1	brown	no	no	1
17	unit III (25 A, z = 324-344)	1,3	brown	no	no	1
18	unit III (25 A, z = 324-344)	1,1	parcial	no	no	1
19	unit III (25 A, z = 324-344)	0,9	brown	no	no	1
20	unit III (25 A, z = 324-344)	1	brown	no	no	1
21	unit III (25 A, z = 324-344)	1	brown	no	no	1
22	unit III (25 A, z = 324-344)	0,9	brown	no	no	1
23	unit III (25 A, z = 324-344)	1,1	brown	no	no	1, 2 and 4
24	unit III (25 A, z = 324-344)	1	brown	no	no	1
25	unit III (25 A, z = 324-344)	1,1	brown	no	no	1
26	unit III (25 A, z = 324-344)	1	brown	no	no	1
27	unit III (25 A, z = 324-344)	1,4	brown	no	no	1
28	unit III (25 A, z = 324-344)	1,1	brown	no	no	1
29	unit III (25 A, z = 324-344)	1,1	brown	no	no	1
30	unit III (25 A, z = 324-344)	1	brown	no	no	1
31	unit III (25 A, z = 324-344)	1,2	brown	no	no	1
32	unit III (25 A, z = 324-344)	1,1	brown	no	no	1, 4
33	unit III (25 A, z = 324-344)	1,4	brown	no	no	1, 4
34	unit III (25 A, z = 324-344)	1,5	parcial	no	no	1
35	unit III (25 A, z = 324-344)	1,3	brown	no	no	1
36	unit III (25 A, z = 324-344)	1	brown	no	no	1, 4
37	unit III (25 A, z = 324-344)	1,5	brown	no	no	1
38	unit III (25 A, z = 324-344)	1,1	parcial	no	no	1
39	unit III (25 A, z = 324-344)	1,1	brown	no	no	1

40	unit III (25 A, z = 324-344)	1,4	brown	no	no	1
41	unit III (25 A, z = 324-344)	1,3	parcial	no	no	1
42	unit III (25 A, z = 324-344)	1,1	parcial	no	no	1
43	unit III (25 A, z = 324-344)	1,5	brown	no	no	1
44	unit III (25 A, z = 324-344)	1,2	brown	no	no	1
45	unit III (25 A, z = 324-344)	1,2	brown	no	no	1, 2 and 3
46	unit III (25 A, z = 324-344)	1,8	brown	no	no	1
47	unit III (25 A, z = 324-344)	1	brown	no	no	1, 4
48	unit III (25 A, z = 324-344)	1	brown	no	no	1
49	unit III (25 A, z = 324-344)	1,3	parcial	no	no	1, 2
50	unit III (25 A, z = 324-344)	1,2	brown	no	no	1
51	unit III (25 A, z = 324-344)	1,3	brown	no	no	1
52	unit III (25 A, z = 324-344)	1,4	brown	no	no	1, 4
53	unit III (25 A, z = 324-344)	1,2	brown	no	no	1
54	unit III (25 A, z = 324-344)	1,1	brown	no	no	1, 4
55	unit III (25 A, z = 324-344)	1,8	brown	no	no	1
56	unit III (25 A, z = 324-344)	1,1	parcial	no	no	1
57	unit III (25 A, z = 324-344)	1,2	brown	no	no	1
58	unit III (25 A, z = 324-344)	1,2	parcial	no	no	1
59	unit III (25 A, z = 324-344)	1,2	brown	no	no	1
60	unit III (25 A, z = 324-344)	1,3	brown	no	no	1, 4
61	unit III (25 A, z = 324-344)	1,3	brown	no	no	1
62	unit III (25 A, z = 324-344)	1,1	brown	no	no	1, 2
63	unit III (25 A, z = 324-344)	1,3	light brown	no	no	1, 3
64	unit III (25 A, z = 324-344)	1,3	light brown	no	no	1
65	unit III (25 A, z = 324-344)	1,2	parcial	no	no	1
66	unit III (26 C, z = 308)	1,5	brown	no	no	1
67	unit III (26 C, z = 308)	1,5	brown	no	no	1
68	unit III (26 C, z = 308)	1,7	brown	no	no	1
69	unit III (26 C, z = 308)	1	brown	no	no	1
70	unit III (26 C, z = 308)	1	brown	no	no	1, 2, and 3

71	unit III (25 A, z = 324-344)	1,2	brown	no	no	1, 4
72	unit III (25 A, z = 324-344)	1,3	brown	no	no	1, 2
73	unit II (30 C, z = 200)	1,1	brown	no	no	1, 4
74	unit II (30 C, z = 200)	0,7	grey-ish	no	no, but flattered	1, 4
75	unit II (30 C, z = 200)	1,2	parcial	no	no	1
76	unit II (30 C, z = 200)	0,8	brown	no	no	1
77	unit II (30 C, z = 200)	1,5	brown	no	no	1, 2 and 4
78	unit II (30 B, until 200)	0,5	brown	no	no	1, 2
79	unit II (30 B, until 200)	1,1	brown	no	no	1, 2
80	unit II (30 B, until 200)	1	brown	no	no	1

Supplementary Table S12. Size of natural foramina, bioerosion, and the anthropic perforation holes present in unmodified and modified osteoderms.

Area (mm^2)		
Natural foramina	Bioerosion	Anthropic perforations
FR1		
0.0007		
0.0040		
0.0080		
0.0050		
FR3A		
0.0500		
0.0500		
0.0400		
0.0500		
0.0500		
0.0500		
0.3400		
0.0300		
0.0100		
0.0100		
FR3B		
0.6200		
0.3300		
FR6		
0.0750	0.0910	
0.0500	1.7570	
0.0330	0.2950	
0.0470	0.0980	

0.0590	0.1140		
0.0240			
0.0787			
0.0300			
0.0800			
0.0140			
FR7			
0.0210			
1.1450			
FR12			
1.2520			
0.0680			
FR14			
1.7880			
0.1550			
0.1090			
0.1220			
SEI6059			
0.0260		3.615	
0.0100		6.033	
0.0510			
0.0300			
0.0270			
0.0860			
0.0360			
0.0210			
0.0110			
0.0160			
SEI6368			
		8.614	
		7.152	
SEI6557			
		2.432	
0.1616	**0.4710**	**5.5692**	**mean value**
0.3625	**0.7238**	**2.5324**	**standard deviation**